Max-Born-Institut
für Nichtlineare Optik
und Kurzzeitspektroskopie
im Forschungsverbund Berlin e.V.

Annual Report 2022

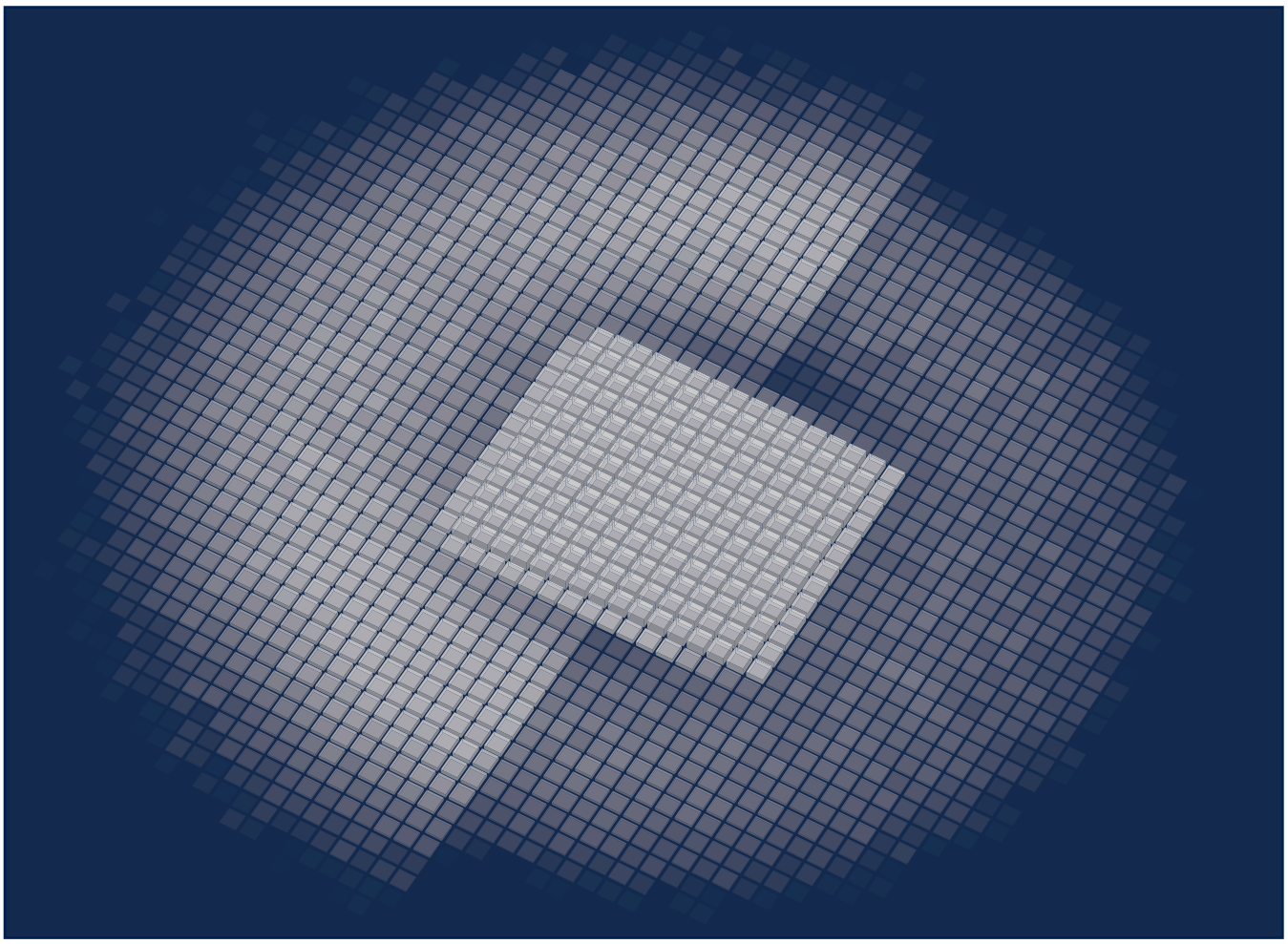

Max-Born-Institut

für Nichtlineare Optik
und Kurzzeitspektroskopie
im Forschungsverbund Berlin e.V.

Annual Report 2022

2022 in Figures

Budget

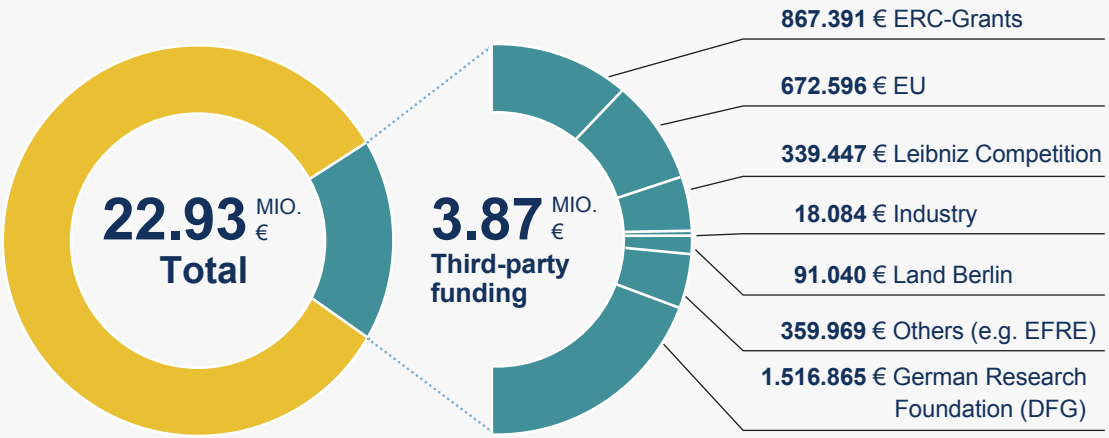

Staff total

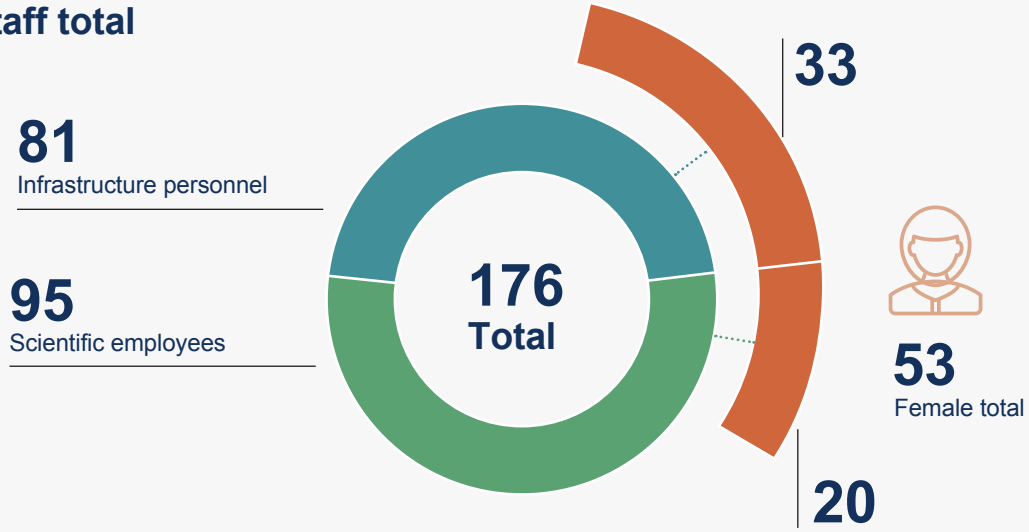

Scientific staff

There are two Junior Research Groups at MBI.

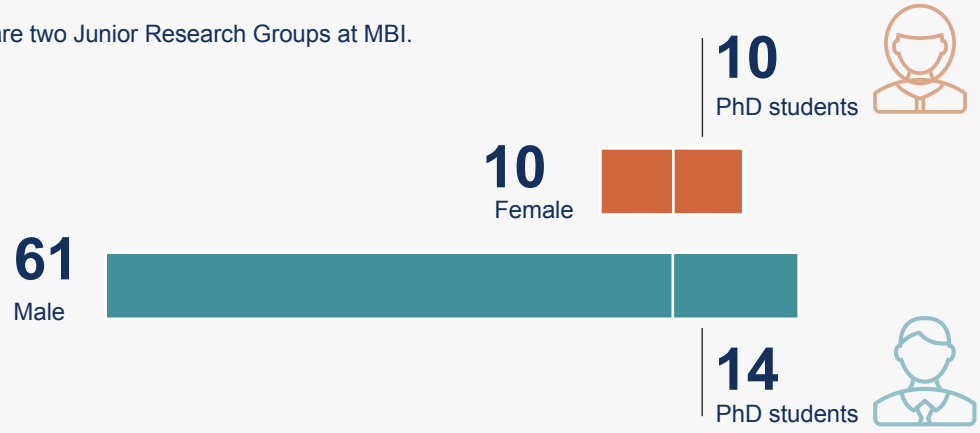

Publications

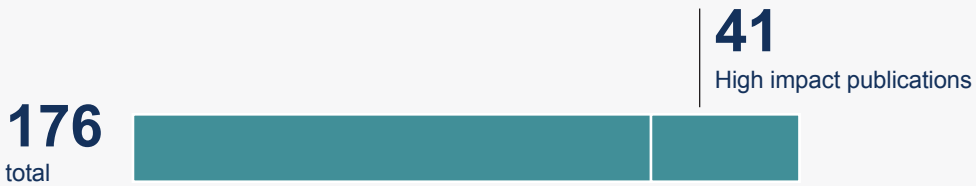

Scientific communication

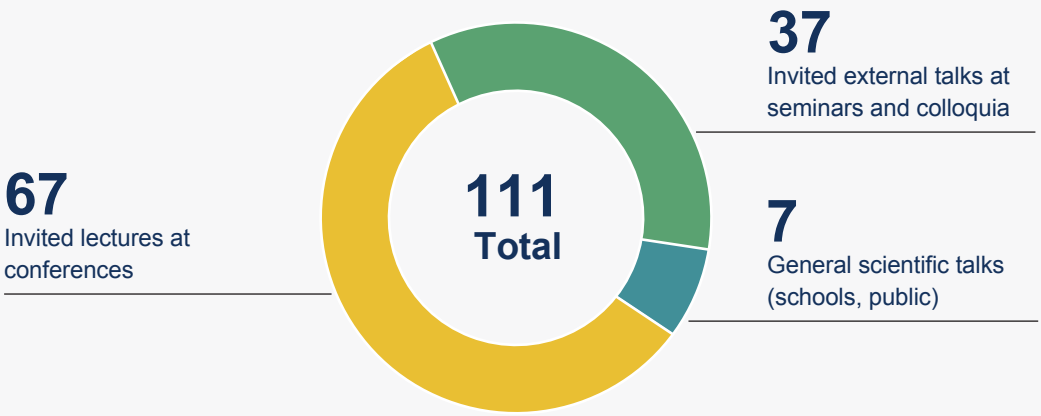

Education and Teaching

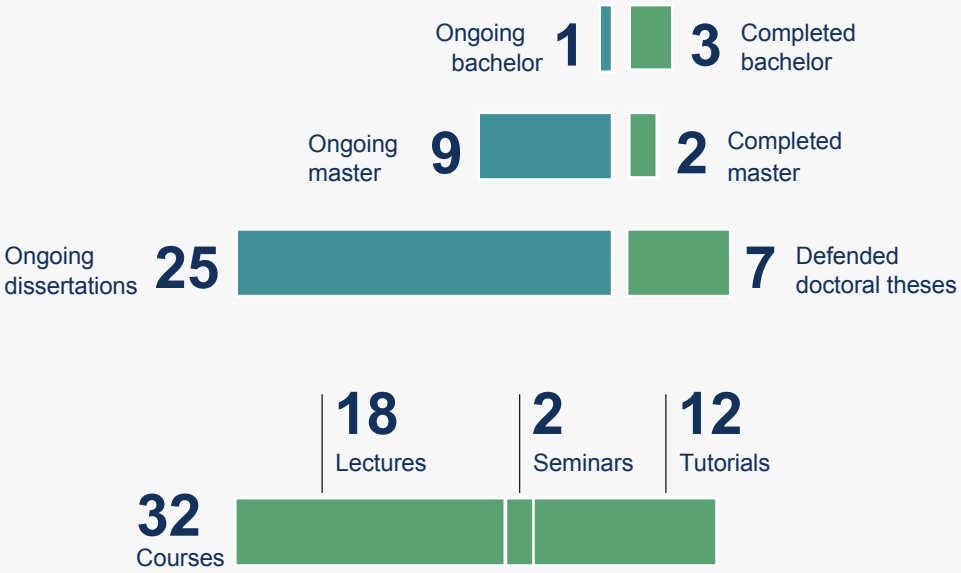

Annual Report 2022

Max-Born-Institut
für Nichtlineare Optik
und Kurzzeitspektroskopie
im Forschungsverbund Berlin e.V.

Max-Born-Straße 2 A
12489 Berlin
Germany
Phone: (++49 30) 63 92 - 15 05
Fax: (++49 30) 63 92 - 15 19
mbi@mbi-berlin.de
www.mbi-berlin.de

Preface

In this Annual Report we present you the achievements of the Max-Born Institute in 2022. The year 2022 has been a very eventful year. On the one hand, it has been a positive year, in that the consequences of the pandemic were felt much less severely than in the two years before. Accordingly, most MBI researchers were again able to carry out their work at the institute, and were able, once more, to directly interact with colleagues at conferences. On the other hand, 2022 was also the year in which Russia invaded Ukraine, with massive consequences for the Ukraine and the world at large. The war in Ukraine led to a large stream of refugees (with MBI happy to be able to accommodate a few), and had an enormous impact on the global economy, with the cost of food and energy, sharply increasing. At MBI, the annual cost of electricity more than doubled, reaching a sum of well over 1 million Euro. Accordingly, 2022 became the year in which, after several years of a gradual tightening of the budgets (due to difference between the annual salary increases and the annual budget increases of the institute) the financial management of the institute took center stage, with the institute having to seriously consider scenarios for a future with financial boundary conditions that might be less favourable than in the past.

Fortunately, 2022 also was a year where fantastic science was performed at the institute. As the many examples in this Annual Report will show, the research activities in MBI´s laboratories and on MBI´s computer facilities were brimming in 2022, and the institute produced and published many important and beautiful results that found their way into an impressive list of high-profile publications. You will be able to read about many of these results in detail in this Annual Report. However, MBI´s research output was not limited to research results in the form of publications, only. Two MBI researchers, Benjamin Fingerhut and Jochen Mikosch, left the institute to assume professorships at, respectively, the LMU München and the University of Kassel. Still, the biggest farewell in 2022 was that of Thomas Elsaesser as the Director of division C. With Thomas, the last member of the original directorate of the institute retired. In a career at MBI spanning 30 years, Thomas played a leading role in the development of MBI to the internationally renowned institute that it is today, combining the establishment of a world-leading research program in division C of the institute with dominant contributions to the management of the institute. For this Thomas deserves our heartfelt thanks. However, Thomas is not completely lost for MBI yet. The next two years he will continue his research at the institute in the framework of his successful ERC Advanced Grant project BIOVIB.

The retirement of Thomas Elsaesser as director of division C is connected with the search for a new director. This search process was started in 2021, and, after a series of interviews, led to the definition of a ranked list containing three very strong candidates in May of 2022, with each of these possible candidates representing very exciting research opportunities and a major gain for the institute. This list has meanwhile been approved by all relevant supervisory bodies, and at the moment that this introduction is written (April 2023) the appointment of a new director appears imminent. In addition to the procedure to hire a new director, a procedure for an appointment at the professor level at the FU Berlin led to a call to Sangeeta Sharma, the head of the Condensed Matter Theory group. We are confident that this call will also result in an appointment soon.

In 2022, a number of MBI researchers received individual honors and awards.

- Olga Smirnova was awarded and ERC Advanced Grant for her research on Ultrafast Molecular Chirality.

- Thomas Elsaesser was awarded the Ahmed Zewail Award for Ultrafast Science and Technology of the American Chemical Society.

- Daniel Schick was awarded a Junior Research Group in the Leibniz Competition, allowing him to set up an independent research group on the topic “Complex Spin Structures in Time and Space”.

We congratulate Olga, Thomas and Daniel on these well-deserved individual recognitions.

In closing, we would like to thank all members of the MBI community for their strong efforts in 2022, and we thank the funding bodies for their consistent support of the institute.

Berlin, April 2023

Marc Vrakking

Stefan Eisebitt

Research Structure of the Max-Born-Institut

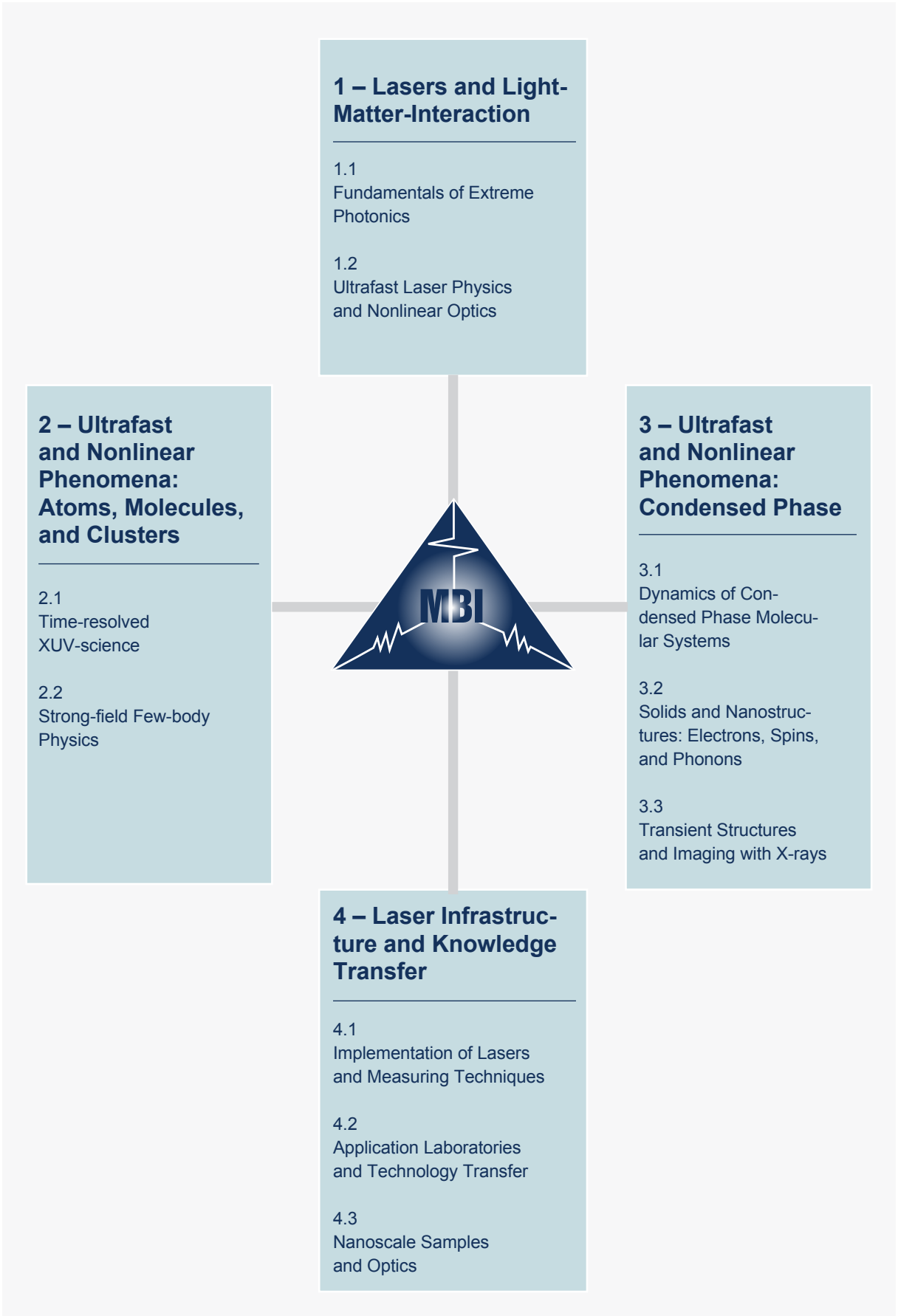

Organizational Structure of the Max-Born-Institut

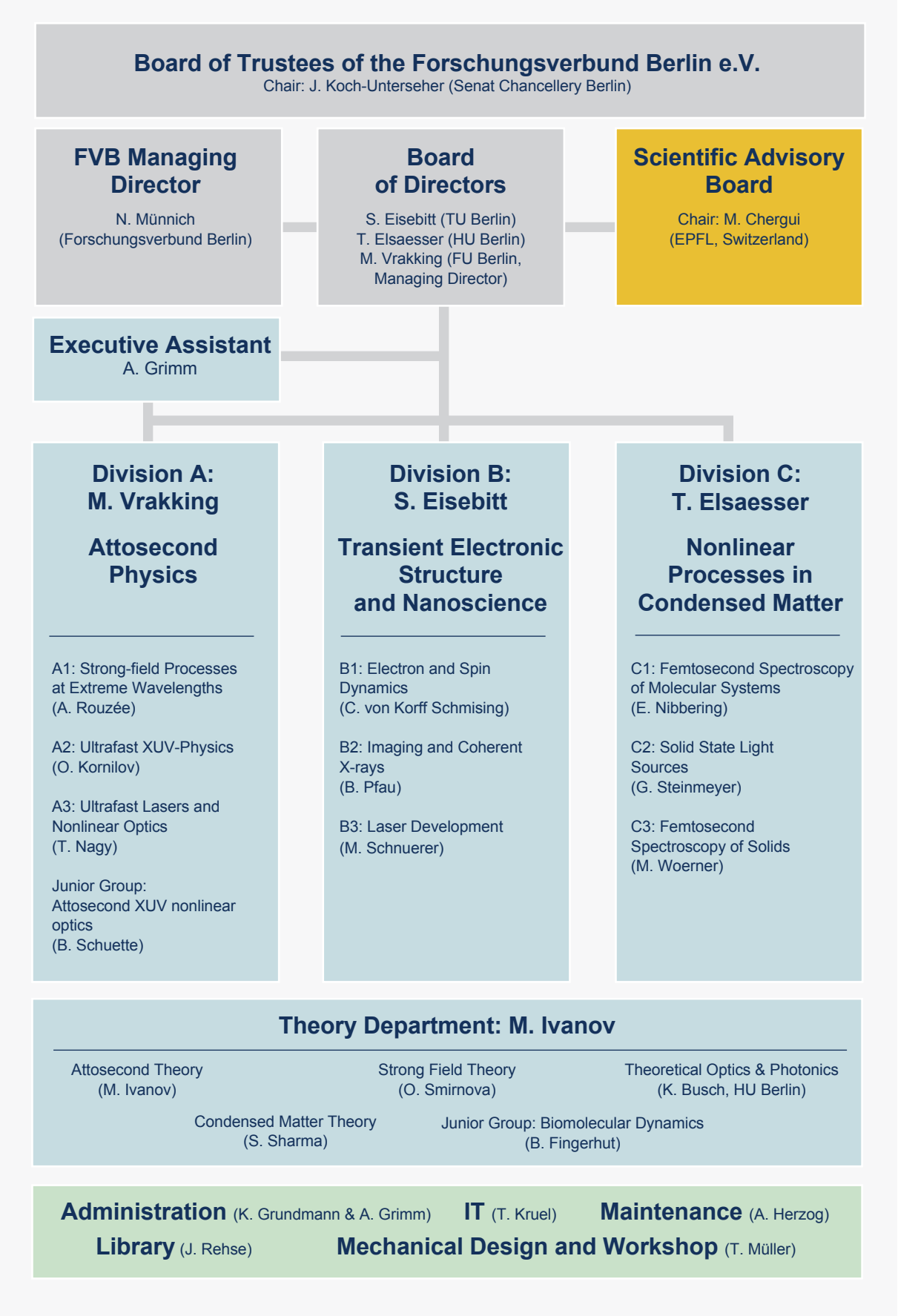

Members of the Scientific Advisory Board

Prof. Dr. Giulio Cerullo
Politecnico de Milano, Dipartimento di Fisica, Italy

Prof. Dr. Majed Chergui (Chair)
École Polytechnique Fédérale de Lausanne (EPFL), Institute of Chemical Sciences and Engineering, Switzerland

Prof. Tony Heinz
Stanford University, Department of Applied Physics, USA

Prof. Dr. Jon Marangos
Imperial College London, Department of Physics, UK

Prof. Dr. Christoph Quitmann
RI Research Instruments GmbH and Lund University, Max IV Laboratory, Sweden

Prof. Dr. Ursula Roethlisberger
École Polytechnique Fédérale de Lausanne (EPFL), Institute of Chemical Sciences and Engineering, Switzerland

Prof. Dr. Regina de Vivie Riedle
Ludwig-Maximilians-Universität München (LMU), Department Chemie, Germany

Prof. Dr. Jan Michael Rost
Max-Planck-Institut für Physik komplexer Systeme, Dresden, Germany

Representatives of the Cooperating Universities

Prof. Dr. Christoph Koch
Humboldt-Universtität zu Berlin, Institut für Physik, Germany

Prof. Dr. Andreas Knorr
Technische Universität Berlin, Institut für Optik und Atomare Physik, Germany

Prof. Dr. Martin Weinelt
Freie Universität Berlin, Fachbereich Physik, Germany

Representatives of the Federal Republic and the State of Berlin

Jan Neitzke
Bundesministerium für Bildung und Forschung, Ref. 711, Bonn, Germany

Aylin Gümüs
Senatskanzlei, Wirtschaft und Forschung, Ref. VI D, Berlin, Germany

MBI is a member of the Leibniz Association

Leibniz Association

Scientific Highlights

Attosecond pulses: 100 times more

T. Witting, M. Osolodkov, F. Schell, F. Morales, S. Patchkovskii, P. Šušnjar, F. H. M. Cavalcante, C. S. Menoni, C. P. Schulz, F. Furch, M. J. J. Vrakking

Attosecond laser pulses in the extreme ultraviolet (XUV) are a unique tool enabling the observation and control of electron dynamics in atoms, molecules, and solids. Most attosecond laser sources operate at a pulse repetition rate of 1 kHz (1000 shots per second), which limits their usefulness in complex experiments. Using a high power laser system developed at MBI we have managed to generate attosecond pulses at 100 kHz repetition rate. This enables new types of experiments in attosecond science.

Light pulses in the extreme ultraviolet (XUV) region of the electromagnetic spectrum, with durations on the order of 100s of attoseconds (1 as = 10^{-18} s) allow scientists to study ultrafast dynamics of electrons in atoms, molecules and solids. Usually experiments are performed using a sequence of two laser pulses with a controllable time-delay between them. The first pulse excites the system, and the second pulse takes a snapshot of the evolving system, by recording an appropriate observable. Usually the momentum distributions of ions or electrons or the transient absorption spectrum of the XUV pulse is measured as a function of delay between the two pulses. By repeating the experiment for different timings between the two pulses a movie of the dynamics under study can be created.

In order to get most detailed insights into the dynamics of the system under investigation, it is advantageous to measure the available information about the time evolution as completely as possible. In experiments with atomic and molecular targets, it can be advantageous to measure the three-dimensional momenta of all charged particles. This can be achieved with a so-called reaction microscope (REMI) apparatus. The scheme works by ensuring single ionization events for every laser shot and detecting electrons and ions in coincidence. This however, has the drawback, that the detection rate is limited to a fraction (usually 10 to 20 %) of the laser pulse repetition rate. Meaningful pump-probe experiments in a REMI are not possible with 1 kHz class attosecond pulse sources.

At MBI we have developed a laser system based on optical parametric chirped pulse amplification (OPCPA). In parametric amplification no energy is stored inside the amplification medium, therefore very little heat is generated. This enables the amplification of laser pulses to much higher average powers than with the current “work-horse” Ti:Sapphire laser, which is most often used in attosecond laboratories around the world. The second advantage of OPCPA technology is the ability to amplify very broad spectra. Our OPCPA laser system directly amplifies few-cycle laser pulses with durations of 7 fs to average powers of 20 W. This is a pulse energy of 200 uJ at 100 kHz repetition rate. With this laser system we have previously successfully generated attosecond pulse trains [1].

In many attosecond experiments it is beneficial to have isolated attosecond pulses instead of a train of multiple attosecond pulses. To enable the efficient generation of isolated attosecond pulses, the laser pulses driving the generation process should have pulse durations as close as possible to a single cycle of light. This way the attosecond pulse emission is confined to one point in time leading to isolated attosecond pulses. In order to achieve near-single-cycle laser pulses we have employed the hollow fiber pulse compression technique. The 7 fs pulses are sent through a 1 m long hollow waveguide filled with neon gas for spectral broadening. Using specially designed chirped mirrors the pulses can

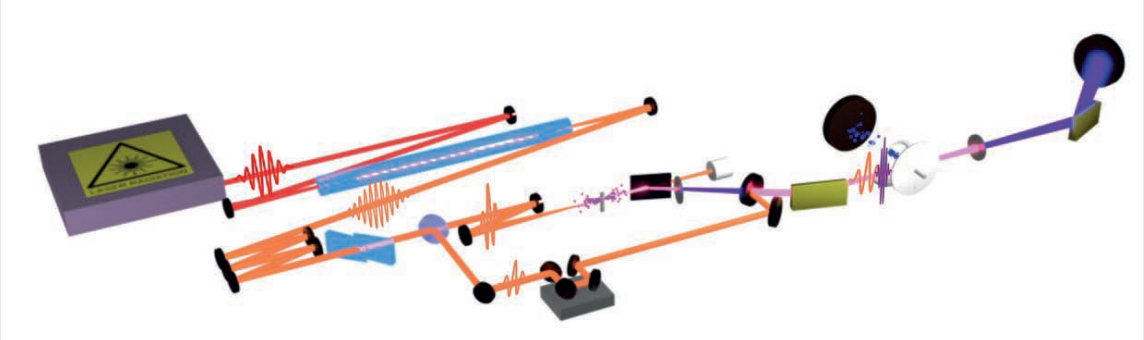

Fig. 1:
Experimental setup. Our home-built OPCPA system provides 7fs pulses at 100 kHz repetition rate. These pulses are shortened to 3.3 fs duration via hollow fiber pulse compression. Attosecond streaking experiments are performed in a purpose-built beamline.

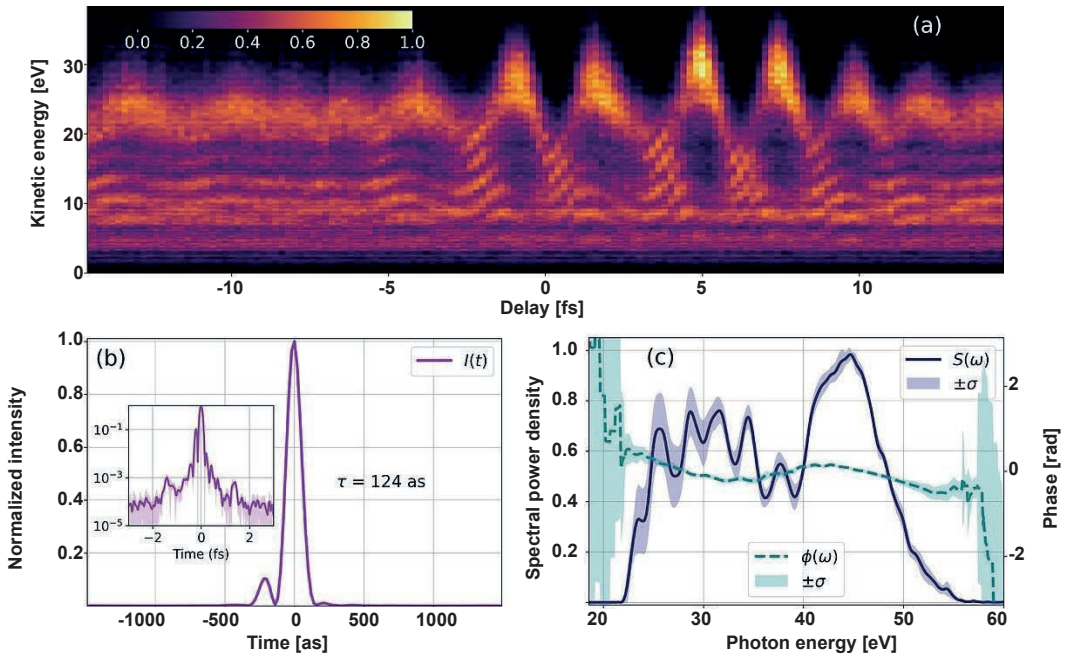

Fig. 2:
Attosecond streaking results. (a) Measured photoelectron streaking trace. (b) Intensity envelope of retrieved isolated attosecond pulse (inset: the intensity profile on logarithmic scale) (c) Retrieved spectral intensity and spectral phase.

be compressed to pulse durations as short as 3.3 fs. These pulses consist of only 1.3 optical cycles.

The 1.3 cycle pulses are sent into an attosecond beamline developed at the MBI. The main part of the energy is used to generate isolated attosecond XUV pulses in a gas cell target. After removal of the high power NIR beam, spectral filtering, and focusing, around 10^6 photons per laser shot (corresponding to an unprecedented photon flux of 10^{11} photons per second) are available for experiments.

In order to characterize the generated attosecond XUV pulses we performed an attosecond streaking experiment. Essentially the XUV pulse is used to ionize an atomic gas medium (neon in our case), while a strong NIR pulse is used to modulate the XUV generated photoelectron wavepackets. Dependent on the exact timing of the XUV and NIR pulses, the photoelectrons are accelerated (gain energy) or decelerated (loose energy) leading to a characteristic 'streaking trace'. From this datamatrix the exact shapes of both the NIR pulse, as well as the XUV pulse can be determined. The attosecond pulse shapes have been retrieved using a global optimization algorithm developed for this project. Our careful analysis shows that the main attosecond pulses have a duration of 124±3 as. The main pulse is accompanied by two adjacent satellite pulses. These stem from the attosecond pulse generation half an NIR cycle before and after the main attosecond pulse generation. The pre- and post-pulse satellites have a relative intensity of only 1×10^{-3} and 6×10^{-4}, respectively. These high flux isolated attosecond pulses open the door for attosecond pump-probe spectroscopy studies at a repetition rate 1 or 2 orders of magnitude above current implementations. We are currently starting experiments with these pulses in a reaction microscope (REMI).

Publications

(for full titles and list of authors see appendix 1)

[1] M. Osolodkov *et al.*; Generation and characterisation of few-pulse attosecond pulse trains at 100 KHz repetition rate; J. Phys. B: At. Mol. Opt. Phys. **53** no. 19 (2020) 194003

[2] WOS22: T. Witting *et al.*; Optica **9** (2022) 145-151

Center stage for quantum mechanical entanglement in an attosecond laser laboratory

L.-M. Koll, L. Maikowski, L. Drescher, T. Witting, and M. J. J. Vrakking

Quantum mechanics is famous for the way that its predictions challenge intuitive human thinking developed through the way that we experience the everyday world around us. Among other things, quantum objects can display both particle- and wave-like character, can interfere and can occur in the form of quantum superpositions. Arguably the biggest challenge of all is brought about by the fact that quantum mechanics does not adhere to our intuitive notion of local realism, that is, the notion that the results of measurements on objects reflect properties that are inherent to these objects. Quantum-mechanical entanglement represents a breakdown of local realism, and introduces the existence of non-locality, implying that the outcomes of measurements on an object A ("Alice") can be influenced by measurements on an object B ("Bob"), without there being any interaction between objects A and B.

Entanglement naturally arises when a quantum system is split into two sub-systems. Common situations are spontaneous parametric down-conversion, where an incoming pump photon is split into a pair of signal and idler photons, and photoionization, where light absorption splits a neutral atom or molecule into an ion and a photoelectron. Afterwards, the wave function of the total system can be written as a sum of one or more product wave functions describing the individual parts. If the wavefunction can be written as just a single product, then measurements that are performed on part A ("Alice") do not affect measurements that are performed on part B ("Bob"). However, if the wavefunction of the composite system can only be written as a sum of such products, then the system is entangled and the remarkable result emerges that measurements on "Bob" (with different outcomes possible according to the quantum-mechanical probability of each of these outcomes) will determine the outcome of subsequent measurements on "Alice", even if "Alice" and "Bob" do not interact.

Based on the above, we may expect quantum entanglement to be a common feature within attosecond science (1 as = 10^{-18} s), the new branch of laser physics that emerged in the early part of this century, where the time-dependent dynamics of electrons is studied on its natural, sub-femtosecond (1 fs = 10^{-15} s) timescale. The generation of attosecond laser pulses via high-harmonic generation necessarily produces laser pulses with photon energies that exceed the binding energy of every conceivable atom, molecule or material, and therefore, photoionization is a common aspect of attosecond experiments. Still, up to now the possible role of entanglement in attosecond experiments did not receive any significant attention.

Attosecond experiments are commonly performed in the form of a pump-probe experiment, where a first laser (the "pump") initiates dynamics of interest in the system under investigation and, after a variable delay, a second laser (the "probe") interrogates the evolving system, producing an observable that can be measured as a function of pump-probe delay. In this manner, pump-probe experiments provide a movie of the evolving dynamics, which can be viewed repeatedly and slowly (frame by frame, if necessary) until the underlying processes are understood. In quantum-mechanical terms, pump-probe experiments rely on coherence, i.e. the existence of well-defined phase relationships between different parts of the system that is formed after interaction with the pump laser pulse. As we have shown in recent theoretical [1] and experimental [2] work, the degree of coherence is significantly reduced in quantum systems that display entanglement.

In the experiments and in the calculations, neutral hydrogen molecules (H_2) were ionized using an attosecond pulse, producing an H_2^+ ion in the lowest-available, bound electronic state. In this state, a vibrational wavepacket was formed, i.e. a coherent superposition of vibrational states, describing the vibration of the molecule between an inner and an outer turning point. The vibration was detected using a near-infrared probe laser, which dissociated the molecule, producing an easily detectable H^+ ion and a neutral H-atom. Given that the probability of this dissociation process strongly depends on the internuclear distance between the two protons, the experiment could observe the vibration of the molecule by monitoring the fraction of molecules near the outer turning point of the vibration as function of pump-probe delay. In line with previous experimental results, the H_2^+ vibrations could readily be measured, demonstrating coherence between the different H_2^+ vibrational states.

This situation radically changed when the attosecond ionization pulse was replaced by a phaselocked pair of attosecond ionization pulses, with a controlled relative delay. For some values of the delay, the H_2^+ vibrations could be observed as before, whereas for other values the vibrations became all but unobservable. An analysis

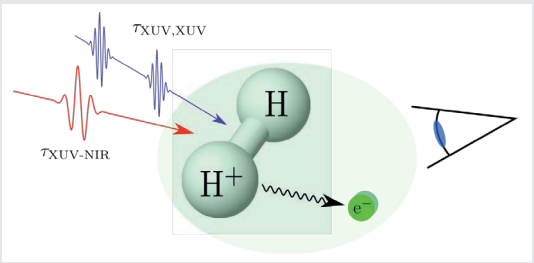

Fig. 1:
Sketch of the experiment. H_2 molecules are ionized by a phase-locked pair of attosecond XUV pulses. The quantum system consisting of molecular ion and photo-electron is probed by few-cycle NIR pulses.

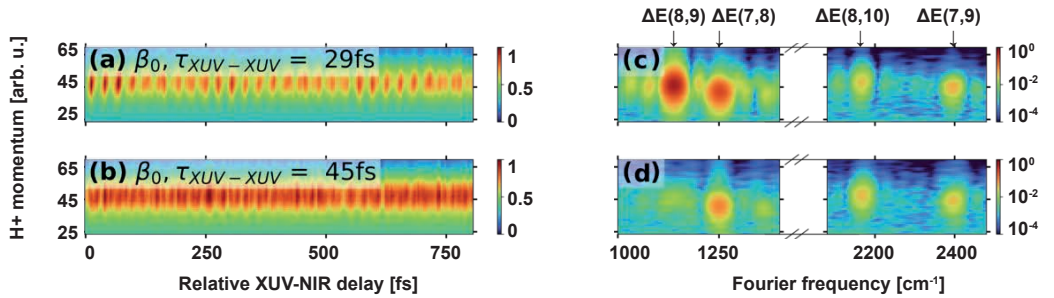

Fig. 2:
Measured momenta of the H^+ ions after ionization by a phase-locked XUV attosecond pulse pair as function of delay to the probing NIR laser pulse (a) for an XUV-XUV delay of 29 fs corresponding to coherent excitation of vibrational wave-packets. (b) for an XUV-XUV delay of 45 fs, where the system is entangled. Via a Fourier transform of the delay scan data individual vibrational quantum beats can be identified (c)+(d). Crucially, the intensity of the peaks corresponding to nearest neighbor coherences (ΔE8,9 and ΔE(7,8)) are very pronounced in the measurement with an XUV-XUV delay of 29 fs, and very weak for an XUV-XUV delay of 45 fs.

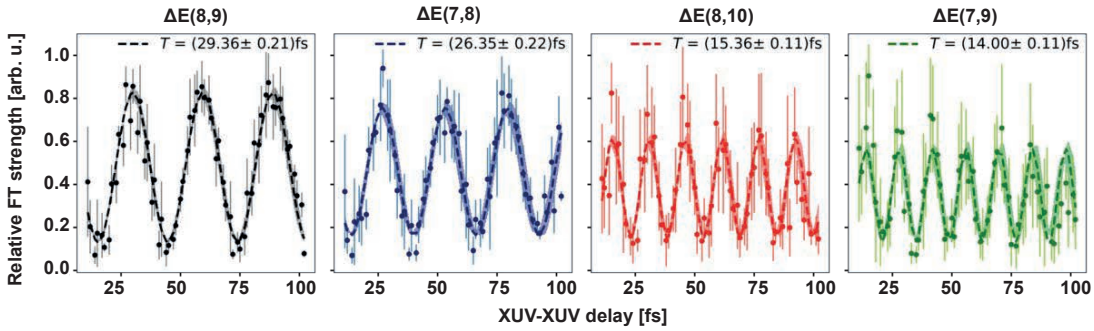

Fig. 3:
Strength of the quantum beats shown in Fig. 2 (c) and (d) as function of XUV-XUV delay.

of the time-delays for which the vibrational coherence was (un)observable, revealed that the degree of vibrational coherence in the H_2^+ cation occurred in competition with the degree of entanglement between the H_2^+ ion and the photoelectron produced in the ionization process. In other words, the experiment provided direct evidence that in attosecond pump-probe experiments involving ionization, entanglement between the ion and the photoelectron that are produced by ionization by the pump laser pulse, constrains the coherence that can be observed when the probe laser interacts with the ion or photoelectron. As such, the experiment provides an important warning to the attosecond community, demonstrating that the outcome of pump-probe experiments is governed by the properties of the wave function of the complete quantum system, even when the experiment may only target observation of the dynamics within one of the sub-systems. The experiment also points at an interesting opportunity in, for example, studies aiming at the observation of attosecond to few-femtosecond charge migration, where the specific electronic coherences underlying the charge migration process can be revealed. Finally, these experiments draw attention to the emerging link between ultrafast laser spectroscopy and the field of quantum information, where the application of attosecond science research tools may create hitherto unsuspected opportunities.

Publications

(for full titles and list of authors see appendix 1)

[1] M. J. J. Vrakking; Control of Attosecond Entanglement and Coherence; Phys. Rev. Lett. **126** (11) (2021) 113203

[2] KMD22a: L.-M. Koll *et al.*; Phys. Rev. Lett. **128** (2022) 043201/1-6

A new mix of extreme ultraviolet and optical light

H. Rottke, D. Schick, M. Borchert, U. Eichmann, C. von Korff Schmising, S. Eisebitt

Free-electron laser sources are shifting the limits for non-linear spectroscopy into the extreme ultraviolet (XUV) and X-ray spectral ranges, where inner shell electrons become involved in the non-linear processes. Exemplarily, we studied the influence of core excitons in a lithium fluoride single crystal on sum- and difference-frequency mixing by employing XUV free-electron and optical laser pulses. This allows probing charge localization with atomic specificity and gives access to otherwise forbidden, dark transitions.

Lithium fluoride (LiF) is an ionic crystal of cubic symmetry. Photoexciting one of the Li 1 s electrons with photons beyond 64 eV can transfer it to the conduction band, where it may freely roam the crystal. Excitation may also form an exciton, with the electron staying colocalized with the core hole at an excitation energy of just 62 eV. This exciton is evidenced by a narrow maximum in linear spectroscopy (Fig. 1b). The energetically close (1s)(2s) Li^+ configuration may also give rise to an exciton. However, it cannot be excited in linear spectroscopy due to dipole selection rules. However, the small shoulder on the low energy side of the pronounced structure in Fig. 1b has been suspected to be based on just this electron configuration, made accessible by breaking the cubic crystal symmetry. Non-linear spectroscopy may help clarify this proposition.

Owing to the symmetry of LiF, the lowest order nonlinear process is of third order: four-wave mixing (FWM) governed by the susceptibility $\chi^{(3)}$. Specifically, we studied sum- (SFG) and difference-frequency (DFG) mixing using extreme ultraviolet free-electron (photon energy E_X) and infrared (IR) laser radiation (photon energy E_{IR}). We then looked for generated radiation at photon energies $E_X + 2E_{IR}$ (SFG) and $E_X - 2E_{IR}$ (DFG), emitted in reflection off the LiF crystal surface as sketched in Fig. 1c.

The measurements were conducted at the FLASH2 beamline FL24 using the MUSIX endstation with the free-electron laser (FEL) photon energy scanned between E_X = 58 eV and 72 eV. The IR laser pulses had a fixed photon energy of E_{IR} = 1.55 eV. The sum- and difference-frequency generated in reflection are separated from the driving IR and FEL beams by a grating spectrometer. Please note that this geometry also allows the investigation of thick samples.

The main experimental result, i.e. the yield of radiation generated by FWM, is shown in Fig. 2a with the FEL photon energy on the horizontal axis and the energy shift of the emitted photons on the vertical axis. A region in the vicinity of the FEL photon energy was blanked out to protect the detector. The integration of the signal over positive (blue) and negative (orange) energy shifts results in the total yield of SFG and DFG, respectively (Fig. 2b).

Significant frequency conversion was only observable with the FEL tuned to the exciton transition (E_{exc} = 62 eV) or offset from E_{exc} by twice the IR photon energy, i.e. ± 3.1 eV (Fig. 2b) and with temporal overlap of both pulses. This verifies the nature of the observed FWM signal. In contrast, no frequency conversion was observed with the FEL tuned to the conduction band, including the 70.5 eV feature, which has been debated to be due to an electron polaron bound to a core hole.

The strong influence of the exciton, with its colocalized electron and hole, in the FWM processes suggests a simplified approach to model $\chi^{(3)}$ of LiF. We used an atomic model with two excitons based on the (1 s)(2 p) and (1 s)(2 s) electron configurations. It turned out that

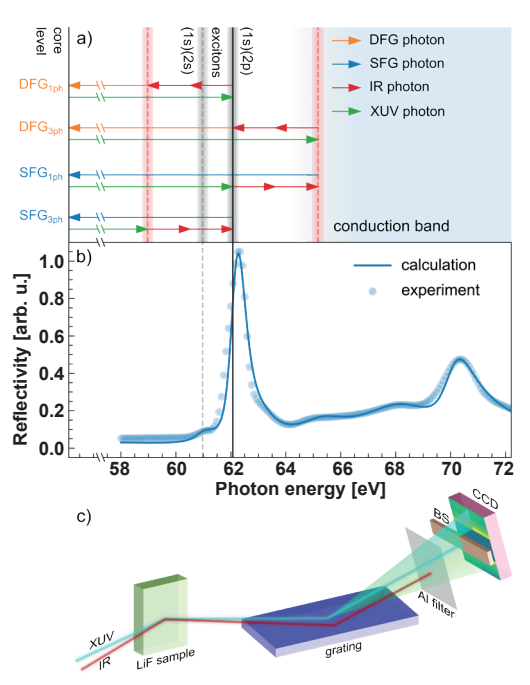

Fig. 1:
a) Schematic of the LiF energy levels relevant for the FWM experiment. The horizontal arrows represent the SFG and DFG generation if in one- or three-photon resonance with the LiF (1 s)(2 p) exciton at around 62 eV. b) Linear reflectivity spectrum in the relevant photon energy range. The dots represent the experimental data, and the solid line is a calculation based on a linear model for the dielectric constant of LiF. c) Sketch of the experimental setup showing the XUV and IR laser beams impinging nearly collinearly on the LiF crystal surface. The reflected IR light is blocked by an Al filter, while the XUV radiation is spectrally dispersed by a grating and detected by a CCD camera. The strong XUV fundamental is blocked by a beam-stop (BS) to avoid saturation.

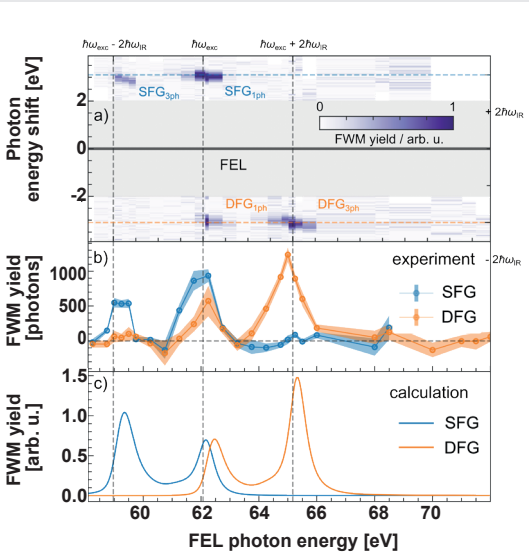

Fig. 2:
a) Density map of the FWM yield. DFG and SFG signals are only observed in one- or three-photon resonance with the Li (1 s)(2 p) exciton at around 62 eV. The corresponding photon energy shift is ± 2E_{IR}. The experimental SFG and DGF yields, shown in b), agree with the simple atomic model for the non-linear susceptibility χ(3) of LiF as shown in panel c).

both excitons, dipole coupled, are necessary to reproduce the experimental yields reasonably (see Fig. 2c). This indicates the presence of an s-type exciton as suspected based on linear spectroscopy.

Our work shows that non-linear XUV spectroscopy under resonant conditions is a sensitive probe of charge localization, enabling atomic specificity even when using wavelengths substantially larger than the unit cell. FWM allows identifying localized excitations, like excitons, even when they are ‘optically dark’. More generally, the presence of excited states, inaccessible or suppressed owing to crystal symmetry in linear spectroscopy, can be uncovered. With the FEL pulse durations decreasing, nonlinear spectroscopy will soon be able to probe the dynamical evolution of these excitations. As the dynamics of transient localization and delocalization of charge at different atomic species is of fundamental importance for a multitude of processes in physics, chemistry, and biology, we expect wave mixing processes in resonance with inner shell excitations to become a particularly fruitful approach for future time-domain studies at FELs.

Publication

(for full titles and list of authors see appendix 1)

RES22: H. Rottke *et al.*; Sci. Adv. **20** (2022) eabn5127/1-20

All-optical switching on a nanometer scale

K. Yao, F. Steinbach, M. Borchert, D. Schick, D. Engel, F. Bencivenga, R. Mincigrucci, L. Foglia, E. Pedersoli, D. D. Angelis, M. Pancaldi, B. Wehinger, F. Capotondi, C. Masciovecchio, S. Eisebitt, and C. v. Korff Schmising

Ultrafast light-driven control of magnetization on the nanometer length scale is key to achieve competitive bit sizes in next generation data storage technology. In this work, we used a novel experimental technique based on the interference of coherent light pulses in the extreme ultraviolet spectral range and successfully demonstrated the ultrafast emergence of nanoscale all-optical magnetization switching. By continuously reducing the wavelength of the light pulses, we optically imprint sinusoidal magnetization gratings with periodicities down to 17 nm. Studying the ultrafast evolution of the grating gives insight into the fundamental spatial limits of all-optical switching, ultimately governed by ultrafast lateral energy transport. The experiments were performed at the free electron laser facility FERMI at Elettra in Trieste, Italy.

The physics of optically driven magnetization dynamics on the femtosecond time scale has become of great interest for two main reasons: first, understanding the fundamental mechanisms of nonequilibrium, ultrafast spin dynamics and, second, the potential application in the next generation of information technology with a vision to satisfy the need for both faster and more energy efficient data storage devices. All-optical switching (AOS) is one of the most interesting and promising mechanisms for this endeavor, where the magnetization state can be reversed between two directions with a single femtosecond laser pulse, serving as “0 s” and “1 s”. While the understanding of the temporal control of AOS has progressed rapidly, knowledge on ultrafast transport phenomena on the nanoscale, important for the realization of all-optical magnetic reversal in technological applications, has remained limited due to the wavelength limitations of optical radiation. An elegant way of overcoming these restrictions is to use short wavelength radiation in the extreme ultraviolet (XUV) spectral range in transient grating experiments. This technique is based on the interference of two XUV beams leading to a nanoscale excitation pattern and has been pioneered at the EIS-Timer beamline of the free-electron laser FERMI in Trieste, Italy.

Here, we excited a transient magnetic grating (TMG) with a periodicity of Λ_{TMG}=87 nm in a ferrimagnetic GdFe alloy sample. We probed the spatial evolution of the magnetization grating by diffracting a time-delayed, third XUV pulse tuned to the Gd *N*-edge at a wavelength of 8.3 nm (150 eV). As AOS exhibits a strongly non-linear response to the excitation, one expects characteristic symmetry changes of the evolving magnetic grating distinct from the initial sinusoidal excitation pattern. This information is directly encoded in the diffraction pattern: in case of a linear magnetization response

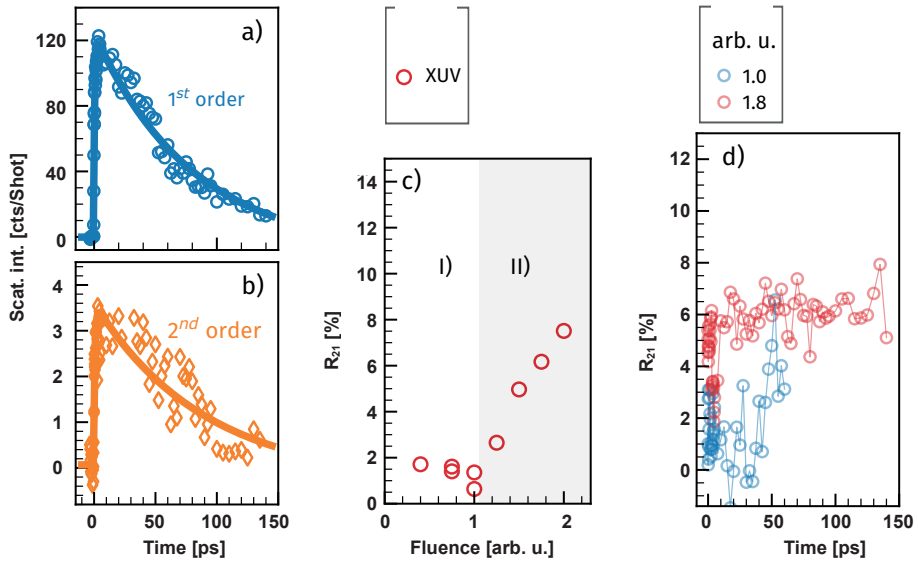

Fig. 1:
a) First and b) second order diffraction intensity as a function of the time delay between the pump and probe beams. c) Intensity ratio between the second and first diffraction order (R_{21}) as a function of excitation fluence at a delay of 50 ps. At a fluence of 1.3 arb. u., the transient magnetization grating starts to change its shape leading to the emergence of the second diffraction order, a fingerprint for AOS. d) Only for a sufficiently high excitation fluence (red circles) R_{21} exhibits a large and constant ratio, which we interpret as the emergence of a stable magnetic structures and therefore as further evidence for AOS on the nanometer spatial scale.

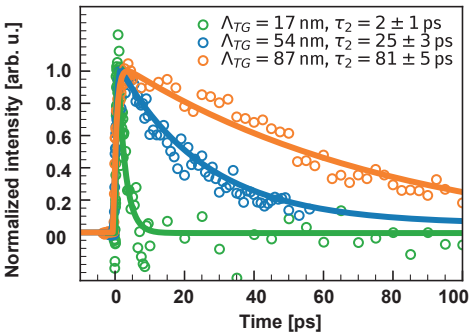

Fig. 2:
Normalized diffraction intensity as a function of time delay for three different periodicities, Λ_{TG} = 87 nm, 54 nm and 17 nm. For the smallest structure, the grating decays within ~ 2 ps via lateral energy transport.

to the excitation and no AOS, a sinusoidal TMG is induced and the second diffraction order is suppressed. However, if AOS occurs, the grating shape changes, now allowing for a pronounced second order diffraction intensity. In other words, we identified the intensity ratio between the second and first order (R_{21}) as a fingerprint observable for AOS in diffraction experiments.

Figure 1 a) and b) show the temporal evolution of the diffracted first and second order intensities, respectively. We find comparable decay times of $\tau_{RE,first}$ = (81 ± 7) ps and $\tau_{RE,second}$ = (90 ± 24) ps, consistent with lateral energy diffusion rates of the nanoscale gratings. Figure 1c), shows the ratio R_{21} as a function of the excitation fluence at a constant pump-probe delay of 50 ps. For low fluence below the threshold of AOS, we observed a constant and small value of R_{21} of around 1 %. Increasing the excitation to lie within the fluence window for AOS, R_{21} rises to ~8 %, providing first evidence for a magnetization reversal on the nanometer length scale. The ratio R_{21} as a function of time is shown in Figure 1d) for two selected excitation fluences. Only for the larger fluence (red circles) R_{21} exhibits an elevated and constant ratio of about 6 % over the measured time interval of 150 ps, indicative of a stable magnetic structure, which we interpret as optically reversed domains, i.e. AOS. Magnetic switching has taken place, transforming the sinusoidal magnetization profile into a prototypical …01010101… bit pattern. We were able to confirm the observations by complementary all-optical measurements in real space using time-resolved Faraday microscopy, where larger bits can be directly imaged. The combination of the techniques allows us to study the dynamics of the AOS process on the relevant nanometer-scale in great detail.

In a follow-up transient grating experiments, we were able to induce much smaller periodicities down to 17 nm (corresponding to 8.5 nm bit size), leading to a significantly accelerated decay of the magnetic grating contrast with rates of only τ_2 = (2±1) ps (cf. Fig. 2). Now ultrafast lateral transport processes present an additional channel for energy dissipation on the time scale of demagnetization and will therefore set the fundamental spatial limits of AOS.

Publication

(for full titles and list of authors see appendix 1)

YSB22: K. Yao *et al.*; Nano Lett. **22** (2022) 4453-4458

High energy few-cycle pulses around 12 µm for ultrafast longwave-infrared spectroscopy

P. Fuertjes, M. Bock, L. v. Grafenstein, D. Ueberschaer, U. Griebner, and T. Elsaesser

Few-cycle pulses at wavelengths longer than 10 µm are important for fundamental studies of the non-equilibrium properties of condensed matter, i.e., solids and liquids, and exhibit a high application potential, for example in optical materials processing. In particular, our interest is on the study of molecular vibrations and/or for performing time resolved two-dimensional infrared (2D-IR) spectroscopy [1]. The comparably small vibrational absorption cross sections require ultrashort pulses of sufficient energy in order to induce a nonlinear vibrational response. The challenge, however, is the limited availability of nonlinear crystals being transparent for the pump and the idler pulses and exhibiting high damage threshold. Consequently, there has been limited improvement of femtosecond longwave-infrared sources over the last 20 years [2-5].

We developed a new light source that delivers ultrashort infrared pulses beyond 10 µm wavelength with record parameters. The extremely compact system is based on the concept of optical parametric chirped pulse amplification (OPCPA), in which a weak ultrashort infrared pulse is amplified by interaction with an intense pump pulse of shorter wavelength in a nonlinear crystal. The infrared source combines a novel type of front-end with the technology of picosecond 2 µm Ho:YLF regenerative amplifiers developed at MBI in recent years.

The OPCPA front-end consists exclusively of a Cr:ZnS oscillator operating at a repetition rate of 79 MHz. The oscillator provides pulses as short as 30 fs with a spectrum spanning from 1.9 µm up to 2.6 µm (30 dB-level) and 12.5 nJ energy. The emitted spectrum is sufficiently broad to seed the pump and the OPCPA at its signal frequency in parallel. The spectral components below 2.1 µm are separated with a dichroic mirror and seed the 2-µm pump, whereas the part above 2.1 µm is used directly as the signal input. The pump is a Ho:YLF regenerative amplifier providing pulses of a 3 ps duration and 13 mJ energy at a 1 kHz repetition rate [6].

The setup of the OPCPA system is shown in Fig. 1. Prior to amplification, the signal pulses with 46 fs pulse duration are stretched in bulk sapphire and phase shaped by an acousto-optic programmable dispersive filter (AOPDF, Dazzler, Fastlite). The first amplification stage is equipped with a 2 mm thick GaSe crystal, the second and the third with a 1 mm thick crystal. GaSe exhibits a high second order nonlinearity of d_{eff} = 54 pm/V and a comparably high damage threshold [7]. In all stages, the

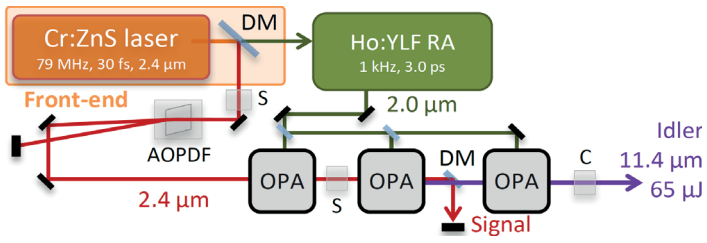

Fig. 1:
Setup of the LWIR OPCPA. The main parts are the front-end with the fs Cr:ZnS oscillator, the Ho:YLF regenerative amplifier (RA) as pump, and the three optical parametric amplifier (OPA) stages based on GaSe crystals. AOPDF, acousto-optic programmable dispersive filter; S, bulk stretcher; C, compressor; DM, dichroic mirror.

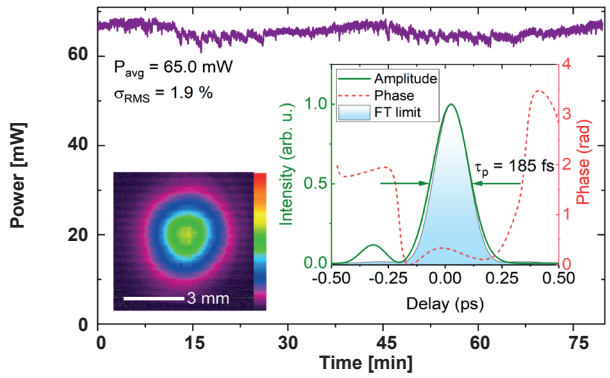

Fig. 2:
Characterization of the OPCPA pulse performance at 11.4 µm. Long-term pulse stability measurement. The average power is 65 mW, the standard deviation σ_{RMS}=1.9 %. Left inset: Far-field intensity distribution. Right inset: Retrieved temporal pulse shape of the few-cycle pulse.

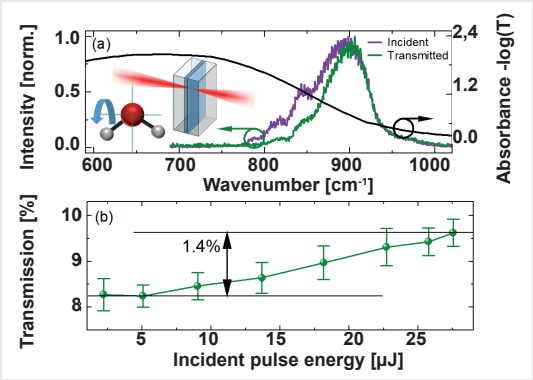

Fig. 3:
Nonlinear transmission of liquid water (12 µm thick film held between two transparent windows) at the librational (L2) band (vibration indicated by the circular arrow). (a) L2 absorption of water (black line) and incident (magenta line) and transmitted (green line) spectra of the 11.4 µm pulses (energy: 25 µJ). (b) Transmission of the water sample as a function of incident pulse energy, showing a nonlinear transmission increase.

type II parametric process is phase matched at an internal angle of 12.2° corresponding to an external angle of 36°. In total, only 6 mJ of the available pump is used for the three OPA stages in GaSe. The performance of the system is mainly limited by the aperture and quality of the commercially available GaSe crystals. All stages are pumped with a fluence of about 50 GW/cm^2. In the first stage, the signal pulses are amplified to 14 µJ, where a small angle of < 0.5° is introduced between pump and signal to prevent the second stage from being seeded with the SHG of the pump. The second collinear stage generates idler pulses of 15 µJ energy at a center wavelength of 11.4 µm, subsequently seeding the third parametric stage. In the last amplification stage, the non-collinearity allows for a clean separation of the pump and the idler pulses. The idler pulses are amplified up to an energy of 70 µJ which corresponds to a total pump-to-idler conversion efficiency of 1.2 %.

The idler pulses are characterized in an autocorrelation setup, generating a second-harmonic frequency-resolved optical gating (SH-FROG) trace using a monochromator (Horiba) with a spectral resolution of 10 nm. As shown in Fig. 3(a), the spectrum has its center at 11.4 µm (877 cm-1) and a full width at half maximum (FWHM) of 0.832 µm supporting a pulse duration of 172 fs. In principle, type II phase matching supports amplification beyond 12 µm. However, the spectral part above 13 µm is not accessible due to the group velocity mismatch in GaSe between the involved pulses. Finally, after compression in bulk ZnSe and additional phase shaping with the AOPDF, we retrieve an idler pulse duration of 185 fs which corresponds to less than five optical cycles of the light wave (Fig. 2).

The compressed idler pulses have an energy of 65 µJ, corresponding to a peak power around 0.4 GW. In the 1 kHz train the pulses are highly stable with a root-mean-square value of 1.9 % and of excellent optical beam quality (Fig. 2) [8]. Output power and repetition rate of the system are scalable.

The potential of this unique source for nonlinear spectroscopy was demonstrated in experiments on liquid water. For the first time, hindered rotations, so-called librations, of water molecules were excited to such an extent that their optical absorption decreased significantly (Fig. 3). From the analysis of this absorption saturation, a lifetime of the librational excitation of 20 to 30 fs is estimated [8].

Publications

[1] S. Ashihara, N. Huse, A. Espagne, E. T. J. Nibbering, and T. Elsaesser, “Ultrafast structural dynamics of water induced by dissipation of vibrational energy,” J. Phys. Chem. A **111**, no. 5 (2007) 743–746, doi: 10.1021/jp0676538

[2] F. Rotermund, V. Petrov, and F. Noack, “Difference-frequency generation of intense femtosecond pulses in the mid-IR (4-12 µm) using $HgGa_2S_4$ and $AgGaS_2$,” Opt. Commun. **185,** no. 1-3, (2000) 177-183, doi: 10.1016/S0030-4018(00)00987-1

[3] R. A. Kaindl, M. Wurm, K. Reimann, P. Hamm, A. M. Weiner, and M. Woerner, “Generation, shaping, and characterization of intense femtosecond pulses tunable from 3 to 20 µm,” J. Opt. Soc. Am. B **17,** no. 12 (2000) 2086, doi: 10.1364/josab.17.002086

[4] F. Junginger, A. Sell, O. Schubert, B. Mayer, D. Brida, M. Marangoni, G. Cerullo, A. Leitenstorfer, and R. Huber, “Single-cycle multiterahertz transients with peak fields above 10 MV/cm,” Opt. Lett. **35**, no. 15 (2010) 2645, doi: 10.1364/ol.35.002645

[5] K. Liu, H. Liang, L. Wang, S. Qu, T. Lang, H. Li, Q. J. Wang, and Y. Zhang, “Multimicrojoule GaSe-based midinfrared optical parametric amplifier with an ultrabroad idler spectrum covering 42-16 µm,” Opt. Lett. **44**, no. 4, (2019) 1003, doi: 10.1364/ol.44.001003

[6] P. Fuertjes, L. von Grafenstein, D. Ueberschaer, C. Mei, U. Griebner, and T. Elsaesser, “Compact OPCPA system seeded by a Cr:ZnS laser for generating tunable femtosecond pulses in the MWIR,” Opt. Lett. **46**, no. 7 (2021) 1704, doi: 10.1364/ol.419956

[7] K. L. Vodopyanov, “Parametric generation of tunable infrared radiation in $ZnGeP_2$ and GaSe pumped at 3 µm,” J. Opt. Soc. Am. B **10**, no. 9 (1993) 1723, doi: 10.1364/josab.10.001723

[8] P. Fuertjes, M. Bock, L. von Grafenstein, D. Ueberschaer, U. Griebner, and T. Elsaesser, “Few-cycle 65 µJ pulses at 11.4 µm for ultrafast longwave-infrared spectroscopy”, Optica **9**, no. 11, (2022) 1303

Proton hydration and proton transfer dynamics elucidated with steady-state and time-resolved soft X-ray spectroscopy

M. Ekimova, C. Kleine, J. Ludwig, S. Eckert, M.-O. Winghart, and E. T. J. Nibbering

Proton hydration, i.e. the involvement of a certain number of water molecules in solvating an excess proton, has been an intensively investigated research topic. It plays a pivotal role in the mediation (transport) mechanisms of energy conversion and signal transduction, ranging from hydrogen fuel cells to transmembrane proteins. However, aqueous solvation of excess protons has also to date been intensely debated because, being a complex quantum object with strong interactions to its surrounding, it is hard to probe. A collaboration of research teams from the Max Born Institute, the University of Hamburg, Stockholm University, Ben Gurion University of the Negev and Uppsala University have obtained key insight into the electronic structure of hydrated proton complexes in solution, that goes beyond the traditional Eigen or Zundel pictures, where four or two water molecules constitute the hydrated proton complex. Using state-of-the-art liquid flatjet sample delivery technology for measurements of the oxygen K-edge spectra at the BESSYII facility, it has been found that not only the electronic structure of three most inner water molecules in an $H_7O_3^+$ complex is drastically modified by the proton, but that the first hydration shell around this inner $H_7O_3^+$ complex, made up by a further 5 water molecules, senses the electric field of the proton by Coulomb interactions.

Textbook chemistry teaches us that bare protons do not exist in aqueous solution, because of the extraordinarily large proton affinity of liquid water. The hydronium ion, H_3O^+, is what is most familiar: one proton combines with one water molecule into a distinguished own species. In the middle of the 20th century two larger hydrated proton complexes with characteristic well-defined structures have been postulated, one by Manfred Eigen and the other one by Georg Zundel. As an acknowledgement to these pioneering scientists, these have been named after them: the Eigen cation $H_9O_4^+$ consists of a central H_3O^+ hydrogen-bonded to three water molecules – $H_3O^+(H_2O)_3$; the Zundel cation $H_5O_2^+$ has a proton shared between two strongly bound water molecules – $H_2O\cdots H^+\cdots OH_2$. The modern view is that both the Eigen and Zundel ions represent limiting structures of the hydrated proton in liquid water, with the actual structure of protonated water still under debate.

Until now, the electronic structure of hydrated proton complexes under room temperature solution conditions has been elusive, even though the electronic structure would provide vital information on all water molecules that are directly affected by the presence of a proton, providing an electronic structural picture that clearly in its refinement will go beyond the two limiting Eigen and Zundel geometries. Ideally, one would need a local probe of electronic charge densities, i.e. a probe such as provided by the electronic orbital structure of the water molecules actively involved in the hydration of the proton. This probe goes clearly beyond a mere determination of local electronic density change from two O-H bonds and two lone pairs, as is the case of the H_2O molecule, to three O-H bonds and only one lone pair, as happens for H_3O^+. In fact, by the formation of hydrogen bonds of different strengths, the electronic orbital structure is expected to change profoundly for all water molecules directly interacting with the proton.

The results show an absence of a distinct pre-edge band and a strong post-edge band in the oxygen K-edge

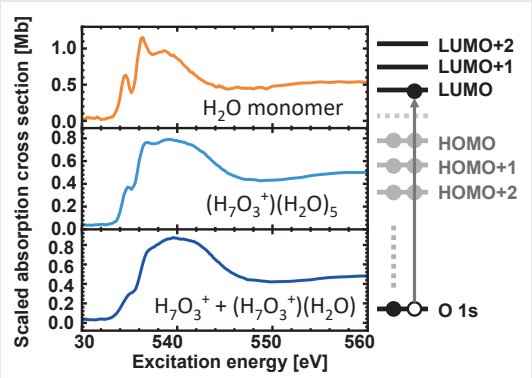

Fig. 1:
Oxygen K-edge spectra of the water monomer, and of hydrated proton complexes formed by mixing HI and H_2O in 1:8 and 1:3.5 mixing ratios respectively, showing the distinct difference in the pre-, main and post-edge band features of monomer water molecules, of hydration shell water molecules and of the inner $H_7O_3^+$ complex.

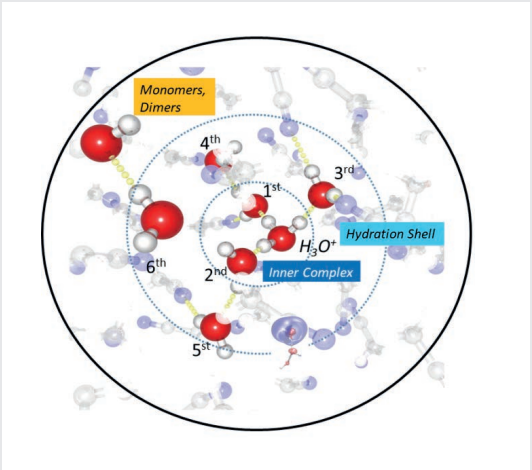

Fig. 2:
A general architectural hierarchy exists in which the proton strongly interacts with the three nearest water molecules to form a hybridized $H_7O_3^+$ core while the first hydration shell is affected by the electric field of the proton's positive charge. Further solvation shells contain bulk-like water molecules.

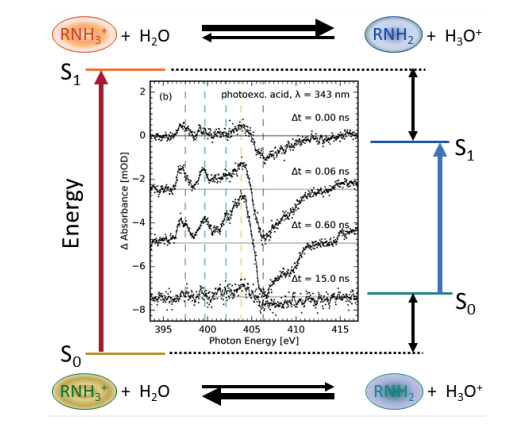

Fig. 3:
Förster cycle of an amine photoacid, showing electronic ground states S_0 and the first excited states S_1 of the acidic (left) and basic (right) species. There are the four stages of photoacid behaviour in aqueous solution, as shown by the cartoons. In the centre transient soft X-ray spectra are shown, measured on 8-aminopyrene-1,3,6-trisulfonate (APTS).

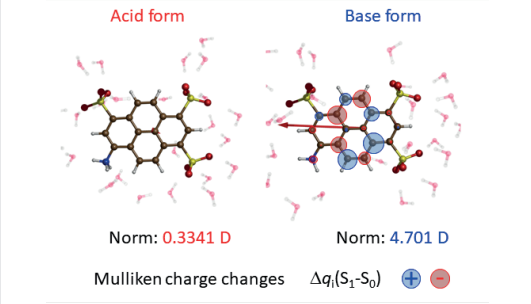

Fig. 4:
Estimated charge distribution changes on the APTS photoacid and conjugate photobase forms, showing major changes in Mulliken charges and in the electric dipole moment upon electronic excitation.

spectrum of $H_7O_3^+$, whereas water molecules have a clear pre-edge and a much smaller post-edge band (Fig. 1). The results obtained on acid/water mixtures dissolved in acetonitrile suggest a general architectural hierarchy for proton hydration, a proton strongly interacting with three water molecules as $H_7O_3^+$, and one hydration shell affected by the electric field of the positive charge of the proton (Fig. 2). These findings will have direct repercussions in the understanding of proton hydration, ranging from protons in bulk aqueous solution, to proton complexes that are anticipated to occur in hydrogen fuel cell devices, and in hydration pockets in transmembrane protein proton channels.

Photoacids are molecules that release a proton upon electronic excitation, thus enhancing the acidity of a liquid. Pioneering work by Theodor Förster has shown the direct relationship between the wavelength position of optical absorption and acidity properties with which the increase in acidity in the first electronic excited state can be quantified. However, underlying full microscopic explanations for the photoacidity phenomenon have remained sparse. With ultrafast X-ray spectroscopy, locally probing the electronic structure of a proton donating group of an amine aromatic photoacid has now provided direct insight in the changes of electronic structure. The long standing open question for photoacidity has now finally been resolved: major electronic structure changes occur on the base side of the so-called Förster cycle, whereas the acid side plays a minor role.

Photoacids have been known for more than 70 years. Theodor Förster has been the first to correctly describe the observations of absorption and fluorescence spectra of photoacids, and connect positions of the electronic transitions giving rise to optical absorption bands to the increased acidity properties of photoacids in the electronic excited state. Many research activities have been pursued in the following decades, but apart from quantum chemical calculations of photoacid molecules of medium size, focussing on the intramolecular electronic charge distribution changes of the proton donating moieties of photoacids, microscopic insight have remained limited. Some of these studies have indicated – in line with previous suggestions based on physical organic principles – that the effects of electronic excitation are much more pronounced on the conjugate photobase side of the Förster cycle (Fig. 3).

Scientists from the Max-Born-Institute in Berlin, Stockholm University, the University of Hamburg, Helmholtz-Zentrum Berlin, Ben-Gurion University of the Negev in Beersheva and Uppsala University, have now successfully pursued a novel combined experimental and theoretical approach to study the electronic charge distributions of photoacids along the four stages of photoacids provide direct microscopic insight into the electronic structural changes of the proton donating amine group of an aminopyrene derivative in aqueous solution. The K-edge X-ray absorption spectra of nitrogen atoms in the molecular structure were measured at the synchrotron BESSY II in transmission mode to locally probe electronic structure on ultrafast time scales. Together with quantum chemical calculations, such results provide a consistent picture of photoacid behaviour (Fig. 4): electronic charge distributions of the proton donating group are only minor on the photoacid side, but substantial on the conjugate photobase side. Yet the overall dipole moment change of the whole molecule is as important as the local charge distribution changes, hence solvation dynamics by the solvent water is the second important factor governing photoacidity.

These achievements obtained on hydrated proton complexes and on photoacid molecules along all stages of the Förster cycle pave the way towards further developments in steady-state and ultrafast soft X-ray spectroscopy. Probing on ultrafast time scales the electronic structural dynamics of acid-base complexes, and those of the hydration shell water, will provide key insight into the elementary steps in proton transport that will affect the electronic charge densities accommodating the dislocation of protons.

Publications

EKL22a and EWK22a

Spin-orbit Larmor clock in high harmonic generation: The unexpected role of ultra-long Rydberg Trajectories

N. Mayer, A. Jimenez-Galan, S. Patchkovskii, O. Kornilov, O. Smirnova, M. Y. Ivanov

High-harmonic generation (HHG) is typically thought of as a sub-laser-cycle process, with the electron's excursion in the continuum lasting a fraction of the optical cycle. However, it was suggested in our earlier works that excitation of long-lived Rydberg states can play an unexpectedly important role in high harmonic generation. This suggestion was triggered by observation of strong symmetry-forbidden harmonics in atoms driven by a combination of counter-rotating circularly polarized fundamental and second harmonic field, also known as the trefoil field. In such fields, symmetry requires that 3N harmonic orders (N integer) are forbidden.

Indeed, long-lived excitations introduce memory in the system, breaking perfect symmetry between the subsequent ionization-recombination events driving the HHG, thus opening a door for generating symmetry-forbidden harmonics. Experimentally, this symmetry breaking is particularly clearly seen when atoms are driven by the combination of the counter-rotating circularly polarized fundamental light field and its second harmonic, i.e. the trefoil field.

In our work [MBJ22] we report detailed theoretical analysis of unexpected properties of HHG in Argon gas driven by trefoil fields. We complement theoretical analysis with direct experimental evidence of long and stable Rydberg trajectories contributing to high-harmonic generation. To this end, we introduce the spin-orbit Larmor clock to characterize the time-scale that the Rydberg electrons, which are driven by strong laser field yet still trapped by the core potential (the so-called frustrated tunneling), spent between ionization and recombination.

The idea of the spin-orbit Larmor clock is depicted in Fig.1 It utilizes the precession of the spin of the hole left in the parent ion upon injection of the active electron into the continuum. The precession of the hole spin affects the recombination probability: the spin of the electron must be aligned with the spin of the hole for the recombination to be possible, introducing periodic modulation of the recombination probability. This periodic modulation leaves a clear trace in the harmonic spectra by splitting the harmonic lines into a doublet, with the splitting equal to the spin-orbit splitting in the ion, provided the delay between ionization and recombination is long enough to resolve this splitting. In Argon, where the experiment was done, this spin-orbit period is equal to 28 fsec, i.e. is about 10 laser cycles long. Thus, our observation of spin-orbit splitting in high harmonic generation in Argon is a direct evidence of the contribution of electron trajectories that spend at least 10 cycles between ionization and recombination oscillating around the core.

Our findings contrast sharply with the general view that long-lived Rydberg orbits should generate negligible contribution to the macroscopic far-field high harmonic response of the medium. Indeed, the usual argument is that long trajectories accumulate large phase associ-ated with the electron wiggling in the laser field. This phase scales with laser intensity and changes substan-tially across the laser focus due to the inhomogeneous intensity distribution, leading to a sharp phase front profile and rapid divergence of the radiation associated with long trajectories, let alone with the ultra-long ones. This well-known issue poses a clear challenge: one has to explain how and why radiation from such long-lived, laser driven Rydberg states, which accumulate very large intensity-dependent phase can lead to well collimated macro-scopic signal in the far field.

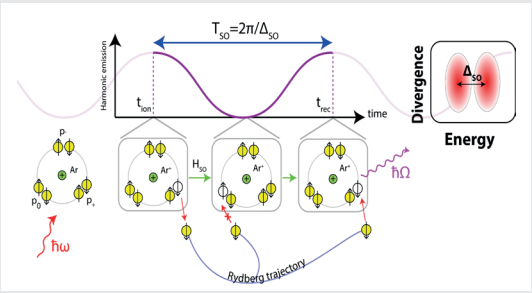

Fig. 1:
Spin-orbit Larmor clock in HHG. Electron-hole recombination is temporally modulated due to the precession of the spin of the hole, leading to a spectral splitting of the harmonic lines (adapted from [MBJ22]).

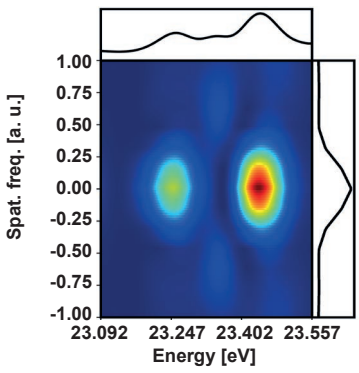

Fig. 2:
Far-field profile of H15 calculated in [MBJ22]. The top panel shows the frequency-resolved, spatially integrated distribution when the spin-orbit modulations are included, while the right panel shows the frequency-integrated, spatially resolved far-field line.

We also resolve this challenge in Ref. [MBJ22]. We found that, for long laser pulses, the frequency-domain analogue of the frustrated tunneling are the so-called Freeman resonances: The Rydberg states are populated when the ponderomotive Stark shift brings them into a multi-photon resonance with the ground state. The dominant contribution with the largest excitation probability is obtained when the resonance is achieved near the peak of the laser pulse, selecting a relatively narrow 'onion shell' inside the laser focus, with well-defined intensity. Thus, the quantum phase associated with the contribution of resonant Rydberg trajectories is large but constant, leading to collimated emission in the far field shown in Fig. 2.

Publication

(for full titles and list of authors see appendix 1)

MBJ22: N. Mayer *et al.*; Phys. Rev. Lett. **129** (2022) 173202

Short Description of Research Projects

1.1: Fundamentals of Extreme Photonics

O. Smirnova, M. Richter (project coordinators)
and M. Y. Ivanov, M. Khokhlova, Á. Jiménez-Galán, W. Becker, F. Morales, I. Babushkin, D. Ayuso, A. Ordonez, R. Heilemann, A. Loehr, Y. Muhammed, P. Maier, N. Mayer, J. Herrmann, A. Gusakov, K. Busch, V. Bender, A. Rodríguez-Echarri, W. Zhao, S. Vengaladas, K. Tschernig, D. Reiche, S. Patchkovskii, R. Ovcharenko, B. Fingerhut, S. Sharma, S. Shallcross, P. Elliott, S. Solovyev

1. Overview

The main objective of the project 1.1 in 2022 has remained to be the development of analytical and numerical methods for the description of light-matter interactions in extreme conditions. These methods are used to investigate the viability of new physical ideas and research questions arising in extreme light-matter interaction. The interaction is studied in both the few-photon limit where the fully quantum description of light is crucial and in the semiclassical regime, where the light can be described classically. When a low number of photons are involved, not only the quantum properties of matter but also those of light play a very important role in the description of the interaction. At high intensities, the description of light as a classical electromagnetic wave is typically adequate, but a precise description of the (often highly nonlinear) quantum response of matter is needed. Moreover, the modification of the incident light via nonlinear-optical processes may also lead to interesting quantum properties of the generated radiation. Non-perturbative theoretical models and methods are developed and applied, focusing on adequate description of system's optical properties and the influence of systems' geometrical structure, especially in the case of chiral molecules, as well as on many-body effects such as electron-electron correlation, coupled electronic and nuclear dynamics, optically induced and controlled spin dynamics, including laser-driven and laser-controlled ultrafast spin and magnetization dynamics in solids, and the role of quantum coherence in these dynamics. The range of material systems involves atoms, molecules, especially chiral molecules, and solids – from dielectrics to semiconductors to magnetic materials, as well as photonic structures such as waveguides.

2. Topics and collaborations

In 2022 the project was initially organized around five general directions, following the main research thrusts of the 5 theory groups:

T1: Theory of attosecond and few-femtosecond electron dynamics

T2: Theory of matter in intense laser fields, focusing on chiral molecules

T3: Theoretical optics and photonics in structured media (Joint HU-MBI Group)

T4: Bio-molecular dynamics in condensed phase

T5: Condensed Matter Theory

Important changes have occurred during 2022, however. The topic T4 was discontinued in 2022 with the departure of the leader of T4 group Dr. Benjamin Fingerhut and the relocation of his T4 theory group. Dr. Fingerhut has taken a professor position at the LMU in Munich.

In the theory of matter in strong laser fields, the acquisition of the 2022 advanced ERC grant by Prof. Olga Smirnova, the head of the T2 group, has led to increased focus on ultrafast chirality, especially on the theory of ultrafast electronic response of chiral matter to intense laser fields.

In-house collaborations with Projects 1.2, 2.1, 2.2, 2.3, 3.1, 3.2

External collaborations: IC London (UK), Kings College (UK), HU Berlin, TU Berlin, The Weizmann Institute (Israel), Technion (Israel), CEA Saclay (France), CELIA and University Bordeaux (France), University of Ottawa (Canada), UCLA (USA), UA Madrid (Spain), University Trieste (Italy), XLIM Limoges (France), University Sherbrook (Canada), University of Central Florida, (USA), University Sarajevo (Bosnia-Herzegovina), University Geneva (Switzerland), MPI Halle (Germany), Hebrew University of Jerusalem (Israel), Ben-Gurion University of the Negev, Beer-Sheva (Israel), University of Colorado and JILA (USA), University of Zurich (Switzerland).

3. Results in 2022

Representative results are given below for a range of general research directions.

T1, T5: All-optical valley switch and clock of electronic dephasing

One of the most interesting features of 2D hexagonal materials such as graphene and gapped graphene (transition metal dichalogenides, TMDCs) is the electron's extra degree of freedom, the valley pseudospin, associated with populating the local minima located at the **K** and **K'** points of the hexagonal Brillouin zone (BZ). Both T1 [SIJ22] and T5 [SES22] have been working on developing ultrafast schemes which would allow one to use valley pseudospin as information carrier on time-scale of tens of femtoseconds.

It has been shown that shining circularly-polarized light allows to achieve close to 100 % of valley polarization, opening the way to valley-based transistors. However,

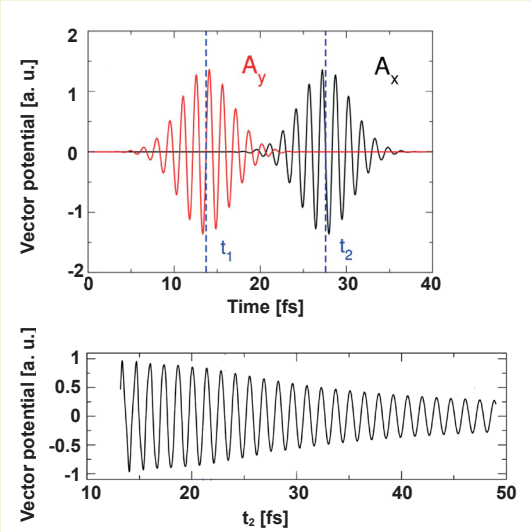

Fig. 1:
Valley-selective excitation with linearly polarized pulses in WSe2, demonstrated theoretically in [SES22]. (Top) The sequence of pulses used by T5 in [SES22]. The two pulses are orthogonally polarized; the vector potentials are shown. (b) Valley polarization as a function of the arrival time of the second pulse, the first is centered around 14 fsec. Strong valley polarization is achieved even when the two pulses no longer overlap.

in this approach one uses long pulses, carefully tuning the carrier frequency on resonance with the minimal band-gap in the valley. Ultrafast switching of the valley polarization is still a key challenge for the practical implementation of such devices due to the short valley lifetimes..

The problem addressed by both T1 and T5 can be formulated as follows: is it possible to control valley polarization and excite a selected valley by using a combination of linearly polarized few-cycle pulses, and how fast can this be done without significant loss of valley selectivity? T1 and T5 have used completely different numerical methods. While the T5 has used their first-principles ELK code, T1 has used the IWERIA code which combines static DFT material input followed by the Wannierization procedure with the semiconductor Bloch equations. The results, however, are in excellent agreement, demonstrating robustness of the analysis.

The core idea of the two works can be understood as follows. A circularly polarized pulse is a combination of two linearly polarized pulses with orthogonal polarizations and a quarter-cycle delay between the peaks of the two. Switching the circularity of the overall pulse from left-handed to right-handed can be done by delaying one of the two polarization components, i.e. one of the two linearly polarized pulses, by one half-cycle. Thus, one can consider the well known valley selective excitation as a function of the sub-cycle delay between the two linear, fully overlapping, and orthogonally polarized pulses.

It is hardly surprising that, as long as the two orthogonal pulses overlap, valley selective excitation will be achieved. The key question is how long can the delay between the two pulses be, so that the valley polarization persists, even – and especially – if the two orthogonally polarized pulses no longer overlap

The typical results are shown in Figure 1 for WSe2, obtained in Ref. [SES22].

In Ref. [SIJ22] similar results have been obtained for two other materials, hBN and MoS2. This confirms that the scheme is completely general.

Next, Ref. [SIG22] considered logic operations using coherence created in the valleys between the valence and the conduction band. The idea is stimulated by the recent progress in ultrashort laser technology, which now allows one to produce trains of few-cycle pulses with controlled phase and polarization between the pulses. Taking advantage of such technology, we introduce a coherent control protocol to turn on, off and switch the valley polarization at faster timescales than electron-hole decoherence and valley depolarization, that is, an ultrafast optical valley switch.

We theoretically demonstrated the protocol for hBN and MoS2 monolayers, using calculations from first principles. To this end, a sequence of four linearly polarized few-cycle pulses has been designed, with orthogonal polarizations between the successive pulses and sub-cycle control of the time delays between each pulse pair in the four-pulse sequence.

The first linearly polarized pulse creates equal excitation in both valleys. The second pulse, polarized orthogonally to the first, is used to select one of the valleys by adjusting the time-delay between the two pulses. The third pulse, polarized orthogonally to the second, re-equilibrates the populations of both valleys. Finally, the last pulse switches dominant excitation to the opposite valley or returns it to the first one, depending on the exact sub-cycle de-

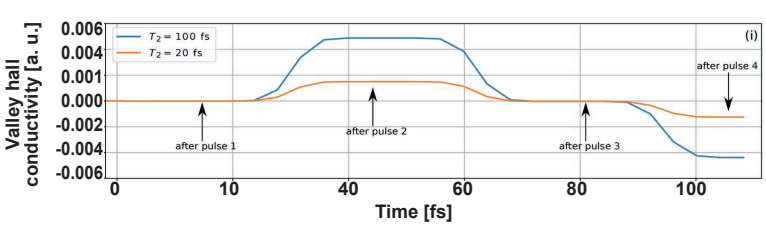

Fig. 2:
Ultrafast optical switch based on valley-selective excitation with linearly polarized pulses in MoS2, demonstrated theoretically in [SIJ22]. Valley polarization as a function of the time-delay relative to the first pulse in the pulse sequence is measured via valley Hall conductivity.

lay. The first option – ultrafast valleytronics-based optical switch – is shown in Fig. 2

Additionally, Ref [SIJ22] shows that one can extract the electronic dephasing time T2 from the valley Hall conductivity. This is clear from the results in Fig. 2, which show valley Hall conductivity for two different dephasing times: the longer the dephasing time, the higher is the contrast. This suggests that simple pair of two pulses, polarized orthogonally to each other, allows one to extract the dephasing time by measuring the contrast in switching valley polarizations as function of the time-delay between the two pulses. The faster the dephasing, the shorter is the memory of the first pulse in the two-pulse sequence, the faster the decay of the contrast in switching the valley polarization between the valleys.

T1-T2: Sub-cycle changes to the light-driven band structure

In this project, which resulted from the collaboration between the T1 and T2 groups, we have addressed a fundamental question: How is the effective band structure of a solid affected by oscillations of strong, low-frequency laser field?

Indeed, imagine applying a DC electric field to a crystal. One naturally expects that its electronic structure will change. When the strength of the DC field approaches volts per nanometer, these changes will be profound. How does it translate to the interaction between a crystal and a low-frequency field, with the carrier well below the bandgap, where the instantaneous field changes its strength on the sub-cycle time-scale from several Volts per nanometer to zero? As the oscillating electric field changes within the driving field's cycle, does the band structure follow and how can it be defined?

Theoretical study of this question has been combined with an experimental measurement at the Weizmann Institute in the group of N. Dudovich, see Ref. [UJO22]. In this work we have both addressed the fundamental question about sub-cycle changes in the effective band structure and demonstrated, both experimentally and theoretically, how high harmonic generation can be used to probe the laser-induced closing of the bandgap between adjacent conduction bands.

From the theoretical point of view, we have been able to extend the concept of adiabatic eigenstates of the quantum system to the regime of strong non-adiabatic transitions on the sub-cycle time-scale.

Adiabatic eigenstates are defined as those states which diagonalize the Hamiltonian depending on the value of the external parameter, and follow the adiabatic changes of this parameter. In our case, this is the instantaneous electric field of the low-frequency pulse. The adiabatic states provide excellent approximation to the instantaneous, adiabatic band structure of a driven solid. However, what happens in the presence of non-adiabatic transitions?

Ref. [UJO22] shows that effective eigenstates and eigen-energies can be defined by following the evolution of the quantum system through the non-adiabatic transition and identifying wavefunctions which exactly reproduce themselves, up to a quantum phase, after passing through the avoided crossing region were the non-adiabatic transition takes place. The derivative of the quantum phase with respect to time spent going through the region yields effective energies. Importantly, our formalism shows that the gap between the adiabatic states closes when non-adiabatic transitions become strong. That is, in the limit of diabatic passage through the avoided crossing, the diabatic states become the effective time-dependent energies of the driven system, exactly as one would expect based on the physical intuition.

The closing of the bandgap is visible in high harmonic generation. If a particular harmonic falls into the gap region, the corresponding quantum electron trajectory acquires substantial imaginary component, i.e. evolves in complex time. Once the gap closes, this imaginary time component disappears. As a result, the behavior of the harmonic intensity as a function of the parameters of the driving field changes drastically and in a very robust way. This change has been observed experimentally exactly when and where it was predicted theoretically, see Ref. [UJO22] for details.

T1: All-optical attosecond spectroscopy of strong field ionization

Recent experiments by Ramos et al. [RSR20] on measuring time-delays during tunnelling of cold atoms through an optically created potential barrier have reinvigorated [ELe19, EBL20, CKH21, KLS22] the debate regarding possible time-delays during light-induced strong field ionization of an atom, also known as optical tunnelling [POS15, EPC08, SSB12, PCS11, LWM14, YKH14, TMK15, NSR16, CYF17, SXW19]. Strong arguments have been used to support completely opposite views, confirming or refuting the existence of finite tunnelling time delays during strong-field ionization.

Importantly, all attempts at measuring tunnelling times during strong field ionization have always been based on photo-electron spectroscopy. The first goal of our recent work [BJC22] was to develop an all-optical approach, which could therefore be applied not only to isolated atoms but also to liquids and solids.

In [BJC22] we have developed an all-optical method and shown how one can augment photo-electron detection in laser-induced tunnelling with detection of light emitted by the tunnelling electron as it moves through the classically forbidden region and emerges on the other side of the tunnelling barrier. This radiation is usually referred to as the Brunel radiation [Bru90]. The polarization of the Brunel radiation is controlled by the direction of the laser field when the electron is 'injected' into the continuum. Therefore, just like the conventional attoclock, it is sensitive to the deflection of the electron by the Coulomb potential or its tunnelling delay, during which the laser field has time to rotate.

In our scheme the circularly polarized fundamental field was augmented with the co-rotating circularly polarized second harmonic. This generates the driving field with clear asymmetry and a single maximum during one la-

ser cycle. As for the harmonics, the combination of these two driving fields leads to the generation of both odd and even harmonics, including the so-called zero-order harmonic. The latter is generated by absorbing two circularly polarized photons of the fundamental and emission of one 2w photon. The emission of the 'zero'-frequency completes the loop. In reality the emitted light is in the THz range due to the final duration of both driving pulses. The polarization of the THz light is given by the Fourier transform of the acceleration,

$$E(\omega) \propto \int dt\, \dot{p}(t) e^{i\omega t}$$

Thanks to the nearly zero frequency, the direction of **E**(ω) is determined by the final electron momentum at the detector. Thus, it yields the same information as the attoclock, but measured optically.

The results are shown in Figure 3. The observable of the optical attoclock is the angle of rotation of the polarization of the THz radiation relative to the major axis of the Lissajous figure generated by the two-color driving field. It is shown on the right vertical axis of the plot. The re-calibration of the rotation angle into the time-delay used the same procedure as for the standard attolock: time=rotation angle/light frequency.

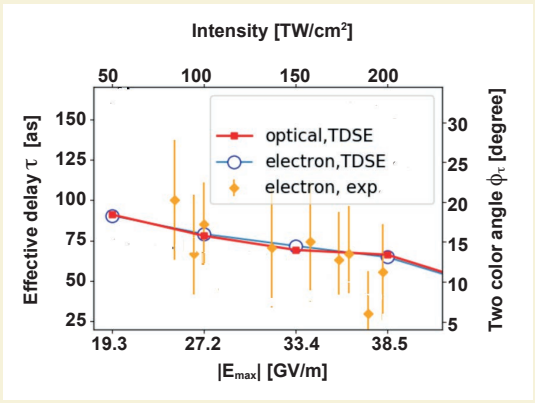

Fig. 3:
Effective tunneling ionization delay as a function of intensity obtained from the polarization rotation of the 0th harmonic (red curve) as determined by TDSE simulations and compared to the results of the photo-electron attoclock, also simulated using TDSE (blue curve), which shows the deflection angle for the center of mass of the electronic wavepacket. The yellow data are from the experiment on the photo-electron attoclock in H atom [SXW19].

Figure 3 shows that the optical attoclock measurements are in excellent agreement with the photo-electron-based measurements, but now the measurement is all-optical. Both results are obtained using the time-dependent Schroedinger equation (TDSE) and solving it numerically, and then extracting radiation or photo-electron spectra.

The key step in interpreting the results of these simulations was similar to that taken in our previous work [TMK15] where we have looked at the photo-electron spectra: to disentangle the effects of the electron deflection due to the Coulomb potential from the change in the electron acceleration due to possible time delays, the same calculations have been repeated for the short-range Yukawa potential supporting only a single ground state. In this case the angle of rotation of the polarization of the THz radiation relative to the major axis of the Lissajous figure generated by the two-color driving field was equal to zero.

T2, T1: Enantiosensitive steering of free-induction decay

Studying ultrafast dynamics of chiral molecules and developing new tools for discriminating left-handed and right-handed versions (enantiomers) of the same molecule has been a major research direction in the T2 group for the past few years. The two enantiomers – the two "mirror twins" – of the same chiral molecule have identical physical and chemical properties, unless they interact with another chiral "object". The goal of the work [KPP22] was to use spatially structured light to induce coherent excitations in a macroscopic ensemble of chiral molecules and then use the free induction decay, i.e. the super-fluorescence of these molecules, to distinguish the left-handed and right-handed enantiomers. This work has built on the concepts of synthetic chiral light [ANO19] and chirality polarized light [AOD21] as well as ultrafast optical rotation [AOI21] developed by us previously. It combined the possibility of structuring light in space, e.g. using vortex beams, with the opportunity to structure light in time by combining several phase locked colors.

Tightly focused vortex beams are well suited to generate longitudinal field component, making non-trivial polarization patterns. When several colors of light are phase locked together and at least one of the colors is structured in space, the resulting light field develops complex and rich 3D polarization patterns in space and time: the light becomes locally chiral, with the Lissajous figure created by the rotation of the light polarization vector in

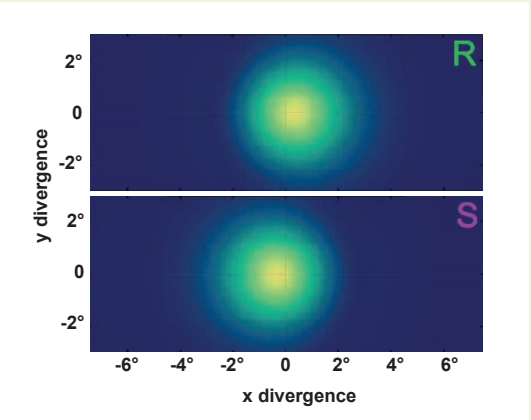

Fig. 4:
Directionality of the free induction decay (coherent fluorescence) from a Rydberg 3 s state of methyloxiran after a gas of methyloxirane molecules is illuminated with a multi-color vortex field, see [KPP22] for details. The two panels show the far-field emission profiles for the two enantiomers: R (green) and S (lilac).

3D drawing a chiral structure, locally, at every point in space. The nonlinear chiral optical response of a chiral molecule to such light is very strong and enantio-sensitive [ANO19, AOD21, AOI21].

When the local chirality of light changes in space, a grating in chiral optical response is generated, affecting the propagation of the chiral optical signal into the far field [KPP22, AOD21]. The gratings are out of phase in the two enantiomers of the chiral molecule, leading to the deflection of the optical response in different directions for the two enantiomers of the same molecule.

The key new result obtained in 2022 in Ref. [KPP22] was to show that multi-color vortex beams are well suited for generating locally chiral light and for controlling the distribution of chirality in space, thus imprinting spatial chirality polarization gratings on excited molecules. As a result, coherent fluorescence of such molecules is deflected differently for left-handed and right-handed molecules, as shown in Figure 4.

T2: Ultrafast chirality: the road to efficient chiral measurements

Today we are witnessing the so-called electric-dipole revolution in chiral measurements, which evolves along two complementary paths, both using controlled light and both relying only on the electric dipole interactions.

Standard circularly polarized light often serves as a model of a chiral optical object, as the electric field of this light traces a corkscrew as the light propagates in space. However, in the dipole approximation this chirality is lost: a circularly polarized light traces a circle in a given point in space. The need to rely on the corkscrew of light forces one to look at optical effects beyond the dipole approximation, and such effects are usually very weak. This is why the development of chiral-sensitive methods that do not require one to look beyond the dipole approximation offer much higher chiral sensitivity.

The electric-dipole revolution has opened routes to extremely efficient enantio-discrimination with a family of new methods. These methods are governed by the same principles but work in vastly different regimes – from microwaves to optical light; they address all molecular degrees of freedom – electronic, vibrational and rotational, and use flexible detection schemes, *i.e.* detecting photons or electrons, making them applicable to different chiral phases, from gases to liquids to amorphous solids.

According to [AOS22], these new types of measurements can be broadly classified in two groups. One group relies on the concept of a chiral observer, formally identified and introduced by A. Ordonez and O. Smirnova in [OSm18]. In this approach, an achiral light is used together with the arrangement of detectors to form a chiral setup, with the photoelectron circular dichroism measurements (PECD) providing one example. There, the measurements are performed in the laboratory frame where the two orthogonal components of the circularly polarized field are complemented by the axis of the detectors to form a chiral reference frame.

The second group relies on using synthetic chiral light discovered in [ANO19]. In this light, the chiral structure is formed not by the pattern that the light electric field draws in space, but by the pattern that it draws in time. If the pattern is chiral, the response of the molecules is enantio-sensitive and can be controlled by controlling the light structure in time.

These two concepts have been unified in [AOS22].

This work also identified new classes of chiral observables that can be obtained using different setups.

The work [AOS22] introduces, for the first time, classification and hierarchy of chiral observables, starting with scalar observables achieved using synthetic chiral light, vectorial chiral observables obtained using simple chiral observer setup, and then introducing tensorial enantio-sensitive observables, where the laboratory setup provides two axes of the overall chiral frame. Tensorial observables emerge, for example, when one uses orthogonally polarized two-color light pulses, combining fundamental and second harmonic. In this setup the instantaneous circularity of the light pulse changes on the sub-cycle time-scale, but even in this case angle-resolved photo-electron spectra carry enantio-sensitive information as long as the photoelectron signal is measured in correlation between two orthogonal laboratory axes.

Last but not least, Ref. [AOS22] identified new properties of the chiro-optical response in the ultrafast and non-linear domains by uncovering the link between geometric magnetism in solids and in the chiral response in photoionization. Remarkably, this link allows one to connect geometric magnetism in ultrafast chiral electronic response and charge directed reactivity, providing a unique example of enantio-sensitive photo-chemical reaction driven by ultrafast chiral currents excited inside a chiral molecule.

T3: Quantum photonics in non-Hermitian optical systems

In 2022, the research in T3 has been concerned with nonlinear and quantum plasmonics as well as with quantum photonics and few-photon nonlinearities in photonic structures waveguide arrays inscribed in glass. Specifically, with regards to quantum photonics, we have investigated possibilities for the rational design of non-Hermitian integrated waveguiding systems that exhibit high-order exceptional points.

Exceptional points are complex-valued spectral singularities that lead to a host of intriguing features such as loss-induced transparency and sensing schemes with enhanced sensitivity. In general, the associated enhancements scale with the order of the exceptional points. Consequently, it is of great interest to devise new strategies to implement realistic devices capable of exhibiting high-order exceptional points. Alas, on the classical such high-order exceptional points are difficult to realize but the use of multi-photon quantum light offers an alternative route.

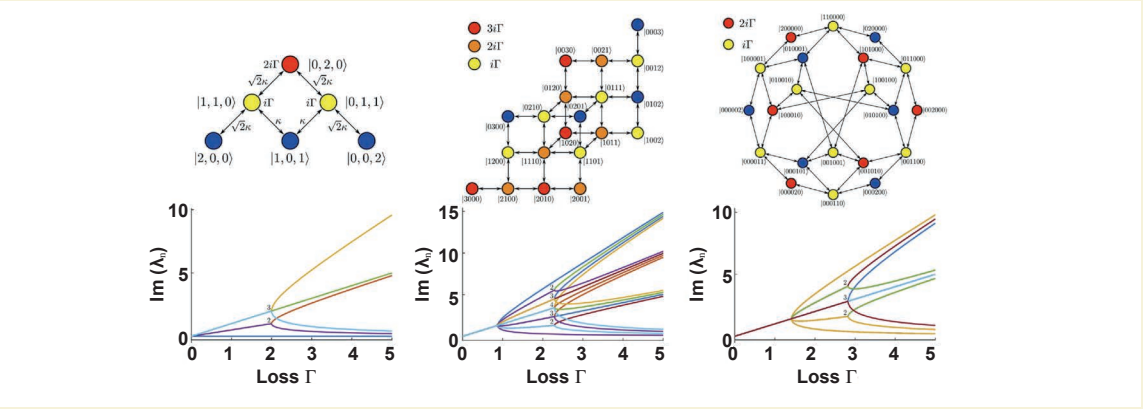

Fig. 5:
Branching of exceptional point of partially lossy waveguide arrays and associated synthetic space representation. Left panel: A balanced waveguide trimer with a lossy central waveguide excited by two photons exhibits two exceptional points of second and third order at the critical dimensionless loss rate Γ=2. Middle panel: Balanced waveguide The Haldane lattice implemented using a honeycomb lattice of helical waveguide tetramer with two lossy waveguides and excited by three photons. In this case the synthetic space representation (Fock graph) becomes non-planar and exhibits multiple multifurcations. Right panel: Two-photon excitation of a ring configuration of six waveguides, alternating lossy and lossless. Adapted from [TBC22].

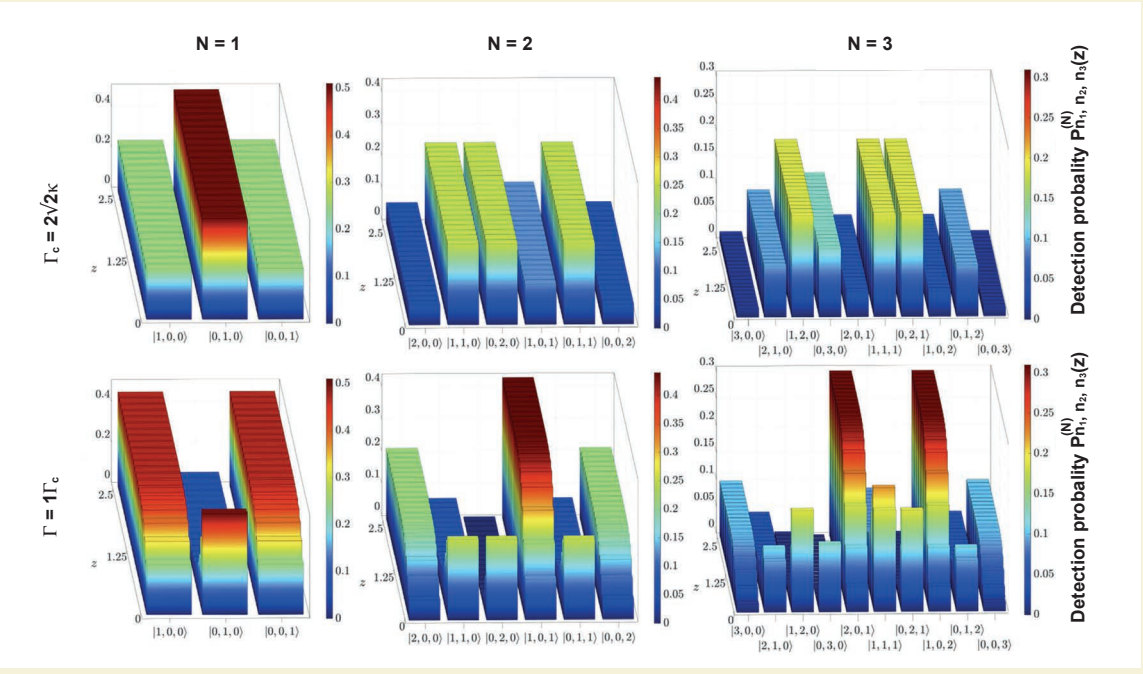

Fig. 6:
Evolution of the post-selected N-photon coherent eigenmode in the waveguide trimer where the central waveguide is lossy (cf. the left panel of Fig. 5). In the top row the system is at the critical point and in the bottom row it is in the super-critical regime. At the critical point, all states are proper eigenstates of the system, while in the supercritical regime more and more photons are detected in the neutral (outer) waveguides. Adapted from [TBC22].

In order to address this question in detail, we have investigated non-Hermitian coupled waveguide systems for which an experimental platform is presently developed within the SAW project LAPTON at MBI. In particular, we have shown that high-order N-photon exceptional points can be generated by exciting non-Hermitian waveguide arrangements with coherent light states. Using photon-number resolving detectors it then becomes possible to observe N-photon enhanced loss-induced transparency in the quantum realm.

Further, we have demonstrated that the number-resolved dynamics occurring in the same non-conservative waveguide arrays will exhibit eigenspectral ramifications having several exceptional points associated to different sets of eigenmodes and dissipation rates.

Specifically, we have shown that arrays of coupled waveguides exhibiting alternating patterns of lossy and lossless sites, give rise to several exceptional points of second order at the single photon or, equivalently, the classical level.

The excitation with the corresponding coherent exceptional mode promotes these exceptional points to an arbitrary order in the emerging synthetic coupled structure in the N-photon Fock-space (see Fig. 5), and this without the need of further fine-tuning of the loss-rates in the underlying physical system (as would be required for high-order exceptional points on the classical level).

Upon utilizing photon-number-resolving detectors, it then becomes possible to exploit the effect of loss-induced transparency in the quantum optical regime. We have outlined this concept for the semi-lossy waveguide beamsplitter, which is excited by its coherent exceptional mode. Further, we generalized this scheme to an arbitrary number of waveguides to show that integrated quantum optics based on multiphoton states is richer than its single-photon counter-part and it requires fewer waveguide elements as it works in synthetic space (see Fig. 6). The challenges of this approach is the need to generate multiphoton states and to have suitable photon-number-resolving detectors. In other words, using coherent states as input, we have greatly alleviate the problem of the generation of multiphoton states but our scheme still relies on photon-number-resolving detectors which is a manageable problem. Since our analysis employs a tight-binding model, we anticipate that this scheme will find applications in numerous other formally equivalent systems, such as coupled micro-cavities, ring resonators, and ultra-cold atoms trapped in an optical lattice.

T5: Femto-phono-magnetism

Femto-magnetism is a growing research field, with the focus on controlling magnetism in matter by laser pulses. In this context, ultrafast laser pulses have recently been shown to enable spin manipulation on the timescales as short as ~10 femtoseconds, i.e. orders of magnitude faster than is achieved with currently available devices.

Several key processes responsible for ultra-fast spin control have been identified, including spin transfer from one magnetic sub-lattice to another by charge-excitations induced by the laser, known as Optical Inter-sublattice Spin Transfer (OISTR) and discovered in our works, see e.g. [DES18, SGO19]. Harnessing these techniques to control magnetization would lead to operational times in the femtosecond regime.

In this context, the key issue is the coupling of electronic and phononic degrees of freedom. In our latest theoretical work [SSE22c] we show how the interplay of phonon excitations with the excitations of spin and charge dynamics leads to femto-phono-magnetism, a powerful route to control magnetic order at ultrafast times.

To address the problem, we have performed state-of-the-art theoretical simulations of coupled spin, charge, and lattice dynamics. Our simulations show strong non-adiabatic spin-phonon coupled modes that dominate early time spin dynamics.

The key outcome of the simulations, shown in Fig. 7, is that excitation of phonon modes can lead to an additional, up to 40 %, loss of spin moment in iron-platinum. The corresponding time scale is about 40 femtoseconds.

We have been able to identify a physical mechanism responsible for this process. In this mechanism, the minority spin current drives an enhanced intersite minority charge transfer, in turn promoting increased on-site spin flips.

Our results demonstrate that the nuclear system, often assumed to play the role of an energy and angular momentum sink, when selectively preexcited, can play a profound role in controlling femtosecond spin dynamics in materials.

Own Publications 2022 ff

(for full titles and list of authors see appendix 1)

AOS22: D. Ayuso *et al.*; Phys. Chem. Chem. Phys. **24** (2022) 26962-26991

BJC22: I. Babushkin *et al.*; Nat. Phys. **18** (2022) 417-422

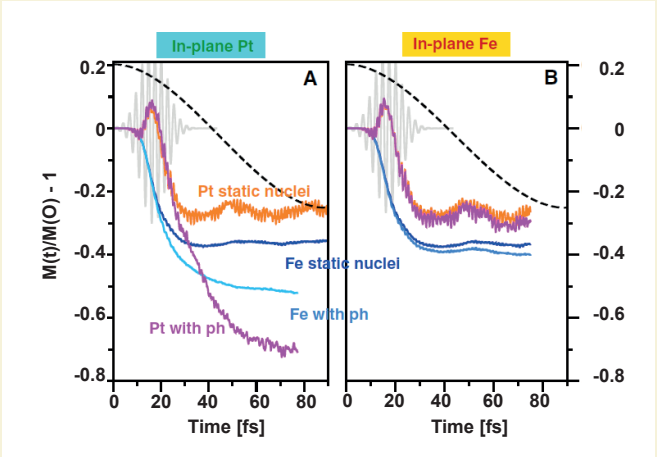

Fig. 7:
Normalized atom-resolved spin moment as a function of time (in femtoseconds) in laser-pumped FePt, with the vector potential of the laser pulse shown in gray. Spin dynamics calculations are performed both for full nuclear dynamics (i.e., including both preexcitation of the phonon and forces generated on the nuclei by momentum transfer from the excited electron system) and in the absence of nuclear dynamics. Displacement of atoms during the phonon modes is shown with black dashed lines. Results are shown for the two most strongly coupled phonon modes at the X-point: (A) the in-plane Pt mode (see Fig. 1D) and (B) the in-plane Fe mode. (Adapted from [SSE22c]).

KPP22: M. Khokhlova *et al.*; Sci. Adv. **8** (2022) eabq1962/1-8

SES22: S. Sharma *et al.*; Optica **9** (2022) 947-952

SIJ22: R. E. F. Silva *et al.*; Opt. Express **30** (2022) 30347-30355

SSE22c: S Sharma *et al.*; Sci. Adv. **8** (2022) eabq202/1-6

TBC22: K. Tschernig *et al.*; Laser Photon. Rev. **16** (2022) 2100707/1-9

UJO22: A. J. Uzan-Narovlansky *et al.*; Nat. photonics **16** (2022) 428-432

Other Publications

RSR20: R Ramos *et al.*; Nature **583** (2020) 529-532 (2020)

ANO19: D. Ayuso *et al.*; Nat. Photonics **13** (2019) 866-871

AOD21: D Ayuso *et al.*; Nat. Comm. **12** (2021) 3951

AOI21: D. Ayuso *et al.*; Optica **8** (2021) 1243-1246

Bru90: F. Brunel; J. Opt. Soc. Am. B **7** (1990) 521-526

CKH21: D. B. Canário *et al.*; Phys. Rev. A **104** (3) (2021) 03310

CYF17: N. Camus *et al.*; Phys. Rev. Lett. **119** (2017) 023201

DES18: J. K. Dewhurst *et al.*; Nano Letters **18** (2018) 1842-1848

EBL20: N. Eicke *et al.*; Phys. Rev. Letters **124** (2020) 043202

ELe19: N. Eicke *et al.*; Phys. Rev. A **99** (2019) 031402

EPC08: P. Eckle *et al.*; Science **322** (2008) 1525-1529

KLS22: M. Klaiber *et al.*; Phys. Rev. Letters **129** (2022) 203201

KMT15: J. Kaushal *et al.*; J. Phys. B **48** (2015) 234002

LKe15: A. S. Landsman *et al.*; Phys. Rep. **547** (2015) 1-24

LWM14: A. S. Landsman *et al.*; Optica **1** (2014) 343-349

NSR16: H. Ni *et al.*; Phys. Rev. Lett. **117** (2016) 023002

OSm18: A. F. Ordonez *et al.*; Phys. Rev. A **98** (2018) 063428/1-20

PCS11: A. N. Pfeiffer *et al.*; Nat. Phys. **8** (2011) 76-80

POS15: O. Pedatzur *et al.*; Nat. Phys. **11** (2015) 815-819

SGO19: F Siegrist *et al.*; Nature **571** (2019) 240-244

SSB12: D. Shafir *et al.*; Nature **485** (2012) 343-346

SXW19: U. S. Sainadh *et al.*; Nature **568** (2019) 75

TMK15: L. Torlina *et al.*; Nat. Phys. **11** (2015) 503-508

TYB16: N. Teeny *et al.*; Phys. Rev. Lett. **116** (2016) 063003

YKH14: E. Yakaboylu *et al.*; Phys. Rev. A **90** (2014) 012116

Invited Talks at International Conferences
(for full titles see appendix 2)

K. Busch; NanoPhoton Conference 2022 (Rungstegaard, Denmark, 2022-06)

K. Busch; MeepCon 2022 (Cambridge, MA, USA, 2022-07)

K. Busch; DokDok 2022 (Arnstadt, Germany, 2022-08)

K. Busch; HIOS Symposium 2022 (Berlin, Germany, 2022-10)

A. Husakou; Crete VII Ultrafast Dynamics Symposium (Crete, Greece, 2022-06)

M. Y. Ivanov; PQE'2022 (Snowbird, Utah, USA, 2022-01)

M. Y. Ivanov, Int. COST/ZCAM School on Computational methods for attosecond processes, (Zaragoza, Spain, 2022-03)

M. Ivanov, 4th Int. Workshop on Quantum and Topological Nanophotonics (Singapore, 2022-04)

M. Y. Ivanov, Int. Workshop on Attosecond Science and Wolf prize award ceremony (Haifa and Jerusalem, Israel, 2022-06)

M. Y. Ivanov, ECAMP conference (Vilnius, Lithunia, 2022-06)

M. Ivanov, ATTO VIII Conference (University of Central Florida, Orlando, FL, USA, 2022-07)

M. Y. Ivanov; EPS Symposium on the Third Generation Metamaterials, METAMATERIALS 3.1 (Cetraro, Calabrien, Italy, 2022-08)

S. Patchkovskii, Int. COST/ZCAM School on Computational methods for attosecond processes, (Zaragoza, Spain, 2022-03)

O. Smirnova; PQE'2022 (Snowbird, Utah, USA, 2022-01)

O. Smirnova, Int. COST/ZCAM School on Computational methods for attosecond processes, (Zaragoza, Spain, 2022-03)

O. Smirnova, 4th Int. Workshop on Quantum and Topological Nanophotonics (Nanyang Technological University, Singapore, 2022-04)

O. Smirnova; Int. Workshop on Attosecond Science and Wolf prize award ceremony (Haifa and Jerusalem, Israel, 2022-06)

O. Smirnova; ATTO FEL Conference (University College, London, UK, 2022-07)

O. Smirnova; Optica Incubator on On-Chip High-Field Nanophotonics, Workshop (Optica Global Headquarters, Washington DC, USA, 2022-07)

O. Smirnova; ATTO VIII Conference (University of Central Florida, Orlando, FL, USA, 2022-07)

O. Smirnova; The 27th Int. Conference on Atomic Physics (Royal Conservatory of Music, Toronto, Canada, 2022-07)

O. Smirnova; EPS Symposium on the Third Generation Metamaterials, METAMATERIALS 3.1 (Cetraro, Calabrien, Italy, 2022-08)

O. Smirnova; The 23rd European Conference on the Dynamics of Molecular Systems (MOLEC 2022) (Hamburg, Germany, 2022-08)

O. Smirnova; The 7th edition of the ELI Summer School (ELISS 2022) (Szeged, Hungary, 2022-08)

S. Sharma; Spin Phenomena Interdisciplinary Center, SPICE- Conferene Ultrafast Antiferromagnetic Writing (Ingelheim, Germany, 2022-05)

S. Sharma; 50+2 years in science theory (Nijmegen, The Netherlands, 2022-05)

S. Sharma; MORIS (Magnetics and Optics Research Int. Symposium) (Shimane, Japan, virtual, 2022-05)

S. Sharma; Psi-k 2022 Conference (Lausanne, Switzerland, 2022-08)

S. Sharma, Paris-Saclay Ultrafast X-ray Science School, Seminar "Femto-Phono-Magnetism" (Paris-Saclay University, France, 2022-10)

S. Sharma; Theory meets XFELs (DESY, Hamburg, Germany, 2022-11

Invited External Talks at Seminars and Colloquia
(for full titles see appendix 2)

M. Y. Ivanov, QUTIF meeting (Bad Honnef, Germany, 2022-08)

M. Y. Ivanov, Limati SFB Retreat Workshop (Gut Ulrichshusen, Germany, 2022-09)

M. Y. Ivanov, Summer school on light-matter interaction at interfaces, (Rostock, Germany, 2022-09)

M. Y. Ivanov, ICFO Colloquium (Barcelona, Spain, 2022-12)

O. Smirnova, Seminar of Kassel University SFB on chirality (Bad Arolsen, Germany, 2022-10)

O. Smirnova, Retreat Workshop of the Technical University (Gustrow, Germany, 2022-10)

S. Sharma, Colloquium (Trinity College Dublin, Ireland, 2022-03)

S. Sharma, joint Seminar/Colloquium (TU Graz and KFU, Austria, 2022-05)

S. Sharma, (TU Kaiserslautern, 2022-09)

S. Sharma, Colloquium (Regensburg, Germany, 2022-11)

1.2: Ultrafast Laser Physics and Nonlinear Optics

T. Nagy, M. Schnürer, and G. Steinmeyer (project coordinators)
M. Bock, S. Dávila Lara, W. Chen, F. J. Furch, P. Fürtjes, U. Griebner, R. Grunwald, N. Jiménez de la Vega, M. Kretschmar, M. Mero, M. Osolodkov, V. Petrov, L. Wang, T. Witting

1. Overview

This project is the home of MBI's research activities in nonlinear optics and laser physics focusing on the development of novel light sources and time-resolved techniques.

Our primary goal is to strengthen MBI's research on ultrafast and nonlinear phenomena in light-matter interaction with state-of-the-art technology from our original research activities. Depending on the planned application of the technology, the focus of the development lies on superior pulse energy, short pulse duration, carrier-envelope phase stability, or high average power and repetition rate. A further goal is to cover a large range of the electromagnetic spectrum from the THz to the soft X-ray region with few-cycle pulses. Consequently, the project encompasses research on primary laser and parametric sources as well as on compression and wavelength conversion of the primary sources.

2. Topics and collaborations

T1: Primary Sources

Partly supported by DFG (GR2115/6-1), DFG (PE 607/14-1, M-0040), AFOSR/PK (FA8655-20-1-7053). and EU Horizon 2020 (871124 Laserlab-Europe, JRA PRISES)

Our research on primary sources is strongly focused on new sources for few-cycle pulses in the mid-IR, employing either parametric conversion or direct laser schemes. To this end, we extended the operation of our mid-IR OPCPA system employing a novel three-stage architecture, resulting in unprecedented pulse parameters in the LWIR near 10 µm. This scheme provides four-cycle pulses with 10 µJ energy at 1 kHz repetition rate. In a separate effort, we investigated novel nonlinear optical materials for generating pulses that are tunable over the entire atmospheric transmission band at 10 µm wavelength. As another highly interesting nonlinear optical material system, we investigated novel ternary cubic semiconductors for quasi-phase matching in the mid-IR. Furthermore, we intensified our research on direct laser-based pulse generation schemes at 2 µm wavelength and beyond, exploiting excitation transfer in co-doped laser materials.

T2: Secondary Sources

Partly supported by DFG (NA1102/3-1) and EU Horizon 2020 (871124 Laserlab-Europe, JRA PRISES)

In 2022, our work on secondary sources mostly focused on pulse compression of high-repetition rate sources. Using a commercial Yb:fiber laser with up to 1 MHz repetition rate, we demonstrated six-fold compression in a multipass cell, resulting in sub-50 fs pulse duration at an average power of 15 W. In a second effort, we started with sub-10 fs pulses from a 100 kHz OPCPA, which were compressed to near-single-cycle duration in a sequence of three 50 µm thin quartz plates. We further refined our novel approach for generating VUV pulses at 150 nm, exploiting dispersive wave generation in a soliton-based hollow-fiber compression scheme. Finally, we explored optimal conditions for maximizing high-harmonic flux using 2 µm driver pulses for the harmonic generation.

Collaboration partners: X. Mateos (Tarragona University, Spain), H. Yu and Z. Pan (Shandong University, Jinan and Qingdao, China), F. Rotermund (KAIST, Daejeon, Korea), A. Agnesi (Pavia University, Italy), V. Pasiskevicius (KTH, Stockholm, Sweden), P. Schunemann (BAE Systems, Nashua, USA), K. Kato (CIST, Chitose, Japan). Z. Heiner (SALSA, HU Berlin, Germany), Y. Zhao (JSNU, Xuzhou, China), G. Zhang (FJIRSM-CAS, Fuzhou, China), K. Miyata (RIKEN, Wako, Japan), V. Tassev (AFRL, Dayton, USA), R. Murray (Imperial College, London, UK). I. Divliansky (CREOL, Orlando, USA), G. Exner (Plovdiv University, Bulgaria), P. Loiko (Caen University, France), T. Metzger (Trumpf Scientific Lasers GmbH, Germany), N. Forget (Fastlite, Antibes, France), C. Mei (Beijing University of Technology, China).

3. Results in 2022

T1: Primary Sources

High-energy few-cycle pulse generation in the longwave-IR at 1 kHz

A large scale midwave-IR (MWIR) OPCPA system is operating at a central wavelength of 5 µm and emits pulses with 80 fs duration and 3 mJ energy at a 1 kHz repetition rate [1]. A stable and reliable operation of the OPCPA system was ensured in 2022 leading to the successful application of the system for its main application as driver for hard x-ray generation (see project 3.3).

The main activities in 2022 were devoted to the extension of our OPCPA systems to the longwave-IR, i.e., emission at wavelengths longer than 10 µm, with few-cycle pulse duration and µJ-level pulse energy. As a result, a novel three-stage LWIR OPCPA emitting at 11.4 µm was successfully implemented [FBG22] – see highlight article.

High-energy few cycle pulses beyond 10 µm were also generated via DFG using the signal and idler of the MWIR OPCPA [1] as driver. The conceptual scheme of the experiments is shown in Fig. 1a.

The 3.5 µm, 30 fs signal pulses are first subject to spectral pulse shaping. In this work a Ge-prism pair was implemented for shaping instead of the spatial light modulator (SLM) usually implemented in our OPCPA [1]. The Ge-prism pair was adjusted in such a way that it reproduces the dispersion parameters that are otherwise realized by the SLM, i.e., for the shortest pulse duration of the idler at 4.9 µm. Applying the idler as seed in OPA4, an output pulse energy of 1.9 mJ is generated in the 1 kHz pulse train. The measured idler spectrum at 4.9 µm exhibits a bandwidth of 0.75 µm (FWHM). The compressed idler, as well as the signal pulses are characterized by the SH-FROG technique. The SH-FROG retrieval reveals a pulse duration of 120 fs (FWHM) for the idler with an estimated energy content of 95 %. The pulses are slightly longer than in [1] which we ascribe to the extremely challenging fine tuning of the individual dispersion orders with the Ge-prism pair used here instead of the SLM.

The amplified signal pulses at 3.5 µm are compressed to nearly the same duration as the idler pulses. For this purpose, we built a Martinez-type compressor comprising two sapphire prisms. The signal pulses generated in OPA3 containing 0.7 mJ energy are used for the DFG experiments because after OPA4 the signal pulses are angularly dispersed due to the non-collinear geometry. Its 0.22 µm broad spectrum (FWHM) is centered at 3.5 µm and supports sub-100 fs duration. The signal pulses are compressed to a duration of 125 fs, i.e., close to the desired duration, that of the idler pulses. Since spectral shaping in OPCPAs is in general only optimally adapted for either the signal or the idler pulse, in our case for the idler, the pulse quality of the signal is not perfect. Due to losses in both OPCPA compressors, the pulse energies applied to the DFG crystal at 3.5 and 4.9 µm were 0.35 and 1.0 mJ, respectively. Taking into account the damage threshold of the DFG crystals the peak intensity was chosen slightly below 200 GW/cm^2. The beams are combined with a dichroic mirror. Two crystals are used for the generation of the DFG: a 0.5-mm-thick Z-cut gallium selenide (GaSe) and a 1-mm-thick silver gallium selenide (AGSe) cut at an angle of 53.3°. In GaSe, the Type-II process is phase-matched at an internal angle of 14.3°. In AGSe, the phase-matching angle is 55.8°. The DFG pulses are characterized behind a long-pass filter (Fig. 1a). A maximum pulse energy of 15.5 µJ and 12.2 µJ are achieved for GaSe and AGSe, respectively, corresponding to external conversion efficiencies of >1 %. The DFG spectra are centered at 11.4 µm and 12.2 µm with FWHM widths being 1.29 µm and 1.74 µm for GaSe and AGSe, respectively (Figs. 1b and 1c, insets). The transform-limited (FTL) pulse duration is thus well below 100 fs, however, the signal as well as the idler are slightly chirped. The dispersion of the DFG pulses is dominated by the dichroic mirror in front of the nonlinear crystals (Fig. 1a). This mirror imposes a high GDD on the 3.5 µm pulses, which needs post compression. The latter is performed by Ge bulk material accompanied by some loss. The DFG pulse characterization is performed with a TPA autocorrelator and pro-

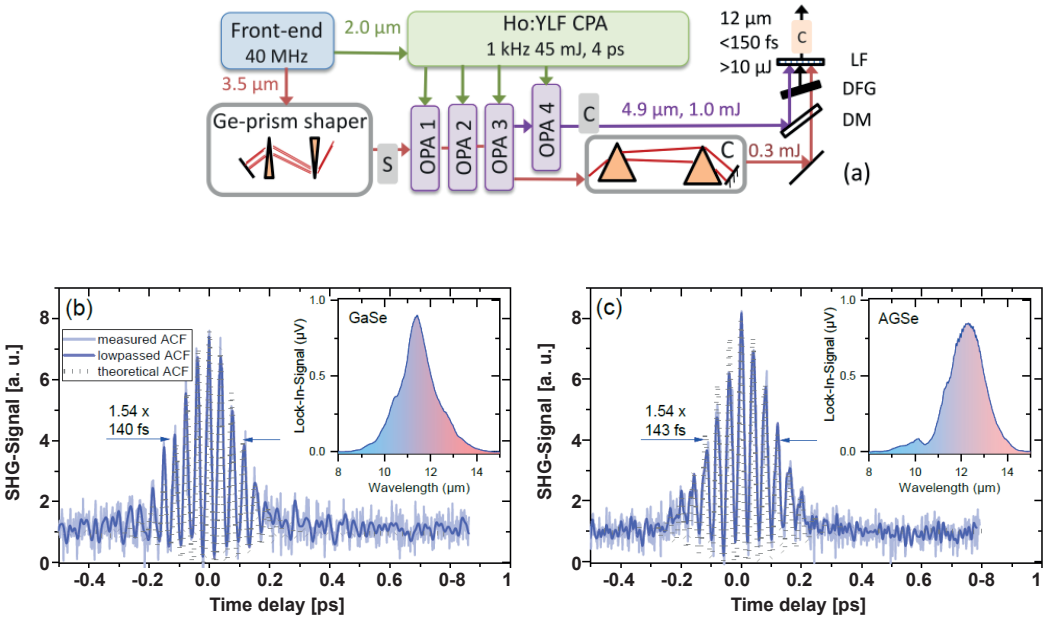

Fig. 1:
(a) Setup of the DFG generation with the driving MWIR OPCPA; S: stretcher, C: compressor, DFG: DFG crystal, DM: dichroic mirror, LF: long-pass filter. (b,c) Characterization of the DFG pulses: measured autocorrelation traces and spectra (insets) using (b) GaSe and (c) AGSe.

vided durations of 140 fs and 143 fs, assuming a sech^2-shape, for GaSe and AGSe, respectively (Figs. 1b and 1c). We attribute the deviation from the FTL duration to the uncompensated TOD imprinted on the 3.5 µm pulses. Hence the generated DFG pulses have a duration of less than four optical cycles and pulse energies as high as 10.2 µJ and 10.0 µJ for GaSe and AGSe, respectively. The beam profile is nearly Gaussian and the power stability is remarkably 1 % rms, measured at 10 mW average power [DGB22].

For wavelengths beyond 10 µm the achieved pulse energy is the highest reported for femtosecond DFG so far [2].

In 2023, the focus will be on the improvement of the LWIR OPCPA performance, i.e., energy scaling by exchanging the GaSe crystals with Ba-compound Se-crystals and increasing the bandwidth by changing the OPA design.

Excitation transfer in $Cr^{2+}Fe^{2+}$:ZnSe

Cr^{2+} and Fe^{2+} doped ZnSe crystals are currently discussed as the Ti:sapphire of the mid-infrared as these materials offer phonon-broadened absorption and emission spectra and provide broadband laser gain in the 2 to 5 µm wavelength range. While Cr^{2+}:ZnSe can be directly excited by commercially available high power Er, Ho or Tm lasers, no such possibility exists for Fe^{2+}:ZnSe. To this end, we have investigated electronic excitation transfer processes between Cr^{2+} and Fe^{2+} ions in co-doped ZnSe as an alternative excitation process. Employing photoluminesence (PL) experiments at unprecedented sub-10 ns temporal resolution [FTG22, STF], we have been able to unveil details of the transfer process that could not be resolved before. Fig. 2(a) and (b) show PL measurements on co-doped ZnSe, where the luminescence from the individual ion species has been separated by suitable bandpass filters. Here the Fe^{2+} luminescence sets in with a marked delay of about 65 ns, and the PL time constant appears prolonged by a factor 3 compared to measurements with direct excitation of the Fe^{2+} ions. The Cr^{2+} PL decay, in contrast, appears significantly accelerated compared to singly-doped Cr^{2+}:ZnSe. Further analysis of the Cr^{2+} PL reveals an ~exp(-gt$^{1/2}$) decay component, which is characteristic for dipole-dipole mediated resonant excitation transfer (Förster transfer). We further analyzed this transfer process using a multirate equation model that comprises 31 groups of interionic distances up to 30 nm. This analysis indicates a transfer efficiency >80 %, exceeding previous expectations by at least an order of magnitude. We explain this remarkably high transfer efficiency by (multi)phonon-assisted excitation transfer, in analogy to the phonon-mediated efficient radiationless decay of the excited Fe^{2+} state. Moreover, as both non-radiative losses and excitation transfer show different temperature scaling, a cryogenic temperature regime was identified that promises overall efficiencies above 50 %, suggesting that Fe^{2+}:Cr^{2+}:ZnSe may be a much more viable alternative to parametric conversion schemes in the mid-infrared range than previously anticipated.

Combined gain in Tm/Ho-doped laser materials

For generation of ultimately short pulses near 2 µm we study Tm,Ho-codoped materials exhibiting intrinsic structural disorder and utilize vibronic interactions and stimulated Raman scattering in mode-locked (ML) lasers, see Fig. 3. In the tetragonal calcium gadolinium aluminate $CaGdAlO_4$ (abbreviated: CALGO), the Ca^{2+} and Gd^{3+} cations are statistically distributed over the same Wyckoff site and the structure disorder originates from the second coordination sphere of the dopant ions. CALGO crystals exhibit a significant inhomogeneous spectral broadening of the absorption and emission bands of the dopant Tm and Ho ions which facilitates the generation of ultrashort pulses in ML lasers. In addition, despite their disordered nature, they feature attractive thermo-mechanical properties, i.e., high thermal conductivity and nearly athermal behavior. From polarized spectroscopy and using a suitable model which takes into account bidirectional energy

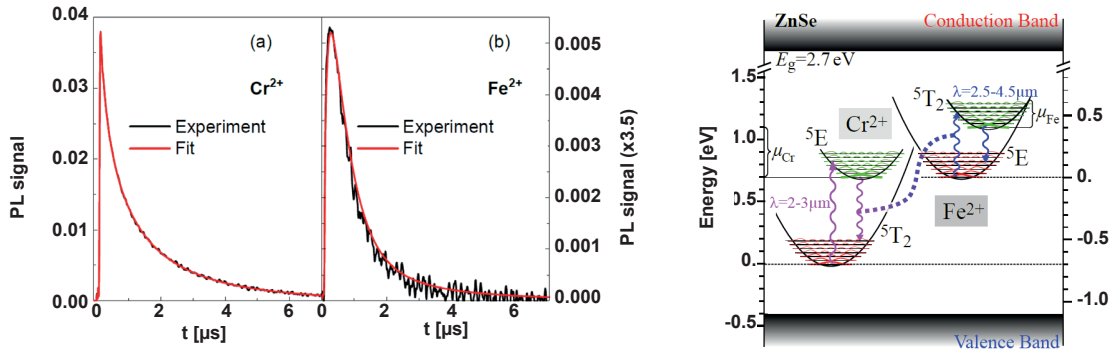

Fig. 2:
Photoluminescence transients taken with 2.05 µm excitation from a Fe^{2+}:Cr^{2+}:ZnSe codoped sample with bandpass filter sets for isolating the Cr^{2+} and Fe^{2+} luminescence, see (a) and (b), respectively. Fits of the data are obtained using a rate equation model that comprises a total of 31 interionic distances. (c) Level scheme of Fe^{2+}:Cr^{2+}:ZnSe, depicting the resonance condition between the ^5E states of Cr^{2+} and Fe^{2+}, enabling efficient Förster transfer between these two ion species in ZnSe.

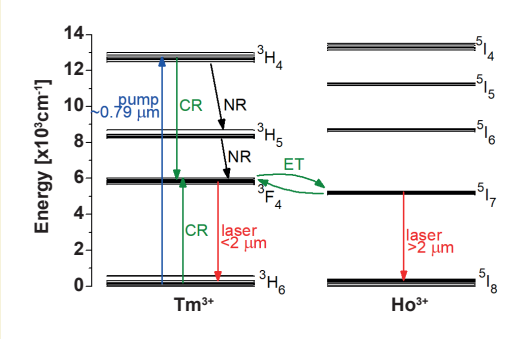

Fig. 3:
Simplified energy-level scheme of Tm^{3+} and Ho^{3+} ions with processes relevant for ~2 µm laser operation: CR – cross-relaxation, NR – non-radiative relaxation, ET – energy-transfer.

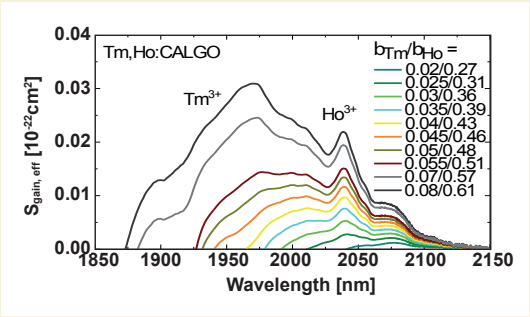

Fig. 4:
Effective gain spectra for the Tm,Ho:CALGO crystal at ~2 µm: $\beta_{Ho} = N(^5I_7)/N_{Ho}$ is the Ho^{3+} inversion rate and $\beta_{Tm} = N(^3F_4)/N_{Tm}$ is the Tm^{3+} inversion rate; σ-polarization.

transfer, we derived inversion dependent effective cross-sections [WLZ22], Fig. 4.

For the laser experiments, a 5 mm thick, AR-coated a-cut sample of a 4.5 at.% Tm, 0.5 at.% Ho:CALGO, was used in an X-shaped laser cavity. Chirped mirrors were used to manage the cavity dispersion with a total round-trip group delay dispersion (GDD) of −1250 fs². We employed an anti-resonant GaSb-based SESAM for self-starting ML operation, designed for a central wavelength of 2060 nm with two InGaAsSb quantum wells.

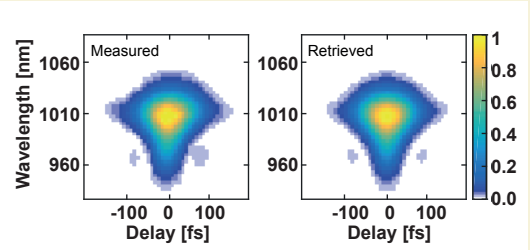

Fig. 5:
SESAM ML Tm,Ho:CALGO laser: SHG-FROG characterization of the shortest pulses achieved with 3 % output coupler: (a) measured and (b) retrieved traces.

In the ML regime and at the maximum pump power used (Ti:sapphire laser), an average output power of 376 mW was obtained with a 3.0 % output coupler at a repetition rate of 86 MHz, corresponding to a pulse energy of ~4.4 nJ. The ML laser operated at a central wavelength of 2015 nm and the emission bandwidth (FWHM) amounted to 82 nm. To characterize the pulse duration properly, we used a home-made second-harmonic generation frequency-resolved optical gating (SHG-FROG) set-up. The measured and retrieved FROG traces on a 128×128 grid size are shown in Fig. 5. A pulse duration (FWHM) of 52 fs was derived, while from the spectral bandwidth, a Fourier-transform limited pulse duration of 45 fs was calculated.

A comparison of the measured spectrum with the gain spectra of the Tm,Ho:CALGO crystal, cf. Fig. 4, indicates that the developed ML laser benefits from the gain originating from both Tm^{3+} and Ho^{3+} ions. It was operating with superior long-term stability for hours without interruption or power degradation. To characterize the stability of the ML operation, radio frequency (RF) spectra were measured with a fast extended InGaAs photodiode. The fundamental beat note displayed an extinction ratio of 85 dBc above carrier, evincing stable mode-locking without any Q-switching instabilities. The main limitation for further pulse shortening is set at present by the dielectric coatings of the cavity mirrors and in particular the output coupler [WLZ22].

Ternary cubic semiconductors for quasi-phase-matching (QPM) in the mid-IR

The most successful among all QPM non-ferroelectric, non-centrosymmetric cubic materials that are transparent in the mid-IR studied to date has been the orientation-patterned GaAs (OP-GaAs). This binary semiconductor combines superior second-order nonlinearity and thermal conductivity with transparency up to 18 µm but suffers from strong two-photon absorption (TPA) and cannot be pumped by pulsed laser sources between 1 and 1.7 µm. Compared to GaAs, the isostructural GaP not only has a negligible TPA in the same spectral range but shows some additional advantages such as higher laser damage threshold, lower refractive index (strict-

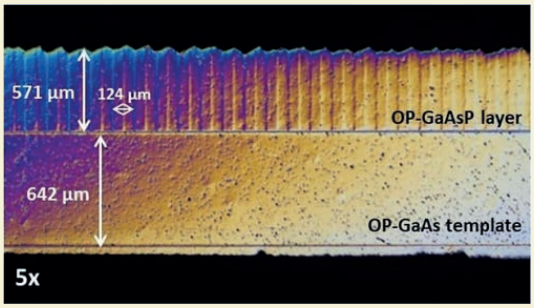

Fig. 6:
A cross section of GaAsP, HVPE grown directly on a patterned inverted layer of an OP-GaAs template without deposition of an encapsulating MBE GaAs layer. The template part used for this sample corresponds to a fan-out structure with a domain width in the 62-63 µm range.

ly correlated with the nonlinear figure of merit and the domain width) and higher thermal conductivity at lower thermal expansion – most of them as a consequence of the increased band-gap. This, however, comes at the expense, again due to the increased band-gap, of somewhat lower nonlinearity and lower transparency upper limit in the mid-IR. In spite of all the progress subsequently achieved with OP-GaP, the low quality of the commercially available GaP wafers, their 5-6 times higher price and extremely narrow market present a huge technological hurdle. Heteroepitaxy, i.e. the growth of one material on another, can be used not only to grow GaP on the cheaper, robust and higher quality GaAs substrates, notwithstanding the relatively large lattice mismatch (3.6 %), but also offers a unique opportunity to grow mixed GaAsP on GaAs with engineerable properties and at reduced lattice mismatch. In 2022, we demonstrated for the first time nonlinear frequency conversion (SHG) in such a ternary OP-GaAsP structure with a nominal P content of 15 %, i.e. OP-$GaAs_{0.85}P_{0.15}$, grown on an OP-GaAs template by our partner at AFRL [WVP22]. The thickness of ~600 µm is the largest achieved so far for such a ternary QPM structure, Fig. 6. The period of the heteroepitaxial ternary OP-GaAsP structure (Λ = 124 µm) corresponds to a fundamental wavelength of ~5450 nm for SHG at room temperature. For the SHG experiments we employed a commercial source available from our collaborator APE, based on difference-frequency generation (DFG) between the signal and idler of an optical parametric oscillator, synchronously pumped by a femtosecond Yb-fiber laser at a repetition rate of 40 MHz.

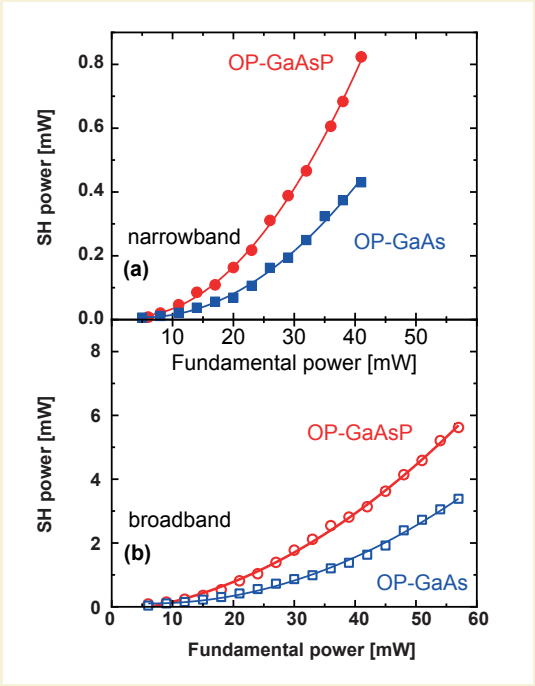

Fig. 7:
Average second-harmonic (SH) power vs. average incident fundamental power in the narrowband (a) and broadband (b) modes: OP-GaAsP (5-mm, red symbols and lines) and OP-GaAs (3.1 mm, blue symbols and lines).

This tunable parametric source offers two modes in terms of spectral width (pulse durations of 700 and 100 fs, respectively). The fundamental beam was focused by a 50 mm lens into the ~5 mm long OP-GaAsP. At the maximum average powers near 5450 nm (41 mW in the narrowband and 57 mW in the broadband mode) the peak on-axis intensity incident on the sample amounted to 5 and 75 MW/cm^2, respectively. The second-harmonic (SH) average power dependence recorded for the OP-GaAsP sample at ~5450 nm is shown in Fig. 7 by red symbols and fits for the narrowband and broadband cases. The maximum SH powers achieved were 0.82 and 5.6 mW, respectively. Correcting for the Fresnel reflections at the uncoated input and exit faces of the OP-GaAsP sample (roughly 28 % per surface) we obtain for the maximum internal SHG conversion efficiency 3.9 % in the narrowband and 19.1 % for the broadband case, i.e., much higher notwithstanding the severe acceptance bandwidth limitation. The performance of the present ternary OP-GaAsP sample grown by heteroepitaxy was not inferior compared to a reference OP-GaAs sample grown by homoepitaxy with a QPM period corresponding to SHG in the same wavelength range [WVP22].

Next steps of this research will include investigation of higher P-content, improved surface polishing and AR coating of the OP-GaAsP structures. Future work will be extended to frequency down-conversion, e.g. synchronously pumped optical parametric oscillators (SPOPOs) by ultrafast Er-fiber lasers near 1.6 µm for which the already achieved layer thickness and sample length are sufficient both in the picosecond and in the femtosecond regime. While ternary structures with a P-content as high as 50 % have been already grown, a P-content of about 30 % will be more than sufficient to avoid TPA at 1.6 µm and still achieve idler wavelengths as long as 14 µm, exceeding the upper transmission limit of GaP.

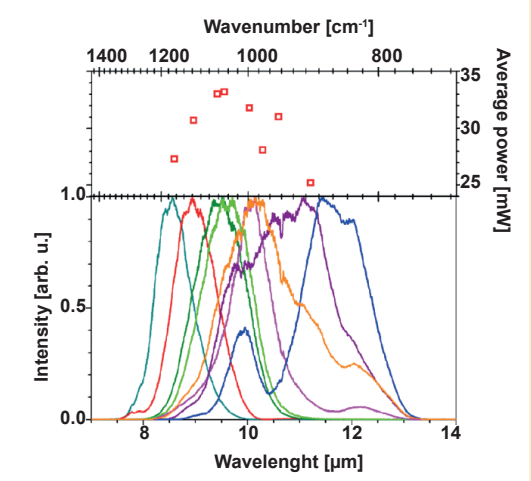

Fig. 8:
Top: Average power of the chirp-compensated idler output beam as a function of center wavelength across the tuning range for a pump power of 1.95 W at 1.03 µm. Bottom: Representative idler spectra across the tuning range.

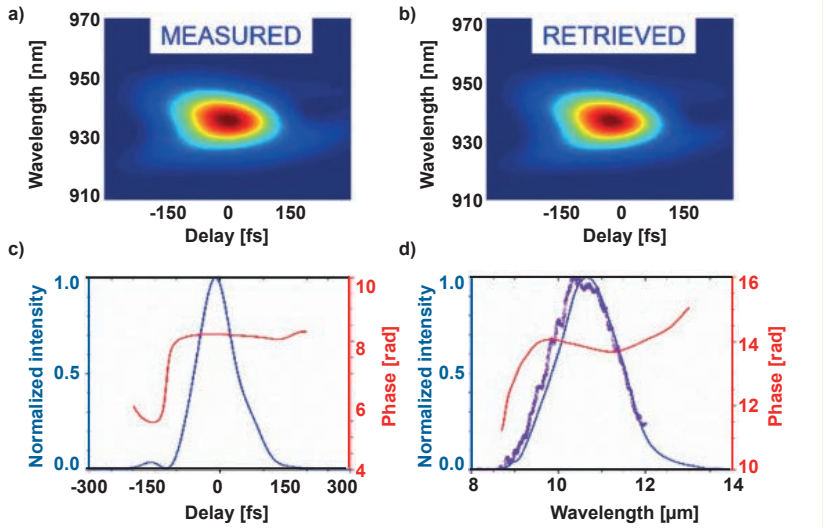

Fig. 9:
(a) Measured and (b) reconstructed X-FROG traces obtained for chirp-compensated idler pulses. Retrieved temporal (c) and spectral (d) intensity and phase. The retrieved pulse duration is 101 fs. The symbols in (d) represent the measured spectrum.

100 kHz OPA covering the 7.5-13.3 μm range

We demonstrated efficient, direct frequency down-conversion of femtosecond 100 kHz, 1.03 μm pulses to the mid-infrared in a supercontinuum-seeded, tunable optical parametric amplifier based on $Cd_{0.65}Hg_{0.35}Ga_2S_4$ [HPP22]. We obtained few-cycle pulses with an average power > 30 mW at center wavelengths between 8.8 and 10.6 μm (Fig. 8), at conversion efficiencies far surpassing that of optical parametric amplification followed by difference-frequency generation or intra-pulse difference-frequency generation. The pulse duration at 10.6 μm was 101 fs corresponding to 2.9 optical cycles with a spectral coverage of 760-1160 cm^{-1} and an average power of 33 mW (Fig. 9). At a center wavelength of 10.6 μm, the practical overall pump-to-idler energy conversion efficiency, defined as the ratio of the idler pulse energy after chirp-compensation and the pump power incident on the OPA crystal, was 1.7 %. $Cd_xHg_{1-x}Ga_2S_4$ is an attractive alternative to other recently developed non-oxide materials, $LiGaS_2$ (LGS) and $BaGa_4S_7$ (BGS), and offers a much higher nonlinear figure of merit compared to those materials.

T2: Secondary Sources

Compression of a commercial fiber CPA in a multipass cell

Commercially available fiber CPA systems delivering tens of Watts of average power at high repetition rates (>100 kHz) with pulse duration in the few-hundred fs are routinely employed around the world for laser material processing applications. At MBI it has been shown that combining high repetition rates and pulse duration

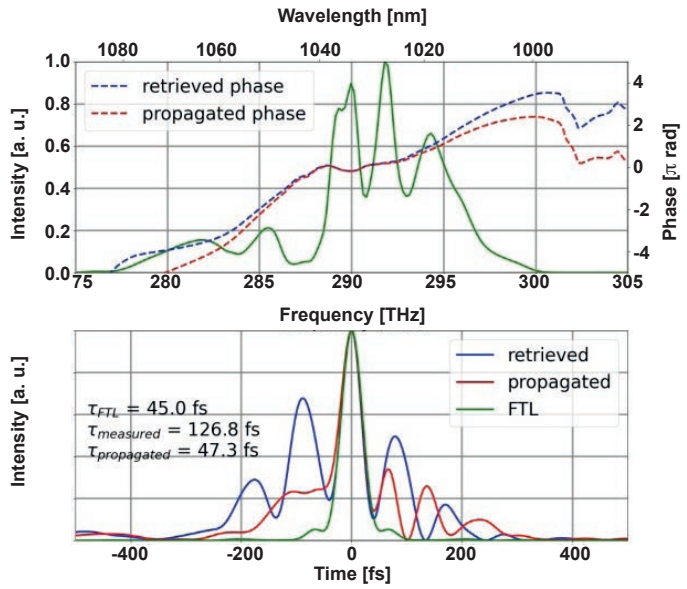

Fig. 10:
Compression of a fiber CPA in a multi-pass cell. Top: Retrieved spectrum and spectral phase (blue) including simulated propagation in fused silica (red). Bottom: Retrieved temporal profile (blue), retrieved pulse after simulated propagation (red) and Fourier-limited pulse (green).

in the order of 10 fs allows accessing new windows of laser material processing, in particular for direct laser writing of surface waveguides [3]. These experiments utilized a fairly complex optical parametric chirped pulse amplification (OPCPA) system. In order to provide a simpler, robust and cost-effective alternative, nonlinear compression of a commercial fiber CPA has been identified as a viable route for the generation of multi-W, sub-20 fs pulses at hundreds of kHz. During 2022 a multi-pass cell setup was designed and built for the post-compression of 300 fs pulses with 18 W average power, at repetition rates between 500 kHz and 1 MHz (Amplitude Satsuma HP). Fig. 10 shows the results of spectral broadening during 28 passes through a 9.5 mm thick window of fused silica located inside the multi-pass cell. Dispersion compensation with chirped mirrors allowed pulse compression to 47 fs with 15 W.

Compression of a high average power OPCPA

Nonlinear compression of sub-10 fs pulses from an OPCPA has been investigated for the generation of near-single-cycle pulses with high average power at 100 kHz in a compact setup. 0.15 mJ, 7 fs pulses from a 100 kHz OPCPA at 800 nm were focused by a 30 cm focal distance spherical mirror. The waist was reproduced two more times by realizing a 1:1 image of the focal plane utilizing 15 cm focal length spherical mirrors. The setup was placed in a compact vacuum chamber and spectral broadening was achieved by placing 50 microns thick quartz plates outside the focal planes. Three plates were sufficient to produce an octave-spanning spectrum. After beam collimation, the pulses were compressed by chirped mirrors. Pulse duration below 4 fs with ~65 % efficiency was achieved. Fig. 11 shows the results of spatio-temporal characterization utilizing a SEA-F-SPIDER setup. The spatio-spectral distributions (a) show that the space-time couplings originated during parametric amplification are still present, while the broadened spectrum contains stronger spectral modulations (integrated spectrum shown in (c)). Similarly, the spatio-temporal distribution (b) shows a pulse shape with dependence on the spatial coordinate and pulse front tilt, although the pulse front tilt could be an artifact of the measurement (small misalignment). The pulse front tilt gives rise to an integrated pulse duration (d) over 5 fs, although at particular points across the spatial profile the pulse duration is below 4 fs and closer to the Fourier transform limit. Although locating the windows for spectral broadening outside the focus allows building a very compact

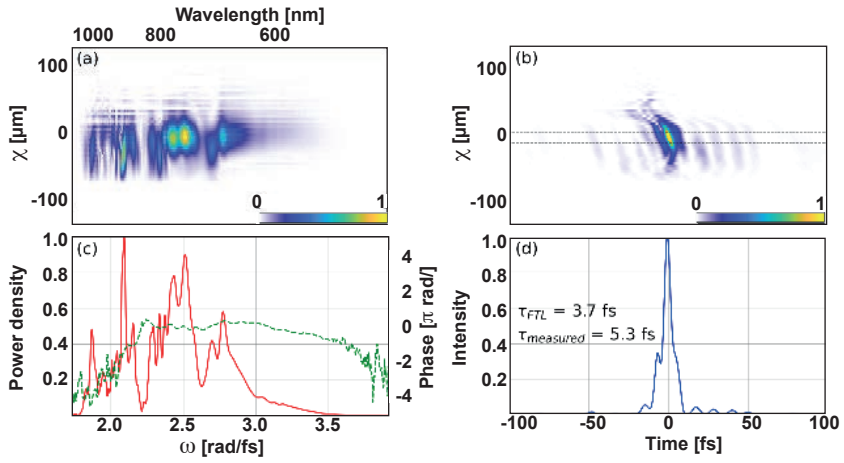

Fig. 11:
Compression of OPCPA pulses: (a) spatio-spectral distribution, (b) retrieved spatio-temporal distribution, (c) spatially integrated spectrum (red) and retrieved spectral phase (green), (d) spatially integrated temporal shape.

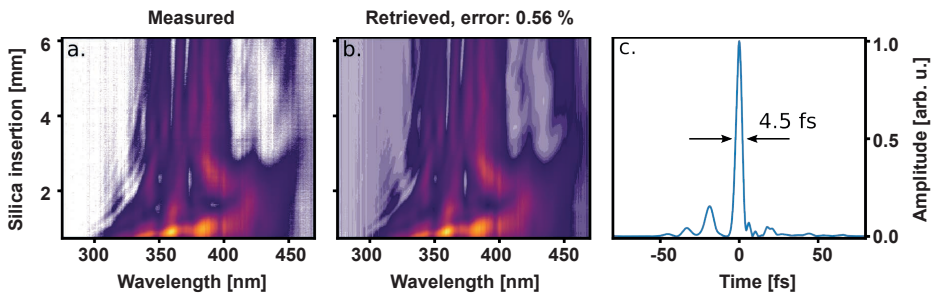

Fig. 12:
Dispersion scan measurement of the NIR pulses in vacuum. Measured and retrieved traces are displayed in (a) and (b), respectively. The well retrieved pulse is sub-5-fs as seen in (c). This corresponds to approximately 1.8 cycles of the electric field. This trace was taken while driving the fiber with 10 fs pulses with 280 µJ of energy, and the fiber was differentially filled with 1.2 bar of helium.

setup, the approach has the disadvantage of translating spatial and spatio-temporal distortions to the nonlinearly broadened field.

Dual source of VUV and visible laser pulses

In this work, intense ultrashort vacuum ultraviolet (VUV) pulses are generated alongside few-cycle near-infrared pulses. In 2021 we showed the generation of VUV pulses, continuously tunable from 140 nm to 200 nm with spectral bandwidths typically between 5 nm and 10 nm. The pulses are generated via resonant dispersive wave generation during soliton compression in a stretched flexible hollow-core fiber. This concept naturally supports the extension of the VUV source by exploiting the soliton self-compressed pulses covering the full visible spectral range, too. Since the pulses have a fixed temporal relationship to each other dictated by the generation process and both are very short, they are ideal for time-resolved pump-probe experiments with a few-fs time resolution.

To that end, the output of the hollow-core-fiber is separated into two independent arms by non-dispersive pulse front splitting. The pulse shape of the infrared arm was characterized in vacuum via the second-harmonic generation dispersion scan method. The results are shown in Fig. 12. The retrieved pulse shape displayed in Fig. 12 (c) confirms the theoretical prediction of self-compression to few-cycle duration.

Regarding the VUV generation, efforts have been made to stabilize the output characteristics of the system.

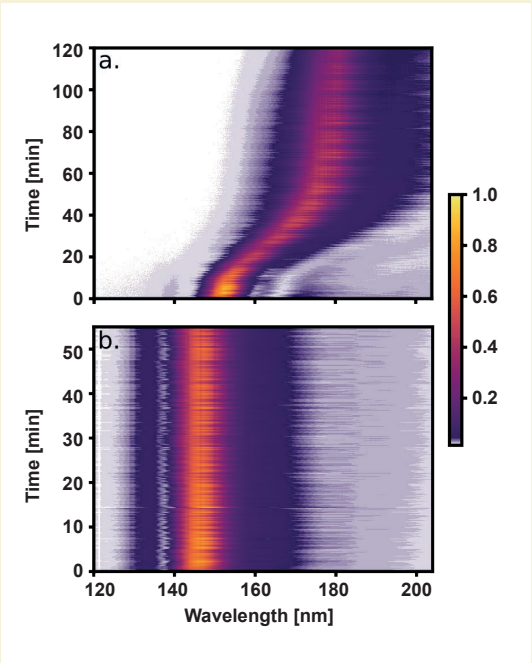

Fig. 13:
Recording the VUV spectrum for an extended period of time (a) before and (b) after optimization of the VUV beamline. Both spectrograms correspond to similar driving conditions: ~300 µJ per pulse input and fiber filled differentially with 1.1 bar He.

degraded rapidly. After careful optimization of the generating parameters, the vacuum and the gas system we managed to achieve stable spectrum, and also the energy drop has been reduced as shown in Fig. 13 (b). This provides confidence that the system can be operated for multi-hour experiments with high reliability.

In 2023 we will perform further characterization, and the source be used in project 3.2 for time-resolved absorption spectroscopy of excited fused silica.

Simulation of High Harmonic Generation (HHG)

In HHG the interplay of different processes provides a complex physical picture. Therefore, we complement secondary source HHG development with numerical simulations. First we compare experimentally found parameter combinations resulting in maximum HHG-flux with numerical code predictions. When this has proven successful, further search of code predictions for global maxima can be done. Because optimization of the high harmonic flux depends on various parameters of the laser driver, beam propagation geometry and the generating medium, which are hampered by experimental constraints, code calculations are an indispensable tool.

Complete simulation of HHG is very time consuming, and parameter search becomes ineffective. Therefore, we pursue the search at first with a code that calculates phase-matching as the basic process for flux enhancement strategies which then can be complemented by pursuing in-depth calculation. The idea is to get confidence in optimum HHG for the existing and upcoming MIR-laser driver systems at MBI.

Code calculations were performed using a Maxwell – solver for beam propagation, accounting for geometrical,

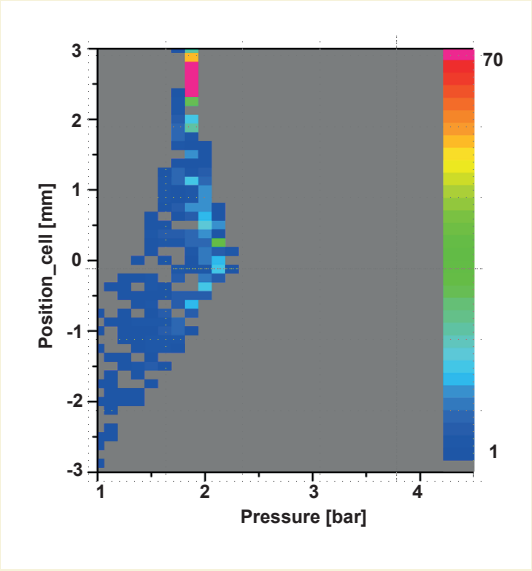

Fig. 14:
Change of FOM² (cf. text) - color coded – with He-pressure (x-axis) in a 3 mm gas cell and entrance position (y-axis) for HHG at 500 eV of a 2.1 µm (28 fs, laser peak intensity 8.2 x 10^{14} W/cm²) driver.

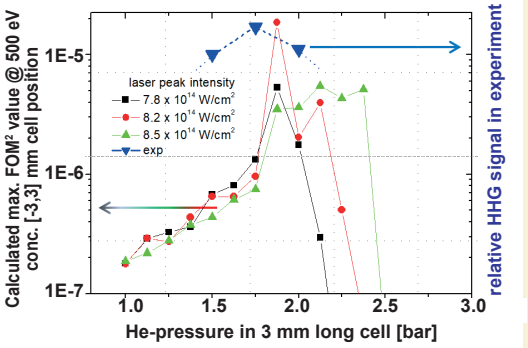

Fig. 15:
Comparison of relative signals (cf. text) in experiment and numerical code calculation.

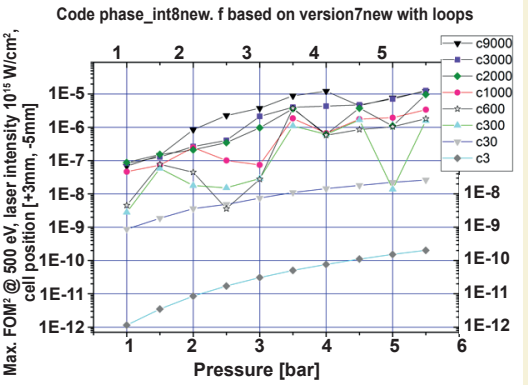

Fig. 16:
Calculated FOM² (laser peak intensity 10^{15} W/cm²) values as a function of He-pressure at optimized cell position and cell-length as parameter. (Label numbers in graph are the cell length in microns).

dipole and dispersive phase shifts. Ionization is derived from an adapted ADK-model. Microscopic HHG of a given selected order is simply assumed if the necessary intensity is reached in the respective beam position. Thus a so-called “figure-of-merit” (FOM)

d(FOM)/dz = pressure * cos (phase) * H (intensity)

in dependence on beam propagation, phase shift and intensity (H is 1 or 0 concerning intensity) is calculated. The FOM indicates regions of phase-matching for a selected harmonic order and we interpret FOM^2 as a relative HHG-signal. Figure 14 displays color-coded FOM^2 values as a function of He-gas pressure in a 3 mm extended gas cell and the entrance position (y-axis) of the cell with respect to the position of the focus (y = 0) of the drive beam.

Within the experimental accuracy of the laser intensity we compare the experimental signal (relative units, integrated spectrum 280 eV-600 eV with max. around 500 eV due to filter transmission, cf. annual report 2021) with the calculated maximum (relative units, for HHG 500 eV) at the optimized cell position. Figure 15 shows reasonable agreement of the pressure values at which the HHG-signal is maximized.

Figure 16 displays an example of parameter calculation concerning the gas cell extension. This provides the valuable information that the used cell length of 3 mm in experiments matches with calculated signal saturation as a function of the HHG-medium extension.

Own Publications in 2022 ff

(for full titles and list of authors see appendix 1)

BBS22: V. V. Badikov *et al.*; J. Alloy. Compd. **907** (2022) 164378/1-5

BWM22: A. A. Boyko *et al.*; SPIE Proc. **11985** (2022) 1-5

CLX22: W. Chen *et al.*; Opt. Lett. **47** (2022) 4728-4731

DGB22: M. Duda *et al.*; Opt. Lett. **47** (2022) 2891-2894

EGB22: G. Exner *et al.*; Opt. Mater. **133** (2022) 112994/1-4

ELB22: K. Eremeev *et al.*; Opt. Mater. Express **12** (2022) 3749-3762

EMV22: U. Elu *et al.*; in *Light Filaments: Structures, challenges and applications*, (SciTech Publishing, IET, Stevenage, U.K., 2022) 103-115

FBG22: P. Fuertjes *et al.*; Optica **9** (2022) 1303-1306

FGM22: P. Fuertjes *et al.*; Opt. Express **30** (2022) 5142-5150

FTG22: P. Fuertjes *et al.*; Opt. Lett. **47** (2022) 2129-2131

FWO22: F. J. Furch *et al.*; J. Phys.: Photonics **4** (2022) 032001/1-26

GBS22: F. Guo *et al.*; Opt. Lett. **47** (2022) 842-845

GJB22a: R. Grunwald *et al.*; Photonics **9** (2022) 9010042/1-13

HPP22: Z. Heiner *et al.*; Sci. Rep. **12** (2022) 5082/1-7

KKB22: H. Kurz *et al.*; Frontiers in Physics **10** (2022) 3389/1-7

KMH22: K. Kato *et al.*; SPIE Proc. **1198505** (2022) 1-5

KSZ22: M. Kowalczyk *et al.*; Opt. Lett. **47** (2022) 1762-1765

KTW22: D. Kühn *et al.*; Opt. Lett. **47** (2022) 750-753

KUB22: K. Kato *et al.*; Appl. Opt. **61** (2022) 10774-10777

LXZ22a: Z.-L. Lin *et al.*; Opt. Lett. **47** (2022) 3027-3030

LXZ22b: Z.-L. Lin *et al.*; Opt. Express **30** (2022) 31986-31997

MBN22: C. Mei *et al.*; Photonics Res. **10** (2022) 01000148/1-7

MGS22: C. Mei *et al.*; Phys. Rev. A **106** (2022) 053527/1-9

MKW22a: K. Miyata *et al.*; Opt. Mater. Express **12** (2022) 963-969

MSY22: C. Mei *et al.*; Phys. Rev. A **105** (2022) 013516/1-12

PLL22: Z. Pan *et al.*; Opt. Mater. Express **12** (2022) 673-684

PLS22: Z. Pan *et al.*; J. Lumin. **246** (2022) 118828/1-10

PLW22: Z. Pan *et al.*; SPIE Proc. **11980** (2022) 198003/1-6

PWC22: Z. Pan *et al.*; SPIE Proc. **11980** (2022) 1198002/1-6

PWV22: V. Petrov *et al.*; SPIE Proc. **1198506** (2022) 1-6

SNB22: G. Steinmeyer *et al.*; SPIE Proc. **11986** (2022) 1198602/1-6

Ste22: G. Steinmeyer, Light-Sci. Appl. **11** (2022) 229/1-2

SZL22: S. Sun *et al.*; Opt. Express **30** (2022) 11861-11871

WLZ22: Y. Wang *et al.*; Opt. Express **30** (2022) 7883-7893

WVP22: L. Wang *et al.*; Phys. Status Solidi-RRL **16** (2022) 2200198/1-4

XLZ22a: W.-Z. Xue *et al.*; Opt. Express **30** (2022) 11825-11832

XLZ22b: W.-Z. Xue *et al.*; Opt. Express **30** (2022) 15807-15818

ZBL22a: L. Zhang *et al.*; SPIE Proc. **11980** (2022) 119800L/1-5

ZBL22b: L. Zhang *et al.*; Opt. Mater. Express **12** (2022) 2028-2040

ZLP22: H.-J. Zeng *et al.*; SPIE Proc. **11980** (2022) 119800M/1-5

ZLW22: N. Zhang *et al.*; Opt. Express **30** (2022) 29531-29538

ZLX22: H.-J. Zeng *et al.*; Opt. Express **30** (2022) 11833-11839

ZWL22: N. Zhang *et al.*; Opt. Express **30** (2022) 23978/1-8

ZZH22: Y. Zhao *et al.*; Laser Photon. Rev. **16** (2022) 2200503/1-9

submitted

FKBU: K. Kato *et al.*; J. Opt. Soc. Am. B

KUB: K. Kato *et al.*; SPIE Proc.

MWC: R. T. Murray *et al.*; SPIE Proc

PLS: Z. Pan *et al.*; J. Lumin.

STF: G. Steinmeyer *et al.*; Phys. Rev. Appl.

ZSZ: N. Zhang *et al.*; Opt. Lett.

Other publications

[1] L. von Grafenstein, M. Bock, D. Ueberschaer, A. Koç, E. Escoto, K. Zawilski, P. Schunemann, U. Griebner, and T. Elsaesser; Multi-millijoule few-cycle 5 µm OPCPA at 1 kHz repetition rate; Opt. Lett. **45** (2020) 5998

[2] R. Budriunas, K. Jurkus, M. Vengris, and A. Varanavicius; Long seed, short pump: converting Yb-doped laser radiation to multi-µJ few-cycle pulses tunable through 2.5-15 µm; Opt. Express **30** (2022) 13009

[3] F. J. Furch, W. D. Engel, T. Witting, A. Perez-Leija, M. J. J. Vrakking, and A. Mermillod-Blondin; Single-step fabrication of surface waveguides in fused silica with few-cycle laser pulses; Opt. Lett. **44** (2019) 4267

Invited Talks at International Conferences

(for full titles see appendix 2)

Z. Pan *together with* Y. Wang, Y. Zhao, W. Chen, L. Wang, H. Yu, H. Zhang, H. Chu, D. Li, F. Rotermund, P. Loiko, J. M. Serres, X. Mateos, U. Griebner, and V. Petrov; LTO2022 The 17th National Conference on Laser Technology and Optoelectronics (Shanghai, China, 2022-08)

W. Chen *together with* P. Loiko, X. Mateos, P. Camy, U. Griebner, and V. Petrov; Europhoton 2022 (Hanover, Germany, 2022-08)

W. Chen; CIOP 2022, 13th Int. Conference on Information Optics and Photonics (Xi'an, China, 2022-08)

U. Griebner *together with* L. von Grafenstein, M. Bock, T. Nagy, and T. Elsaesser; VII Ultrafast Dynamics and Metastability & Ultrafast Bandgap Photonics 2022 (Hersonissos, Crete, Greece, 2022-06)

G. Steinmeyer, Int. Conference on Laser Filamentation (COFIL), Chania, Greece (2022-07)

G. Steinmeyer, 25th Congress of the International Commission for Optics (ICO25), Dresden (2022-09)

G. Steinmeyer, Workshop on Nonlinear Photonics and Applications, Helsinki, Finland (2022-10)

2.1: Time-resolved XUV-science

A. Rouzée, S. Patchkovskii (project coordinators)
and K. Amini, F. Branchi, F. Furch, M. O. S. Guzmán, C. A. Granados Buidrago, E. Ikonnikov, M. Ivanov, A. Jiménez Galàn, A. Husakov, L.-M. Koll, O. Kornilov, M. Kretschmar, Sebastián Dávila Lara, N. Mayer, M. Mero, F. Morales Moreno, T. Nagy, M. Osolodkov, M. Richter, F. Rodriguez Diaz, C. P. Schulz, B. Schütte, A. Sen, O. Smirnova, E. Svirplys, M. T. Talluri, M. J. J. Vrakking, T. Witting, Z.-Y. Zhang

1. Overview

The main goal of project 2.1 is to visualize, understand, and steer electron and atomic motion during the transformation of finite quantum systems, starting from few-body systems to isolated nanoparticles. The project has both experimental and theoretical components. Experimentally, we are developing a framework of closely interconnected time-resolved methods, unified by the application of novel XUV/X-ray light sources, both table-top, such as obtained by high harmonic generation (HHG), as well as free electron laser facilities. These novel light sources allow us to combine the ultimate temporal resolution (attoseconds) with atomic-scale spatial resolution. Using photoionization as a probe step in a pump-probe configuration, we investigate attosecond electron motion in atoms, molecules and nanoparticles as well as coupling of the electron motion to the nuclear motion. Our experimental framework is complemented by an advanced theory program aiming at (i) tracking and resolving correlated multi-electron dynamics on the attosecond time scale, and (ii) understanding the impact of coherently excited attosecond multi-electron dynamics on the longer, femtosecond-scale nuclear motion. Our common goal is to push atomic and molecular science beyond the present state-of-the-art by looking at the new time scale in chemical and physical processes.

2. Topics and collaborations

Presently, the project is organized in four topics:

T1: Attosecond electronic dynamics in strongly driven systems

T2: Strongly-coupled electronic and nuclear dynamics in photoexcited neutral molecules

T3: Ultrafast electronic decay and fragmentation dynamics at XUV and X-ray wavelengths

T4: Ultrafast electron diffraction in photo-excited molecules

Collaborations with: A. Rudenko, D. Rolles (Kansas State University, USA); J. Küpper (Center For Free-Electron Laser, Hamburg); H. Stapelfeldt (Aarhus University, Denmark); A. Vilesov (UCLA, USA), F. Calegari (CFEL, Hamburg); F. Lépine (Institut Lumière et Matière, France); D. Holland (Science and Technology Facility Council, UK); Th. Pfeiffer (Max Planck Institute for Nuclear Physics, Germany); K. Varju (University of Szeged, Hungary); L. Banares (Universidad Compulense de Madrid, Spain); K.H. Meiwes-Broer, I. Barke (Universität Rostock); B. v. Issendorff (Universität Freiburg); P. Piseri (Università di Milano, Italy); P. Hommelhoff (FAU Erlangen); T. Brabec (University of Ottawa, Canada); G.G. Paulus (University Jena); C. Menoni (Colorado State University, USA), A. Orr-Ewing, M. Ashfold (University of Bristol, UK), F. Stienkemier (University of Freiburg), J. Osterhoff (DESY), A. Emmanoulidou (University College London, UK), B. Major (ELI-ALPS), V. Tosa (National Institute for Research and Development of Isotopic and Molecular Technologies, Romania); J. Luiten (Technical University of Eindhoven, The Neterhlands); B. Siwick (McGill University, Canada), F. Martin (Universidad Autonoma de Madrid, Spain).

In-house collaborations with projects 1.1, 1.2, 2.2, 3.1, 3,2, 4.1 and 4.3.

3. Results in 2022

T1: Attosecond electronic dynamics in strongly driven systems

Attosecond coincidence spectroscopy at 100 kHz

Investigation of attosecond electron dynamics in small molecules is the goal of this activity. To gain the most complete information about the laser-induced processes a so-called reaction microscope (ReMi) is used. This is an electron-ion coincidence spectrometer, which allows to determine the full (3D) momentum vector of all charged particles created in the interaction of a gaseous target with a combination of XUV attosecond and ultrashort NIR femtosecond pulses. The latter ones are produced by a state of the art 100 kHz OPCPA laser system combined with a high harmonic source, which can deliver either short XUV pulse trains or isolated attosecond pulses [WOS22].

Already in 2021 ionization phases of the N_2^+ C state have been determined by employing the RABBITT (reconstruction of attosecond beating by interference of two-photon transitions) technique, where the kinetic energy of the photoelectron from a target molecule is registered as a function of the delay between an XUV pulse train and an IR pulse. In the reporting period we collaborated with the theory group of Prof. Fernando Martin (Universidad Autónoma de Madrid). The group did elaborate calculations to determine the ionization delays of the N_2^+ C state. The agreement between the measured and calculated time delays is very good for low photon energies up to 10 eV.

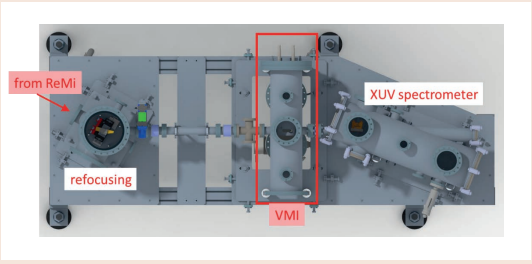

Fig. 1:
Schematic of the beamline extension located downstream of the ReMi. It consists of three chambers: The refocusing chamber, the VMI and the XUV spectrometer. For details see text.

In 2022 the main activity in the 100 kHz attosecond laser lab was the extension of the attosecond beamline downstream of the ReMi. One major limitation in exploiting the full capacity of the ReMi when performing coincidence detection experiments is its inability to quickly characterize the laser fields that trigger the ionization events. In coincidence experiments the ionization rate should not exceed 0.2 ionization events per laser pulse to keep the rate of false coincidences low (< 5 %). Even at 100 kHz repetition rate RABBITT or streaking scans typically used for pulse characterization take hours in a ReMi to achieve sufficient statistics.

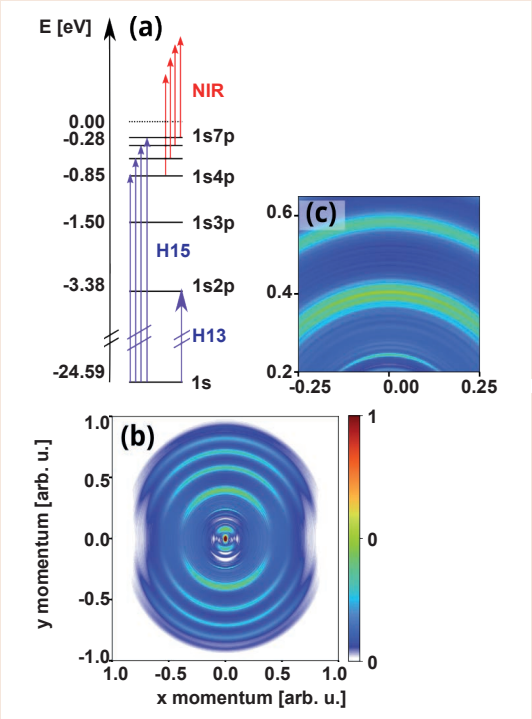

Fig. 2:
Photoionization of Helium by a phase-locked pair of attosecond pulses (a) Schematic energy level diagram showing the Rydberg states in helium excited by an XUV pulse and ionized by a near infrared laser pulse. (b) inverted VMI image for one XUV-XUV-delay. (c) Zoom into the VMI image showing the spectral fringes within the photoelectron spectra from each harmonic.

To improve the situation a beamline extension was installed. It consists of three main chambers as depicted in Fig. 1. The first one contains a toroidal mirror mounted on a three-axis motorized stage. It refocuses the focal spot from the ReMi into a velocity map imaging (VMI) spectrometer in a 2f-2f configuration. Compared to the ReMi a VMI spectrometer allows much higher ionization rates to determine the momenta of either electrons or ions with sufficient precision and strongly reduces the time needed for pulse characterization runs. The third chamber is a newly designed compact XUV spectrometer. It contains a Hitachi aberration-corrected concave grating to diffract the incoming XUV pulses onto an MCP/Phosphor assembly enabling to continuously monitor the spectral profile of the XUV pulses. A differential pumping chamber (not shown in Fig. 1) was installed between the ReMi and the new beamline extension. It acts not only as differential pumping stage to maintain the ultrahigh vacuum within the ReMi, but it also contains a retractable photodiode used to monitor the flux of XUV photons.

Phase-locked pairs of XUV pulses and application in atomic and molecular science

In order to enable a new class of XUV interferometry experiments, we have developed a phase-locked Mach-Zehnder interferometer, which allows to generate phase-locked pairs of few-cycle pulses, which are then used to generate pairs of phase-locked XUV pulses. The whole setup is compatible with near-single cycle NIR pulses; this allows for the generation of pairs of isolated attosecond pulses. The new setup enables experiments with three mutually phase-stable pulses, two locked XUV attosecond pulses, and one near-single cycle NIR pulse. The XUV phase-stability has been experimentally confirmed to be in the order of 6 as [KMD22b]. As a test of the setup we performed XUV Fourier transform photoelectron spectroscopy on helium (see Fig. 2). We recorded the photoelectron spectra formed through ionization of helium by an XUV pulse pair as a function of the delay between those XUV pulses. At each photoelectron momentum corresponding to an XUV energy $\hbar\omega_{XUV}$ - Ip we observe oscillations of the photoelectron signal with frequency ω_{XUV} with respect to the delay $\tau_{XUV\text{-}XUV}$ (see Fig. 3(a)). The Fourier transform power spectrum of the delay scan reveals the energies of the 1s4p, 1s5p, 1s6p, and 1s7p Rydberg states of helium (see Fig. 3(b)) with a spectral resolution of < 15 meV and an accuracy better than 1 meV.

Using this setup, we investigated and steered the degree of entanglement between the photoelectron and photoion produced in the XUV photoionization of hydrogen molecules [KMD22a]. By controlling the XUV-XUV delay, we influenced the degree of electron-ion entanglement, which was quantified in our experiment by monitoring the strength of vibrational quantum beats observed when probing the H^+ ion momentum distributions that resulted from the dissociation of the H_2^+ ion by a time-delayed NIR pulse. We have extended these studies to observe how the entanglement can also affect electron localization occurring in H_2^+ ions formed in a combined XUV pulse pair and NIR laser pulse. Fig. 4 shows the observed asymmetry of H^+ ions (charac-

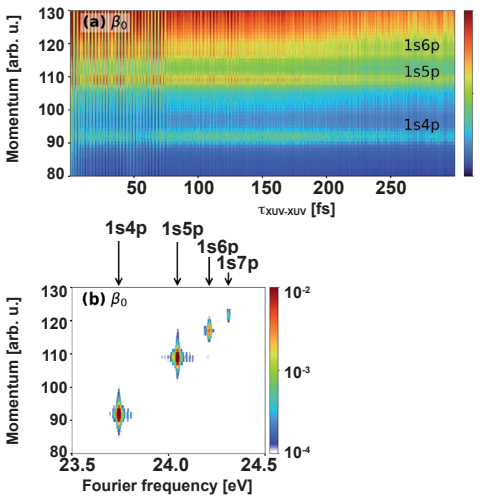

Fig. 3:
Photoionization of Helium by a phase-locked pair of attosecond pulses (a) photoelectron spectra as a function of XUV-XUV pulse delay. (b) Fourier transform power spectrum of the delay scan shown in (a) clearly revealing the excited Rydberg states.

terized by the normalized difference between H^+ ions ejected in opposite directions) in the photoionization of H_2 molecules as a function of delay between the XUV pulse pair and the NIR probe pulse. When repeating this experiment for a range of XUV-XUV delays, and therefore for different degrees of entanglement, we could also influence the degree of asymmetry. Our studies show that both electronic and nuclear coherences induced by ionization of a molecule with a broadband XUV pulse are affected by the degree of electron-ion entanglement.

T2: Strongly coupled electronic and nuclear dynamics in photoexcited neutral molecules

High-order harmonic generation is a powerful method that allows for the generation of ultrashort pulses of short wavelength radiation by ionizing an atomic gas target with a femtosecond laser pulse. The maximum photon energy achieved in this process is proportional to the ponderomotive energy of the laser pulse (given by Up-[eV]=9.33xI[10^{14}W/cm^2]xλ[μm]^2) and can therefore be tuned by increasing the laser wavelength. However, it is also well known that the efficiency of the process scales very poorly when increasing the laser wavelength, limiting the flux that can be achieved at high photon energies.

In collaboration with project 3.1, we have recently developed a new high harmonic beamline at the Max Born Institute that provides ultrashort soft x-ray pulses in the water window spectral range covering both the C K-edge (~280 eV) and the N K-edge (~400 eV) with an estimated minimum total flux at the source of (7.4 ± 1.0).10^6 photons·s^{-1} [KEG19]. In addition and in collaboration with the Institute of Applied Photonics (IAP), a highly efficient soft x-ray spectrometer was developed

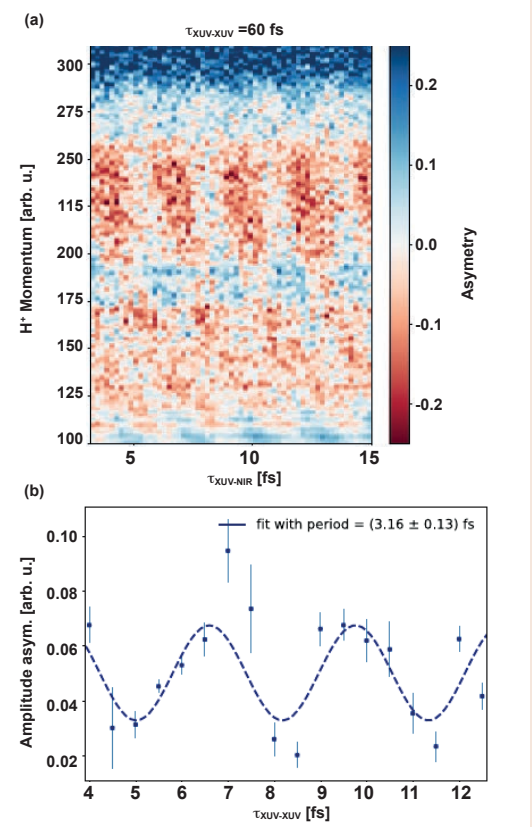

Fig. 4:
(a) asymmetry of H^+ photoion spectra as a function of time-delay between an XUV pulse pair and the probe NIR pulse. (b) Strength of the asymmetry as a function of XUV-XUV delay.

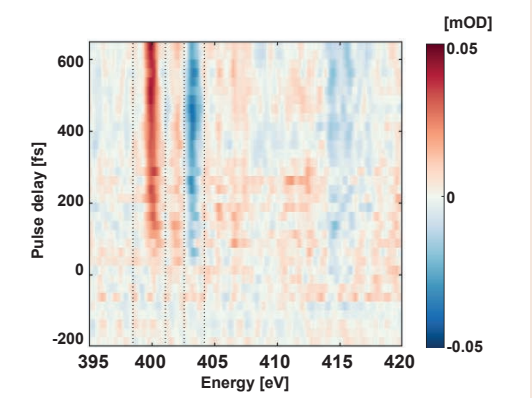

Fig. 5:
Transient N K-edge absorption spectrum recorded in UV-excited NO_2. A strong depletion (blue signal) is observed at a photon energy of 403 eV that is assigned to depletion of the ground state molecule. In addition, a new absorption feature is observed at a photon energy of 400 eV corresponding to the NO 1s – 2π resonance that reflects the formation of NO fragments following dissociation of the NO_2 molecules induced by the UV pulse.

and tested for transient absorption spectroscopy experiments with our table-top high harmonic source [KEW21].

The spectrometer is based on a Hettrick–Underwood design and incorporates a reflective zone plate (RZP) as a dispersive element. We demonstrated a resolving power of 890 at a photon energy of 410 eV and a total of ~400 photons/eV/s detected photons at the N K-edge.

The source together with the newly developed spectrometer was used to perform first femtosecond transient absorption spectroscopy experiments at the N K-edge in gases [KWZ22b] and in aqueous solution. The strong field ionization and fragmentation dynamics of N_2 upon interaction with an ultrashort 800 nm laser pulse was directly probed by monitoring the change of absorption of a time-delayed extreme high harmonic pulse at the N K-edge [KWZ22b]. Transitions indicative of the formation of N_2^+ ions in its first three electronic states, i.e. the electronic ground $X^2\Sigma^+_g$, first excited $A_2\Pi_u$, and second excited $B^2\Sigma^+_u$ states, were observed and used to determine the time-dependent electronic state population distribution dynamics of N_2^+. In addition, fragmentation of N_2^+ into N and N^+ on a timescale of several tens of picoseconds was observed and assigned to significant collisional dynamics in the plasma resulting from the strong field ionization of N_2.

The unimolecular dissociation dynamics of NO_2 upon single photon excitation by a femtosecond UV laser pulse was also investigated by transient absorption measurements at the N K-edge. The ultrafast dissociation of NO_2 is known to involve conical intersection (CI) dynamics between the first electronically excited A^2B_2 and the ground electronic X^2A_1 states. Upon single photon excitation at ~3 eV, the nuclear wavepacket propagates on the potential energy surface of the A^2B_2 state along the bending coordinate before returning to the electronic ground state by internal conversion. This leads to a significant vibrational excess energy, larger than the first dissociation threshold (3.115 eV) resulting to a prompt dissociation into neutral NO and O fragments. In our measurements, we observe a strong bleach of the core-hole excited B1 absorption feature of NO_2 at 403.26 eV upon photoexcitation of ground state NO_2 (see Fig. 5). In addition, we observe a new absorption feature at 402 eV appearing within the time resolution of the experiment, which we attribute to the vibrationally hot electronic ground state that is formed following internal conversion. This feature exhibits a notable decay in the first few hundred femtoseconds. A new broad absorption band centered at 399.8 eV is also observed and can be assigned to the NO 1s-2π resonance. Its spectral position and intensity directly reflect the photodissociation process. This work demonstrates that femtosecond soft X-ray absorption spectroscopy is a particularly well-adapted technique to investigate coupled electronic and nuclear dynamics in photoexcited molecules.

T3: Ultrafast electronic decay and fragmentation dynamics at XUV and x-ray wavelengths

Femtosecond pump-probe spectroscopy has revolutionized the understanding of extremely fast processes and was awarded with the Nobel prize in chemistry in 1999. Some processes in nature are even faster and take place on attosecond timescales (1 attosecond = 10^{-18} seconds). Ideally, the investigation of processes occurring on such fast timescales requires to use a sequence of two attosecond XUV pulses, one attosecond pulse to initiate the process and a second attosecond XUV pulse to interrogate the system under investigation. However, so-called attosecond-pump attosecond-probe spectroscopy has been very limited so far and only demonstrated for relatively simple processes involving the absorption of two photons. Most experiments in attosecond science have relied on the use of only one attosecond (pump or probe) pulse in combination with one femtosecond pulse.

Recently, we have been able to demonstrate a pump-probe experiment, in which complex multi-photon ionization processes were studied using two attosecond pulse trains. This experiment required the generation of very intense attosecond pulses, for which the TW OPCPA in the Extreme Photonics Laboratory was used.

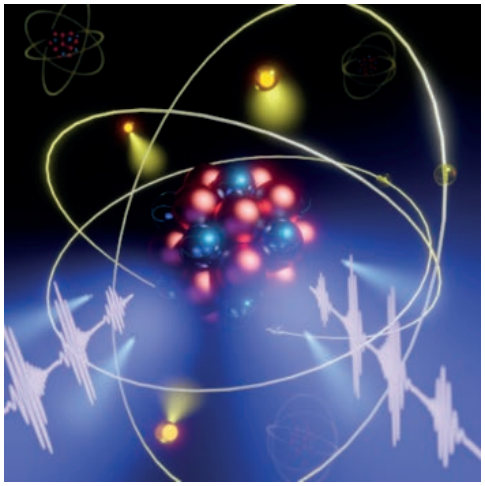

Fig. 6:
Two intense attosecond pulse trains (white) interact with an atom, resulting in the emission of three electrons (yellow). During this process four photons (blue) are absorbed. The probability of this process can be controlled by varying the temporal and the spatial overlap between the two attosecond pulses.

An artistic visualization of the experiment is presented in Fig. 6, showing two attosecond pulse trains interacting with an argon atom. Following the absorption of four photons from the attosecond pulses, three electrons were removed from the atom. There are many possible ways in which this multi-photon absorption may take place. To find out in detail how the electrons were removed from the atom, we varied the time delay between the two attosecond pulses and observed how many ions were generated.

As shown in Fig. 7, the yield of the doubly-charged Ar^{2+} ions (red curve) was almost independent of the time delay. In contrast, the yield of triply-charged Ar^{3+} ions (blue curve) shows pronounced oscillations when varying the time delay between the two attosecond pulses. We were able to conclude that the multi-photon absorption occurred in three steps: In each of the first two steps a

single photon was absorbed, whereas in the third step two photons were absorbed at the same time. These results were confirmed by simulations that were carried out at University College London and at ELI ALPS.

The developed experimental technique can be used in the future to study complex processes not only in atoms, but also in molecules, solids and nanostructures. An exciting question that we hope to answer is how several electrons interact with each other. This could help to understand the most fundamental processes on the shortest timescales.

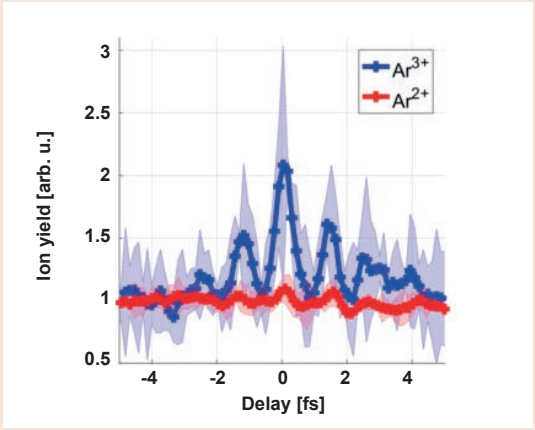

Fig. 7:
Ar^{2+} and Ar^{3+} ion yields as a function of the time delay between two attosecond pulse trains. (a) The Ar^{2+} ion yield (red curve) is only weakly modulated as a function of the XUV-XUV time delay, whereas clear oscillations with a period of 1.3 fs are observed in the delay-dependent Ar^{3+} ion yield (blue curve). These results indicate that Ar^{2+} is generated via the sequential absorption of two photons. Subsequently, two additional photons are simultaneously absorbed to form A^{3+}.

T4: Ultrafast electron diffraction of photoexcited molecules

We have optimized our 100 kHz nonrelativistic ultrafast electron diffraction (UED) source, achieving reciprocal- and real-space resolutions of <0.085-$Å^{-1}$ and <14.4-pm, respectively (see Fig. 8b) as confirmed by static electron diffraction of monocrystalline gold and polycrystalline aluminum thin films (see Fig. 8a). We have also measured the lattice structures of bismuth selenide and vanadium dioxide. Simulated electron diffraction data (see red/pink data in Fig. 8a) calculated with a powder electron diffraction simulation software called CrystalMaker show a very good agreement with corresponding measured data (see white data in Fig. 8a). The coherence length of our electron beam was estimated to be 6.2 nm. Moreover, we characterized and improved our electron beam's pointing stability to 60 µm (FWHM) and intensity fluctuation to the <1 % level (see Fig. 8c). We also achieved first optical-pump electron-probe time-resolved signal of transient space-charge effects from the formation of a plasma at a metal needle tip illuminated by a >10^{12} W/cm^2 optical pump pulse with a fluence of >40 mJ/cm^2. The temporal resolution was on the order of <25 ps (see Fig. 8d). In the next steps, we will upgrade our UED instrument for improved electron beam size manipulation that is compatible with the implementation of a radio-frequency (RF) compression of electron

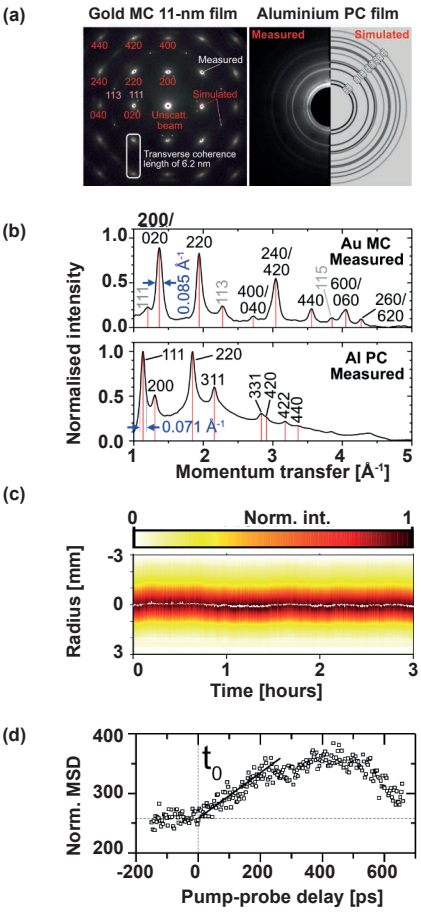

Fig. 8:
(a) Measured (white) and simulated (red) static 70-keV electron diffraction images of monocrystalline (MC) gold 11-nm film and polycrystalline aluminium (PC) film. The simulated data were calculated using a powder electron diffraction simulation software called CrystalMaker. The transverse coherence length was estimated to be 6.2 nm. (b) Reciprocal-space distributions extracted from the diffraction patterns shown in panel (a). The reciprocal- and real-space resolution are <0.085-Å-1 and 14.4 pm, respectively. (c) Beam pointing stability and intensity measurement of the electron pulse over 3 hours. The corresponding FWHM changes are 60 µm and <1 %. (d) First time-resolved 800 nm pump electron-probe measurement of space-charge dispersion of the primary electron beam following the generation of a plasma at a 50 µm metal tip illuminated with an 800 nm pulse with fluence of 40 mJ/cm^2, pulse duration of <60 fs, focused to a spot of 100 µm 1/e2 diameter. The mean square difference (MSD) in the change of the electron beam intensity between the pump-probe and electron-only data is shown. The temporal overlap of the two pulses, t0, is determined with sub-25 ps resolution.

pulses using an RF microwave cavity. Electron compression by RF fields will enable to improve our instrument's temporal resolution to the sub-few-hundred femtosecond timescale. The RF-laser time-of-arrival jitter will be corrected with an active synchronization system designed in close collaboration with Prof. Brad Siwick and Prof. Jom Luiten/DrXWorks. We will also implement a gas jet delivery system, and we plan to test a direct electron detector with our beamline towards the latter stages of 2023.

Own Publications 2022 ff

(for full titles and list of authors see appendix 1)

BJC22: I. Babushkin *et al.*; Nat. Phys. **18** (2022) 417

DWK22: L. Drescher *et al.*; Phys. Rev. A **105** (2022) L011101/1-6

FLT22: A. J. Feinberg *et al.*; Phys. Rev. Res. **4** (2022) L022063/1-6

FWO22: F. J. Furch *et al.*; J. Phys.: Photonics **4** (2022) 032001/1-26

GSE22: E. Granados, *et al.*; Appl. Phys. Lett. **120** (2022) 151101/1-6

GGA22: E. Granados *et al.*; Optica **9** (2022) 317-324

KLA22: H. Köckert *et al.*; J. Phys. B **55** (2022) 014001/1-13

KHM22: M. Kretschmar *et al.*; Optica **9** (2022) 639-644

KMD22a: L.-M. Koll *et al.*; Phys. Rev. Lett. **128** (2022) 043201/1-6

KMD22b: L.-M. Koll *et al.*; Opt. Exp. **30** (2022) 7082-7095

KSU22: K. Kolatzki *et al.*; Phys. Fluids **34** (2022) 012002/1-12

KWZ22b: C. Kleine *et al.*; Phys. Rev. Lett. **129** (2022) 123002/1-7

LOC22: B. Langbehn *et al.*; New J. Phys. **24** (2022) 113043/1-15

MBJ22: N. Mayer *et al.*; Phys. Rev. Lett. **129** (2022) 173202/1-5

PPR22: C. Peltz *et al.*; New J. Phys. **24** (2022) 043024/1-17

SKZ22: L. Seiffert *et al.*; Advanced in Physics: X7 **online** (2022) 2010595/1-60

SNC22: A. K. Schnack-Petersen *et al.*; J. Chem. Phys. **157** (2022) 214305/1-14

Vra22: M. J. J. Vrakking; J. Phys. B **55** (2022) 134001/1-9

WOS22: T. Witting *et al.*; Optica **9** (2022) 145-151

Own Publications in press

(for full titles and list of authors see appendix 1)

BVR: F. Braußе *et al.*; J. Phys. B: At. Mol. Opt. Phys.

Other Publications

KEG19: C. Kleine *et al.*; Soft X-ray absorption spectroscopy of aqueous solutions using a table-top femtosecond soft X-ray source, J. Phys. Chem. Lett. **10** (2019) 52–58

KEW21: C. Kleine *et al.*, Highly efficient soft x-ray spectrometer for transient absorption spectroscopy with broadband table-top high harmonic sources, Structural Dynamics **8** (2021) 034302/1-6

Invited Talks at International Conferences

(for full titles see appendix 2)

B. Schütte; ATTO FEL 2022 (London, UK, 2022-06)

A. Rouzée; QUTIF Final Colloquium (Bad Honnef, Germany, 2022-08)

M. J. J. Vrakking; ATTO conference SOAL-2022 (Dongguan, China, 2022-01)

M. J. J. Vrakking; APS March Meeting 2022 (Chicago, USA, 2022-03)

M. J. J. Vrakking; ATTO-FEL 2022 (London, UK, 2022-06)

M. J. J. Vrakking; Int. Workshop on Photoinization IWP & Resonant Inelastic X-ray Scattering (RIXS) (Zao-cho, Japan, 2022-11)

2.2: Strong-field Few-body Physics

F. Morales Moreno, B. Schütte (project coordinators)
and D. Ayuso, W. Becker, U. Bengs, U. Eichmann, M. Ivanov, Á. Jiménez, T. Kalousdian, M. Merö, D. B. Milošević, A. Ordoñez, S. Patchkovskii, M. Richter, A. Rouzée, O. Smirnova, P. Stammer, M. T. Talluri, N. Zhavoronkov

1. Overview

On a sub-femtosecond temporal and Ångström spatial scale the project aims at

- understanding strong field induced dynamics in atoms and molecules,
- employing strong field processes as a tool for imaging and comprehending atomic and molecular electron dynamics and molecular structural changes,
- using tailored light pulses to manipulate electronic motion, generate high-order harmonics with specific polarization characteristics and investigate chiral phenomena.

We put specific focus on the fundamental aspects of strong field-induced multi-electron dynamics, on the excitation of neutrals, on the forces exerted on these neutrals, on the role played by molecular structure and dynamics and on manipulating electronic dynamics. The strong field regime of interaction of light with matter is typically entered at light intensities beyond 10^{13} Watt/cm^2 in the infrared spectral range. There, the electric field of the light wave starts to become comparable with the intra-atomic/intra-molecular field experienced by the valence electrons.

2. Topics and collaborations

We address our objectives via experiment and closely linked theory focusing on the topics:

T1: Recollision physics and dynamic imaging in intense laser fields

T2: Strong-field processes in few-body systems

T3: Strong field excitation and HHG in tailored fields

Collaboration partners: S. P. Goreslavski, S. V. Popruzhenko (National Research Nuclear University (MEPhi), Moscow, Russia), A. Saenz (HU Berlin), Y. Mairesse (CELIA, Université Bordeaux, Bordeaux, France), N. Dudovich (Weizmann Institute, Rehovot, Israel), X. J. Liu (Chinese Academy of Sciences, Wuhan, China), J. Chen (Beijing Univ., Beijing, China). T. Marchenko (Université Pierre et Marie Curie, Paris, France), J. M. Bakker, G. Berden, B. Redlich (FOM-Institute for Plasma Physics, Rijnhuizen, The Netherlands), A. Stolow, A. E. Boguslavskiy (National Research Council of Canada, Ottawa, Canada and University of Ottawa), F. Martín (Universidad Autónoma de Madrid, Madrid, Spain), H. Stapelfeldt (Aarhus Univ., Aarhus, Denmark), J. Küpper, A. Rubio (Center for Free Electron Laser, Univ. Hamburg), T. Fennel (Univ. Rostock), V. R. Bhardwaj (Univ. of Ottawa, Canada), R. Cireasa (Institut des Sciences Moléculaires d'Orsay, France), F. Legare (ALLS Montreal, Canada), H. Köppel (Univ. Heidelberg), V. S. Makhija, (University of Mary Washington, USA), J. P. Wolf (Univ. Geneva, Switzerland), M. Kleber (TU München), R. Forbes (Stanford, USA), M. Spanner (National Research Council, Ottawa, Canada)

In-house collaborations with Projects 1.1, 2.1 and 4.1.

3. Results in 2022

T3: Strong-field excitation and HHG in tailored fields

Elliptically polarized high harmonics

High-harmonic generation (HHG) is a strong-field process, driven by the nonlinear interaction of laser radiation with different gases and solids. During this interaction, the driving field is up-converted through a process commonly described using the three-step model, where an electron is tunnel-ionized at the peak of the field, accelerated and brought back to the core by the same field. Following recombination, coherent radiation at very short wavelengths is emitted, with durations down to a few tens of attoseconds (1 as=10^{-18} s). Many frontiers of attosecond science, which studies the behaviour of electrons in atoms and molecules, rely on HHG technology not only as a source of radiation with unique properties, but also as an analytic tool for high-harmonic spectroscopy.

Controlling the amplitude, frequency and polarization of the generated XUV radiation is essential to unlock the true potential of HHG as a source for advanced experiments. In particular controlling the polarization state of the generated harmonics, as a fundamental property of light, is a strong motivation in order to enable attosecond-resolved measurements of chiral-sensitive electron dynamics. In principle, synchrotron and free-electron laser sources with tuneable polarization can provide the brightness and cover the spectral range for such measurements. However, pulse durations in the attosecond region have not been achieved in the XUV region. Additionally, in large-scale facilities the availability is limited, making a table-top source highly attractive.

The difficulty to generate harmonics with different polarization states has its origin in the recollision nature of HHG: the polarization of the generated harmonics follows the atomic dipole direction, which is directly related to the driving laser beam polarization. However, even

moderate ellipticity drastically decreases the recombination probability and the efficiency of the harmonic generation.

Alternatively, the polarization of high harmonics generated by a linearly polarized laser can be converted to elliptical polarization using a reflective phase retarder. Although the robustness and seeming simplicity of this approach still attracts numerous groups to contribute to this topic [KWN17], it has serious drawbacks: It is technically challenging to realize, it leads to high losses and it suffers from a narrow bandwidth.

There is another approach, based on the application of tailored driving laser fields that was shown to be feasible: A two-colour bi-circular (TCBC) collinear scheme was introduced by a pioneering experimental work [EEN95] and developed further for the generation of isolated attosecond pulses [BZh21]. The TCBC approach also offers full polarization control of the generated harmonics without drastically decreasing the up-conversion efficiency. However, even when the generated high harmonics are circularly polarized with $|\varepsilon| \approx 1$, the same does not necessarily apply to the generated attosecond pulses. Since neighbouring harmonics have helicities alternating between +1 and −1, by combining a group of such harmonics, instead of obtaining a circularly polarized attosecond pulse train, one obtains a pulse with unusual polarization properties, i.e. a starlike structure with linearly polarized pulses. However, if the harmonics of a particular helicity are stronger, i.e., if there is an intensity asymmetry in a high-harmonic energy interval, then it is possible to generate an elliptic or even circular pulse train. Recent studies, however, show the possibility to select harmonics of one helicity [BZh21], resulting in an increased spectral chirality and in overall elliptically polarized pulses.

The exact spectral position and separation of the harmonic orders depend on the spectral content of the driving radiation. Another advantage of the TCBC approach is the possibility to tune the ratio between the intensities of the two counter-rotating fields, I(ω1)/I(ω2), which leads to a spectral shaping of the generated XUV spectrum. Another control aspect is the frequency ratio of driving fields, which is decisive for the selection rules. Using the dynamical symmetry of bi-circular fields, the following selection rule for the generating harmonic and its ellipticity ε_n can be derived [Mil18]:

$$\varepsilon_n = +/-1 \text{ for } n = q(r + 1) +/-1 \text{ (q-integer)} \quad (1)$$

where r = (ω1)/(ω2). The combined laser field describes a Lissajous figure, with some maxima per fundamental period depending on “r”. Examples of the resulting field for r=2, r=3 and r=4 are shown in Fig.1.

Each of the leaves in the Lissajous figures generates an attosecond burst, totalling three, four or five bursts per laser cycle. In the frequency domain, the ω+2ω field produces circularly polarized harmonic peaks at (3N+1) and (3N+2) values, with the helicity of the fundamental field and the second harmonic, respectively, while 3N harmonic lines are symmetry forbidden. In the ω+3ω variant only odd harmonics ((4N+1) and (4N+2)) are

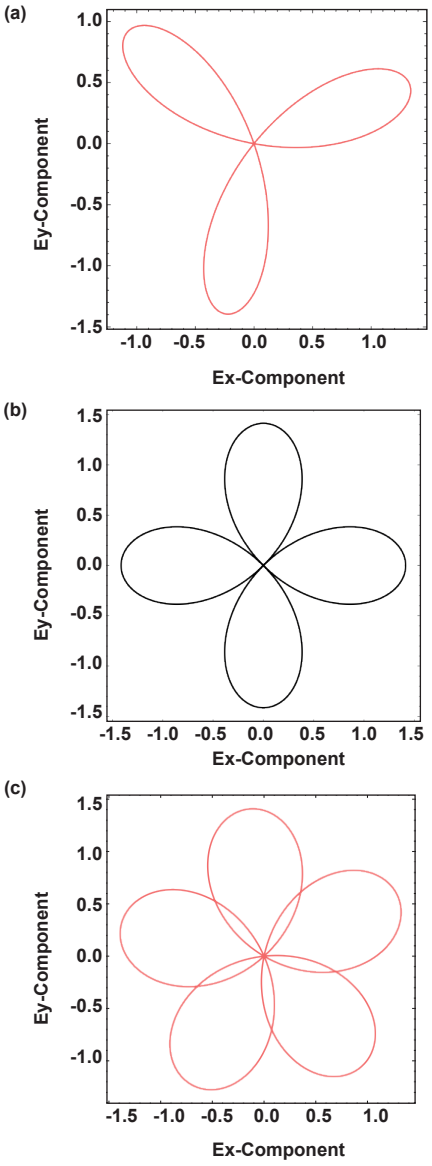

Fig. 1:
Combined laser fields for ω+2ω (a), ω+3ω (b) and ω+4ω bi-circular field with equal intensity for both field components.

allowed with the helicity having opposite signs for any neighbouring harmonics. The ω+4ω option allows the generation of only two of five consecutive harmonics, i.e. (5N+1) and (5N+2). So far most of the efforts were directed to explore the ω+2ω variant of the TCBC approach, promising the generation of highly elliptical XUV radiation via pulse trains [ZIv17] as well as isolated attosecond pulses [BZh21]. In this project we investigate the ω+3ω and ω+4ω variants of the TCBC approach aiming to explore its potential for the generation and characterisation of circularly polarized attosecond pulses.

Experiments were performed using a Ti:sapphire-based laser system, producing 35 fs pulses with up to 6 mJ energy and a central wavelength of 795 nm at 1 kHz. Part of the beam was directed towards an OPA obtaining

1200 nm and 1600 nm radiation, while the other part of the beam was compressed and frequency doubled with a BBO crystal. Both beams passed through corresponding achromatic broadband λ/2 and λ /4 wave plates to generate elliptically polarized pulses with an ellipticity up to ε=0.95 at 400 nm for the ω field and ε=0.92 at 1200 nm and 1600 nm, for 3ω and 4ω respectively.

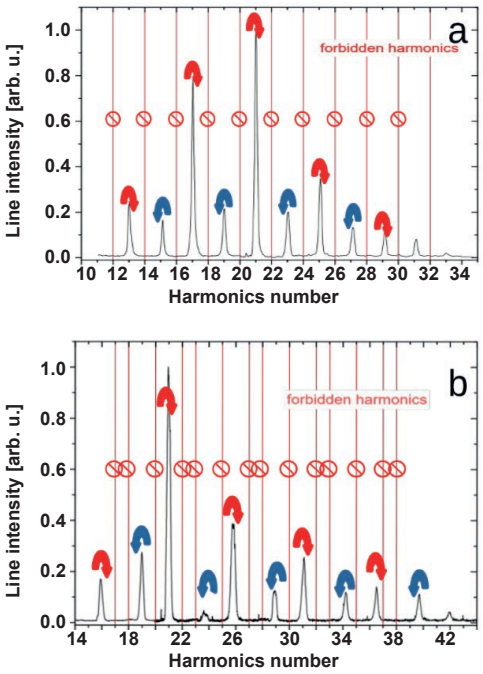

Fig. 2:
XUV spectra for ω+3ω (a) and ω+4ω combined driving field.

Fig. 2 shows the obtained XUV spectra for bi-circular ω+3ω and ω+4ω driving fields, with an ellipticity of each harmonic as expected. In the case of ω +3ω (Fig 2(a)), the 4n+1 and 4n-1 orders should have helicities corresponding to the 3ω and ω fields, respectively. For the ω+4ω driving field, only harmonics with 5N±1 orders are allowed, as is shown in Fig. 2(b), leading to an increase of two orders of the separation between neighbouring 5N±1 groups of harmonics.

This feature of the ω+4ω case has two advantages. First, it may be possible to develop a new type of pulse characterization on the basis of the dynamics of the forbidden harmonics. Second, this increased spectral separations for driving schemes with r > 2 is a path to avoid depolarization. The most drastic impact on the ellipticity of the individual harmonics has its origin in the spectral overlap of harmonics with opposite helicity (orders rN + 2 and rN + 1).

We have further determined the polarization state of the generated XUV continuum by utilizing a polarizer setup, developed in [BZh21], and based on the Stokes-vector formalism. The intensity of the spectrally isolated harmonic was measured as a function of the azimuthal angle of a Brewster mirror, both for right-handed (e.g.

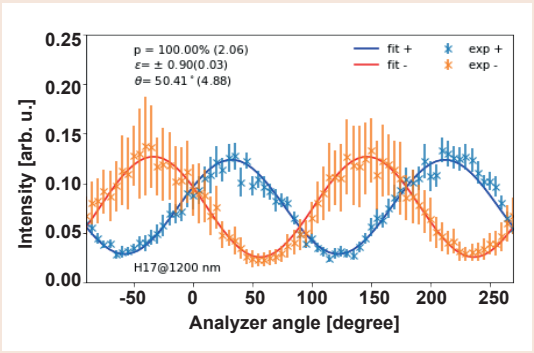

Fig. 3:
Measured intensities of the harmonic order 17 for a ω+3ω driving field in the cases of positive (blue, '+') and negative (red, 'x') helicity.

I(α; S1, S2, + S3)) and left-handed polarization (I(α; S1, S2, − S3)), see Fig. 3. An ellipticity up to |ε|=0.9 was demonstrated for H17, without any unpolarized content. Moreover, the spectra observed with the best possible ellipticity demonstrate the highest contrast between left and right polarised harmonics. The larger the difference in the emission of right- versus left-circularly polarized high harmonics, the larger is the final ellipticity of the generated APT.

In conclusion, we have demonstrated that tuning the ellipticity of the driving fields in the ω+3ω and ω+4ω variants of the TCBC approach presents a simple and practical possibility to decrease the unpolarized content of the harmonics and to control the ellipticity of attosecond pulses in a smooth and predictable way. The mutual contribution of rN+1 and rN-1 can be changed in a broad range, leading to a tuneable chirality of APTs.

Generation of intense attosecond pulses

Performing attosecond-pump attosecond-probe spectroscopy (cf. project 2.1) requires the generation of intense attosecond pulses. Since the conversion efficiency in high-harmonic generation is low, the development of such sources is challenging and has so far been limited to low repetition rates between 10 and 100 Hz. At the same time, the large and complex laser systems that have been used so far resulted in substantial fluctuations of the output parameters. Typical applications of attosecond-pump attosecond-probe spectroscopy, however, require both a high repetition rate and a high stability. To achieve both of these goals, we have developed a new setup that makes use of a commercial Ti:sapphire laser system operating at 1 kHz. The output pulses were temporally compressed using hollow-core fiber technology in combination with chirped mirrors, resulting in sub-4 fs pulses with a pulse energy of about 1 mJ. High harmonics were generated by focusing the driving laser pulses a few Rayleigh lengths behind a dense gas jet. This optimizes the XUV photon flux and leads to a small virtual source size of the XUV beam [MGK21]. By further demagnifying the XUV source size using a short focal-length spherical mirror, high XUV intensities up to 10^{14} W/cm^2 can be obtained.

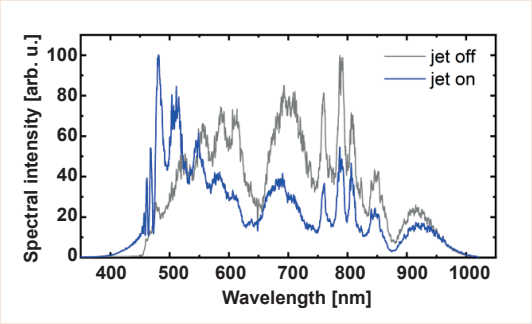

Fig. 4:
Driving laser spectrum for HHG when the Kr jet used for HHG is turned off (gray curve) and when it is turned on (blue curve).

Fig. 4 shows the driving laser spectrum used for HHG (gray curve). When switching on a Kr jet, the driving laser pulses are substantially blue-shifted (blue curve), which is attributed to ionization-induced self-phase modulation occurring within the HHG medium. Since the HHG conversion efficiency scales with the driving wavelength approximately as λ^{-6}, this results in an enhancement of the HHG conversion efficiency.

The obtained XUV pulses were applied to demonstrate an XUV-XUV experiment relying on the simultaneous absorption of two XUV photons by an Ar atom. The results are shown in Fig. 5, where oscillations with a period of 1 fs are observed with a main peak at zero delay. Since an attosecond burst is generated during each half cycle of the driving laser pulse, this shows that the harmonics are effectively generated with a 600 nm driving field (which has an oscillation period of 2 fs). Compared to a driving laser pulse at 800 nm, the HHG conversion efficiency is expected to increase by a factor of about 5-6. This increased conversion efficiency was the key to demonstrate for the first time attosecond-pump attosecond-probe spectroscopy at a repetition rate of 1 kHz.

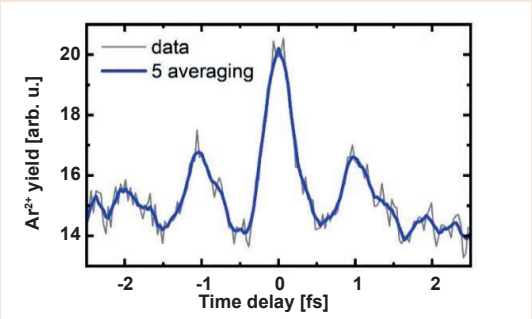

Fig. 5:
Ar^{2+} ion yield as a function of the time delay between two very short attosecond pulse trains. An oscillation period of about 1 fs is observed.

The modest driving pulse energy of about 1 mJ used in this experiment means that attosecond-pump attosecond-probe spectroscopy could be performed at repetition rates as high as 100 kHz in the near future, where corresponding laser systems are already available and further systems are under development. To further improve the capabilities of our setup, we plan to tailor the gas jet properties, which promises a further increase of the HHG flux and the available attosecond intensities.

Own Publications 2022 ff

(for full titles and list of authors see appendix 1)

BPI22: U. Bengs *at al.*; Phys. Rev. Lett. **4** (2022) 023135/1-8

MKW22b: T. Mullins *et al.*; Nat. Commun. **13** (2022) 1431/1-7

Own Publication in press

(for full titles and list of authors see appendix 1)

MKS: B. Major *et al.*; Phys. Rev. A

Other Publications

KWN17: C. von Korff Schmising, D. Weder, T. Noll, B. Pfau, M. Hennecke, C. Strüber, I. Radu, M. Schneider, S. Staeck, C. M. Günther, J. Lüning, S. Merhe, J. Buck, G. Hartmann, J. Viefhaus, R. Treusch, and S. Eisebitt; Generating circularly polarized radiation in the extreme ultraviolet spectral range at the free-electron laser FLASH; Rev. Sci. Instrum. **88** (2017) 053903

EEN95: H. Eichmann, A. Egbert, S. Nolte, C. Momma, B. Wellegehausen, W. Becker, S. Long, and J. K. McIver; Polarization-dependent high-order two-color mixing; Phys. Rev. A **51** (1995) R3414

BZh21: U. Bengs and N. Zhavoronkov; Elliptically polarized high harmonic radiation for production of isolated attosecond pulses; Scientific Reports **11**, (2021) 9570

Mil18: D. B. Milosevic; Control of the helicity of high-order harmonics generated by bicircular laser fields; Phys. Rev. A **98** (2018) 033405

ZIv17: N. Zhavoronkov and M. Ivanov; Extended ellipticity control for attosecond pulses by high harmonic generation; Opt. Lett. **42** (2017) 4720

MGK21: B. Major, O. Ghafur, K. Kovács, K. Varjú, V. Tosa, M. J. J. Vrakking, and B. Schütte; Compact intense extreme-ultraviolet source; Optica **8** (2021) 960-965

3.1: Dynamics of Condensed Phase Molecular Systems

E. T. J. Nibbering, O. Kornilov (project coordinators)
and M.-A. Codescu, B. P. Fingerhut, C. Granados, P. Han, C. Kleine, A. Kundu, M. Oßwald, R. Ovcharenko, D. Rana, H.-H. Ritze, J. Schauss, M.-O. Winghart, J. Zhang

1. Overview

This This project aims at a real-time observation of ultrafast molecular processes in the condensed phase, addressing the dynamics of elementary excitations, photoinduced chemical reactions and ultrafast changes of the electronic and/or chemical structure of molecular systems. The project makes use of a broad range of experimental techniques including all-optical pump-probe spectroscopy in a range from the soft-X-ray to mid-infrared, infrared photon-echo and multidimensional vibrational spectroscopies, and photoelectron spectroscopy using ultrashort VUV, XUV, and soft-X-ray pulses.

2. Topics and collaborations

Research in this project has been structured into four major topical directions:

T1: Dynamics and interactions in hydrated biomimetic and biomolecular systems

Collaboration partners: J. T. Hynes (University of Colorado, Boulder, USA), D. Laage (École Normale Supérieure, Paris, France), W. Scherer (Universität Augsburg, Germany), P. Macchi (Politecnico Milano, Italy, R. Netz (FU Berlin, Germany)

T2: Water-mediated proton transport dynamics between acids and bases

Collaboration partners: M. Odelius (Stockholm University, Sweden), Ph. Wernet (Uppsala University, Sweden), N. Huse (University of Hamburg, Germany), E. Pines (Ben Gurion University of the Negev, Beer-Sheva, Israel). D. Sebastiani (Martin-Luther-University Halle-Wittenberg, Germany), V. Batista (Yale University, New Haven, CT, USA).

T3: Electron transport dynamics in donor-acceptor molecular systems

Collaboration partner: M. Kowalewski and M. Odelius (Stockholm University, Sweden)

T4: Electronic excited state dynamics in molecular model systems

Collaboration partners: O. Rader (Helmholtz-Zentrum Berlin), L. Banares (Compulensa University, Madrid, Spain). R. Mitrić (Universität Würzburg, Germany), S. Haacke (University of Strasbourg, France), M. Olivucci (University of Siena, Italy), S. Gozem (State University of Georgia, Atlanta, USA), H. Fielding and G. Worth (University College London, UK), P. Slvicek (University of Prague, Czech Republic), B. Feringa (University of Groningen, The Netherlands), B. Winter (Fritz Haber Institute, Berlin, Germany).

Internal collaborations with Projects 1.1, 2.1 and 3.3 have been established.

3. Results in 2022

T1: Dynamics and interactions in hydrated biomimetic and biomolecular systems
(ERC-2018-ADG-BIOVIB, ERC-2018-STG-NONABVD)

Biomimetic and biomolecular systems and their interactions with water and ions are studied to unravel couplings between the different molecular entities and the fluctuating water shells in the electronic ground state. Hydration dynamics and solvation structures of molecular ions, electric interactions of and ion arrangements around native and artificial DNA and RNA systems, and theory and simulation of such processes at the molecular level are the main topics. In 2022, a combined experimental and theoretical study gave new insight into the properties of sulfate (SO_4^{2-}) ions in water and their interaction geometries with magnesium (Mg^{2+}) ions [KMB22a,b]. A second topic was the ultrafast vibrational response of activated C-D bonds in a chloroform-platinum ($CHCl_3$/Pt) complex in the liquid phase [ZKE22].

Liquid water responds to the presence of an ionic solute by changing local molecular arrangements and hydrogen bond structure. The influence of negatively and positively charged ions is usually classified via the phenomenological Hofmeister series, which ranks ions based on their ability to structure the water around them or to disrupt the water structure. The microscopic origin and molecular mechanisms of the Hofmeister series are still controversial and requires further clarification by experiment and theory.

Sulfate (SO_4^{2-}) ions are prototypical in this context, given their abundance in a broad range of minerals and their key role in biochemical and physiological processes. To elucidate sulfate-water interactions most directly, the asymmetric SO_4^{2-} stretching vibration is introduced as a local probe of the dynamic aqueous environment. This vibration has a frequency of approximately 1100 cm^{-1} and displays a broad infrared absorption band (spectral width ~65 cm^{-1}) consisting of several sub-components. Femtosecond two-dimensional infrared (2D-IR) spectroscopy was applied to map vibrational dynamics

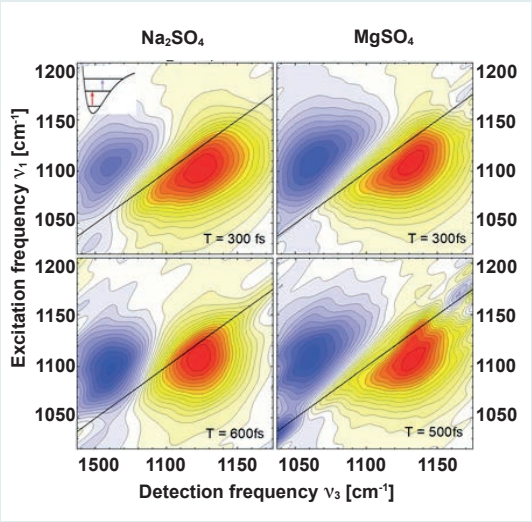

Fig. 1:
Two-dimensional infrared (2D-IR) spectra of the asymmetric stretching vibration of the SO_4^{2-} ion for sodium sulfate (Na_2SO_4, left column) and magnesium sulfate ($MgSO_4$, right column) in water. The absorptive 2D-IR signal is plotted as a function of the excitation frequency ν_1 and the detection frequency ν_3. Yellow-red contours correspond to excitations of the fundamental vibrational transition between the v=0 and 1 states of the vibration (red arrow in the inset image at top left), while blue contours are due to overtone excitations (v=1 to 2, blue arrow). For sodium sulfate, the change in the red-yellow contour from an elliptical line shape (top left) to a round shape (bottom left) within about 300 fs is due to rapidly fluctuating forces exerted on the sulfate ion by the water environment. For magnesium sulfate in contrast (right column), the elliptical line shape is preserved on this time scale because fast fluctuations are largely suppressed by the presence of magnesium ions in the vicinity of the sulfate ion.

at a comparably low sulfate concentration of 0.2 M and in the presence of sodium (Na^+) or magnesium (Mg^{2+}) ions. With Na^+ ions present, the 2D-IR spectra shown in Fig. 1 display a pronounced change of the 2D line shapes on a time scale of a few hundred femtoseconds. The initially elliptic envelope of the 2D-IR spectrum is transformed into a nearly circular shape, a manifestation of fast spectral diffusion induced by fluctuating forces from the solvent. In contrast, the elliptic shape is preserved in the presence of Mg^{2+} ions, demonstrating a reduction of ultrafast fluctuations of the water shell around a sulfate ion, which leads to a specific slowdown in the solvation dynamics of hydrated $MgSO_4$ compared to aqueous Na_2SO_4 solutions.

Extensive theoretical simulations provide a microscopic view of the observed dynamics and reveal a molecular picture in which the slowdown of the water dynamics arises from structural features of SO_4^{2-} - Mg^{2+} ion pairs that share water molecules in their hydration shells (Fig. 2). Contrary to the widespread account in the literature, the described effects are of short range and limited to the first 1-2 water layers around the sulfate ion. In contrast to the Hofmeister series, which classifies the effect of ion types on the water structure, the new results demonstrate a particular relevance of individual solvation geometries of specific ion pairs for the dynamics of dilute aqueous systems.

C-H bonds are one of the most abundant chemical motifs but of a mainly inert chemical character. Metal-induced C-H bond activation in transition metal complexes represents an important concept for functionalizing or activating C-H bonds in chemical reactions such as olefine polymerization and others. The molecular mechansims of C-H bond activation are a subject of current research, requiring experimental access to electronic structure and related properties such as electric bond polarizabilities.

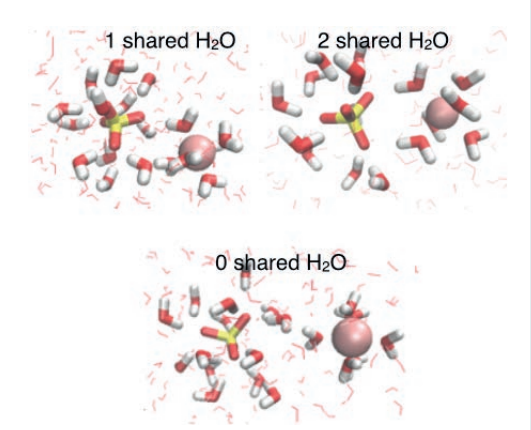

Fig. 2:
Structural representation of Mg^{2+} - SO_4^{2-} ion pairs in aqueous solution. The simulations yield a molecular picture in which the slowdown of hydration dynamics results from structural features of SO_4^{2-} - Mg^{2+} ion pairs that share 1 or 2 water molecules in their hydration shells (top), whereas ion pairs with separate, complete hydration shells (bottom) have little effect on water dynamics. Sulfur atoms are shown in yellow, magnesium atoms in pink, oxygen atoms in red and hydrogen atoms in white.

Vibrational spectroscopy is a most sensitive probe of local interactions, affecting the frequency position, line shape, and strength of vibrational transitions. In recent experiments, femtosecond infrared spectroscopy has been applied for the first time to the prototypical chloroform-platinum(II) complex $[Pt(C_6H_5)_2$(btz-N,N′)$\cdot CDCl_3$ (Fig. 3a, btz = 2,2′-bi-5,6-dihydro-4H-1,3-thiazine], in which the non-classical Pt···D−C interaction induces an effective C-D activation [ZKE22].

The linear C-D stretching absorption of the activated C-D bonds is plotted in Figs. 3(b,c), where panel (b) includes the C-D absorption of the non-complexed $CDCl_3$ molecules as a benchmark. Compared to the free solvent molecule, the stretching band of the activated C−D bond displays a red shift of 119 cm^{-1}, a strong broadening, and an 8-fold enhancement of spectrally integrated absorption. The vibrational lifetime was measured in femtosecond pump-probe experiments and has a value of approximately 5 ps.

To explore the origin of the strong broadening of the absorption band of the activated bonds, 2D-IR spectra were measured and analyzed with the help of density-matrix theory for the third-order response. The frequency fluctuation correlation function of the solvent was approximated by a sum of two Kubo terms. The experimental 2D-IR spectrum is presented in Fig. 4(a), and the result of the simulation in Fig. 4(b). In the 2D-IR spectra, signals originating from the 0-1 transition (yellow-red contours) and the red-shifted 1-2 transition (blue contours) of the C-D vibration are well separated. The analysis gives a large diagonal anharmonicity of 85 cm^{-1} of the vibration. The two contributions to the 2D-IR spectra exhibit elliptic envelopes with the long axis markedly tilted relative to the frequency diagonal $\nu_1=\nu_3$ (black solid line), a signature of fast spectral diffusion. The strong broadening of the vibrational line shape is dominated by spectral diffusion on 200 fs and 2 ps time scales, induced by the strong coupling to the fluctuating solvent $CDCl_3$.

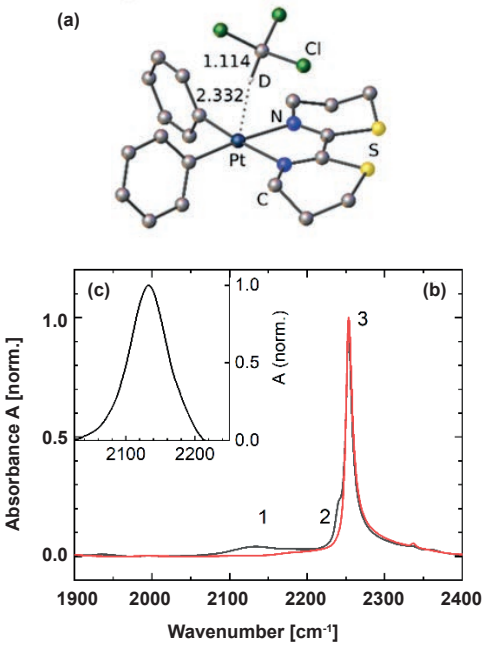

Fig. 3:
(a) Molecular structure of the chloroform-platinum(II) complex studied by femtosecond infrared spectroscopy. (b) ***Normalized*** *infrared absorption spectrum of the complex in $CDCl_3$ (black line), with (1) the stretching absorption band of the complexed C-D groups, (2) a shoulder probably due to C-D groups in hydrogen bonds with dissociated btz ligands, and (3) the stretching absorption band of uncomplexed C-D groups. The red line gives the spectrum of the neat solvent $CDCl_3$. (c) Normalized infrared absorption in the range of the C-D stretching mode of the complex.*

It is important to note that the stretching vibration of activated C-D bonds is much more susceptible to solvent fluctuations than the C-D bonds of the solvent molecules, the latter displaying a much narrower infrared band. This behavior originates from the strongly enhanced anharmonicity of the C-D vibration in the complex. The strong enhancement of infrared absorption is due to the modified electronic structure of the C-D groups interacting with the metal complex. More specifically, it reflects a strong increase of electric polarizability. This conclusion is confirmed by detailed DFT calculations of electronic structure and polarizabilities, benchmarked by calculations for other complexes. The key mechanism consists in the coordination of the C-D bond to the 16 valence electrons of the Pt(II) complex.

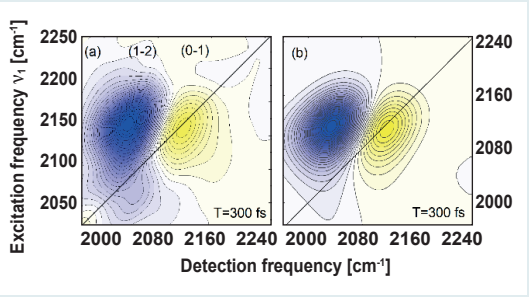

Fig. 4:
(a) 2D-IR spectrum of the C-D stretching vibration of the Pt(II) complex. The absorptive 2D signal measured at a waiting time T=300 fs is plotted as a function of excitation frequency ν_1 and detection frequency ν_3. Yellow-red contours represent signals on the v=0 to 1 transition corresponding to an absorption decrease while blue contours are due to the v=1 to 2 transition and represent an absorption increase. The signal change between neighboring contour lines is 2 %. (b) Simulated 2D-IR spectrum.

T2: Water-mediated proton transport dynamics between acids and bases
(DFG NI 492/13-1; ERC-2017-ADG-XRayProton)

Aqueous acid-base neutralization predominantly proceeds in a sequential way via water bridging acid and base molecules. This line of research builds on previous ultrafast studies of aqueous proton transfer using photoacids. Experimental techniques include transient UV/IR and UV/soft-X-ray absorption spectroscopies. Mid-IR absorption spectroscopy probes vibrational marker modes of particular species generated during proton transport between acid and base, as well as locally monitors hydrogen bond interactions of these species. X-ray absorption spectroscopy (XAS) probes transitions from inner-shell levels to unoccupied molecular orbitals, making it a tool to monitor electronic structure with chemical element specificity. Ultrafast UV/IR spectroscopy enables the elucidation of proton transfer pathways and the associated time scales for individual proton transfer steps [CWB22]. Much effort has been devoted in recent years to develop steady-state [EKL22a, EKL22b] and time-resolved soft-x-ray spectroscopy of acids and bases in water-poor and water-rich solutions [EWK22a, EWK22b WHZ22]. For the recently published results on the oxygen K-edge of hydrated proton complexes and on the N K-edge of photoacid molecules, obtained with beamtimes at BESSYII, we refer to the Scientific Highlight.

In a collaboration between the MBI and Yale University a detailed numerical study has been pursued on ultrafast charge relocation dynamics in intramolecular enol−keto tautomerization monitored with a local soft-x-ray probe [SVN22]. A full quantum treatment of the electronic and nuclear dynamics of 2-(2'-hydroxyphenyl) benzothiazole upon electronic excitation reveals how the spectral features of local nitrogen and oxygen 1 s core excitations to frontier orbitals provides direct insight into the distinctly different stages of charge relocation of the H atom, hydroxyphenyl oxygen atom donating and benzothiazole nitrogen atom accepting sites. Coherent modulations of the frequency positions of the pre- and main-edge transitions of the nitrogen and oxygen K-edges are due to coherently excited Raman-active vibrational modes with large displacements on the $S_0 \rightarrow S_1$ electronic excitation (Fig. 5). Our findings demonstrate that with ultraviolet-pump soft-x-ray-probe spectroscopy one can determine how the interplay of proton and electronic charge distribution motions facilitate the underlying mechanism of proton-coupled electron transfer responsible for enol−keto tautomerization reactions.

We have continued proton transport studies within the collaboration between the MBI and Martin-Luther-University. We have further explored the proton transport mechanism between the proton donating OH-group and the proton accepting quinoline unit of the bifunctional photoacid 7-hydroxyquinoline (7HQ). We continued our study on the role of bases added to the solution, with which a possible change in reaction pathways can be imposed onto 7HQ. Results on the 7HQ-imidazole reaction pair in methanol have shown that the outcome of the proton transfer dynamics can be quantitatively changed for high base concentrations (2.0 – 4.0 M).

Whereas proton exchange from the proton accepting quinoline unit towards the proton donating OH-group of 7HQ occurs through a proton vacancy methoxide transfer hopping mechanism along a methanol solvent bridge (with 7HQ following the neutral N* → cationic C* → zwitterionic tautomer Z* pathway), the added amphoteric imidazole acts as a base by accelerating the first proton transfer to take place from the 7HQ OH-group (converting 7HQ as neutral N* tautomer → anionic A* on femtosecond time scales) [CWB22, CKW]. A slower proton exchange from a second imidazole molecule, now acting as an acid, towards the quinoline unit of the 7HQ on a two-to-three fold longer time scale facilitates a completion of the tautomerization reaction, by converting the 7HQ A* anion → zwitterionic tautomer Z*. The observed subpicosecond time scale for the first N* → A* reaction step indicates a basically barrierless reaction for "tight" contact 7HQ-imidazole acid-base pairs, in line with previously investigated photoacid-carboxylate systems. Instead, even for "tight" contact reaction conditions, the proton abstraction from imidazole by the quinoline nitrogen atom in "tight" contact pair conditions has a pronounced acid-base reaction barrier. Electronic excited-state calculations of the 7HQ-imidazole complexes confirm the existence of a major reaction barrier, rationalizing the observed time scales for the A* anion → zwitterionic tautomer Z*

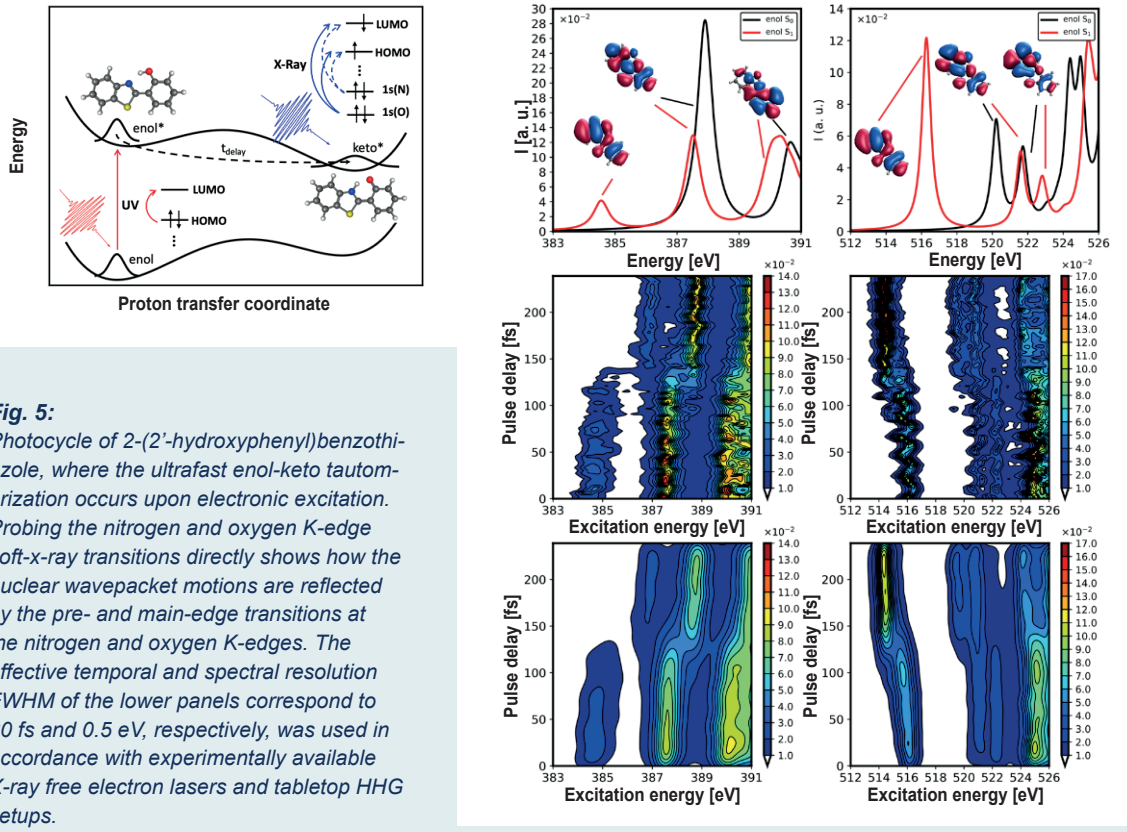

Fig. 5:
Photocycle of 2-(2'-hydroxyphenyl)benzothiazole, where the ultrafast enol-keto tautomerization occurs upon electronic excitation. Probing the nitrogen and oxygen K-edge soft-x-ray transitions directly shows how the nuclear wavepacket motions are reflected by the pre- and main-edge transitions at the nitrogen and oxygen K-edges. The effective temporal and spectral resolution FWHM of the lower panels correspond to 20 fs and 0.5 eV, respectively, was used in accordance with experimentally available X-ray free electron lasers and tabletop HHG setups.

in these “tight” contact 7HQ-imidazole complexes, that cannot be understood by simple assessments using empirical free energy-reactivity relationships.

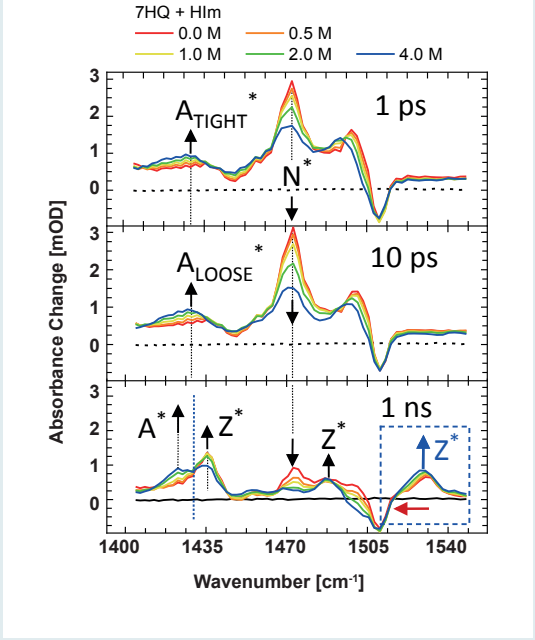

Fig. 6:
Comparison of transient UV/IR pump-probe spectra of 7HQ in CD_3OD measured at 1 ps, 10 ps and 1 ns pulse delay times for different imidazole (HIm) base concentrations. Dotted lines are reference lines denoting the frequency positions of N (1473 cm^{-1}), Z* (1437 cm^{-1} and 1530 cm^{-1} and A* (1422 cm^{-1}) 7HQ-species.*

T3: Electron transport dynamics in donor-acceptor molecular systems
(ERC-2017-ADG-XRayProton, SMART-X)

In this topical area, elementary charge transport dynamics in solution are investigated from the viewpoint of their functional role in biochemical processes. The objective is to elucidate the underlying mechanisms for electron transfer, proton transfer as well as proton-coupled electron transfer in donor-acceptor molecular systems. This line of research builds on previous ultrafast studies of photoinduced electron transfer processes in donor-acceptor complexes. Experimental techniques include, besides ultrafast UV/IR spectroscopy, ultrafast UV/soft-X-ray measurement methods using laboratory-based table-top laser systems and large-scale facilities (storage rings, free electron lasers). For the table-top approach we have recorded ultrafast soft-x-ray spectra of both molecular systems in the gas phase and in aqueous solution, using extreme high-order harmonic (HHG) probe pulses covering 200-450 eV and an X-ray spectrometer with a frequency resolution of about 0.5 eV, clearly sufficient to distinguish different electronic states in small molecules in the gas phase [KWZ22a, KWZ22b, ZKH22], but also to monitor pre-edge and main-edge spectral features typical for mid-sized organic molecules in solution.

Results on strong field ionization of molecular nitrogen in the gas phase has been published, and results on photoinduced dissociation on nitrogen dioxide have been measured and analyzed (see Project 2.1). Preliminary experiments have shown the feasibility of probing photoinduced charge flow in molecular systems in solution, using the table-top ultrafast soft-X-ray spectroscopic approach.

T4: Electronic excited state dynamics in molecular model systems
(DFG KO 4920/1-1)

Photoelectron spectroscopy is one of the most powerful analytical tools for studies of molecular electronic structure. In particular, time-resolved photoelectron spectroscopy (TRPES) is considered to be one of the most viable methods to study dynamics at conical intersections. In this topical area TRPES methods have been extended to the liquid phase employing an XUV time delay-compensating monochromator beamline based on a high-order harmonic generation source. The setup provides pulsed, wavelength-selected XUV radiation for the probe in the traditional pump-probe configuration of time-resolved experiments. The beamline is coupled to a microliquid jet endstation, which allows for studies of molecules in solutions. An NIR/vis pump pulse is used to excite organic solute molecules, which are ionized by the probe XUV pulses. The photoelectrons are detected using a magnetic bottle time-of-flight spectrometer. The first application of the technique was demonstrated in 2018 in the investigation of intramolecular proton transfer in Quinoline Yellow molecules. In 2019 a collaboration with one of the leading theory groups in this field, the group of Prof. Roland Mitrić (University of Würzburg) was established. In 2021 a joint publication on ultrafast relaxation of aminoazobenzenes demonstrated that the TRPES method is sensitive enough to allow choosing a DFT functional most suitable for the description of molecular dynamics.

In 2022 the main focus of research was on the biomimetic photoactuators: molecular switches and motors, which can be used in biological environments. In 2022 a collaboration network involving R. Mitrić (Würzburg) S. Haacke (Strasbourg), M. Olivucci (Siena), H. Fielding (UCL), P. Slavicek (Prague), S. Crespi (Groningen), B. Winter (Berlin) submitted a proposal for a European doctoral network. The results of the evaluation are expected in April 2023. In the meantime, joint investigations were developed. The MBI group conducted transient absorption experiments at the facilities in Strasbourg on aminoazobenzene molecules in a continuation of the time-resolved photoelectron spectroscopy data previously obtained at the MBI. The main focus of these studies is the investigation of the solvent influence on the dynamics of the switches, in particular the p*H* and viscosity. The results are currently under evaluation and will be complemented by further TRPES measurements. The TRPES of biomimetic switches NAIP and HDIOP, as well as the oxyindole-based switches of the group of B. Feringa have been attempted. The experimental campaign, however, was delayed, because the protocols for working with these new samples had to be

developed. In the meantime, a new collaboration with S. Gozem (GSU) was established. The ab initio calculations of S. Gozem compare with the previously measured static spectra of NAIP and HDIOP and emphasize the importance of proper description of solvation including counterions. Publication of the results is underway.

Further activities in the project include collaboration with the Institute for Zoo- and Wildlife (IZW) research and the Immunology institute of Free University of Berlin. The topic of collaboration is investigation of the non-linear interaction of laser radiation with living organisms, such as cells or common worm parasites. In 2019 a femtosecond laser laboratory was temporarily established at IZW. In 2022 a new assay for analysis of the viability of larvae was developed with small contributions from the MBI (mostly by the FU partners). In 2022 a scaling of the method was conducted to allow larger output of the treated eggs and larvae, which will facilitate application of statistical analysis and, after further development, application of the treated eggs to animals. The MBI is responsible for the optical parts of the project, while all biological applications are pursued by the IZW and FU groups.

Own Publications 2022 ff

(for full titles and list of authors see appendix 1)

CWB22: M.-A. Codescu *et al.*; in *Ultrafast Phenomena 2022*, F. Légaré, T. Tahara, J. Biegert, T. Brixner, and N. Dudovich (eds.) (Optica Publishing Group, Montreal, Quebec, Canada, 2022) Tu1A.4/1-2

EKL22a: M. Ekimova *et al.*; Angew. Chem. Int. Edit. **61** (2022) e202211066/1-9

EKL22b: M. Ekimovaat *et al.*; Angew. Chem. **134** (2022) e202211066/1-10

EWK22a: S. Eckert *et al.*; Angew. Chem. Int. Edit. **61** (2022) e202200709/1-7

EWK22b: S. Eckert *et al.*; Angew. Chemie **134** (2022) e202200709/1-8

KMB22a: A. Kundu *et al.*; in *Ultrafast Phenomena 2022*, F. Légaré, T. Tahara, J. Biegert, T. Brixner, and N. Dudovich (eds.) (Optica Publishing Group, Montreal, Quebec, Canada, 2022)

KMB22b: A. Kundu *et al.*; ACS Phys. Chem Au **2** (2022) 506-514

KWZ22a: C. Kleine *et al.*; in *Ultrafast Phenomena 2022*, F. Légaré, T. Tahara, J. Biegert, T. Brixner, and N. Dudovich (eds.) (Optica Publishing Group, Montreal, Quebec, Canada, 2022) M2A.4/1-2

KWZ22b: C. Kleine *et al.*; Phys. Rev. Lett. **129** (2022) 123002/1-7

SVN22: M. B. Soley *et al.*; J. Phys. Chem. Lett. **13** (2022) 8254-8263

WHZ22: M.-O. Winghart *et al.*; in *Ultrafast Phenomena 2022*, F. Légaré, T. Tahara, J. Biegert, T. Brixner, and N. Dudovich (eds.) (Optica Publishing Group, Montreal, Quebec, Canada, 2022) Th4A.6/1-2

ZKE22: J. Zhang *et al.*; J. Phys. Chem. Lett. **13** (2022) 4447-4454

ZKH22: Z.-Y. Zhang *et al.*; in *Ultrafast Phenomena 2022*, F. Légaré, T. Tahara, J. Biegert, T. Brixner, and N. Dudovich (eds.) (Optica Publishing Group, Montreal, Quebec, Canada, 2022) Th4A:29/1-2

Own Publications submitted

ARF: N. Acharyya *et al.*; Phys. Rev. Research

CKW: M.-A. Codescu *et al.*; J. Phys. Chem. Lett.

Invited Talks at International Conferences

(for full titles see appendix 2)

T. Elsaesser; Workshop ‘Advances of Multidimensional Vibrational Spectroscopy in Water, Biology, and Materials Science’ (Telluride, CO, USA, virtual, 2022-07)

T. Elsaesser; Nobel Symposium 173 ‘Exploring complex molecular and condensed phase processes and functions by multidimensional spectroscopy from THz to X-rays’ (Baståd, Sweden, 2022-08)

T. Elsaesser; 2nd European Symposium on Ultrafast Laser-Driven Biophotonics (Jena, Germany, 2022-09)

B. P. Fingerhut; Undergraduate Research Conference on Molecular Sciences (URCUP) (Kloster Irsee, Germany, 2022-10)

E. T. J. Nibbering; Ultrafast X-Ray Science@SXL (Stockholm, Sweden, 2022-06)

3.2: Solids and Nanostructures: Electrons, Spins, and Phonons

C. von Korff Schmising, S. Sharma, and M. Woerner (project coordinators)
and V. Bender, M. Borchert, K. Busch, J. R. Cardoso de Andrade, V. DeMichele, P. Elliot, T. Elsaesser, A. Ghalgaoui, R. Grunwald, M. Hennecke, S. Jana, P. Jürgens, T. Kang, Q. Li, A. Mermillod-Blondin, T. Noll, A. Perez-Leija, B. Pfau, L. Rammelt, K. Reimann, J. Richter, M. Runge, P. Scheid, D. Schick, P. Singh, S. Shallcross, T. Sidiropoulos, N. Singh, P. Singh, R. Smith, F. Steinbach, N. Stetzuhn, K. Taehee, J. W. Tomm, K. Tschernig, K. Yao

1. Overview

This project addresses ultrafast and nonlinear phenomena in solids and nanostructures. In correlated condensed-matter systems, interaction of electrons, phonons and spins lead to a broad range of novel and unusual phenomena, which are interesting both from a fundamental as well as applied research perspective. To gain new insight into microscopic phenomena in this field of research, experiments are performed with ultrafast time resolution and in a very wide spectral range extending from terahertz to X-ray frequencies. The work includes studies in the regime of nonperturbative light-matter interactions.

Our basic research is complemented by studies of light-matter interactions in materials processing with ultrashort optical pulses and by work on optoelectronic materials and devices. The project includes five topics.

2. Topics and collaborations

Research in this project has been structured into five major topical directions:

T1: Nonlinear THz and mid-infrared spectroscopy
(DFG WO 558/14-1)

Cooperation partners are K. Biermann, Paul-Drude-Institut, Berlin, C. Flytzanis, Ecole Normale Supérieure, Paris, France, A. Tkatchenko, University of Luxembourg, G. Cassabois and B. Gil, Université de Montpellier, France, M. Lazzeri, Sorbonne, Paris, France, G. Fugallo, Université de Nantes, France, M. Fiebig, ETH Zürich, Switzerland.

T2: Material modification with femtosecond laser pulses
(SAW LAPTON, DFG-ANR NA 1102/3-1, SFB 1477 LiMatI.)

Collaborations: Thomas Fennel (University of Rostock, Germany), Gunnar Bottger (Fraunhofer IZM, Berlin, Germany) Razvan Stoian and Jean-Philippe Colombier (LabHC, Saint-Etienne, France), Peter Balling (University of Aarhus, Denmark).

T3: Optoelectronic devices

Main subjects of the experimental work in this topic are optoelectronic materials and devices based on semiconductors. This includes diode lasers, light emitting diodes (LED), and semiconductor-based gain materials such as ZnSe:Cr^{2+}+Fe^{2+}.

InGaN-based diode lasers are studied together with W. Trzeciakowski from UNIPRESS Warsaw. A new concept of quantum wells (QWs) called “wide QWs” was analyzed in detail.

AlGaN-based UV-LEDs as well as InGaAs semiconductor structures designed for the infrared region were explored with scientists such as J. Ruschel, S. Einfeld and M. Weyers of the Ferdinand-Braun-Institut Berlin.

T4: Magnetism and transient electronic structure

Cooperation partners are various principal investigators within the Collaborative Research Center TRR 227 “Ultrafast Spin Dynamics” (MBI projects: A02, A04). Furthermore, we collaborate with M. Ramsteiner and J. M. J. Lopes, Paul-Drude-Institut, Berlin, J. Lüning, HZB, Berlin, S. Bonetti, Stockholm University, Uppsala University, Sweden, Flavio Capotondi, FERMI, Trieste, Italy, Christian Gutt, University Siegen, M. Albrecht, Augsburg University, E. K. U. Gross, MPI Halle, M. Schultze, TU Graz, Austria, M. Münzenberg, Greifswald University.

T5: Joint HU-MBI Group on Theoretical Optics

Projects: within the DFG-SPP-1839 “Tailored Disorder”, project Bu 1107/10-1, Bu 1107/10-2 “Light-path engineering in disordered waveguiding systems” and Bu 1107/12-2 “Non-Markovian continuous-time quantum random walks of multiple interacting particles”.

Cooperation partners: W. Pernice, University of Münster, A. Szameit, University of Rostock, N. A. Mortensen, University of Southern Denmark, R. de Jesus Leon-Mortiel, Universidad Nacional Autonoma de Mexico, and S. Linden, University of Bonn.

3. Results in 2022

T1: Nonlinear THz and mid-infrared spectroscopy

In 2022, we extended our recent study of coherent underdamped polarons in water to various liquid alcohols [SZG22a]. After femtosecond generation of solvated electrons in alcohols of varying polarity by means of femtosecond 800 nm pulses, we observe long-lived coherent polaron oscillations of longitudinal character, which modulate the terahertz (THz) dielectric properties of the liquids and give rise to THz emission.

The electron solvated in polar liquids represents an archetypal quantum system in condensed matter physics, physical chemistry and radiology. It resembles in many

aspects a single particle localized in a self-consistent potential well. While single-particle pictures, e.g., the established cavity model, account for properties such as the optical absorption band of the electron, collective electronic and nuclear degrees of freedom and their dynamics have remained essentially unexplored. Very recently, we reported the first evidence for polaronic many-body excitations in water, clearly showing the existence of hybrid modes of electronic and vibrational character. In 2022, we extended this study, i.e., we demonstrated the broad relevance of polaron excitations in polar liquids through a systematic and comparative study of such many-body excitations in water and alcohols of different polarity.

The experiments make use of two-color two-dimensional (2D) spectroscopy with an optical excitation pulse and a THz probe pulse which is detected by electro-optic sampling in an amplitude- and phase-resolved way. The excitation pulse generates free electrons by multiphoton ionization of solvent molecules. Such electrons undergo an ultrafast relaxation process to their localized ground state. The THz pulse maps the resulting nonlinear response of the excited liquid as a function of pump-probe delay τ and real time t, the latter being the temporal coordinate along which the THz field is measured. A gravity-driven liquid jet of isopropanol (IPA), ethylene glycol (EG) and water (H2O) serves as sample to avoid artefacts from windows. The sample is excited with 65 fs 800 nm pulses to generate electron concentrations between 1 and 100 µM. The THz pulse with a spectral maximum around 0.7 THz and a duration of ~1 ps is transmitted through the sample and recorded by free-space electrooptic sampling. The nonlinear THz signal is given by $E_{NL}(t,\tau) = E^{ex}_{pr}(t,\tau) - E_{pr}(t)$, where $E^{ex}_{pr}(t,\tau)$ and $E_{pr}(t)$ are the THz electric fields transmitted through the sample with and without excitation.

Figure 1(a) displays the nonlinear-signal field $E_{NL}(t,\tau)$ as a function of real time t and delay time τ for an electron concentration c_e = 70 µM in IPA. A Fourier transform of the transmitted pulses $E^{ex}_{pr}(t,\tau)$ and $E_{pr}(t)$ along real time

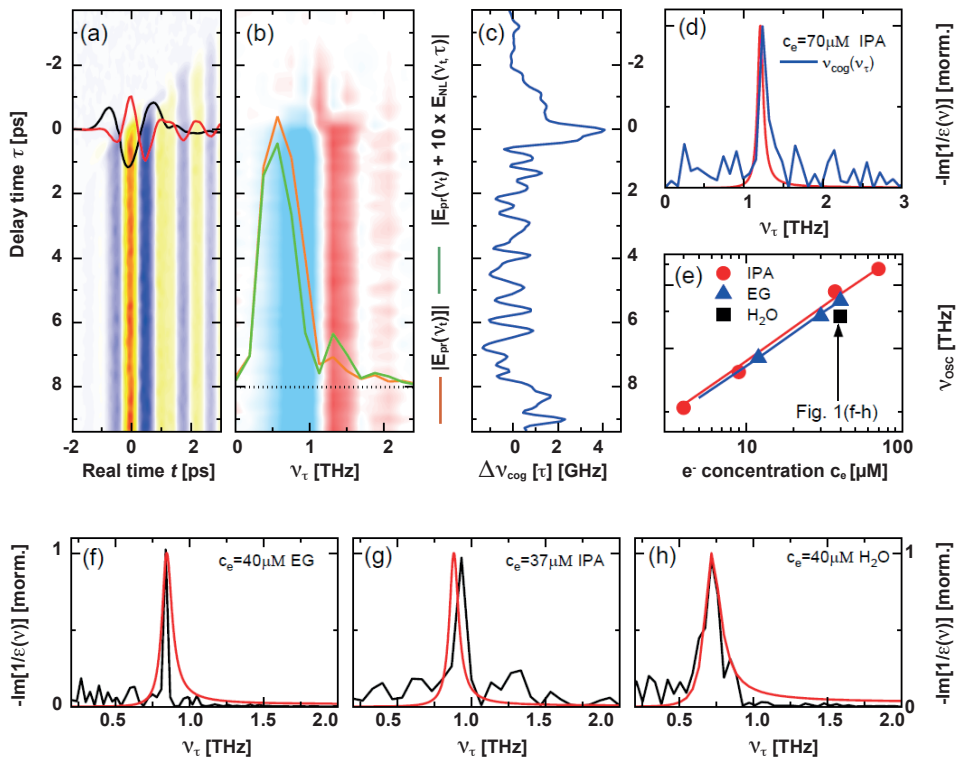

Fig. 1:
(a) 2D scan of the nonlinear signal field $E_{NL}(t,\tau)$ along real time t and pump-probe delay τ for an electron concentration c_e = 70 µM in IPA. Black solid line: Cut of probe pulse transmitted through the unexcited sample. Red line: Cut of $E_{NL}(t,\tau)$ at τ= 0. (b) Orange curve: Amplitude spectrum $|E_{pr}(\nu_t)|$ of the transmitted probe pulse without excitation. Green curve: Amplitude spectrum $|E_{pr}(\nu_t) + 10 \times E_{NL}(\nu_t, \tau = 8ps)|$ with a calculated tenfold enhancement of the nonlinear signal. Contour plot: difference spectrum $\Delta E_{pr}(\nu_t, \tau) = |E^{pu}_{pr}(\nu_t, \tau)| - |E_{pr}(\nu_t)|$. (c) Blue line: transient center of gravity $\Delta\nu_{cog}(\tau)$ calculated from Eq. (1). (d) Blue curve: Fourier transform of $\Delta\nu_{cog}(\tau)$ from (c) taken between τ = 1 ps and 9 ps. Red curve: Theoretical curves for the dielectric function $-\mathrm{Im}[1/\varepsilon(\nu,c_e)]$ for c_e = 70 µM IPA calculated from the Clausius-Mossoti model. (e) Polaron frequency as a function of electron concentration c_e for IPA, EG and H2O (symbols). The solid lines are calculated from the Clausius- Mossotti analysis. (f)-(h) Black curves: Fourier transforms of $E_{osc}(0,\tau)$ for comparable concentrations ($c_e \approx$ 40µM) of electrons in EG, H_2O and IPA. Red curves: Theoretical results for the dielectric function $-\mathrm{Im}[1/\varepsilon(\nu,c_e)]$ at the respective electron concentration c_e.

t yields the amplitude spectra $|E^{ex}_{pr}(\nu_t, \tau)|$ and $|E_{pr}(\nu_t, \tau)|$. The amplitude spectrum of the nonlinear signal is given by $\Delta E_{pr}(\nu_t, \tau) = |E^{pu}_{pr}(\nu_t, \tau)| - |E_{pr}(\nu_t)|$ shown as a contour in Fig. 1(b). As a function of τ, $\Delta E_{pr}(\nu_t, \tau)$ consists of a step-like kinetics, arising from the long-lived changes the presence of solvated electrons causes in the THz absorption of the liquid. A probe spectrum calculated with a ten-fold enhancement of the nonlinear signal (green line, τ = 8 ps) illustrates the amplitude decrease, i.e., enhanced absorption, observed below ν_t = 1.1 THz, and an amplitude enhancement/absorption decrease above. The step-like kinetics is superimposed by oscillations as a function of τ, most clearly visible around ν_t = 2 THz.

For a uniform analysis of the oscillatory signals observed in the different liquids for a wide range of electron concentrations c_e, we define the transient center of gravity (cog) of the transmitted probe spectrum according to

$$\nu_{cog}(\tau) = \int \nu_t \, |E^{ex}_{pr}(\nu_t, \tau)| d\nu_t \, / \int |E^{ex}_{pr}(\nu_t, \tau)| d\nu_t \qquad (1)$$

The quantity $\Delta\nu_{cog}(\tau) = \nu_{cog}(\tau) - (\nu_{cog})_{pr}$ [$(\nu_{cog})_{pr}$ is the cog of the probe pulse transmitted through the unexcited sample] is plotted in Fig. 1(c) (blue line) and displays pronounced oscillations. The Fourier spectrum of such long-lived oscillations [Fig. 1(d)] peaks at 1.2 THz. The same method of analysis was applied to a large data set recorded with electrons solvated in EG, IPA and H2O, which display a very similar transient THz response. Figures 1(f)–(h) show results for these liquids at a similar electron concentration $c_e \approx 40$ µM. The experimentally observed frequencies as a function of c_e are shown in Fig. 1(e).

The oscillatory signals are due to coherent oscillations of polaron wavepackets, which are impulsively excited by the ultrafast relaxation of photogenerated electrons to their localized ground state. For an analysis of the oscillation frequencies, we apply a Clausius-Mossotti model of the frequency dependent complex dielectric function $\varepsilon_{solvent}(\nu, c_e)$. The calculations reproduce the observed oscillation frequencies in a wide range of electron concentrations [solid lines in Fig. 1(e)] and, thus, reveal the longitudinal character of the polarons. The red curves in Figs. 1(d) and (f) to (h) show the imaginary part of the inverse dielectric function $-\mathrm{Im}[1/\varepsilon_{solvent}(\nu, c_e)]$, which governs the spectral profile of the polaron resonances. The long decoherence times of the polaron oscillations reveal a weak coupling of longitudinal excitations to the transverse low-frequency excitations of the liquid. At the molecular level, polaron formation is caused by the long-range Coulomb interaction between an excess electron and several thousands of polar solvent molecules.

T2: Material modification with femtosecond laser pulses

The interaction of ultrashort pulses (i.e. with a sub-ps duration) with the surface of solid dielectrics may produce periodic nanostructures (the so-called LIPSS) or, when the fluence exceeds a few J/cm², in direct ablation. Recently, we have demonstrated that it is possible

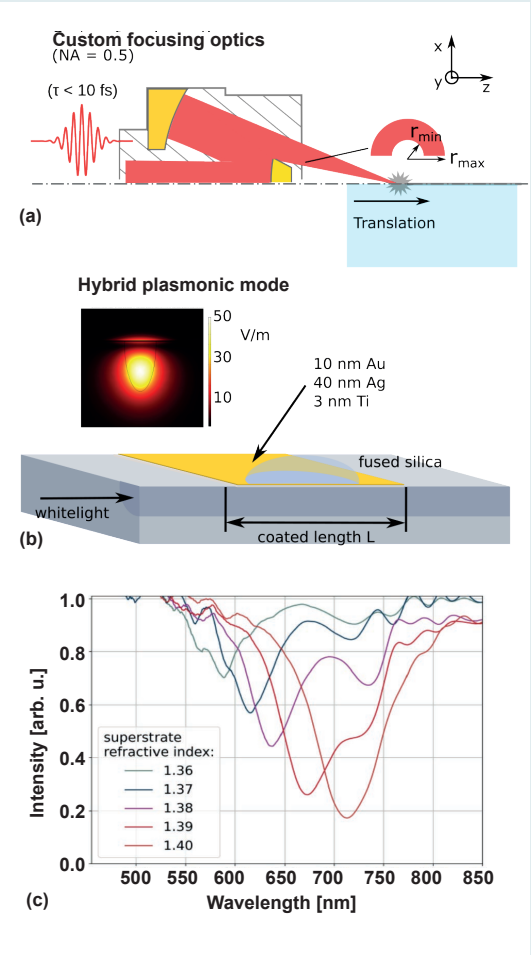

Fig. 2:
Demonstration of plasmonic sensing relying on a surface waveguide photoinscribed in fused silica. (a) Experimental setup for the photoinscirption process (b) Schematic description of the plasmonic sensor. (c) Spectral transmittance of the microsensing platform as a function of n_{sup}, the refractive index of the superstrate.

to induce surface microcompaction by using few-cycle laser pulses (with a <10 fs duration). Surface microcompaction occurs when the few-cycle pulses are focused tightly (i.e. with a numerical aperture close to 0.5) in a grazing incidence scheme (see Fig. 2 (a)). Upon continuous irradiation and translation of the sample in the direction of the laser beam, we were able to fabricate optical waveguides onto the surface of a (pure) fused silica substrate. The eigenmodes of the optical microstructures include an evanescent component which is localized near the air/glass interface (i.e. the region of space defined as the superstrate). The resonant conditions evolve with the refractive index of the superstrate (n_{sup}) and influences the mode formation. This effect can be exploited to perform evanescent field sensing. Evanescent field sensing usually offers an excellent sensitivity but only in a reduced sensing range located near the effective modal refractive index (ca. 1.46 here). In our experiments, by contrast, we propose to use the surface waveguides as a platform for plasmonic sensing, with the goal to extend the sensing range. The su-

perstrate is coated with a plasmonic stack composed of an adhesion layer (Ti, 3 nm thick), a 40 nm thick silver layer and a 10 nm thick gold layer (with the goal to prevent corrosion of the Ag layer) and the evanescent component of the mode is exploited to excite a surface plasmon polariton (SPP) wave. In Fig. 2 (b), we show the experimental setup employed as well as the structure of the (hybrid) mode predicted numerically (with the help of Comsol). The energy consumed in the excitation process is removed from the propagating field and a (spectral) dip appears at the frequency of the SPP excitation. Here, just as in the evanescent sensing scenario, the excitation conditions depend on the refractive index of the superstrate and it is possible to establish an unequivocal relationship between the position of the dip and n_{sup}. An experimental characterization of the transfer function is shown in Fig. 2 (c). We emphasize that (i) the sensing range spans over 0.04 refractive index units (RIU), (ii) there is a clear relation between the position of the 'plasmonic' dip and n_{sup}, and (iii) such a micro-integrated sensing platform exhibits a sensitivity as high as 4230 nm/RIU in the refractive index range 1.38 to 1.40.

As an outlook, these characteristic can be improved and tailored by optimizing the nature (materials and thicknesses) of the plasmonic stack.

T3: Optoelectronic devices

We analyze the photoluminescence (PL) kinetics of polar structures with a 25 nm $In_{0.17}Ga_{0.83}N$ QW, a so-called "wide QW" [BTM], and compare the results with reference structures with narrower QWs. A special feature of InGaN QW structures, which are widely used in diode lasers and LEDs, could make the use of "wide QWs" in devices generally very useful. For technology and cost reasons, such devices are nowadays grown on so-called c-plane substrates. These generate internal fields in the QWs, which reduce the emission efficiency via the quantum confined Stark effect (QCSE). Figure 3 (a) shows this for a conventional structure. The overlap of the wave functions in the ground states, which determines the emission efficiency, is significantly reduced by the distortion (tilt) of the band structure due to the QCSE. This effect also occurs for the lowest ground states in the "wide QWs", see (b), but the multitude of excited states above them, forming almost a continuum, should actually allow efficient optical transitions and thus enable brighter luminescence. The ps-PL experiment shown in (c) clearly confirms this thesis. Not only do the baselines (dashed lines) differ, but in the "wide QW" sample there is additional kinetics that is likely dominated by radiative recombination. The time constants are 1.5 and 8 ns at 6 and 300 K, respectively. This emission most likely originates from a set of excited states, while the ground state decays only extremely slowly on a µs-to-ms time scale, i.e. long-living charge accumulates there. We also quantify this population spectroscopically by applying short reverse voltage pulses (not shown); see [BTM]. These findings point to a possible route to improved polar device architectures.

The aging behavior of QWs in UVB-emitting (280-325 nm) devices is analyzed [RTG]. The results allow us to distinguish between the different contributions that lead to the aging of the devices. Spectrally resolved transient PL results show that the strongest reduction in the PL decay time appears 100 meV redshifted with respect to the PL peak. This suggests that aging enhances non-radiative recombination preferentially at localization sites in the QW. In conjunction with the modeling, we find that the aging-induced increase in spatial inhomogeneity of the PL is an important element of the aging process, which then directly affects the spatially integrated transient PL behavior including the experimentally observed PL decay time.

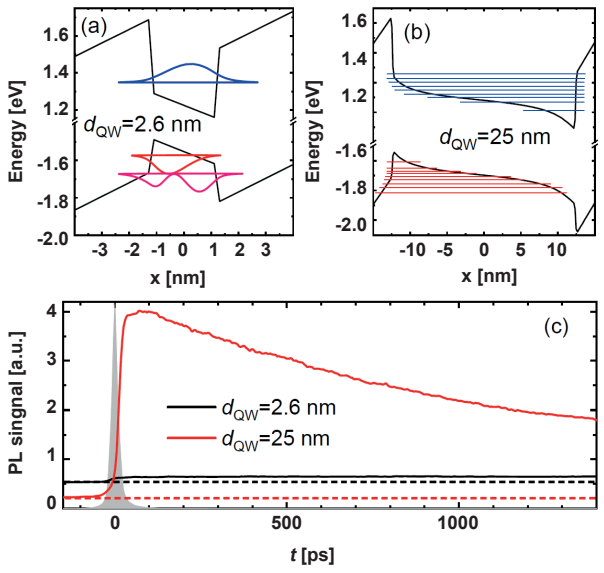

Fig. 3:
Energy band diagram with QW energy levels calculated (a) for the reference sample with a QW width d_{QW}=2.6 nm (including wavefunctions) and (b) the "wide" QW sample with d_{QW}=25 nm. The spatial extension of the wave function in growth direction is represented here by the width of the levels (red and blue lines). (c) Original PL transients vs. temperature for the two samples. The baselines are dashed. The gray shaded curve represent the impulse response function of the streak camera measured with the 100-fs excitation pulses.

We study the $Cr^{2+} \rightarrow Fe^{2+}$ energy transfer in co-doped ZnSe:$Cr^{2+}Fe^{2+}$ [FTG22, STF,TSF], which is a potential active element in novel solid-state lasers emitting in the 2-5 µm infrared spectral region. PL kinetics as well as PL intensities measured upon resonant and indirect excitation are taken and interpreted. The observed $Cr^{2+} \rightarrow Fe^{2+}$ transfer is significantly more efficient than predicted by elementary excitation transfer theory. On the other hand, our analysis also indicates a strong influence of non-radiative losses at excited Fe^{2+} ions, which decrease the overall PL quantum yield to less than 4 %. Strategies to address this problem for practical laser applications involve cooling of the ZnSe:$Cr^{2+}Fe^{2+}$ laser crystals..

T4: Magnetism and transient electronic structure

Magnetic functionality often emerges via the interaction of elements with distinct properties in complex magnetic systems, such as multicomponent alloys or heterostructures. In femtomagnetism, a prominent example is all-optical switching in rare-earth transition metal systems, where excitation with a single femtosecond laser pulses leads to the deterministic reversal of the magnetization direction. Of further great interest are systems with large magnetic anisotropies, based on 3*d* transition and 5*d* heavy metals, such as Co/Pt multilayers or FePt nanoparticles. These systems are characterized by an *intrinsic* magnetic 3*d* and an *induced* 5*d* moment caused by band hybridization between neighboring Co/Fe and Pt atoms. For the exploration and further development of new material properties that arise via a non-equilibrium, transient state of matter, a thorough understanding of the microscopic processes is essential. Therefore, we have continued to apply and to develop magnetic circular dichroism (MCD) techniques in the extreme ultraviolet (XUV) spectral range as well as all-optical Kerr and Faraday microscopy to probe transient magnetization on an ultrafast time scale. Our experiments are guided by state-of-the-art time-dependent density functional theory.

Magneto-optical observables in the XUV spectral range

In 2022, we have increased our efforts to establish a more complete understanding of the magneto-optical observables in the XUV spectral range, giving access to element-specific magnetization. In particular, we investigated how magnetic information is encoded within the reflected intensity off a magnetic thin film. We emphasize that such work is the crucial prerequisite to connect experiment to theory and predictions on microscopic processes during ultrafast demagnetization. Surprisingly, such systematic studies are still largely missing in current literature. We were able to show that reflection of broadband radiation around core to valence band transitions can yield accurate information on nanometer depth dynamics in magnetic films [HSS22]. We explored under which circumstances the relationship between magnetization and observable becomes highly counterintuitive and nonlinear. We were able to identify previously unknown experimental geometries, greatly extending the range of systems that can be studied. Using linearly polarized light, we identified substantial magnetic sensitivity for (i) parallel alignment between polarization and magnetization as well as (ii) for out-of-plane magnetization directions. Finally, we demonstrated that a combination of dedicated magnetic scattering simulations and time resolved measurements, allows a very accurate assignment of different elemental contributions [KJY]. This is of par-

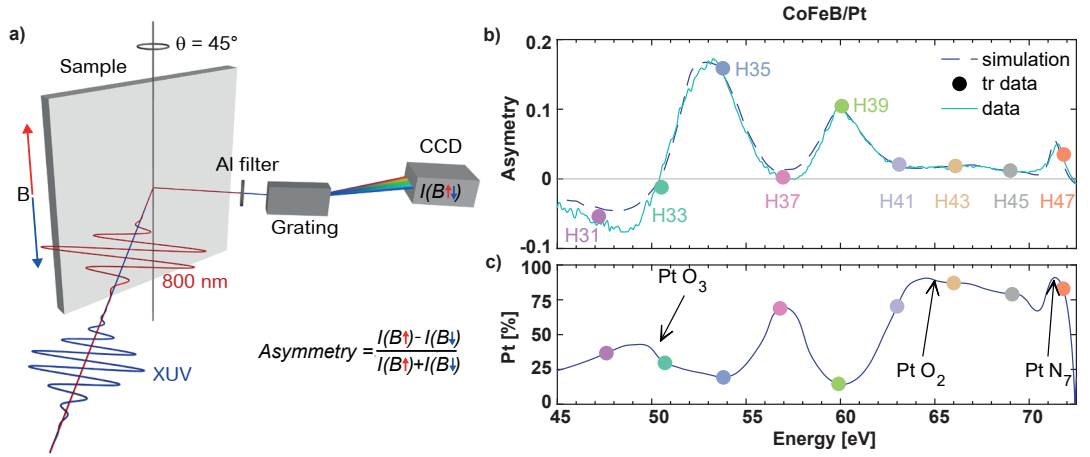

Fig. 4:
Geometry of the experiment: broadband, p-polarized XUV radiation is reflected off the sample and then dispersed by a grating and detected by a CCD camera. The magnetic asymmetry, A, is defined as the normalized difference between two opposite magnetization directions set by external magnetic field, B. b) Measured and calculated magnetic asymmetry as a function of photon energy for a CoFeB/Pt bilayer. The colored dots mark the photon energies where time resolved data was measured. H35 and H39 predominately measure the Fe (80%) and Co (85%) magnetic moment at their respective $M_{2,3}$ resonances. c) Relative sensitivity to the interfacial magnetization of Pt due to the Pt $O_{2,3}$ and Pt N_7 edge. The largest contribution of Pt to the asymmetry is found around H47. Adapted from [KJY].

ticular importance as in the XUV spectral range, resonances tend to be broad and closely spaced, often leading to a substantial spectral overlap.

Ultrafast dynamics of induced and intrinsic magnetic moments

Disentangling the different elemental contributions to ultrafast magnetization dynamics was crucial in an experiment, where we systematically investigated how *intrinsic* and *induced* moments in a CoFeB/Pt bilayer behave upon femtosecond, optical excitation [KJY]. In Figure 4, we show the geometry of the experiment: *p*-polarized XUV pulses are incident on the magnetic film at an incident angle of 45°, close to the Brewster condition, reflected, dispersed by a grating and then detected by a CCD camera. We toggle the magnetization of the CoFeB/Pt bilayer by applying an external magnetic field, *B*, aligned perpendicular to the XUV polarization, facilitating the transverse magneto-optical Kerr Effect (T-MOKE) geometry. Here, the experimental observable is defined as the normalized difference between the reflected intensity for the two antiparallel magnetization directions and denoted as magnetic asymmetry, *A*. In Fig. 4 (b), we show the measured and simulated asymmetry as a function of photon energy and additionally mark the position of the HHG emission peaks, H31 to H47, for which we performed time resolved experiments. H35 and H39 predominately probe the $M_{2,3}$ edge of Fe and Co at 54 eV and 60 eV, respectively. The relative elemental contribution of the *induced* moment of Pt is caused by its $O_{2,3}$ and N_7 edge and are shown in panel (c). We can identify photon energies that exhibit a strong mixture of Co/Fe and Pt and spectral regions where Pt dominates the response. We emphasize that the quantitative separation of the different elements Co, Fe and Pt relies on careful magnetic scattering simulations and knowledge of the respective atomic and magnetic form factors.

In Figure 5, we show the ultrafast magnetic asymmetry at three selected photon energies, reflecting predominately the dynamics of Fe, Co and Pt moment. While the Fe and Co moments exhibit a very similar behavior, Pt demagnetizes much more efficiently and loses its moment already within ~200 fs. Such distinct dynamics between *intrinsic* and *induced* moment is a priori surprising and hence presents an opportunity to test current microscopic models of femtomagnetism. We suggest two explanations: first, enhanced spin-flip probabilities due to the higher spin-orbit coupling localized at the heavy metal Pt compared to Fe and Co, and second a potentially emerging incoherent magnon population within the ferromagnetic CoFeB film that has been predicted to result in an overproportional reduction of the *induced* magnetic moment of Pt. The latter hypothesis is interesting, because it would imply that our experiment presents a novel approach to differentiate between spin-flip processes and spin wave excitations, associated with the Stoner versus Heisenberg model of ferromagnetism. Closer inspection of Fig. 5 shows that the response of Co/Fe and Pt only diverge after approximately 50 fs, which may then be interpreted as the time scale on which spin wave excitations emerge. We anticipate that combining time-dependent density of state calculations with experiments reaching a significantly improved

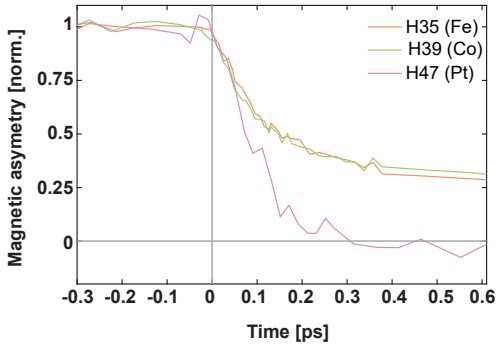

Fig. 5:
Magnetic asymmetry of a CoFeB/Pt bilayer as a function of time after optical excitation. While the intrinsic moments of the magnetic layer Co and Fe exhibt identical demagnetization dynamics, the induced interfacial dynamics of Pt demagnetizes significantly more efficiently. Adapted from [KJY].

temporal resolution, one may be able to disentangle the different microscopic processes in the time domain.

Femto-Phono-Magnetism

In most of the works on ultrafast spin dynamics, the lattice plays the vital role of an energy and momentum reservoir into which the angular momentum lost due to demagnetization is transferred. The importance of the lattice in demagnetization suggests that it could also provide a route to directly control spin dynamics via excitation of phonon modes before the laser pulse induces the spin dynamics.

In our recent work [SSE22c], we show that coupling phonon excitations of the nuclei to spin and charge leads to femto-phono-magnetism, a powerful route to control magnetic order at ultrafast times. With state-of-the-art theoretical simulations of coupled spin- charge- and lattice-dynamics, we identify strong non-adiabatic spin-phonon coupled modes that dominate early time spin dynamics. Activating these phonon modes, leads to an additional (up to 40 % extra) loss of moment in FePt occurring within 40 femtoseconds of the pump laser pulse (see Fig. 6). Underpinning this enhanced ultrafast loss of spin moment we identify a physical mechanism in which minority spin-current drives an enhanced inter-site minority charge transfer, in turn promoting increased on-site spin flips. Our finding demonstrates that the nuclear system, often assumed to play the role of an energy and angular momentum sink, when selectively pre-excited can play a profound role in controlling femtosecond spin-dynamics in materials.

T5: Joint HU-MBI Group on Theoretical Optics

In 2022, research in T5 has been concerned with the development of nonlinear material models for plasmonic systems and the development of novel concepts for

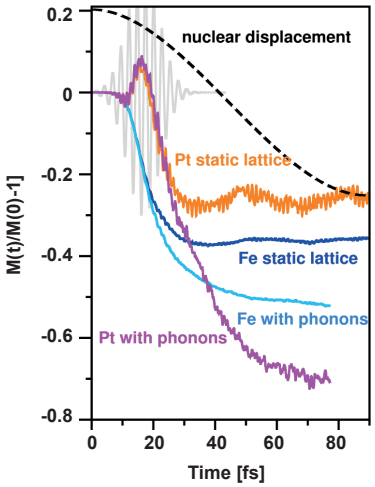

Fig. 6:
Normalized atom-resolved spin moment as a function of time (in fs) in laser pumped FePt, with the vector potential of the laser pulse shown in grey. Spin dynamics calculations are performed both for full nuclear dynamics (i.e. including both pre-excitation of the phonon and forces generated on the nuclei by momentum transfer from the excited electron system) as well as in the absence of nuclear dynamics. Displacement of atoms during the phonon modes are shown with black dotted lines. Pre-exciting specific phonon modes (in-plane Pt mode in this case), strongly impacts the spin dynamics in femtosecond time-scales (See Ref. [SSE22c] for further details).

micro-resonators in integrated optical circuits, including non-Hermitian systems.

Metasurface-design with Bayesian shape-optimized scatterers

Specifically, regarding novel concepts of micro-resonators, we have addressed the question whether a uniform distribution of gain or loss can also lead to nontrivial non-Hermitian effects in linear systems, beyond just signal amplification or decay.

In fact, we have been able to demonstrate that the application of uniform gain to a symmetric photonic molecule, i.e. a system of two coupled resonances, can reverse the optical energy distribution inside the structure. For a photonic molecule composed of two coupled resonators, this translates into changing the optical energy distribution inside the resonators (see Fig. 7). For a photonic molecule formed through scattering or defect-induced intermodal coupling in a ring resonator, the applied gain, despite being uniform and symmetric, can impose a strong chirality and switch the direction of light propagation from dominantly clockwise to dominantly counter-clockwise (see Fig. 8). We have confirmed these predictions by using both coupled mode formalism and full-wave finite-element simulations. Our work establishes a different direction in the field of non-Hermitian optics where interesting behavior can be engineered not only by unbalancing the non-Hermitian parameter but also by changing its average value – a feature that was overlooked in previous works.

To further emphasize these findings, we have checked that our results indeed extend to larger systems such as those made of three coupled resonators. In fact, these results raise some important questions. For instance, several recent studies investigated localization properties in disordered non-Hermitian waveguide arrays, which fall into the class of initial value problems. In that case, the average value of the gain does have a trivial impact on the outcome; namely, it acts as an amplification factor. Our above described work indicates that the situation could be very different in a system of disordered driven-dissipative coupled resonators. In particular, the relationship between wave localization and transport properties in driven-dissipative systems under variation of average loss (or gain) values is not at all clear. Another interesting question is whether one can devise optical systems whose topological features can be controlled by applying uniform gain.

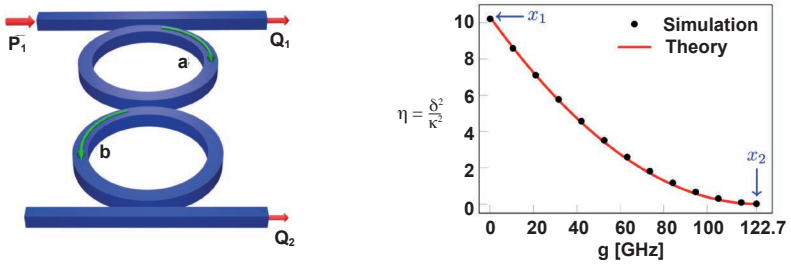

Fig. 7:
Left panel: Schematic of system of two coupled micro-cavities with two waveguide channels for excitation and collection as indicated by the red arrows. In this example, ring resonators are used but the analysis if valid for other types of resonators such as photonic crystals and coupled clockwise and counter-clockwise modes in a single ring (for the latter, see Fig. 2). Right panel: Plot of the asymmetry parameter h that characterizes the ratio of energy in resonator a to that of resonator b as a function of the uniform gain g under resonant condition. The red solid line represents the results obtained via analytical calculations based on temporal coupled-mode theory wheras the dots represent the results of full numerical computations, both for silicon-nitride based integrated optics elements. Adapted from [HBO22].

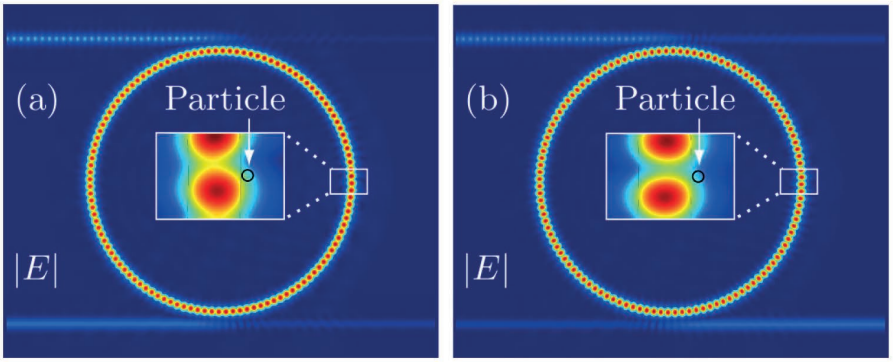

Fig. 8:
Left panel: Steady-state electric field distribution for a waveguide-coupled ring resonator with uniform gain that is excited from port P_1. This is system is conceptually similar to the system depicted in Fig. 1 – here, the presence of a nano-particle leads to a coupling between clock-wise and counter-clockwise mode. Left panel: No gain is applied (analogous to point X_1 in Fig. 1) and only 4% of the energy resides in the counter-clockwise mode, leading to a predominant out-coupling to the lower-left port. Right panel: Uniform gain is applied (analogous to point X_2 in Fig. 1) so that 92% of the energy resides in the counter-clockwise mode, leading to a predominant out-coupling to the lower-right port. Adapted from [HBO22].

Own Publications 2022 ff

(for full titles and list of authors see appendix 1)

AMI22: F. Allum *et al.*; Nat. Comm. Chem. **5** (2022) 42/1-10

BCC22: P Bonfà *et al.*; Electron. Structure **4** (2022) 024002

BDK22b: M. Belitsch *et al.*; Micro. Nano. Eng. **17** (2022) 100167/1-27

DSR22: J. K. Dewhurst *et al.*; Appl. Phys. Lett. **120** (2022) 042401/1-6

EEC22: P. Elliott *et al.*; Advanced Materials Interfaces **20** (2022) 2201233/1-9

FTG22: P. Fuertjes *et al.*; Opt. Lett. **47** (2022) 2129-2131

GRe22: A. Ghalgaoui *et al.*; Appl. Phys. Lett. **120** (2022) 162103/1-6

GSQ22: R. Gupta *et al.*; Phys. Rev. B **106** (2022) 115126/1-11

HBO22: A. Hashemi *et al.*; Phys. Rev. Res. **4** (2022) 043169

HSS22: M. Hennecke *et al.*; Phys. Rev. Research **4** (2022) L022062/1-7

JLK22a: P. Jürgens *et al.*; ACS Photonics **9** (2022) 233-240.

JLK22b: P. Jürgens *et al.*; in Ultrafast Phenomena 2022, F. Légaré, T. Tahara, J. Biegert, T. Brixner, and N. Dudovich eds. (Montreal, Quebec, Canada, 2022)

KYA22: J. N. Kirchhof *et al.*; Nano. Lett. **22** (2022) 8037-44

KZS22: A. Kimel *et al.*; J. Phys. D **55** (2022) 463003/1-64

PSD22: C. Pellegrini *et al.*; Phys. Rev. B **105** (2022) 134425/1-6

PSF22: M. Pancaldi *et al.*; J. Synchrot. Radiat. **29** (2022) 969-977

RES22: H. Rottke *et al.*; Sci. Adv. **20** (2022) eabn5127/1-20

RKB22a: M. Runge *et al.*; in Ultrafast Phenomena 2022, F. Légaré, T. Tahara, J. Biegert, T. Brixner, and N. Dudovich eds. (Montreal, Quebec, Canada, 2022)

RSE22: H. Rottke *et al.*; Physik in unserer Zeit **53** (2022) 216-217

SES22: S. Sharma *et al.*; Optica **9** (2022) 947-952

SHR22: R. Shayduk *et al.*; Appl. Phys. Lett. **120** (2022) 202203/1-5

SKE22: S. Shallcross *et al.*; Phys. Rev. B **106** (2022) L060302/1-6

SLD22: S. Shallcross *et al.*; Appl. Phys. Lett. **120** (2022) 032403/1-6

SSE22a: F. Steinbach *et al.*; Appl. Phys. Lett. **120** (2022) 112406/1-7

SSE22b: S. Sharma *et al.*; Appl. Phys. Lett. **120** (2022) 062409/1-8

SSE22c: S. Sharma *et al.*; Sci. Adv. **8** (2022) eabq2021/1-6

SZG22a: P. Singh *et al.*; PNAS Nexus **1** (2022) pgac078/1-8

SZG22b: P. Singh *et al.*; in *Ultrafast Phenomena 2022*, F. Légaré, T. Tahara, J. Biegert, T. Brixner, and N. Dudovich eds. (Optica Publishing Group, Montreal, Quebec, Canada, 2022)

WFE22: M. Woerner *et al.*; J. Phys. Chem. B **126** (2022) 2621-2634

WSM22: C. Y. Wang *et al.*; Phys. Rev. B. **105** (2022) 174509/1-13

ZJS22: D. Zahn *et al.*; Phys. Rev. Res. **4** (2022) 013104 /1-13

Submitted

KJY: C. von Korff Schmising *et al.*; Phys. Rev. Res.

RRW: M. Runge *et al.*; Phys. Rev. Lett.

RTG: J. Ruschel *et al.*; Appl. Phys. Lett.

STF: G. Steinmeyer *et al.*; Phys. Rev. Appl.

TSF: J. W. Tomm *et al.*; J. Electron. Mater.

Invited Talks at International Conferences
(for full titles see appendix 2)

S. Eisebitt; 12th Ultrafast Surface Dynamics Conference (USD12) (ICFO/Centro de Ciendias de Benasque Pedro Pascual, Spain, 2022-05)

P. Elliott; Magnetofon, Joint Meeting of Working Groups 1 & 2 (Messina, Italy, 2022-03)

P. Elliott; 5th Ultrafast Magnetism Conference (UMC 2022) (Nancy, France, 2022-09)

P. Elliott; 12th Ultrafast Surface Dynamics Conference (USD12) (ICFO/ Centro de Ciendias de Benasque Pedro Pascual, Spain, 2022-05)

S. Sharma, Paris-Saclay Ultrafast X-ray Science School, Seminar “Femto-Phono-Magnetism” (Paris-Saclay University, France, 2022-10)

S. Sharma; Theory meets XFELs (DESY, Hamburg, Germany, 2022-11)

S. Sharma; Spin Phenomena Interdisciplinary Center, SPICE- Conferene Ultrafast Antiferromagnetic Writing (Ingelheim, Germany, 2022-05)

S. Sharma; 50+2 years in science theory (Nijmegen, The Netherlands, 2022-05)

S. Sharma; MORIS (Magnetics and Optics Research Int. Symposium) (Shimane, Japan, virtual, 2022-05)

S. Sharma; Psi-k 2022 Conference (Lausanne, Switzerland, 2022-08)

T. P. H. Sidiropoulos; 12th Ultrafast Surface Dynamics Conference (USD12) (ICFO/ Centro de Ciendias de Benasque Pedro Pascual, Spain, 2022-05)

3.3: Transient Structures and Imaging with X-rays

B. Pfau, M. Woerner (project coordinators)
and M. Borchert, J. Braenzel, D. Engel, K. Gerlinger, I. González Vallejo, L.-M. Kern, C. Klose, A. Koç, C. von Korff Schmising, T. Noll, S. Priyadarshi, D. Schick, M. Schneider, H. Stiel, J. Tümmler, S. Wittrock

1. Overview

The aim of project is the development and application of XUV and X-ray sources for structure analysis and imaging with high spatial and temporal resolution down to atomic length scales and femtosecond time scale. The current applications focus on ultrafast optically induced structural dynamics as, e.g., strain waves, phase transitions, as well as transient charge and spin densities investigated with time-resolved X-ray scattering and absorption spectroscopy. A second focus is on imaging lateral spin textures in nanometer-scale magnetic materials in equilibrium and after excitation. The evaluation of new imaging techniques utilizing the light from coherent, highly brilliant soft-X-ray sources as well as the user operation of a laboratory-based X-ray microscope for the water window region are subjects of collaboration with partners from academia and industry.

2. Topics and collaborations

T1: Nanoscale imaging and spectroscopy with soft X-rays

The topic is centered around imaging, scattering, and spectroscopy to investigate nanometer-scale structures with XUV and soft-X-ray radiation produced at synchrotron-radiation sources and free-electron lasers, as well as by laser-driven laboratory sources. Part of the research in this topic is performed in the framework of the Berlin Laboratory for Innovative X-ray Technologies (BLiX) which is jointly operated by the TU Berlin and MBI (cf. Project 4.2).

Collaborations: F. Büttner (HZB, Berlin, Germany), G. S. D. Beach (MIT, USA), S. Wintz, G. Schütz (MPI-IS, Stuttgart, Germany), Y. Mokrousov, S. Blügel (FZ Jülich, Germany), C. M. Günther (ZELMI, TU Berlin, Germany), A. S. Johnson (ICFO, Barcelona, Spain), S. Wall (Aarhus University, Denmark), I. Mantouvalou (HZB, Berlin, Germany), A. Erko (IAP eV. Berlin, Germany), T. Krist (NOB GmbH, Berlin, Germany), K. Schadow (PREVAC GmbH Berlin, Germany), R. Kemmler (greateyes GmbH Berlin, Germany), H. Fiedorowicz (WAT, Warszawa, Poland), H. A. Dürr (Uppsala University, Sweden), S. Bonetti (Stockholm University, Sweden), A. Scherz (European XFEL, Hamburg, Germany), K. Höflich (FBH, Berlin, Germany).

T2: Femtosecond X-ray diffraction and absorption

Investigation of phase transitions and structural dynamics in solids, in close collaboration with projects 3.2 and 4.1..

Collaborations: Michael Horn-von Hoegen and Klaus Sokolowski-Tinten (University of Duisburg-Essen, Duisburg, Germany).

3. Results in 2022

T1: Nanoscale imaging and spectroscopy with soft X-rays

Research at x-ray free-electron lasers

One of the primary scientific topics in the MBI project 3.3 is the research of photo-induced magnetization and charge dynamics in solids on the nanometer length scale. To achieve the temporal and spatial resolution required, many of these experiments are carried out at free-electron laser sources (FEL) operated by large-scale facilities such as European XFEL (Hamburg), FERMI@Elettra (Trieste, Italy), or PAL (Pohang, South Korea). FELs deliver highly brilliant, femtosecond-long pulses of x-ray radiation with tunable wavelength allowing to specifically address electronic states and atomic magnetic moments. Researchers in topic 1 are, therefore, very active in different scientific collaboration pursuing research at FELs, leading to a number of publications in highly ranked journals in 2022.

In the work of Yao et al., we demonstrate the first time-resolved observation of all-optical magnetic switching on the nanometer scale [YSB22]. The experiment performed at FERMI is based on an elaborate pump-probe scheme where the optical excitation of the magnetic thin film is structured into a grating by interference of two inclined XUV beams and the material's response is probed by diffraction from this grating. More details on this work can be found in the highlight section of the annual report.

Another approach to introduce nanoscale magnetization dynamics is structuring the magnetic sample itself. In an experiment performed at European XFEL, an international team including researchers from MBI studied magnetic FePt nanoparticles where femtosecond laser excitation leads to the formation of spin-wave solitons in the particles [TVW22]. The spin-wave solitons are detected via diffraction from coherent phonons generated by the in-plane magnetization precession via magneto-elastic forces. In combination with micromagnetic modeling the spin-wave solitons are assigned to sub-10-nm edge modes at the boundary of the FePt particles.

Nanoscale heterogeneity also plays a role during phase transitions in solids. In 2022, an international collaboration with scientists from MBI studied the insula-

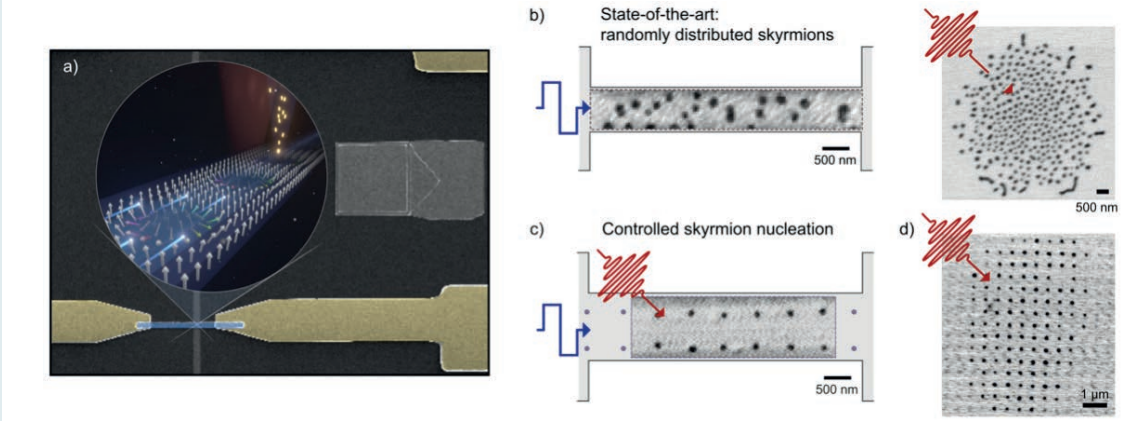

Fig. 1:
Spatial control over skyrmion creation in thin magnetic multilayer films. (a) Artistic schematic view of the approach using He-ion irradiation. Background image: pseudo-color scanning electron microscopy image showing the magnetic track in blue and gold contacts to apply an electric current. The inset sketches a racetrack with magnetic moments represented by arrows. The track is irradiated with He-ions at specific locations where later the skyrmions form induced by laser (red beam) or electric current (dots with blue tail) (b) Skyrmion creation with current or laser pulses in unstructured magnetic films, leading to random distributions. (c,d) Laser and current-induced creation of skyrmions at predefined sites using He-ion irradiation (c) or using a backside metallic mask structuring the laser excitation (d).

tor-to-metal phase transition in VO_2 on ultrashort time scales by triggering the transition with a laser pulse [JPS22b]. Using an approach to directly image the co-existing phases with additional spectral sensitivity, the researchers found that pressure plays a much larger role in the light-induced phase transition than assumed so far. While previous studies without spatial resolution have suggested the transient emergence of a truly non-equilibrium phase in the material, such exotic phases cannot be seen in the time-resolved x-ray images with nanometer resolution. Instead, the ultrafast transition within tiny regions of the sample intrinsically strains the crystal lattice locally which in turn changes the properties of the generated metallic phase. These changes remain until the strain relaxes on a time scale of 5 ps. Using hyperspectral X-ray imaging, the researchers concluded that in the case studied, the dynamics observed can be explained based on strain arguments alone, without having to postulate the existence of an exotic phase.

Nanometer spatial control of magnetic skyrmions: Generation and Motion

In recent years, great advances have been reported in generating, annihilating, and moving magnetic skyrmions in magnetic thin films. A prime tool for investigating these nano- to micrometer-scale magnetic textures is to directly image them – either with visible light or x-rays. Time-resolved imaging to study the dynamical properties of skyrmions typically requires repetitive pump-probe measurements, in order to collect the signal needed to form the images. To enable such measurements, the dynamics of the magnetic skyrmion has to be controllable and deterministic. In 2022, we have established two methods to reliably create skyrmions at desired positions in the magnetic thin film and to guide their motion – essential steps towards recording videos of moving skymions.

A first method relies on irradiation of the magnetic film hosting the skyrmions with a focused helium-ion beam to flexibly create patterns of different shapes and sizes in the magnetic material (Fig. 1(a)) [KPD22]. Importantly, this local modification with very light ions only affects the magnetic properties (in particular, the anisotropy) of the material while the film remains structurally intact. Using this approach, it is possible to predefine positions where skyrmions appear after triggering their creation with a short pulse of electrical current or laser light (see Fig. 1(c), where skyrmions are nucleated in two rows of isolated dots). In particular, the magnetic modification turns out to be gentle enough to even allow for a controlled detachment of the skyrmion from its generation site and its subsequent unimpeded motion. Moreover, by combining such a skyrmion creation site with a guiding channel, we were able to show continuous motion of a magnetic skyrmion driven by electrical current pulses over tens of micrometers back and forth in a so-called magnetic racetrack – fully suppressing any undesired sideways motion, known as the skyrmion Hall effect.

In a second approach to predefine skyrmion nucleation sites, we have designed nanopatterned reflective masks on the backside of the magnetic material [KPS22]. These masks allow to control the excitation amplitudes reached when hitting the magnetic film with a laser, resulting in nanometer-scale precision on the spatial distribution of magnetic skyrmions created (see Fig. 1(d), where skyrmions are nucleated on a square grid). As the masks are prepared on the backside of the magnetic film opposite to the laser-illuminated surface, the approach retains free frontside access to the magnetic film for, e.g., detection of the skyrmions. The application of this backside mask

approach with its unhindered access to the magnetic film can easily be transferred to other photo-induced switching phenomena in order to add nanometer control on the switched areas.

New Leibniz Junior Research Group: Following Complex Spin Structures in Time and Space

Starting in January 2023, the research portfolio of the Max Born Institute will be complemented by a new Junior Research Group led by Dr. Daniel Schick. His proposal "Following Complex Spin Structures in Time and Space" was granted an overall funding of 1.5 million euros over five years within the 2022 Leibniz "Best Minds" Competition. He will establish an independent junior research group focusing on fundamental aspects of ultrafast magnetization dynamics on the nanoscale, taking advantage of the unique opportunities provided by laser-driven soft-X-ray sources developed at MBI.

In particular, the group will utilize ultrashort laser pulses to manipulate magnetic order in technologically relevant nanostructures, which are at the heart of many current and future technologies, e.g., for storing and processing information. Gaining actual functionalities from such laser-driven processes relies on progress in the fundamental understanding of the light-induced spin dynamics on the relevant pico- to femtosecond time scales. This ultimately requires access to the transient spatial magnetization profiles, which have been hardly accessible in experiments so far. The new Junior Research Group will use resonant soft-X-ray scattering as a versatile tool that can provide the missing information, in particular, when combined with polarization-sensitive scattering simulations. The study of such complex spin structures in laser laboratories as opposed to large-scale facilities allows studying fundamental aspects of photoinduced spin dynamics in a more systematic way than before, in order to identify ultrafast and more-energy efficient pathways to control magnetic order.

T2: Femtosecond X-ray diffraction and absorption

In 2022, we performed first femtosecond x-ray diffraction experiments using the new x-ray source based on the 5 µm OPCPA laser system providing 80 fs pulses with an energy of 3 mJ at a 1 kHz repetition rate. In our first study, we performed femtosecond x-ray diffraction experiments performed on single-crystal bismuth excited by 5 µm laser pulses and complementary nonlinear THz experiments. Our results point to a new excitation quantum pathway at longer excitation wavelengths allowing for coherent phonon excitation at the X point in the Brillouin zone.

The ultrafast optical excitation response of bismuth has been intensively studied for the past decades by means of different spectroscopic techniques. This prototypical semimetal displays an A_{1g} optical phonon (i.e., full symmetry of the crystal) that, so far, has been displacively excited via interband excitation with 800 nm pulses. Such previous studies suggest a strong softening of the phonon frequency associated to this coherent mode, with a red shift from 2.9 THz down to 1 THz. A much more specific excitation below the direct band gap at the T point is possible with mid-infrared pulses, but has not been explored so far.

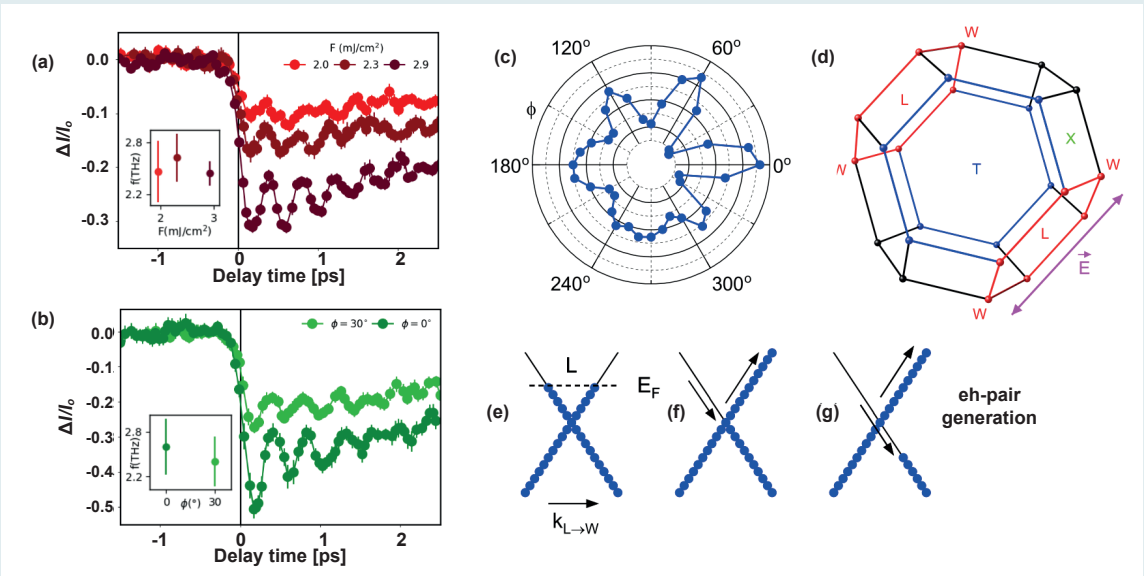

Fig. 2:
(a) Transient intensity changes of the (111) diffraction peak at different incident fluence and with a polarization angle of φ = 15° (inset: peak frequency of the oscillation). (b) Transient intensity changes at a constant incident fluence of 2.6 mJ/cm² for two different polarization angles φ (inset: peak frequency of the oscillation). (c) Azimuthal dependence of the THz pump-probe amplitude at the maximum of the trace. The radial scale is from 0.091 to 0.098. (d) Reciprocal unit cell of Bi; the basal plane is perpendicular to the [111] direction. The hexagons in red are fully parallel to the electric field. (e)-(g) Schematic electron distributions around the L points for different values of the vector potential A; (e) at A = 0, (f) at A = $E_F/(ev_F)$, and (g) for A > $E_F/(ev_F)$, which corresponds to coherently reversible electron-hole pair generation.

In this study, we present femtosecond x-ray diffraction and nonlinear THz experiments on a 45 nm bismuth thin film excited with 5 µm wavelength pulses. Our femtosecond x-ray diffractometer consists of a 5 µm OPCPA driven table-top x-ray source delivering x-ray pulses at 8 keV with a temporal resolution of 120 fs at 1 kHz repetition rate. In our measurements we track the intensity changes of the (111) diffraction peak within the first 3 ps as a function of the incident fluence and the polarization angle. The THz-pump-probe experiments were performed with single-cycle THz pulses centered at 1.2 THz and a pump electric-field amplitude of 600 kV/cm. Fig. 2(a) shows the transient intensity changes of the (111) Bragg reflection different incident fluences as indicated, with φ = 15° as the polarization angle relative to the [11-2] crystallographic direction. The transient intensity shows a fast decay followed by a coherent oscillation with a peak frequency centered at 2.6 THz. The experimentally observed oscillation does not present a softening within our experimental sensitivity (see inset). Fig. 2(b) shows the transient intensity changes at a constant incident fluence of 2.6 mJ/cm^2 at two different polarization angles φ. The amplitude of the fast intensity decrease and of the coherent oscillation are strongly dependent on φ. These results point to a new phonon excitation pathway.

In order to further explore this phenomenon, we performed THz-pump/THz-probe measurements at different polarization angles. Fig. 2(c) shows the azimuthal dependence of the signal maximum of the THz-pump pulse induced transmission change for the THz probe pulse, where a clear six-fold symmetry is observed. This polarization dependence reveals an anisotropy of nonlinear absorption, showing the highest signal when the electric field is aligned along the W−L−W path in the Brillouin zone (Fig. 2(d)). At the L point bismuth presents a small bandgap of 15 meV, with an electronic band dispersion reminiscent of a Dirac cone. This band dispersion plays a crucial role in the excitation process at 5 µm, where the interaction between the electric field and the carriers at L induces a non-perturbative electron-hole generation similar to the one observed in graphene.

This process is illustrated in Figs. 2(e)−(g): at equilibrium, with the vector potential (i.e., time integral of the driving electric field) A = 0, the valence band around the L point is fully occupied and the conduction band up to the Fermi energy E_F. As the vector potential increases to A = E_F/(ev_F) one has the situation depicted in Fig. 1(f) and for even higher A, it generates additional electron-hole pairs, as shown in Fig. 2(g). For the case shown in Fig. 2(d), there is a predominant population at the red hexagons, while for the other L valleys (black hexagons) the carrier generation is essentially zero. This asymmetric carrier distribution at the L points explains the different signal amplitudes for different φ. More importantly, this asymmetry induces a reduction of the crystal symmetry by back folding of the X point in the Brillouin zone into the Γ point, making phonons at the X point now accessible for displacive excitation. The nearly constant frequency 2.5 THz measured in our experiments at different fluences or polarization angles is fully compatible with displacive excitation of coherent phonons at the X point of bismuth's Brillouin zone. It presents a new quantum pathway of coherent optical phonon excitation which might be also present at high excitation levels for driving pulses at shorter wavelengths.

Own Publications 2022 ff

(for full titles and list of authors see appendix 1)

GJB22b: I. González-Vallejo *et al.*; Struct. Dyn. **9** (2022) 014502/1-9

GKR22a: I. González-Vallejo *et al.*; Struct. Dyn. **9** (2022) 024501/1-10

GKR22b: I. González-Vallejo *et al.*; in *Ultrafast Phenomena 2022*, F. Légaré, T. Tahara, J. Biegert, T. Brixner, and N. Dudovich (eds.) (Optica Publishing Group, Montreal, Quebec, Canada, 2022)

HSK22: N. Z. Hagström *et al.*; J. Synchrotron Rad. **29** (2022) 1454-1464

JPS22: A. S. Johnson *et al.*; in *Ultrafast Phenomena 2022*, F. Légaré, T. Tahara, J. Biegert, T. Brixner, and N. Dudovich (eds.) (Optica Publishing Group, Montreal, Quebec, Canada, 2022)

KPD22: L.-M. Kern *et al.*; Nano Lett. **22** (2022) 4028-4035

KPS22: L.-M. Kern *et al.*; Phys. Rev. B **106** (2022) 054435/1-10

KBH22: C. Klose *et al.*; Phys. Rev. B **105** (2022) 214425/1-9

MPS22b: E. Malm *et al.*; Opt. Express **30** (2022) 38424-38438

MCN22: G. Mercurio *et al.*; Opt. Express **30** (2022) 20980-20998

PGH22: S. Priyadarshi *et al.*; Phys. Rev. Lett. **128** (2022) 136402/1-6

PRW22: C. Pratsch *et al.*; Opt. Express **30** (2022) 15566-15574

SAH22: S. Staeck *et al.*; Nanomaterials **12** (2022) 3766/1-13

TVW22: D. Turenne *et al.*; Sci. Adv. **8** (2022) 0523/1-10

WPG22: M. Woerner *et al.*; in *Ultrafast Phenomena 2022*, F. Légaré, T. Tahara, J. Biegert, T. Brixner, and N. Dudovich (eds.) (Optica Publishing Group, Montreal, Quebec, Canada, 2022)

YSB22: K. Yao *et al.*; Nano Lett. **22** (2022) 4453-4458

In press (as of Jan. 2023)

CMB: J. Correa *et al.*; J. Synchrotron Rad.

HWE: C. Hauf *et al.*; in *Structural Dynamics with X-ray and Electron Scattering*, K. Amini, A. Rouzée, and M. J. J. Vrakking (eds.)

JPS: A. S. Johnson *et al.*; Nat. Phys.

KBH: C. Klose *et al.*; Nature

PEi: B. Pfau *et al.*; in *Structural Dynamics with X-ray and Electron Scattering*, K. Amini, A. Rouzée, and M. J. J. Vrakking (eds.)

Submitted

EAA: R. Y. Engel *et al.*; Phys. Rev. Lett.

GLS: K. Gerlinger *et al.*; Phys. Rev. Lett.

GPH: K. Gerlinger *et al.*; Struct. Dyn.

KGR: A. Koç *et al.*; Phys. Rev. Lett

Invited Talks at International Conferences

(for full titles see appendix 2)

S. Eisebitt; 762. WE-Heraeus-Seminar “Diffraction Limited Synchrotron Light Sources and Next Generation Free Electron Lasers” (Bad Honnef, Germany, 2022-03)

B. Pfau; 16th Meeting of GMM Working group “Materials for Nonvolatile Memories” (Dresden, virtual, 2022-03)

A. Koç; CLEO 2022 (California, USA 2022-05)

B. Pfau; The world congress on optics and photonics ICO-25 and 16th Congress of the internatinal society on optics within life sciences (OWLS) (Technische Universität Dresden, Germany, 2022-09)

B. Pfau; XFEL School for condensed matter, dense plasma physics and extreme conditions 2022 (Aussois, France 2022-10)

4.1: Implementation of Lasers and Measuring Techniques

F. Furch, U. Griebner, I. Will (project coordinators)
and M. Bock, S. Dávila Lara, C. Kleine, G. Klemz, M. Kretschmar, L. Lochner, T. Nagy, T. Noll, M. Oso-lodkov, J. Tümmler, T. Witting

1. Overview

The general goal of this project is the development of laser-based sources and optical measurement systems tailored to applications specific to the MBI or laboratories of collaboration partners.

Some of the unique OPCPA systems developed in the last few years within the institute are now ready to be implemented in particular applications. The goal within this project is to further engineer these systems and optimize their characteristics to the needs of the particular applications in Program Areas 2 and 3.

2. Topics and collaborations

T1: Lasers for particle accelerators

This topic contributes to the development of Free Electron Lasers (FELs) and other advanced accelerator-based x-ray sources by providing highly specialized photo injector drive lasers and laser systems for application experiments. This work is carried out in cooperation with the Helmholtz-Zentrum Berlin für Materialien und Energie (HZB), the Helmholtz-Zentrum Dresden-Rossendorf (HZDR) and DESY.

T2: OPCPA engineering

Several OPCPA systems in the near- and mid-infrared have been developed in the last years. The implementation of these OPCPA sources into particular experiments in Program Areas 2 and 3 requires robust, reliable and reproducible day-to-day operation of these systems. Therefore, the constant improvement and engineering of these OPCPAs is the focus of this topic. The topic is divided in three subtopics:

Terawatt OPCPA

A high-power OPCPA system that is pumped by a high-power thin-disk laser was developed and installed in the previous years. Since 2019 this OPCPA system was applied for the generation of high energy XUV pulses through high-order harmonic generation. It is capable of delivering pulses with a peak power >4 TW, having a pulse energy of 40 mJ with < 9 fs duration. The system runs at a repetition rate of 100 Hz.

Near-IR high repetition rate OPCPAs

The development of high repetition-rate non-collinear OPCPA systems (repetition rate ≥100 kHz) is the goal of this topic. Two OPCPAs have been established. A 100 kHz OPCPA that delivers carrier-envelope phase stable sub-7 fs pulses with up to 190 µJ of energy and a 400 kHz OPCPA that delivers sub-10 fs pulses with up to 10 µJ of energy. During 2022 the design of an energy upgrade for the 100 kHz OPCPA has begun, with the goal of reaching 1 mJ pulse energy. The design of the new OPCPA is carried out in collaboration with the Forsvarets Forskningsinstitutt, Norway. These OPCPA systems are intended for experiments in attosecond pump-probe spectroscopy with coincidence detection (project 2.1) and novel material processing applications (project 3.2)

Midwave-IR OPCPA driver for x-ray generation

This midwave-IR OPCPA system operates at 1 kHz repetition rate and delivers 80 fs pulses with up to 3.2 mJ of energy at a central idler wavelength of 5.0 µm. The system is pumped at 2.0 µm by a Ho:YLF CPA developed in-house. The application for this OPCPA is to serve as the driver laser for a Cu-K_α source utilized for time-resolved x-ray diffraction experiments (project 3.3).

T3: Implementation of experimental and measuring techniques

The topic is concerned with the improvement of particular technologies, experimental methods and measuring techniques and their implementation within the institute for the benefit of Program Areas 2 and 3.

3. Results in 2022

T1: Lasers for particle accelerators

This topic deals with the development and systematic improvement of photocathode lasers for linear accelerators (Linacs) of FELs, as well as with other lasers used at particle accelerators and storage rings. During 2022, we ensured proper operation of our lasers at HZDR (Rossendorf), PITZ (DESY Zeuthen), and bERLinPro (HZB Berlin). These lasers developed at the MBI are being used at these service facilities to allow for dedicated experiments and user operation.

In 2022, a large part of our work was dedicated to the improvement of the MBI laser at the MAXYMUS scanning transmission x-ray microscope (STXM) at BESSY II, where the laser pulses are transported into the STXM to allow for pump-probe experiments in conjunction with raster-scan imaging.

The initial version of this laser was designed to generate pulses at 50 MHz repetition rate and with duration comparable to the length of the BESSY bunches and

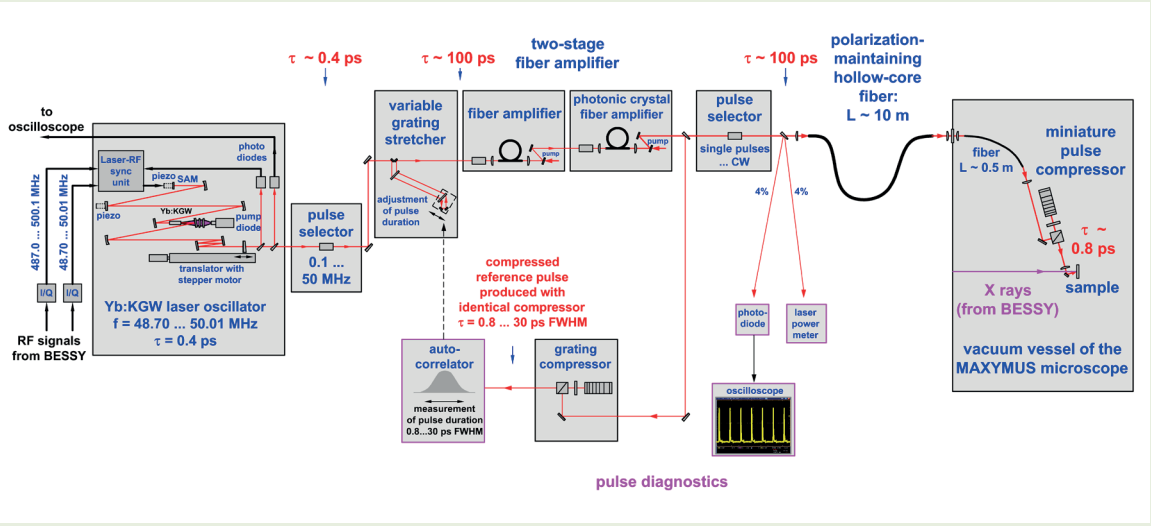

Fig. 1:
Scheme of the laser at the MAXYMUS STXM in 2022.

has been routinely used for experiments in this configuration. Novel experiments require shorter pulses (< 1 ps) with one order of magnitude higher energy than the initial setup. An additional margin in pulse energy is desired to speed up the alignment of the focusing system, in order to compensate for a reduced intensity due to the initially imperfect focussing of the laser beam.

To fit the increased demands on pulse energy, we have improved both the laser setup and the system that transfers the pulses from the laser to the sample in the vacuum chamber of the STXM.

Fig. 1 shows a scheme of the current laser setup. The laser contains an Yb:KGW oscillator synchronized to the bunches of the BESSY synchrotron. A two-stage amplifier with up to ~10 W output power increases the pulse energy by up to two orders of magnitude. Two acousto-optic modulators are used for reducing the repetition rate of the output pulses to a programmable frequency between 0.5 Hz and 50 MHz.

The main extension introduced in 2022 was a hollow-core polarization-preserving fiber that delivers the amplified laser pulses to the vacuum chamber without nonlinear perturbation.

In the vacuum chamber of the STXM, the pulses are still transmitted by a 0.5 m long standard fiber. Although this short fiber adds some moderate amount of nonlinear perturbation to the pulse, it produces a well-defined profile of the output beam, leading to a well-defined focus at the target. Finally, the pulses are compressed in a tiny Mini-Compressor (see MBI annual report 2021) to approximately 0.8 ps duration and focussed onto the sample to a spot of ~7 µm diameter.

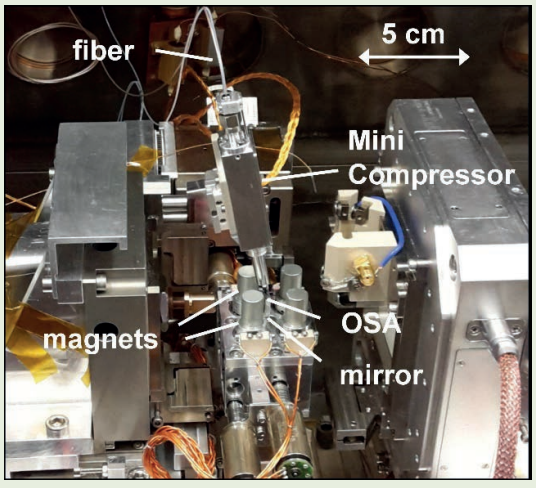

Fig. 2:
Miniature pulse compressor (cover removed) with focussing optics for the laser at the MAXYMUS magnetic microscope.

Fig. 2 shows the densely populated sample area of the STXM with the miniature pulse compressor, Order Selecting Aperture (OSA) and magnets for generating the programmable magnetic field at the sample. The laser was successfully used in two beamtimes by Projects 3.2 and 3.3 for the following experiments:

1. Demonstration of all-optical switching of magnetization in rare-earth/transition-metal alloys on the nanometer-scale based on He-ion patterning of the material or shaping of the excitation by plasmonic structures on the sample. These experiments were made possible by the installation of a hollow-core fiber, allowing the laser to operate with constant pulse duration of 0.8 ps in the full range of pulse energy.

2. Investigation of the nucleation of magnetic skyrmions in a ferromagnetic multilayer, including the first time-resolved imaging experiments on this process. Previous work in this research area which also used the laser at the MAXYMUS microscope has already been published in 2022 (see project 3.3) [KPS22, KPD22].

T2: OPCPA engineering

Terawatt OPCPA system

The major goal of this topic is the reliable supply of few-fs TW-level driver pulses for high-order harmonic generation (HHG). The description of the OPCPA amplifier setup and the application of the resulting high energy near-infrared (NIR) driving pulses for HHG have been published in [1]. A schematic setup of the high power OPCPA is shown in Fig. 3. The HHG source is capable of delivering XUV pulses centered at 25 eV with an energy >500 nJ (at the source) for the application in project 2.1; T3 and T4):

- XUV-pump XUV-probe experiments investigating XUV-driven intensity autocorrelations to further understand the underlying multiphoton multi-electron dynamics.
- time-resolved coherent diffractive imaging studies (not used in 2022).

Since the demands for the experiments changed from high pulse energy with medium repetition rate to lower pulse energy with higher repetition rate, the project will not be continued..

Near-IR high repetition rate OPCPAs

Two high repetition rate OPCPAs have been developed within this topic and utilized for different applications related to projects 1.2, 2.1, 2.2 and 3.2 in the last few years. Both OPCPAs operate at a central wavelength of 800 nm, and are seeded by ultra-broadband Ti:Sapphire oscillators. In both systems, a small fraction of the oscillator spectrum around 1030 nm is also used to seed a chirped pulse amplification (CPA) system that provides, after frequency doubling, the pump pulses for the OPCPA stages. In one OPCPA the pump pulses are provided by a CPA based on an Yb:YAG thin-disk regenerative amplifier operating at 100 kHz. The second OPCPA is pumped by a fiber-CPA operating at 400 kHz.

In 2021 the 400 kHz system, delivering sub-10 fs pulses with energy per pulse exceeding 8 µJ, was commissioned for experiments in the SAW project “On-Chip Laser written Photonic Circuits for Classical and Quantum Applications” linked to project 3.2. During 2022 the pulse duration on target was characterized utilizing a time-domain ptychography setup, and the pulse shape was optimized in order to improve the experimental results. Fig. 4 shows the results on the pulse characterization.

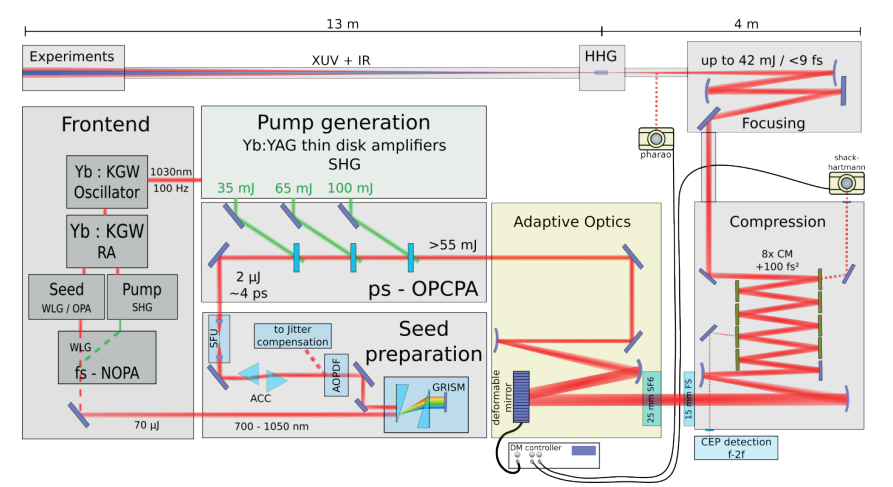

Fig. 3:
Schematic setup of the Terawatt OPCPA and HHG with the beam line to the experimental station.

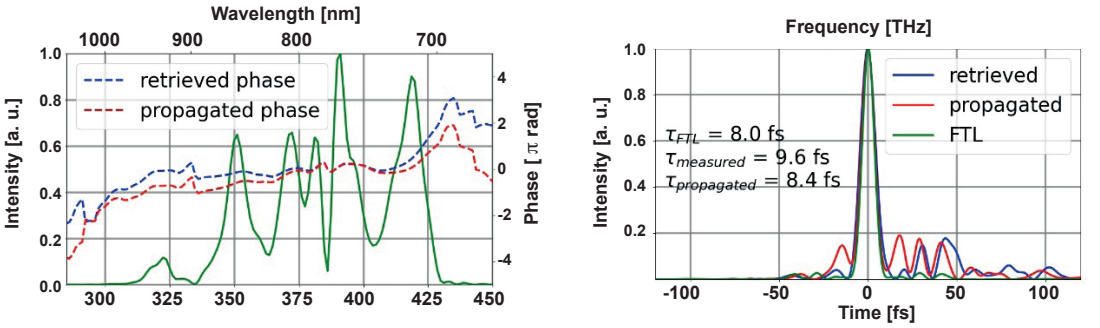

Fig. 4:
Pulse characterization in the target region of the material processing experiments. Left: Spectra and retrieved spectral phase. Right: reconstructed temporal pulse shape.

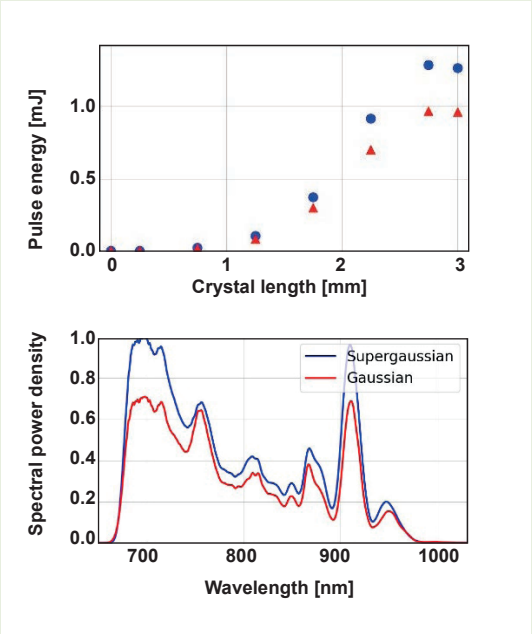

Fig. 5:
Simulations results for the 100 kHz NIR OPCPA utilizing the nonlinear propagation code Sisyfos. Top: Output energy as a function of crystal thickness. Bottom: Output spectra.

During 2022 the 100 kHz OPCPA continued to be commissioned for attosecond pump-probe experiments with electron-ion coincidence detection (see project 2.1). In addition, the preparation began for the planned upgrade of the system. With this upgrade it is intended to reach a 5-fold increase in pulse energy at the output of the OPCPA, reaching the 1 mJ level. The increase in pulse energy will enable the generation of ultrafast UV pulses at high repetition rate, in combination with XUV radiation from high harmonic generation. This will allow a new class of experiments in which ultrafast dynamics in atoms and molecules will be accessed in pump-probe experiments through single photon processes, in combination with the unique detection capabilities of a reaction microscope (electron-ion coincidence detection).

In order to achieve the targeted increase in pulse energy, a multi-pass booster amplifier based on thin-disk technology has been acquired from Trump Scientific Lasers and it will be delivered during 2023. The new amplifier will increase the energy of the existing OPCPA pump laser (before frequency doubling) from 2.3 mJ to 13 mJ (before compression) at the current repetition rate of 100 kHz. Besides small modifications to the existing laboratory infrastructure, new parametric amplification stages have to be designed. To guide the design of the OPA stages, 3D+1 nonlinear propagation simulations were performed utilizing the code Sisyfos (collaboration with Dr. Gunnar Arisholm, from Forsvarets Forskningsinstitutt, Norway). Fig. 5 shows simulation results of a two-stage parametric amplifier based on BBO crystals. The results compare the performance of the second parametric amplifier utilizing a pump delivering 1 ps pulses, 6 mJ at 515 nm with a Gaussian beam profile (red) or Super-Gaussian beam profile of order 4 (blue).

Midwave-IR high repetition rate OPCPAs

The large scale midwave-IR (MWIR) OPCPA system operating at 5 µm wavelength developed in project 1.2 was successfully implemented as driver for hard X-ray generation in 2020, its intended application in MBI's time-resolved X-ray diffraction research (see project 3.3). The system emits at a central wavelength of 5 µm and operates at a 1 kHz repetition rate. The stability and reliability of the OPCPA system was continuously improved. As a consequence, the system was virtually uninterrupted available as driver laser for the Cu-K_α source in 2022 which allowed to setup the X-ray pump-probe line. The latter was tested successfully and first X-ray pump-probe experiments are demonstrated (see project 3.3).

The experimental scheme of the laser-driven hard X-ray source operating at a 1 kHz repetition rate is shown in Fig. 6. Details of our MWIR OPCPA have been reported in [2]. The 40 MHz front-end, based on a Er:fiber laser, provides femtosecond pulses at 1.0 µm, 1.5 µm and 2.0 µm wavelength. The latter are the seed pulses for the pump whereas the 1.0 µm and 1.5 µm pulses generate the signal pulses at 3.5 µm by means of DFG. The DFG exhibits a duration of 30 fs with 0.5 pJ energy. The parametric amplifier consists of four stages which are pumped at 2.05 µm by a Ho:YLF chirped pulse amplifier system. AR-coated $ZnGeP_2$ crystals are used as nonlinear crystals in all four OPA stages. Prior to the parametric amplification, adaptive phase control of the signal pulses at 3.5 µm is conducted by a spatial light modulator. The idler spectrum covers a range from

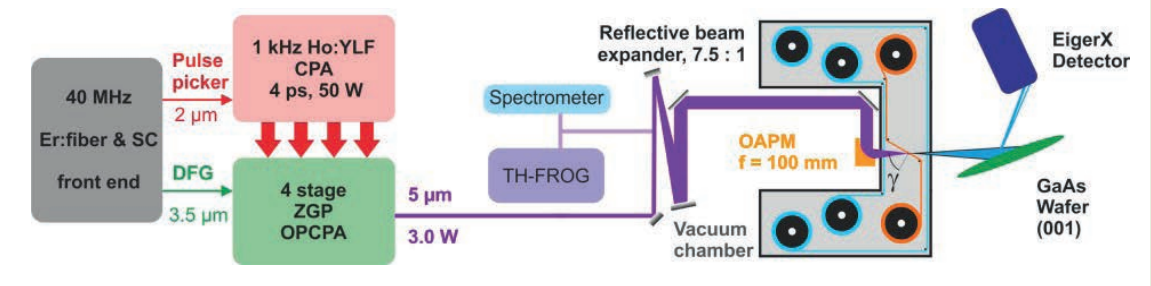

Fig. 6:
Conceptual scheme of the 5-µm OPCPA driver and the setup for the generation and characterization of the hard X-ray pulses.

4.2 to 5.4 µm (at $1/e^2$) supporting a Fourier transform-limited pulse duration of 70 fs. The pulse retrieval delivers a temporal shape with a duration 85 fs. Effectively pumped with 33 mJ, an idler pulse energy of 3.4 mJ is generated, which is still the highest value among fs mid-IR sources beyond 4 µm.

These exceptional output parameters qualify the 5 µm idler pulses of the OPCPA as driver for ultrafast hard X-ray generation. The 5 µm beam is focused to a spot size of 19 µm onto a 20 µm thick Cu target. The characteristic K_α emission in the transmission geometry fills the full solid angle of 4π. In order to calculate the total number of the photons in the full solid angle 4π, X-ray emission in a solid angle of 5.16×10^{-3} is diffracted from a single crystalline GaAs wafer and recorded with an area detector.

This is plotted in Fig. 7 as a function of the electric field of the 5 µm driving pulse perpendicular to the Cu-target surface (blue symbols). First at all an excellent agreement of the measured X-ray flux values with the theoretical prediction (magenta line) has to be emphasized. From these data, a maximum flux of 1.5×10^9 photons per pulse, corresponding to 1.5×10^{12} photons per second in the full solid angle is retrieved [3]. These numbers surpass the X-ray flux when using a Ti:sapphire laser driver at 0.8 µm by 30 times, indicated by the experimental and theoretical values in Fig. 7 (black symbols and red line).

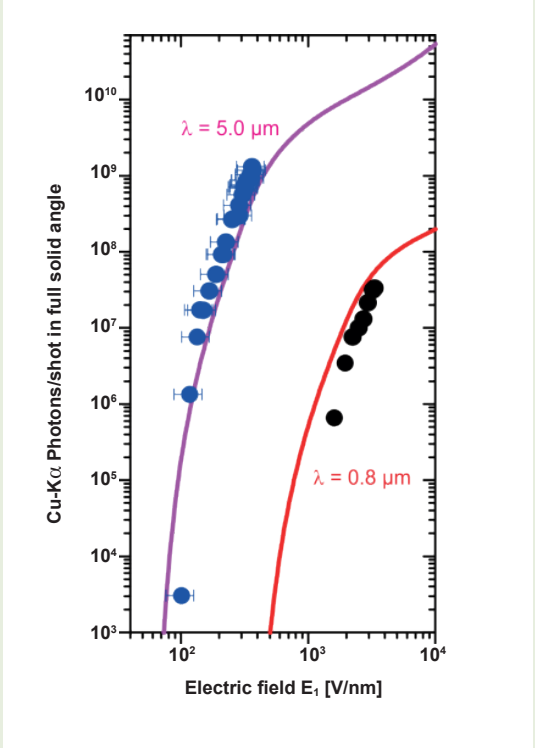

Fig. 7:
Cu-Kα photon number per pulse in 4π as a function of the optical electric field perpendicular to the target surface generated using the 5 µm OPCPA (blue circles) and a Ti:sapphire laser driver (black circles). The solid lines represent the respective theoretical predictions.

T3: Implementation of experimental and measuring techniques

A new pulse characterization device based on time-domain ptychography was developed during 2022. The device also employs sum-frequency mixing, thereby retaining the benefits of the SEA-F-SPIDER, however the setup is simpler to build and easier to use. This new device has been used for the characterization of 1030 nm MPC compressed pulses, the characterization of the 400 kHz OPCPA (T2), and the characterization of near-single cycle pulses from MPC compression of a 100 kHz 800 nm OPCPA (project 1.2). In a collaboration with the ELI-ALPS facility in Szeged both SEA-F-SPIDER and time-domain ptychography devices where employed to characterize spatio-temporal couplings of their SYLOS high energy OPCPA system.

Figure 8 shows experimental results taken with the time-domain ptychography device. For the results in Fig. 8, the output pulses of the 100 kHz OPCPA (T2) were spectrally broadened in a multipass cell setup and after dispersion compensation with chirped mirrors sub-4 fs pulse duration was achieved (see project 1.2).

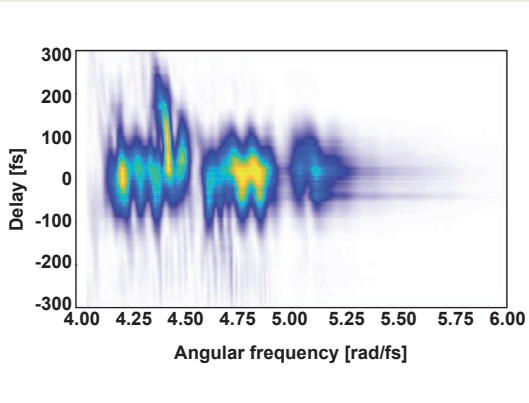

Fig. 8:
Pulse characterization utilizing the time-domain ptychography technique. Example of experimental trace for the characterization of sub-4 fs pulses at 800 nm.

Own Publications

[1] M. Kretschmar, J. Tuemmler, B. Schütte, A. Hoffmann, B. Senfftleben, M. Mero, M. Sauppe, D. Rupp, M. J. J. Vrakking, I. Will, T. Nagy, «Thin-disk laser-pumped OPCPA system delivering 4.4 TW few-cycle pulses», Opt. Express **28** (2020) 34574-34585

[2] L. von Grafenstein, M. Bock, D. Ueberschaer, A. Koç, E. Escoto, K. Zawilski, P. Schunemann, U. Griebner, and T. Elsaesser, "Multi-millijoule few-cycle 5 µm OPCPA at 1 kHz repetition rate," Opt. Lett. **45** (2020) 5998–6001

[3] A. Koç, C. Hauf, M. Woerner, L. von Grafenstein, D. Ueberschaer, M. Bock, U. Griebner and T. Elsaesser, "Compact high-flux hard X-ray source driven by femtosecond mid-infrared pulses at a 1 kHz repetition rate," Opt. Lett. **46** (2021) 210-213

4.2: Application Laboratories and Technology Transfer

NanoMovie – Application Laboratory for nanoscopic spectroscopy and imaging

M. Schnürer, H. Stiel (project coordinators)
J. Bränzel, L. Ehrentraut, P. Friedrich, A. Heilmann, G. Kommol

1. Overview

The application laboratory NanoMovie is part of the Extreme Photonics Laboratory (XPL) at MBI and focuses on providing different soft X-ray technologies. The aim is to establish a reliable experiment and testing platform for internal and external users, including SMEs.

The NanoMovie project realizes laser based secondary soft X-ray sources together with setups for spectroscopy and/or scattering in different photon energy ranges.

Of particular interest are studies of dynamic processes

- in the spectral region around 150 eV where the giant N5,4-edge absorption resonances give access to the f-electrons in the lanthanides via magnetically dichroic transitions,
- in systems with light elements (carbon, nitrogen, oxygen) which are of particular interest in biology and chemistry, where the 1 s core levels can be accessed in the so-called water window (284 eV-543 eV),
- in systems with 3d transition metals where the spin-orbit split L-edges exhibiting strong magnetic dichroism with photon energies beyond 450 eV are reached. Here, the ability to probe the d-electron system with element sensitivity is important e.g. in research of magnetic materials or of metal-organic compounds on an ultrafast timescale.

Femtosecond soft X-ray pulses are generated via High Harmonic Generation (HHG) with long-wavelength drivers in the NIR – IR spectral range. Towards this end, two high average power OPCPA systems with integration of cutting-edge commercial components are constructed. Both, the pump-lasers (500 W Thin Disk Laser (TDL) DIRA500 by *Trumpf Scientific GmbH - TSL*) and frontends (*Fastlite*) are “first of its kind” products. The infrared wavelengths of the two systems (2.1 µm and 3.1 µm) are chosen such that soft X-ray generation via HHG is enabled in spectral regions of 100 eV-600 eV and 500 eV-900 eV, respectively. The challenge, especially at higher photon energies, is the low photon flux of the HHG-sources. Therefore IR-drivers with high flux are needed which perform at high stability, in conjunction with efficient soft X-ray optics. Further development is carried out with the support of projects 1.2 and 4.1 and optimization of the HHG process is aided by numerical simulations within project 1.1 (cf. results in 1.2). Also in 2022, a significant amount of in-house technical work was necessary to keep the performance of the pump lasers (DIRA 500) as well as the frontends (Fastlite) at the specifications. Notably, the two pump lasers DIRA500 perform quite different which causes significant downtime of the 3.1 µm OPCPA system under development. Research and development efforts together with TSL are ongoing to solve the performance issues.

2. Results in 2022

The NanoMovie 2.1 µm and 3.1 µm systems feature a monolithic concept, deriving the seed and the pump beam for the OPCPA stages from the same pump laser. This compact approach, techniques and key parameters have been described in detail within the last annual reports, together with the beamline and spectrometer setup. With 2.1 µm-driven HHG, the system is now in routine operation for application experiments with very high stability and reliability. Work on the 3.1 µm system is ongoing to get into routine operation.

The 2.1 µm OPCPA system with 10 kHz pulse repetition rate excels with stable and reproducible operation. Standard parameters are 28 W to drive the HHG for the probe beam and additional 2 W for the pump beam. The pulse duration is about 26 fs. (Absolute best values are 38 W output without further pulse manipulation.) Pump-probe experiments studying the magnetization dynamics in $Gd_{24}Fe_{76}$ thin film samples via resonant reflectivity measurements in systematically varied scattering geometries have been very successfully performed at the magnetically dichroic Gd $N_{4,5}$ absorption resonance in the spectral region around 150 eV and published (cf. publication [HSS22] described within project 3.2). Research in 2022 was focused at further elevated photon energies, focusing on systems where spectroscopy at the Ti L-edge and N K-edges is instrumental.

Performance of the High Harmonic Source

While high resolution broadband spectra can be recorded in a matter of seconds in the 150 eV region, experiments in the soft X-ray region > 400 eV photon energy are much more challenging given the available photon flux. Irrespective of counting statistics, the noise floor that can be reached is limited by shot-to-shot variations of the source intensity leading to 0.5 % rms (Fig.1) at 10 seconds accumulation, which currently cannot be normalized away at given repetition rate of 10 kHz in conjunction with 2D detection of the dispersed radiation.

Soft x-ray absorption spectra with a total integration time of 80 s for a TiO_x thin film are presented in Fig. 2. Clearly visible is the chemical shift of the Ti $2p_{3/2,1/2}$ core level binding energy for samples with progressive oxidation, starting from the metallic sample (x=0, black line). Time resolved experiments are currently under way.

In order to pump specific electronic transitions in a variety of sample materials of interest, pump beams at wavelengths different from the 2 µm beam will be provided in the future. Towards that end, a NIR-VIS-UV OPCPA synchronized to the 2 µm drive beam will be implemented in 2023/24.

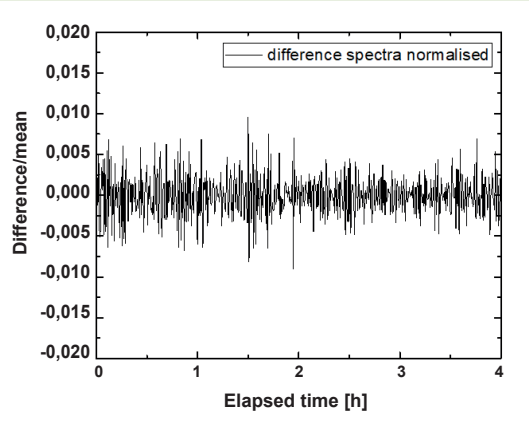

Fig. 1:
Normalized difference of the integral count number obtained at a spectral range of 250-600 eV. Successive integration slots are 10 seconds. Spectra are recorded with a Hitachi VLS-grating.

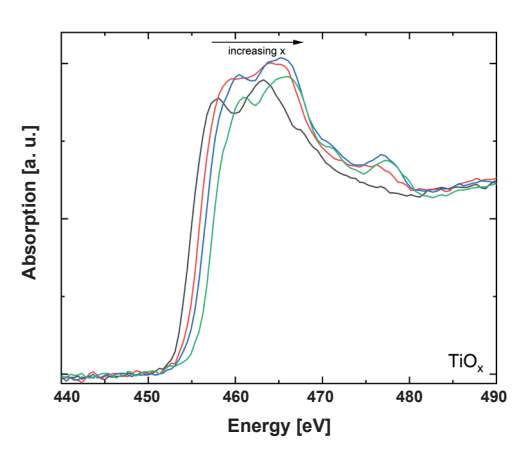

Fig. 2:
Static absorption spectra recorded at the Ti $L_{3,2}$-edge for a thin film of Ti at different stages of the formation of (sub)oxides, i.e. TiOx with increasing x. The resulting chemical shift of the core level is clearly visible.

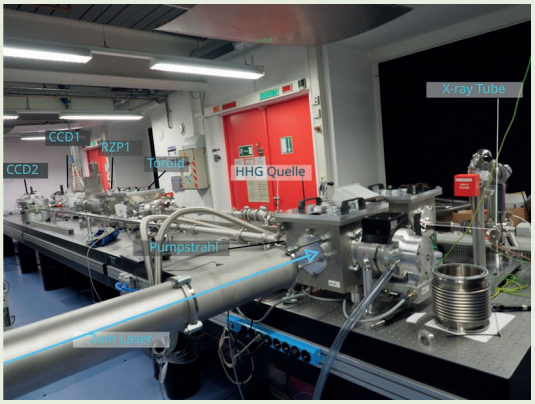

Fig. 3:
View of the MOSFER spectrometer: The setup is based on modular vacuum chambers for beam turning and focussing, HHG-cell, IR-reflector, filter unit, toroidal mirror for soft X-ray beam transport and refocussing, reference RZP1, sample chamber with first CCD1, analysing RZP2 and second CCD2 for sample spectrum. The whole setup is about 9 m long and placed on an optical table. A soft X-ray tube is mounted for adjustment and calibration purposes.

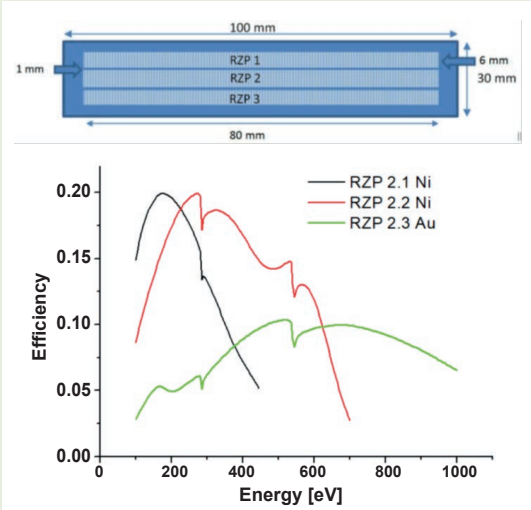

Fig. 4:
Schematic of the analyzing RZP substrate with three different RZP structures optimized for different photon energy ranges. The calculated characteristic reflectivity designed for 3 different spectral bands are shown below. First analysis of calibration measurements at selected photon energies confirms the design values: 21.2 % @ 183 eV, 20.6 % @ 277 eV, 10.7 % @ 525 eV.

Different functionality tests of the second OPCPA system operating at 3.1 µm were performed. The pulse stretching (bulk material) and compression (chirped mirrors) are working successfully, delivering output pulses with 50 fs duration. Although a total output power of up to 17 W with two LiO3 OPA-stages could be obtained, no long term operation without crystal degradation and destruction is cur-rently possible. Therefore work is continuing to find stable crystal OPA configuration with commercially available material, guided by numerical OPA simula-tions

MOSFER

The ProFIT-funded project „Modular Spectrometer with Femtosecond Resolution for soft X-ray radiation" (MOSFER) aims at the design and construction of an efficient and modular soft X-ray spectrometer for use with laboratory sources. The design is aiming for commercialization, taking requirements of ultrafast time-resolved spectroscopy into account. Proofs of concept and performance tests are carried out at two demonstrators, one optimized for HHG sources (set up at NanoMovie, see scheme in annual report 2021) and one optimized for a laser-produced plasma (LPP) source (see section

on 4.2-BLiX, in context with research in projects 3.2, 3.3). The installation of the HHG-adapted system started in 2022, with commissioning planned for April 2023. The innovative optical design relies on the development and production of highly efficient reflection zone plates (RZP) on bent substrates as dispersive elements. The work is organized in the framework of an industrial research project between MBI, PREVAC GmbH, IAP eV. and nob GmbH.

Users and Publications

MBI-users: project 3.2

External users in context with MOSFER: PREVAC GmbH, IAP eV. and nob GmbH

Publications are listed within 3.2 and 1.2.

Berlin Laboratory for innovative X-ray Technologies (BLiX)

H. Stiel, M. Schnürer (project coordinators),
J. Braenzel, J. Tümmler

1. Overview

The Berlin Laboratory for innovative X-ray Technologies (BLiX) is jointly operated by the Institut für Optik und Atomare Physik (IOAP) of the Technische Universität Berlin and the Max-Born-Institut (MBI). BLiX is a „Leibniz-Applikationslabor“ of MBI.

BLiX operates at the interface of scientific research and industrial application with the goal to transfer research results into instrument prototypes, with a focus on instruments and techniques that can be used in a laboratory environment without the need for large scale facilities. BLiX is supposed to be a place of collaborative technology development in the knowledge triangle of research - innovation – education. In 2021, the joint research group SyncLab between the Helmholtz-Zentrum Berlin and BLiX was established. This joint research group will identify and promote the advantages of combining the laboratory methods developed at BLiX with the capabilities offered by large scale facilities like BESSY.

The main fields of activity in BLiX are:
- Soft X-ray imaging using laboratory X-ray microscopy
- Confocal micro X-ray fluorescence analysis
- Detection of chemical species
- Soft and hard X-ray absorption and emission spectroscopy in the laboratory
- Customer inspired development of hard and soft X-ray spectrometers based on advanced X-ray optics

MBI contributes to BLiX predominantly via:
- The support of development and operation of a soft X-ray absorption spectroscopy beamline based on a laser produced plasma X-ray source and novel X-ray optics
- The upgrade of a full field laboratory transmission X-ray microscope (LTXM) capable of tomographic nanoscale imaging and support of LTXM user operation
- The transfer of know-how concerning the development and application of laser based sources, optics and detectors for the soft X-ray region.

Near-edge X-ray absorption fine structure spectroscopy in the laboratory

A laser produced plasma (LPP) source based on long time experience of MBI in laser plasma dynamics has been implemented at BLiX in collaboration between IOAP/TU Berlin and BESTEC GmbH. The pump laser is a high average power commercial Yb:YAG – thin disk laser system (TRUMPF Laser Technology) which has been modified with a variable pulse length seed-diode (AMPHOS, 0.5 ns-30 ns) in order to adapt the pulse duration to the experimental needs. The laser pulses are focused onto a rotating and translating metal cylinder, forming a small hot dense plasma, which emits the desired soft X-rays. The target material can be exchanged with Cu and W the standard materials for line emission or quasi-continuous spectra, respectively. A real-time feedback system ensures source position stability, while the laser and the emission intensity are monitored during measurements. Two beamlines offer the possibility of two simultaneous experiments. The LPP source delivers soft X-ray pulses in the photon energy range between 200 and 1200 eV at a maximum average brightness in selected emission lines of up to 10^{11} ph/s*mm^2*mrad^2.

For investigations of samples relevant for users from life and environmental sciences an X-ray absorption beamline has been implemented. It is equipped with a novel two-channel reflection zone-plate (RZP) spectrometer combining a probe and a reference channel (collaboration with HZB and nob GmbH, Berlin) for near edge X-ray absorption fine structure (NEXAFS) spectroscopy investigations with a spectral resolution up to $E/\Delta E = 1000$ at the carbon, nitrogen and oxygen K-edges as well as on L-edges of transition metal compounds. A beam splitter inserted in the laser beamline in conjunction with a delay line allows for pump-probe experiments with a sub-ns resolution.

Taking advantage of existing laser-driven X-ray sources developed by MBI and operated within the BLiX and NanoMovie laboratories, the ProFIT-funded project „Modular Spectrometer with Femtosecond Resolution for soft X-ray radiation (MOSFER)“ is ongoing. MOSFER is a joint research activity by MBI, IAP eV, Nano Optics Berlin GmbH and Prevac GmbH. The project aims at the conception and construction a soft X-ray spectrometer in a modular design on an optical table in spite of the vacuum requirements, allowing for easy customization by combining standardized units. Furthermore, the development and production of highly efficient reflection zone plates on bent substrates as dispersive elements is part of the project. After commissioning of a prototype spectrometer the demonstration of its performance will be pursued in application experiments within MBI research projects 3.1, 3.2 and 3.3.

Laboratory X-ray microscopy

The full field laboratory transmission X-ray microscope (LTXM) operated at BLiX enables the detection of high quality nanoscopic images at 500 eV with a magnification up to 1000 in a field of view of about 30 µm, a spatial resolution of 30 nm and a typical data accumulation time of less than one minute.

The LTXM is equipped with a high-precision cryo-stage for tomographic measurements.

The soft X-ray radiation of the LTXM is provided by a laser-generated plasma. A high average power laser beam (60 mJ, 0.5 ns, 500 Hz) is focused onto a nitrogen cryo-jet. Line emission at 500 eV from the resulting hot dense plasma is collected by a multilayer condenser mirror (Optixfab GmbH, Jena), monochromatized and focused on the sample. Behind the sample, a zone plate objective (collaboration with X-ray Microscopy department, HZB), projects the image onto a cooled back illuminated X-ray CCD-camera (ALEX, greateyes GmbH, 2048x2048 pixels, 18-bit dynamic range).

2. Results in 2022

Results with direct participation of MBI personnel

Pump-probe NEXAFS spectroscopy in the photon energy range 200-1200 eV

Our pump-probe NEXAFS spectroscopy investigations with sub-ns resolution were extended to new sample systems relevant for catalysis and energy harvesting processes. Among these systems are titanium compounds such as TiN, TiO_2 anatase, TiO_2 nanoparticles doped with C_{60} molecules (collaboration SyncLab HZB and Bergakademie Freiberg). Special procedures to prepare these compounds as very thin layers on Si_3N_4 and Al substrates have been developed. These samples were initially characterized regarding their thermal behaviour during NEXAFS pump-probe investigations with high average pump power, with time-resolved experiments now ongoing at the sub-ns setup at TUB as well as at the ps NEXAFS setup at MBI (see below).

In addition, major improvements in applications of energy-dispersive soft X-ray spectroscopy using modified sCMOS detectors have been achieved (cp. [B2-P-2022.09]).

Ultrafast lab based NEXAFS based on reflection zone plates (RZP) on curved substrates as novel high resolution dispersive optics

MOSFER

In the framework of the MOSFER project (see above) two spectrometer setups were developed. A NEXAFS spectrometer based on two RZPs on curved substrates provided by the industrial partner Nano Optics Berlin GmbH has been commissioned at MBI. The soft X-radiation is provided by a laser produced plasma (LPP) source. (100-1500 eV, 100 Hz, pulse duration < 10 ps, see also Project 3.3). In contrast to an RZP on a planar substrate, the new design with curved RZPs allows high spectral resolution of up to $\Delta E/E = 1000$ on the detector for a broad spectral range while in a spectrometer with planar RZPs the spatial resolution quickly deviates from the design photon energy. Furthermore, no butterfly-like smearing out of intensity perpendicular to the dispersion direction is present on the detector. This enables to record a spectrum while retaining one detector dimension to encode a spatial coordinate, similar to spectrometers based on Varied Line-Spaced (VLS) gratings. In contrast to a VLS, a RZP on a curved substrate offers a high efficiency up to 25 % in a large spectral range. Combining these optics with advanced data acquisition systems based on fast sCMOS detectors, NEXAFS spectra with a very high data quality can be recorded. As an example, figure 1 shows the NEXAFS spectra of Ti and TiN recorded using the NEXAFS setup at the MBI ps-LPP source.

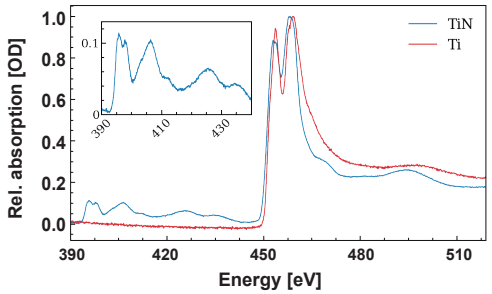

Fig. 1:
NEXAFS spectra of Ti and TiN recorded at the nitro-gen K-edge and titanium L-edge using the NEXAFS spectrometer and the ps LPP-source. Due to the high efficiency of the RZPs and the application of a sCMOS detector (AXIS Photoniques Inc., Canada) the data acquisition time was only 20 s.

This spectrometer concept is also tested and further refined at the NanoMovie HHG source, where a system optimized to match the source properties of a HHG source is currently under commissioning. Here, the focus is on the key ability to perform pump-probe X-ray absorption experiments down to 30 fs temporal resolution in the photon energy range 100-900 eV.

Nanoscale imaging in the water window

In order to increase the usability and availability of the LTXM for external users (see below) several improvements were achieved. Implementation of a tailored pump laser system based on thin disk technology provided by MBI increases the stability and the average flux of the source. A new cryo-jet system (in collaboration with Advanced Microliquids Systems GmbH, Göttingen), comprising a more robust nozzle set-up for the creation of a laminar liquid nitrogen flow as well as a custom manufactured catcher unit has been implemented to increase the durability and reliability of the laser-plasma source (cp. Fig. 2). Furthermore, a custom-built control-software was implemented. The implementation of the software not only further increases the ease of use of the LTXM, but also allows for the automation of several processes such as the automatic stabilization of the laser-plasma source or increasing the field of view by stitching image sequences. Figure 3 shows an image of a diatom recorded with the LTXM after its upgrade.

Besides scientific qualification works (master thesis on image recognition with deep learning algorithms), the

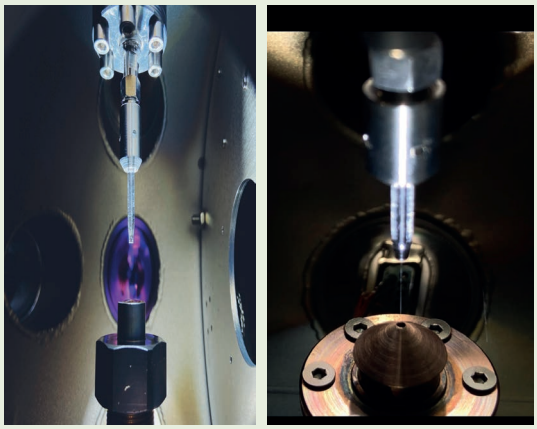

Fig. 2:
Setup of the upgraded cryo-jet system, nozzle (left) and catcher (right). The system delivers a stable laminar cryo-jet as a prerequisite for a stable soft X-ray emission from the plasma.

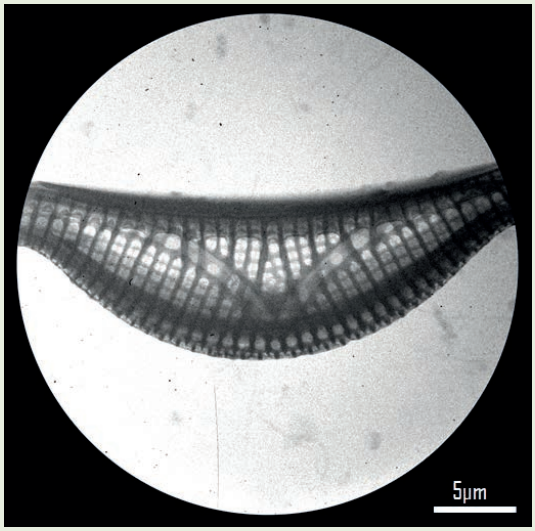

Fig. 3:
Image of a diatom test object recorded with the LTXM at a magnification of 750 (exposure time 120 s) showing a uniform illumination over the full field of view after the LTXM upgrade.

device is mainly used in the Collaborative Research Center 1340. The CRC 1340 “Matrix in Vision” is dedicated to systematically exploring the interaction of magnetic nanoparticles with glycosamino-glycans (GAGs) as a basis for non-invasive imaging of inflammatory diseases such as atherosclerosis. Investigations within the CRC 1340 are performed in close collaboration with various research groups from Charité, HU Berlin. As an example, the very intricate sample preparation of THP-1 cells has been optimized in several iteration steps and the obtained cryo-fixated samples will be analysed in the near future.

Results by TU Berlin personnel, without participation of MBI scientists.

In the following, results by non-MBI staff within BLiX are briefly summarized to allow for a complete picture of the BLiX activities.

The instrumentation for X-ray spectroscopy and microscopy developed in BLiX has reached a state, where it can be used in applications. The development of three X-ray absorption spectrometers for the Max-Planck-Institute for Chemical Energy Conversion (MPI-CEC) was continued. Two instruments are operating in the hard X-ray region and are optimized for XANES and EXAFS respectively. The third instrument employs a laser-plasma source for the soft X-ray range below 1 keV. The instrument for EXAFS and the one for soft X-ray spectroscopy were successfully installed at MPI-CEC.

During 2022 the application experiments at BLiX in research applications were continued in interdisciplinary collaborations in the fields of chemistry, material science and medical science. In 2022, further steps toward in situ and operando XANES experiments were undertaken.

X-ray absorption spectroscopy (XANES, EXAFS)

The BLiX spectrometer is capable of producing XANES spectra with moderate energy resolution and excellent EXAFS spectra within reasonable acquisition times. Application projects are carried out with various partners:

- Catalysis within the Cluster of Excellence ‘Unifying Systems in Catalysis’, UniSysCat (XANES and EXAFS)
- Environmental Chemistry Removal of toxic chromium from water
- Quantitative analysis of species mixtures

First steps towards the application of laboratory XANES for in-situ experiments were made. Together with the group of Prof. Aleksander Gurlo (TU Berlin), changes of the chemical state of catalytic active nanoparticles with changing temperature and during the reaction with gases shall be investigated. In 2022, the instrumentation for sample heating was considerably improved and spin flips could be observed for the first time.

Confocal micro-X-ray fluorescence spectroscopy (XRF)

A dedicated laboratory for micro-XRF and confocal micro-XRF is operated within BLiX. In 2021, the main focus was on biomedical samples as well as samples from the field of cultural heritage. Ongoing application projects focus on:

- Mineral exchange between host plant and cuscuta parasite
- Interface dynamics in teeth close to restauration
- Metal distribution in cacao beans
- Zn localization and speciation in honey bees and larvae
- Provenance studies of marble artifacts from ancient

Greece
- Material characterization of ancient ceramics (Greece) and coins (Greece, Germany)

lAngle-resolved X-ray fluorescence spectroscopy (XRF)

Three different setups for angle-resolved XRF are operational, in part with custom hardware solutions developed at BLiX. They are dedicated to nanoscale elemental depth-profiling for low and high Z elements and diffusion in the sub-µm range, respectively. The setup for the latter application is routinely used in student education. In cooperation with the PVcomB, opportunities for the analysis of compositional gradients in CIGSe and Perovskite solar cells are investigated. The main focus for the two setups with nanometer resolution is on methodological improvement for the investigation of 2D nanostructures relevant for the semiconductor industry. First measurements in the soft X-ray range with the laser-produced plasma source have been conducted and, in cooperation with the X-ray Spectrometry group at PTB and support from HZB, compared to synchrotron measurements at BESSY II. The cooperation with the PTB will continue to establish and validate the method in the laboratory.

Design of X-ray optics

The BMBF-funded joint research project Optiecs4Xi with the University of Hamburg was continued. It aims at the design and application of highly annealed pyrolytic graphite (HAPG) based X-ray optics for X-ray fluorescence imaging at high photon energies for medical applications. An optic for pencil beam formation with a laboratory source was developed and first test were made. A patent application for the optic design was filed.

People

Johannes Tümmler (MBI); Julia Bränzel (MBI); Christian Seim (TUB); Aurélie Dehlinger (TUB); Maria Meitinger (TUB); Ioanna Mantouvalou (HZB); Adrian Jonas (TUB, now at PTB); Daniel Grötzsch (TUB); Christopher Schlesiger (TUB); Wolfgang Malzer (TUB); Birgit Kanngießer (TUB); Leona Bauer (HZB); Richard Gnewkow (HZB); Frank Förste (TUB)

Users & Collaborations

Charité Berlin; The Arctic University of Norway, Tromsö Institutes of TU Berlin: Chemistry, Food Technology, Environment Protection, Construction Engineering; MPI for Chemical Energy Conversion, Mühlheim; Leibniz Institut für Gewässerökologie und Binnenfischerei, Berlin; TU Bergakademie Freiberg; Forschungszentrum Jülich; FhG-ILT, Aachen; optixFab GmbH, Jena; greateyes GmbH, Berlin; HZB/BESSY, Berlin; PTB, Berlin; KTH, Stockholm, Sweden; BESTEC GmbH, Berlin; PREVAC GmbH, Berlin; Institut für angewandte Photonik e.V., Berlin; Nano Optics Berlin GmbH, Berlin; Excillum Ltd, Kista, Sweden; Helmut Fischer GmbH, Berlin/Sindelfingen; Optigraph GmbH; Université P. & M. Curie, Paris, Frankreich; Hamburg University; Leibniz Universität Hannover; hp-spectroscopy GmbH

Own Publications 2022 ff

All publications involving MBI scientists which have emerged from work in BLiX and MOSFER are listed under the relevant research projects (cp. Project 3.3).

Publications related exclusively to TU Berlin personnel, without contribution of MBI scientists:

J. Baumann *et al.*; Int. J. Mol. Sci. 23 (9) 2022

F. Förste *et al.*; J. Anal. At. Spectrom. 37 (8) 2022, 1687-1695

S. Staeck *et al.*; Nanomaterials, 12 (21) 2022

R. Margreiter *et al.*; Archeometry, 64 (6) 2022, 1465-1478

D. K. Nezhad *et al.*; Cat. Sci. Techn., 12 (4) 2022, 1229-1244

4.3: Nanoscale Samples and Optics

W. D. Engel (project coordinator)
and D. Sommer, M. Schneider

1. Overview

As its main task, the Laboratory for Nanoscale Samples and Optics supports a variety of experiments in different scientific projects of the MBI. We develop and produce thin-film sample systems on various substrates with the focus on magnetic multilayers, alloys and metal foils using magnetron sputtering and thermal evaporation. The close integration of deposition, structuring and characterization of these systems with experiments promotes fast feedback on sample performance and rapid development cycles. We collaborate closely with several MBI projects as well as with external cooperation partners to provide custom sample-related services.

To enable new experimental techniques as for example Spin Hall Effect measurements and skyrmion nucleation via high current density, a UV-lithography system is used to create masks, which enables necessary structuring and lift-off processes. Topographic and magnetic characterization is carried out via atomic and magnetic force microscopy (AFM/MFM), electron microscopy (SEM, EDX), X-ray reflectivity and diffraction, Kerr-magnetometry and Kerr-microscopy.

In close cooperation with the central facility for electron microscopy (ZELMI) at the TU Berlin the 3D patterning on a few-micrometer and nanometer scale via electron beam lithography (EBL) and focused ion beam milling (FIB) is carried out.

Main external collaborations: ZELMI (TU Berlin), N. Pontius (Helmholtz-Zentrum Berlin, HZB), R. Ernstorfer (TU Berlin), A. Scherz (XFEL), G.S.D. Beach (Massachusetts Institute of Technology, MIT), S. Bonetti (Stockholm University), C. Gutt (Siegen University), S. Wall (ICFO), K. Höflich (Ferdinand-Braun-Institut, FBH), T. Kampfrath (FU Berlin)

2. Results in 2022

In 2022, the focus was on the preparation of oxide layer systems, ferro- and ferrimagnetic single- and multilayer systems, as well as filter/calibration systems prepared free-standing with a large aperture for a wide variety of experiments within MBI. As a new segment, the preparation of 2D materials, both on different substrates and free-standing - depending on the requirements of the experiments, has been added.

Example: Integrated devices to study spatially controlled creation and motion of magnetic skyrmions

Magnetic skyrmions are topological quasi-particles that attract interest both for fundamental questions related to the emergence of topology as well as their technological applications in next-generation data storage and processing schemes. Studies in these fields demand a comprehensive control over skyrmion nucleation sites and their movement paths, not only to create new functionality, but also to make it experimentally accessible in deterministic pump–probe experiments. In the example highlighted here, Project 4.3 covers the entire manufacturing process for the samples exemplary shown in Fig. 1, which were used in the study in Ref. [KPD22]. The manufacturing included: (i) DC and RF magnetron sputtering to deposit suitable magnetic thin-films with tailored properties, such as magnetic domain size, saturation magnetization, x-ray transmission through the film, presence of Dzyaloshinskii–Moriya interaction etc. Here, the multilayer stack developed has a nominal composition of (thickness values in nanometer): Ta(3)/Pt(4)/[Pt(2.5/Co60Fe25B15(0.95)/MgO(1.4)]$_{\times 15}$/Pt(2) (ii) Combinations of optical, electron-beam and focused ion-beam lithography to pattern the magnetic layer into functional devices. This includes the preparation of striplines and contact strips by lift-off lithography for current-induced skyrmion nucleation. The writing of complex H^+-ion dose profiles to define nucleation sites and motion channels is performed in collaboration with the Ferdinand-Braun-Institut (K. Höflich) using a ZEISS Orion Nanofab at the Helmholtz-Zentrum Berlin. The magnetic film was locally irradiated with 30 kV He^+-ions with doses between 25 and 400 ions/nm^2 in predefined zero-, one-, and two-dimensional patterns with a spatial resolution below 10 nm.

(iii) Thermal as well as electron-beam evaporation of additional layers and their structuring using focused Ga^+-

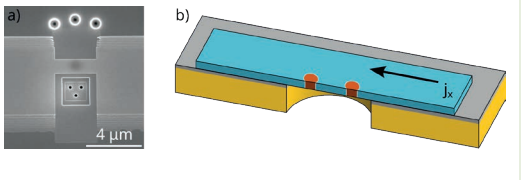

Fig. 1:
(a) SEM image and (b) schematic cross-section of a skyrmion device used in a X-ray Fourier transform holography (FTH) imaging experiment. The finalized samples are a complex, monolithic device comprising the FTH mask (yellow) and magnetic stripline (blue) on a silicon nitride membrane (gray), prepared by a combination of various deposition and lithography techniques. They enable site-controlled skyrmion nucleation (red dots) from electrical current- (jx), and optical laser pulses (not shown).

ion beam lithography. These layers serve experimental purposes, i.e., as local heat sinks and integrated optical elements for static and time-resolved X-ray imaging.

Details on the experiments performed as well as an overview of key results obtained from these samples are highlighted in the project report of Project 3.3.

Example: 2D materials - polycrystalline Bi2Se3

In addition to samples prepared in our laboratory by exfoliation on copper TEM grids consisting of a few monolayers, polycrystalline films of Bi_2Se_3 on Si_3N_4-membranes were prepared for the first time.

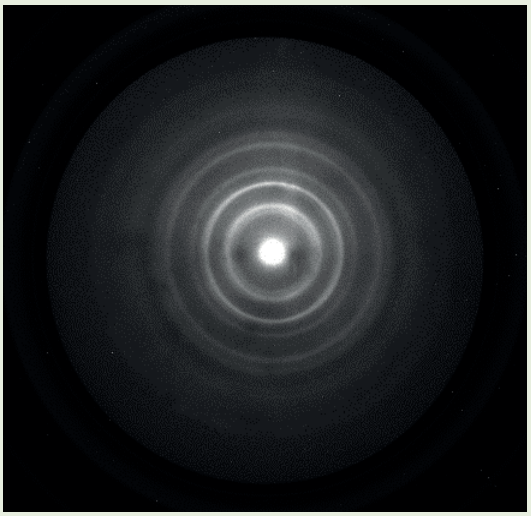

Fig. 2:
Static electron diffraction pattern of a 60 nm thick polycrystalline Bi_2Se_3 film on a Si_3N_4 membrane.

The 60 nm thick films were deposited by magnetron sputtering from a stoichiometric 2" target on a 20 nm thick Si_3N_4 membrane with a free window aperture of 1 mm x 1 mm. This type of films served as a test system for the newly built ultrafast electron diffraction (UED) setup within Topic 4 of Project 2.1, which enables time- and space-dependent lattice dynamics experiments. As a first result, the static electron diffraction pattern of such a sample can be seen in Fig. 2, which clearly shows the polycrystalline phase of the system. For further details see project 2.1.

Example: New MOKE setup

In the sputtering laboratory, in addition to the production of the predominantly magnetic thin-film systems, the characterization of these samples with respect to various properties is also important. A central measurement method for magnetic pre-characterization is MOKE magnetometry. Using the magneto-optical Kerr effect, the magnetic films are measured in a dipole electromagnet.

In our new setup (Fig. 3) we achieve for the first time magnetic fields larger than 2 Tesla, we can rotate the samples in the magnetic field around the optical axis of the incident laser light and we have for the first time a light source with four different wavelengths. In addition, we have built a special sample carrier for this setup, which can be used to heat the samples up to 600 °C during the MOKE measurement and simultaneously measure the magnetoresistance in a Van der Pauw geometry. This opens up to us the quantitative evaluation of hysteresis for a better pre-characterization and thus for an optimal preparation of samples for the experiments.

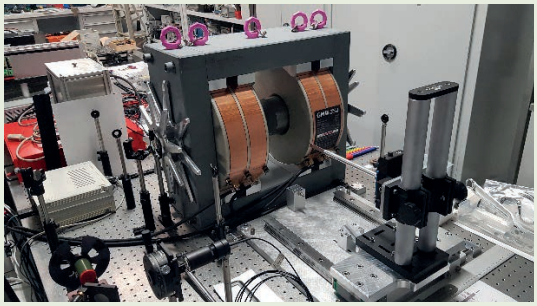

Fig. 3:
Overview of the home build MOKE setup with the new modular specimen holder.

Own Publications 2022 ff

(for full titles and list of authors see appendix 1)

ZJS22: D. Zahn *et al.*; Phys. Rev. Res. **4** (2022) 013104/1-13

Publication in press

RCB: R. Rouzegar *et al.*; Phys. Rev. Appl.

The other publications which have emerged from work in this project are listed under the respective projects 3.2 and 3.3.

Appendices

Appendix 1

Publications

AAB22: M. Arkhipov, R. Arkhipov, I. Babushkin, and N. Rosanov; Self-stopping of light; Phys. Rev. Lett. **128** (2022) 203901/1-6

AMI22: F. Allum, V. Music, L. Inhester, R. Boll, B. Erk, P. Schmidt, T. M. Baumann, G. Brenner, M. Burt, P. V. Demekhin, S. Dörner, A. Ehresmann, A. Galler, P. Grychtol, D. Heathcote, D. Kargin, M. Larsson, J. W. L. Lee, Z. Li, B. Manschwetus, L. Marder, R. Mason, M. Meyer, H. Otto, C. Passow, R. Pietschnig, D. Ramm, K. Schubert, L. Schwob, R. D. Thomas, C. Vallance, I. Vidanović, C. v. K. Schmising, R. Wagner, P. Walter, V. Zhaunerchyk, D. Rolles, S. Bari, M. Brouard, and M. Ilchen; A localized view on molecular dissociation via electron-ion partial covariance; Comm. Chem. **5** (2022) 42/1-10

AOD22: D. Ayuso, A. F. Ordonez, P. Decleva, M. Y. Ivanov, and O. Smirnova; Strong chiral response in non-collinear high harmonic generation driven by purely electric-dipole interactions; Opt. Express **30** (2022) 4659-4667

AOS22: D. Ayuso, A. F. Ordonez, and O. Smirnova; Ultrafast chirality: the road to efficient chiral measurements; Phys. Chem. Chem. Phys. **24** (2022) 26962-26991

Ayu22: D. Ayuso; New opportunities for ultrafast and highly enantio-sensitive imaging of chiral nuclear dynamics enabled by synthetic chiral light; Phys. Chem. Chem. Phys. **24** (2022) 10193-10200

BBS22: V. V. Badikov, D. V. Badikov, G. S. Shevyrdyaeva, K. Kato, N. Umemura, K. Miyata, V. L. Panyutin, and V. Petrov; Crystal growth and characterization of a new quaternary hexagonal nonlinear crystal for the mid-IR: $Ba_2Ga_8GeS_{16}$; J. Alloy. Compd. **907** (2022) 164378/1-5

BCC22: P. Bonfà, S. Chicco, F. Cugini, S. Sharma, J. K. Dewhurst, and G. Allodi; Magnetic phase diagram of the austenitic Mn-rich Ni-Mn-(In, Sn) Heusler alloys; Electron. Structure **4** (2022) 024002/1-11

BDK22a: I. Babushkin, A. Demircan, M. Kues, and U. Morgner; Wave-shape-tolerant photonic quantum gates; Phys. Rev. Lett. **128** (2022) 090502/1-7

BDK22b: M. Belitsch, D. N. Dirin, M. V. Kovalenko, K. Pichler, S. Rotter, A. Ghalgaoui, H. Ditlbacher, A. Hohenau, and J. R. Krenn; Gain and lasing from CdSe/CdS nanoplatelet stripe waveguides; Micro. Nano. Eng. **17** (2022) 100167/1-27

BDM22: I. Babushkin, A. Demircan, U. Morgner, and A. Savel'ev; High-order harmonics and supercontinua formed by a weak optical pump in the presence of an extreme terahertz field; Phys. Rev. A **106** (2022) 013115/1-9

BJC22: I. Babushkin, Á. J. Jiménez-Galán, J. R. C. d. Andrade, A. Husakou, F. Morales, M. Kretschmar, T. Nagy, V. Vaičaitis, L. Shi, D. Zuber, L. Bergé, S. Skupin, I. A. Nikolaeva, N. A. Panov, D. E. Shipilo, O. G. Kosareva, A. N. Pfeiffer, A. Demircan, M. J. J. Vrakking, U. Morgner, and M. Y. Ivanov; All-optical attoclock for imaging tunnelling wavepackets; Nat. Phys. **18** (2022) 417-422

BKS22: V. A. Birulia, M. A. Khokhlova, and V. V. Strelkov; Generation of attosecond pulses with a controllable carrier-envelope phase via high-order frequency mixing; Phys. Rev. A **106** (2022) 023514/1-10

BMi22: W. Becker and D. B. Milošević; Elliptic dichroism in strong-field ionization of atoms subjected to tailored laser fields; Phys. Chem. Chem. Phys. **24** (2022) 7014-7027

BPI22: U. Bengs, S. Patchkovskii, M. Y. Ivanov, and N. Zhavoronkov; All-optical Stückelberg spectroscopy of strongly driven Rydberg states; Phys. Rev. Lett. **4** (2022) 023135/1-8

BWM22: A. A. Boyko, L. Wang, O. Mhibik, I. B. Divliansky, A. Zukauskas, K. Moelster, W. Chen, L. B. Glebov, V. Pasiskevicius, and V. Petrov; High-energy, narrowband, non-resonant PPKTP optical parametric oscillator; SPIE Proc. **11985** (2022) 119850G/1-5

CBD22: S. Carlström, M. Bertolino, J. M. Dahlström, and S. Patchkovskii; General time-dependent configuration-interaction singles. II. Atomic case; Phys. Rev. A **106** (2022) 042806/1-15

CDI22: S. Carlström, J. M. Dahlström, M. Y. Ivanov, and S. Patchkovskii; Rydberg atomic antenna in strongly driven multielectron atoms; Phys. Rev. A **106** (2022) 043114/1-7

CLX22: W. Chen, Z.-L. Lin, W.-Z. Xue, H.-J. Zeng, G. Zhang, P. Loiko, Y. Zhao, X. Xu, J. Xu, X. Mateos, H. Lin, L. Wang, and V. Petrov; Kerr-lens mode-locked Yb:$YAlO_3$ laser generating 24-fs pulses at 1085 nm; Opt. Lett. **47** (2022) 4728-4731

CSP22: S. Carlström, M. Spanner, and S. Patchkovskii; General time-dependent configuration-interaction singles. I. Molecular case; Phys. Rev. A **106** (2022) 043104/1-13

CWB22: M.-A. Codescu, M. Weiß, M. Brehm, O. Kornilov, D. Sebastiani, and E. T. J. Nibbering; Ultrafast proton transfer pathways mediated by imidazole; in *Ultrafast Phenomena 2022*, F. Légaré, T. Tahara, J. Biegert, T. Brixner, and N. Dudovich (eds.) (Optica Publishing Group, Montreal, Quebec, Canada, 2022) Tu1A.4/1-2

DGB22: M. Duda, L. v. Grafenstein, M. Bock, D. Ueberschaer, P. Fuertjes, L. Roškot, O. Novák, and U. Griebner; 10-µJ few-cycle 12-µm source based on difference-frequency generation driven by a 1-kHz mid-wave infrared OPCPA; Opt. Lett. **47** (2022) 2891-2894

DSR22: J. K. Dewhurst, S. Shallcross, I. Radu, P. Elliott, C. v. K. Schmising, and S. Sharma; Ab initio study of ultrafast spin dynamics in $Gd_x(FeCo)_{1-x}$ alloys; Appl. Phys. Lett. **120** (2022) 042401/1-6

DWK22: L. Drescher, T. Witting, O. Kornilov, and M. J. J. Vrakking; Phase dependence of resonant and anti-resonant two-photon excitations; Phys. Rev. A **105** (2022) L011101/1-6

EEC22: P. Elliott, A. Eschenlohr, J. Chen, S. Shallcross, U. Bovensiepen, J. K. Dewhurst, and S. Sharma; Transient Spin Injection Efficiencies at Ferromagnet-Metal Interfaces; Advanced Materials Interfaces **20** (2022) 2201233/1-9

EGB22: G. Exner, A. Grigorov, V. Badikov, and V. Petrov; Hardness and Young's modulus of $BaGa_4S_7$ and $BaGa_4Se_7$ nonlinear optical crystals; Opt. Mater. **133** (2022) 112994/1-4

EKL22a: M. Ekimova, C. Kleine, J. Ludwig, M. Ochmann, T. E. G. Agrenius, E. Kozari, D. Pines, E. Pines, N. Huse, P. Wernet, M. Odelius, and E. T. J. Nibbering; From local covalent bonding to extended electric field interactions in proton hydration; Angew. Chem. Int. Edit. **61** (2022) e202211066/1-9

EKL22b: M. Ekimova, C. Kleine, J. Ludwig, M. Ochmann, T. E. G. Agrenius, E. Kozari, D. Pines, E. Pines, N. Huse, P. Wernet, M. Odelius, and E. T. J. Nibbering; Von lokalen kovalenten Bindungen zu langreichweitigen elektrischen Wechselwirkungen der Protonenhydratation; Angew. Chem. **134** (2022) e202211066/1-10

ELB22: K. Eremeev, P. Loiko, A. Braud, P. Camy, J. Zhang, X. Xu, Y. Zhao, P. Liu, S. Balabanov, E. Dunina, A. Kornienko, L. Fomicheva, X. Mateos, U. Griebner, V. Petrov, L. Wang, and W. Chen; Spectroscopy of solid-solution transparent sesquioxide laser ceramic $Tm:LuYO_3$; Opt. Mater. Express **12** (2022) 3749-3762

EMV22: U. Elu, L. Maidment, L. Vamos, F. Tani, D. Novoa, M. H. Frosz, V. Badikov, D. Badikov, V. Petrov, P. S. J. Russell, and J. Biegert; Extreme temporal compression of ultra-broadband mid-infrared pulses; in *Light Filaments: Structures, challenges and applications*, J.-C. Diels, M. C. Richardson, and L. Arissian (eds.) (SciTech Publishing, IET, Stevenage, U.K., 2022) 103-115

EWK22a: S. Eckert, M.-O. Winghart, C. Kleine, A. Banerjee, M. Ekimova, J. Ludwig, J. Harich, M. Fondell, R. Mitzner, E. Pines, N. Huse, P. Wernet, M. Odelius, and E. T. J. Nibbering; Electronic structure changes of an aromatic amine photoacid along the Förster cycle; Angew. Chem. Int. Edit. **61** (2022) e202200709/1-7

EWK22b: S. Eckert, M.-O. Winghart, C. Kleine, A. Banerjee, M. Ekimova, J. Ludwig, J. Harich, M. Fondell, R. Mitzner, E. Pines, N. Huse, P. Wernet, M. Odelius, and E. T. J. Nibbering; Änderungen der elektronischen Struktur einer Amino-Photosäure entlang des Förster Zyklus; Angew. Chemie **134** (2022) e202200709/1-8

FBG22: P. Fuertjes, M. Bock, L. v. Grafenstein, D. Ueberschaer, U. Griebner, and T. Elsaesser; Few-cycle 65-µJ pulses at 11.4 µm for ultrafast nonlinear longwave-infrared spectroscopy; Optica **9** (2022) 1303-1306

FGM22: P. Fuertjes, L. v. Grafenstein, C. Mei, M. Bock, U. Griebner, and T. Elsaesser; Cr:ZnS-based soliton self-frequency shifted signal generation for a tunable sub-100 fs MWIR OPCPA; Opt. Express **30** (2022) 5142-5150

FLT22: A. J. Feinberg, F. Laimer, R. M. P. Tanyag, B. Senfftleben, Y. Ovcharenko, S. Dold, M. Gatchell, S. M. O. O'Connell-Lopez, S. Erukala, C. A. Saladrigas, B. W. Toulson, A. Hoffmann, B. Kamerin, R. Boll, A. D. Fanis, P. Grychtol, T. Mazza, J. Montano, K. Setoodehnia, D. Lomidze, R. Hartmann, P. Schmidt, A. Ulmer, A. Colombo, M. Meyer, T. Möller, D. Rupp, O. Gessner, P. Scheier, and A. F. Vilesov; X-ray diffractive imaging of highly ionized helium nanodroplets; Physical Review Research **4** (2022) L022063/1-6

FTB22: B. Fetić, M. Tunja, W. Becker, and D. B. Milošević; Extracting photoelectron spectra from the time-dependent wave function. II. Validation of two methods: projection on plane waves and time-dependent surface flux; Phys. Rev. A **105** (2022) 053121/1-10

FTG22: P. Fuertjes, J. W. Tomm, U. Griebner, G. Steinmeyer, S. S. Balabanov, E. M. Gavrishchuk, and T. Elsaesser; Kinetics of excitation transfer from Cr^{2+} to Fe^{2+} ions in co-doped ZnSe; Opt. Lett. **47** (2022) 2129-2131

FWO22: F. J. Furch, T. Witting, M. Osolodkov, F. Schell, C. P. Schulz, and M. J. J. Vrakking; High power, high repetition rate laser-based sources for attosecond science; J. Phys.: Photonics **4** (2022) 032001/1-26

GBS22: F. Guo, E. Boursier, P. Segonds, A. Pena, J. Debray, V. Badikov, V. Panyutin, D. Badikov, V. Petrov, and B. Boulanger; Second-order nonlinear optical coefficients of the monoclinic crystal $BaGa_4Se_7$; Opt. Lett. **47** (2022) 842-845

GGA22: E. Granados, C. Granados, R. Ahmed, K. Chrysalidis, V. N. Fedosseev, B. A. Marsh, S. G. Wilkins, R. P. Mildren, and D. J. Spence; Spectral synthesis of multimode lasers to the Fourier limit in integrated Fabry–Perot diamond resonators; Optica **9** (2022) 317-324

GJB22a: R. Grunwald, M. Jurke, M. Bock, M. Liebmann, B. P. Bruno, H. Gowda, and U. Wallrabe; High-flexibility control of structured light with combined adaptive optical systems; Photonics **9** (2022) 9010042/1-13

GJB22b: I. González-Vallejo, V. L. R. Jacques, D. Boschetto, G. Rizza, A. Hadj-Azzem, J. Faure, and D. L. Bolloch; Time-resolved structural dynamics of the out-of-equilibrium charge density wave phase transition in $GdTe_3$; Struct. Dyn. **9** (2022) 014502/1-9

GKR22a: I. González-Vallejo, A. Koç, K. Reimann, M. Woerner, and T. Elsaesser; Underdamped longitudinal soft modes in ionic crystallites - lattice and charge motions observed by ultrafast x-ray diffraction; Struct. Dyn. **9** (2022) 024501/1-10

GKR22b: I. González-Vallejo, A. Koç, K. Reimann, M. Woerner, and T. Elsaesser; Underdamped longitudinal soft mode dynamics in KDP observed by ultrafast x-ray diffraction; in *Ultrafast Phenomena 2022*, F. Légaré, T. Tahara, J. Biegert, T. Brixner, and N. Dudovich (eds.) (Optica Publishing Group, Montreal, Quebec, Canada, 2022)

GOP22: Q. Guo, R. Ovcharenko, B. Paulus, Y. Dedkov, and E. Voloshina; Electronic and magnetic properties of the graphene/RE/Ni(111) (RE: La, Yb) intercalation-like interfaces: A DFT analysis; Adv. Theory Simul. **5** (2022) 2100621/1-8

GRe22: A. Ghalgaoui and K. Reimann; Excitation of tunable plasmons in silicon using microwave transmission through a metallic aperture; Appl. Phys. Lett. **120** (2022) 162103/1-6

GSE22: E. Granados, G. Stoikos, D. T. Echarri, K. Chrysalidis, V. N. Fedosseev, C. Granados, V. Leask, B. A. Marsh, and R. P. Mildren; Tunable spectral squeezers based on monolithically integrated diamond Raman resonators; Appl. Phys. Lett. **120** (2022) 151101/1-6

GSQ22: R. Gupta, S. Shallcross, J. Quintanilla, M. Gradhand, and J. Annett; Distinguishing d_{xz}+id_{yz} and d_{x2-y2} pairing in Sr_2RuO4 by high magnetic field H−T phase diagrams; Phys. Rev. B **106** (2022) 115126/1-11

GTH22: C. Granados, E. Titov, J. Hummert, E. Ikonnikov, S. Haacke, R. Mitric, and O. Kornilov; Ultrafast relaxation of solvated organic molecules studied by XUV time-resolved photoelectron spectroscopy; in *Ultrafast Phenomena 2022*, F. Légaré, T. Tahara, J. Biegert, T. Brixner, and N. Dudovich (eds.) (Optica Publishing Group, Montreal, Quebec, Canada, 2022)

HBC22: A. Hashemi, K. Busch, D. N. Christodoulides, K. Ozdemir, and R. El-Ganainy; Linear response theory of open systems with exceptional points; Nat. Commun. **13** (2022) 3281/1-10

HBM22: D. Habibović, W. Becker, and D. B. Milošević; High-order harmonic generation by two linearly polarized laser fields with an arbitrary angle between their polarization axes; Phys. Rev. A **106** (2022) 023119/1-13

HBO22: A. Hashemi, K. Busch, Ş. K. Özdemir, and R. El-Ganainy; Uniform optical gain as a non-Hermitian control knob; Phys. Rev. Res. **4** (2022) 043169/1-8

Her22: J. Herrmann; Towards a unified theory of the fundamental physical interactions based on the underlying geometric structure of the tangent bundle; Eur. Phys. J. C **82** (2022) 947/1-23

HPP22: Z. Heiner, V. Petrov, V. L. Panyutin, V. V. Badikov, K. Kato, K. Miyata, and M. Mero; Efficient generation of few-cycle pulses beyond 10 µm from an optical parametric amplifier pumped by a 1-µm laser system; Sci. Rep. **12** (2022) 5082/1-7

HSE22: C. M. Heyl, M. Seidel, E. Escoto, A. Schönberg, S. Carlström, G. Arisholm, T. Lang, and I. Hartl; High-energy bow tie multi-pass cells for nonlinear spectral broadening applications; J. Phys.: Photonics **4** (2022) 014002/1-9

HSK22: N. Z. Hagström, M. Schneider, and et al; Megahertz-rate ultrafast X-ray scattering and holographic imaging at the European XFEL; J. Synchrotron Rad. **29** (2022) 1454-1464

HSS22: M. Hennecke, D. Schick, T. Sidiropoulos, F. Willems, A. Heilmann, M. v. Moerbeck-Bock, L. Ehrentraut, D. Engel, P. Hessing, B. Pfau, M. Schmidbauer, A. Furchner, M. Schnuerer, C. von Korff Schmising, and S. Eisebitt; Ultrafast element- and depth-resolved magnetization dynamics probed by transverse magneto-optical Kerr effect spectroscopy in the soft x-ray range; Phys. Rev. Research **4** (2022) L022062/1-7

HWT22: A. Heßler, S. Wahl, P. Trøst Kristensen, M. Wuttig, K. Busch, and T. Taubner; Nanostructured In_3SbTe_2 antennas enable switching from sharp dielectric to broad plasmonic resonances; Nanophotonics **11** (2022) 3871-38821

IRB22: F. Intravaia, D. Reiche, and K. Busch; In der Unruhe liegt die Kraft; Physik Journal **21** (2022) 35-40

JLK22a: P. Jürgens, B. Liewehr, B. Kruse, C. Peltz, T. Witting, A. Husakou, A. Rouzée, M. Y. Ivanov, T. Fennel, M. J. J. Vrakking, and A. Mermillod-Blondin; Characterization of laser-induced ionization dynamics in solid dielectrics; ACS Photonics **9** (2022) 233-240

JLK22b: P. Jürgens, B. Liewehr, B. Kruse, C. Peltz, T. Witting, A. Husakou, A. Rouzée, M. Y. Ivanov, T. Fennel, M. J. J. Vrakking, and A. Mermillod-Blondin; Reconstruction of strong-field-driven carrier generation dynamics from injection harmonics in solid dielectrics; in *Ultrafast Phenomena 2022*, F. Légaré, T. Tahara, J. Biegert, T. Brixner, and N. Dudovich (eds.) (Optica Publishing Group, Montreal, Quebec, Canada, 2022)

JNS22: M. Janssen, L. Nahon, O. Smirnova, and A. Stolow; Fundamentals and applications of molecular photoelectron spectroscopy – Festschrift for Ivan Powis; Phys. Chem. Chem. Phys. **24** (2022) 24611-24613

JPS22: A. S. Johnson, D. Pérez-Salinas, K. M. Siddiqui, S. Kim, S. Choi, K. Volckaert, P. E. Majchrzak, S. Ulstrup, K. Hallman, R. F. Haglund, C. M. Günther, B. Pfau, S. Eisebitt, D. Backes, F. Maccherozzi, A. Fitzpatrick, S. Dhesi, P. Gargiani, M. Valvidares, H. Choi, D. Jang, A. Katoch, S. Kwon, S. H. Park, H. Kim, and S. E. Wall; Ultrafast X-Ray hyperspectral imaging of the photo-induced phase transition in VO_2; in *Ultrafast Phenomena 2022*, F. Légaré, T. Tahara, J. Biegert, T. Brixner, and N. Dudovich (eds.) (Optica Publishing Group, Montreal, Quebec, Canada, 2022)

KAF22: O. Kneller, D. Azoury, Y. Federman, M. Krüger, A. J. Uzan, G. Orenstein, B. D. Bruner, O. Smirnova, S. Patchkovskii, M. Y. Ivanov, and N. Dudovich; A look under the tunnelling barrier via attosecond-gated interferometry; Nat. Photonics **16** (2022) 304-310

KBH22: C. Klose, F. Büttner, W. Hu, C. Mazzoli, G. S. D. Beach, S. Eisebitt, and B. Pfau; Photon correlation spectroscopy with heterodyne mixing based on soft-x-ray magnetic circular dichroism; Phys. Rev. B **105** (2022) 214425/1-9

KHM22: M. Kretschmar, A. Hadjipittas, B. Major, J. Tümmler, I. Will, T. Nagy, M. J. J. Vrakking, A. Emmanouilidou, and B. Schütte; Attosecond investigation of extreme-ultraviolet multi-photon multi-electron ionization; Optica **9** (2022) 639-644

KKB22: H. Kurz, M. Kretschmar, T. Binhammer, T. Nagy, D. Ristau, M. Lein, U. Morgner, and M. Kovacev; High-order harmonic spectroscopy in an ionized high-density target; Frontiers in Physics **10** (2022) 3389/1-5

KLA22: H. Köckert, J. W. L. Lee, F. Allum, K. Amini, S. Bari, C. Bomme, F. Braußе, M. Brouard, M. Burt, B. C. d. Miranda, S. Düsterer, P. Eng-Johnsson, B. Erk, M. Géléoc, R. Geneaux, A. S. Gentleman, R. Guillemin, G. Goldsztejn, D. M. P. Holland, I. Ismail, L. Journel, T. Kierspel, J. Küpper, J. Lahl, S. R. Mackenzie, S. Maclot, B. Manschwetus, A. S. Mereshchenk, T. Mullins, P. K. Olshin, J. Palaudoux, F. Penent, M. N. Piancastelli, D. Rompotis, A. Rouzée, T. Ruchon, A. Rudenko, N. Schirmel, M. Simon, S. Techert, O. Travnikova, S. Trippel, C. Vallance, E. Wang, J. Wiese, F. Ziaee, T. Marchenko, D. Rolles, and R. Boll; UV-induced dissociation of CH_2BrI probed by intense femtosecond XUV pulses; J. Phys. B **55** (2022) 014001/1-13

KMB22a: A. Kundu, S. I. Mamatkulov, F. N. Brünig, D. J. Bonthuis, R. R. Netz, T. Elsaesser, and B. P. Fingerhut; Short-range slowdown of water solvation dynamics around SO_4^{2-} - Mg^{2+} ion pairs in *Ultrafast Phenomena 2022*, F. Légaré, T. Tahara, J. Biegert, T. Brixner, and N. Dudovich (eds.) (Optica Publishing Group, Montreal, Quebec, Canada, 2022)

KMB22b: A. Kundu, S. I. Mamatkulov, F. N. Brünig, D. J. Bonthuis, R. R. Netz, T. Elsaesser, and B. P. Fingerhut; Short-range slowdown of water solvation dynamics around SO_4^{2-} - Mg^{2+} ion pairs; ACS Phys. Chem Au **2** (2022) 506-514

KMD22a: L.-M. Koll, L. Maikowski, L. Drescher, T. Witting, and M. J. J. Vrakking; Experimental control of quantum-mechanical entanglement in an attosecond pump-probe experiment; Phys. Rev. Lett. **128** (2022) 043201/1-6

KMD22b: L.-M. Koll, L. Maikowski, L. Drescher, M. J. J. Vrakking, and T. Witting; Phase-locking of time-delayed attosecond XUV pulse pairs; Opt. Express **30** (2022) 7082-7095

KMH22: K. Kato, M. Mero, Z. Heiner, T. Kinoshita, V. V. Badikov, K. Miyata, and V. Petrov; Refined Sellmeier equations of $CdGa_2S_4$ for prediction of phase-matching in mixed $Hg_{1-x}Cd_xGa_2S_4$ nonlinear crystals; SPIE Proc. **1198505** (2022) 1-5

KPD22: L.-M. Kern, B. Pfau, V. Deinhart, M. Schneider, C. Klose, K. Gerlinger, S. Wittrock, D. Engel, I. Will, C. M. Günther, R. Liefferink, J. H. Mentink, S. Wintz, M. Weigand, M.-J. Huang, R. Battistelli, D. Metternich, F. Büttner, K. Höflich, and S. Eisebitt; Deterministic generation and guided motion of magnetic skyrmions by focused He+-ion irradiation; Nano Lett. **22** (2022) 4028-4035

KPP22: M. Khokhlova, E. Pisanty, S. Patchkovskii, O. Smirnova, and M. Y. Ivanov; Enantiosensitive steering of free-induction decay; Sci. Adv. **8** (2022) eabq1962 /1-8

KPS22: L.-M. Kern, B. Pfau, M. Schneider, K. Gerlinger, V. Deinhart, S. Wittrock, T. Sidiropoulos, D. Engel, I. Will, C. M. Günther, K. Litzius, S. Wintz, M. Weigand, F. Büttner, and S. Eisebitt; Tailoring optical excitation to control magnetic skyrmion nucleation; Phys. Rev. B **106** (2022) 054435/1-10

KSU22: K. Kolatzki, M. L. Schubert, A. Ulmer, T. Möller, D. Rupp, and R. M. P. Tanyag; Micrometer-sized droplets from liquid helium jets at low stagnation pressures; Phys. Fluids **34** (2022) 012002/1-12

KSZ22: M. Kowalczyk, Ł. A. Sterczewski, X. Zhang, V. Petrov, and J. Sotor; Dual-dispersion-regime dual-comb mode-locked laser; Opt. Lett. **47** (2022) 1762-1765

KTW22: D. Kühn, A. Treffer, F. Wyrowski, and R. Grunwald; Simultaneous spatio-temporal focusing with pulse front symmetrization; Opt. Lett. **47** (2022) 750-753

KUB22: K. Kato, N. Umemura, V. V. Badikov, D. V. Badikov, and V. Petrov; Temperature-dependent phase-matching properties of $BaGa_2GeS_6$ in the 0.767–10.5910 µm spectral range; Appl. Opt. **61** (2022) 10774-10777

KWZ22a: C. Kleine, M.-O. Winghart, Z.-Y. Zhang, M. Ekimova, S. Eckert, M. J. J. Vrakking, E. T. J. Nibbering, and A. Rouzée; Ultrafast N K-edge spectroscopy of strong field ionization and fragmentation dynamics of molecular nitrogen; in *Ultrafast Phenomena 2022*, F. Légaré, T. Tahara, J. Biegert, T. Brixner, and N. Dudovich (eds.) (Optica Publishing Group, Montreal, Quebec, Canada, 2022) M2A.4/1-2

KWZ22b: C. Kleine, M.-O. Winghart, Z.-Y. Zhang, M. Richter, M. Ekimova, S. Eckert, M. J. J. Vrakking, E. T. J. Nibbering, A. Rouzée, and E. R. Grant; Electronic state population dynamics upon ultrafast strong field ionization and fragmentation of molecular nitrogen; Phys. Rev. Lett. **129** (2022) 123002/1-7

KYA22: J. N. Kirchhof, Y. Yu, G. Antheaume, G. Gordeev, D. Yagodkin, P. Elliott, D. B. d. Araújo, S. Sharma, S. Reich, and K. I. Bolotin; Nanomechanical Spectroscopy of 2D Materials; Nano Lett. **20** (2022) 8037-8044

KZB22: A. Kalita, Q. Zhong, K. Busch, and R. El-Ganainy; Quantum-inspired multicore optical fiber; Opt. Lett. **47** (2022) 2526-2529

KZS22: A. Kimel, A. Zvezdin, S. Sharma, S. Shallcross, N. d. Sousa, A. Garcia-Martin, G. Salvan, J. Hamrle, O. Stejskal, J. McCord, S. Tacchi, G. Carlotti, P. Gambardella, G. Salis, M. Muenzenberg, M. Schultze, V. Temnov, I. V. Bychkov, L. N. Kotov, N. Maccaferri, D. Ignatyeva, V. Belotelov, C. Donnelly, A. H. Rodriguez, I. Matsuda, T. Ruchon, M. Fanciulli, M. Sacchi, C. R. Du, H. Wang, N. P. Armitage, M. Schubert, V. Darakchieva, B. Liu, Z. Huang, B. Ding, A. Berger, and P. Vavassori; The 2022 Magneto-Optics Roadmap; J. Phys. D **55** (2022) 463003/1-64

LOC22: B. Langbehn, Y. Ovcharenko, A. Clark, M. Coreno, R. Cucini, A. Demidovich, M. Drabbels, P. Finetti, M. D. Fraia, L. Giannessi, C. Grazioli, D. Iablonskyi, A. C. LaForge, T. Nishiyama, V. O. Á. d. Lara, C. Peltz, P. Piseri, O. Plekan, K. Sander, K. Ueda, T. Fennel, K. C. Prince, F. Stienkemeier, C. Callegari, T. Möller, and D. Rupp; Diffraction imaging of light induced dynamics in xenon-doped helium nanodroplets; New J. Phys. **24** (2022) 113043/1-15

LXZ22a: Z.-L. Lin, W.-Z. Xue, H.-J. Zeng, G. Zhang, P. Zhang, Z. Chen, Z. Li, V. Petrov, P. Loiko, X. Mateos, H. Lin, L. Wang, and W. Chen; Kerr-lens mode-locked ytterbium-activated orthoaluminate laser; Opt. Lett. **47** (2022) 3027-3030

LXZ22b: Z.-L. Lin, W.-Z. Xue, H.-J. Zeng, G. Zhang, Y. Zhao, X. Xu, J. Xu, P. Loiko, X. Mateos, H. Lin, V. Petrov, L. Wang, and W. Chen; Semiconductor saturable absorber mirror mode-locked Yb:YAP laser; Opt. Express **30** (2022) 31986-31997

LYL22: X. Liang, Y. Yi, S. Li, P. Zhu, X. Xie, H. Liu, G. J. Mu, Z. G. Liu, A. Guo, J. Kang, Q. Yang, H. Zhu, Q. Gao, M. Sun, H. Lu, Y. Ma, S. Mondal, D. Papp, S. Majorosi, Z. Lécz, A. Andreev, S. Kahaly, C. Kamperidis, N. A. M. Hafz, and J. Zhu; A laser wakefield acceleration facility using SG-II petawatt laser system; Rev. Sci. Instrum. **93** (2022) 033504/1-11

MAI22: N. Mayer, D. Ayuso, M. Y. Ivanov, and O. Smirnova; Synthetic chiral vortices for highly-sensitive chiral discrimination; in *Frontiers in Optics 2022* (Optica Publishing Group, Rochester, New York, USA, 2022)

MBe22: D. B. Milošević and W. Becker; Negative-travel-time quantum orbits in strong-field ionization by an elliptically polarized laser field; Phys. Rev. A **105** (2022) L031103/1-7

MBJ22: N. Mayer, S. Beaulieu, Á. Jiménez-Galán, S. Patchkovskii, O. Kornilov, D. Descamps, S. Petit, O. Smirnova, Y. Mairesse, and M. Y. Ivanov; Role of spin-orbit coupling in high-order harmonic generation revealed by supercycle Rydberg trajectories; Phys. Rev. Lett. **129** (2022) 173202/1-5

MBN22: C. Mei, I. Babushkin, T. Nagy, and G. Steinmeyer; Spatial cage solitons - taming light bullets; Photonics Res. **10** (2022) 01000148/1-7

MCN22: G. Mercurio, J. Chalupský, I.-T. Nistea, M. Schneider, V. Hájková, N. Gerasimova, R. Carley, M. Cascella, L. L. Guyader, L. Mercadier, J. Schlappa, K. Setoodehnia, M. Teichmann, A. Yaroslavtsev, T. Burian, V. Vozda, L. Vyšín, J. Wild, D. Hickin, A. Silenzi, M. Stupar, J. T. Delitz, C. Broers, A. Reich, B. Pfau, S. Eisebitt, D. L. Civita, H. Sinn, M. Vannoni, S. G. Alcock, L. Juha, and A. Scherz; Real-time spatial characterization of micrometer-sized X-ray free-electron laser beams focused by bendable mirrors; Opt. Express **30** (2022) 20980-20998

MGS22: C. Mei, U. Griebner, and G. Steinmeyer; Thermodynamic and nonlinear optical analysis of solid-state multipass cells for compression of picosecond pulses in the 2-µm range; Phys. Rev. A **106** (2022) 053527/1-9

MHB22: B. Maaß, D. Hartley, K. Busch, and D. Rätzel; Modulated light potentials for state manipulation of quasiparticles in ultra-cold Bose gases; New J. Phys. **24** (2022) 043014/2-23

MKW22a: K. Miyata, K. Kato, S. Wada, and V. Petrov; Thermo-optic dispersion properties of CdSe for parametric nonlinear interactions; Opt. Mater. Express **12** (2022) 963-969

MKW22b: T. Mullins, E. T. Karamatskos, J. Wiese, J. Onvlee, A. Rouzée, A. Yachmenev, S. Trippel, and J. Küpper; Picosecond pulse shaping for strong three-dimensional field-free alignment of generic asymmetric-top molecules; Nat. Commun. **13** (2022) 1431/1-7

MPM22: N. Mayer, S. Patchkovskii, F. Morales, M. Y. Ivanov, and O. Smirnova; Imprinting chirality on atoms using synthetic chiral light fields; Phys. Rev. Lett. **129** (2022) 243201/1-6

MPS22a: R. J. MacDonell, S. Patchkovskii, and M. S. Schuurman; A comparison of partial atomic charges for electronically excited states; J. Chem. Theory Comput. **18** (2022) 1061-1071

MPS22b: E. Malm, B. Pfau, M. Schneider, C. M. Günther, P. Hessing, F. Büttner, A. Mikkelsen, and S. Eisebitt; Reference shape effects on Fourier transform holography; Opt. Express **30** (2022) 38424-38438

MRI22: F. Morales, M. Richter, M. Y. Ivanov, and A. Husakou; Non-instantaneous third-order optical response of gases in low-frequency fields; Opt. Express **30** (2022) 23579-23586

MSY22: C. Mei, G. Steinmeyer, J. Yuan, X. Zhou, and K. Long; Intermodal synchronization effects in multimode fibers with noninstantaneous nonlinearity; Phys. Rev. A **105** (2022) 013516/1-12

NLM22: Z. Nie, F. Li, F. Morales, S. Patchkovskii, O. Smirnova, W. An, C. Zhang, Y. Wu, N. Namb, D. Matteo, K. A. Marsh, F. Tsung, W. B. Mori, and C. Josh; Highly spin-polarized multi-GeV electron beams generated by single-species plasma photocathodes; Phys. Rev. Research **4** (2022) 033015/1-8

NNM22: Z. Nie, N. Nambu, K. A. Marsh, E. Welsh, D. Matteo, C. Zhang, Y. Wu, S. Patchkovskii, F. Morales, O. Smirnova, and C. Joshi; Cross-polarized common-path temporal interferometry for high-sensitivity strong-field ionization measurements; Opt. Express **30** (2022) 25696-25706

ORE22: M. Oelschläger, D. Reiche, C. H. Egerland, K. Busch, and F. Intravaia; Electromagnetic viscosity in complex structured environments: From black-body to quantum friction; Phys. Rev. A **106** (2022) 052205/1-16

OSm22a: A. F. Ordonez and O. Smirnova; A geometric approach to decoding molecular structure and dynamics from photoionization of isotropic samples; Phys. Chem. Chem. Phys. **24** (2022) 13605-13615

OSm22b: A. F. Ordonez and O. Smirnova; Disentangling enantiosensitivity from dichroism using bichromatic fields; Phys. Chem. Chem. Phys. **24** (2022) 7264-7273

OSm22c: A. F. Ordonez and O. Smirnova; Propensity rules for photoelectron circular dichroism in strong field ionization of chiral molecules; Phys. Chem. Chem. Phys. **24** (2022) 5720-5728

PGH22: S. Priyadarshi, I. González-Vallejo, C. Hauf, K. Reimann, M. Woerner, and T. Elsaesser; Phonon-induced relocation of valence charge in boron nitride observed by ultrafast x-ray diffraction; Phys. Rev. Lett. **128** (2022) 136402/1-6

PLL22: Z. Pan, Z.-L. Lin, P. Loiko, G. Zhang, H.-J. Zeng, W.-Z. Xue, P. Camy, V. Petrov, S. Slimi, X. Mateos, F. Díaz, H. Lin, L. Wang, and W. Chen; Polarized spectroscopy and diode-pumped laser operation of disordered Yb:Ca3Gd2(BO3)4 crystal; Opt. Mater. Express **12** (2022) 673-684

PLM22: A. Prokhorov, K. Lamonova, R. Minikayev, J. Lančok, and A. Prokhorov; Ligand hyperfine coupling and electron structure features in the EPR spectra of Cu-doped multicomponent borate crystals: an interpretation based on the concept of the Jahn-Teller effect; Eur. Phys. J. Plus **137** (2022) 1349/1-12

PLS22: Z. Pan, P. Loiko, S. Slimi, H. Yuan, Y. Wang, Y. Zhao, P. Camy, E. Dunina, A. Kornienko, L. Fomicheva, L. Wang, U. Griebner, V. Petrov, R. M. Solé, F. Díaz, M. Aguiló, and X. Mateos; Tm,Ho:Ca(Gd,Lu)AlO_4 crystals: Crystal growth, structure refinement and Judd-Ofelt analysis; J. Lumin. **246** (2022) 118828/1-10

PLW22: Z. Pan, P. Loiko, Y. Wang, Y. Zhao, H. Yuana, J. M. Serres, W. Chen, L. Wang, U. Griebner, V. Petrov, M. Aguiló, F. Díaz, and X. Mateos; Diode-pumped and tunable laser operation of Tm,Ho-codoped modified CNGG-type disordered crystals; SPIE Proc. **11980** (2022) 198003/1-6

PPR22: C. Peltz, J. A. Powell, P. Rupp, A. Summers, T. Gorkhover, M. Gallei, I. Halfpap, E. Antonsson, B. Langer, C. Trallero-Herrero, C. Graf, D. Ray, Q. Liu, T. Osipov, M. Bucher, K. Ferguson, S. Möller, S. Zherebtsov, D. Roll, G. Coslovich, R. N. Coffee, C. Bostedt, A. Rudenko, M. F. Kling, and T. Fennel; Few-femtosecond resolved imaging of laser-driven nanoplasma expansion; New J. Phys. **24** (2022) 043024/1-17

PRW22: C. Pratsch, S. Rehbein, S. Werner, P. Guttmann, H. Stiel, and G. Schneider; X-ray Fourier transform holography with beam shaping optical elements; Opt. Express **30** (2022) 15566-15574

PSD22: C. Pellegrini, S. Sharma, J. K. Dewhurst, and A. Sanna; Ab initio study of ultrafast demagnetization of elementary ferromagnets by terahertz versus optical pulses; Phys. Rev. B **105** (2022) 134425/1-6

PSF22: M. Pancaldi, C. Strüber, B. Friedrich, C. E. Pedersoli, D. D. Angelis, I. P. Nikolov, M. Manfredda, L. Foglia, S. Yulin, C. Spezzani, M. Sacchi, S. Eisebitt, C. v. K. Schmising, and F. Capotondi; The COMIX polarimeter: a compact device for XUV polarization analysis; J. Synchrotron Rad. **29** (2022) 969-977

PTL22: U. Peschel, M. Thümmler, T. Lettau, S. Gräfe, and K. Busch; Two-particle tight-binding description of higher-harmonic generation in semiconductor nanostructures; Phys. Rev. B **106** (2022) 245307/1-14

PWC22: Z. Pan, L. Wang, W. Chen, J. E. Bae, F. Rotermund, Y. Wang, Y. Zhao, P. Loiko, X. Mateos, U. Griebner, and V. Petrov; Sub-100 fs SWCNT-SA mode-locked Tm,Ho:LCLNGG laser; SPIE Proc. **11980** (2022) 1198002/1-6

PWV22: V. Petrov, L. Wang, S. R. Vangala, and V. L. Tassev; Transmission and absorption measurements of GaAsP layers grown from the vapor phase; SPIE Proc. **1198506** (2022) 1-6

RES22: H. Rottke, R. Y. Engel, D. Schick, J. O. Schunck, P. S. Miedema, M. C. Borchert, M. Kuhlmann, N. Ekanayake, S. Dziarzhytski, G. Brenner, U. Eichmann, C. von Korff Schmising, M. Beye, and S. Eisebitt; Probing electron and hole colocalization by resonant four-wave mixing spectroscopy in the extreme ultraviolet; Sci. Adv. **20** (2022) eabn5127/1-20

RIB22: D. Reiche, F. Intravaia, and K. Busch; Wading through the void: Exploring quantum friction and nonequilibrium fluctuations; APL Photonics **7** (2022) 030902/1-9

RKB22a: M. Runge, T. Kang, K. Biermann, K. Reimann, M. Woerner, and T. Elsaesser; Intersubband shift currents in asymmetric quantum wells as a source of mono-cycle terahertz pulses; in *Ultrafast Phenomena 2022*, F. Légaré, T. Tahara, J. Biegert, T. Brixner, and N. Dudovich (eds.) (Optica Publishing Group, Montreal, Quebec, Canada, 2022) Tu5A.3/1-2

RKB22b: J. Reislöhner, D. Kim, I. Babushkin, and A. N. Pfeiffer; Onset of Bloch oscillations in the almost-strong-field regime; Nat. Commun. **13** (2022) 7716/1-8

RLP22: J. Rivera-Dean, T. Lamprou, E. Pisanty, P. Stammer, A. F. Ordóñez, A. S. Maxwell, M. F. Ciappina, M. Lewenstein, and P. Tzallas; Strong laser fields and their power to generate controllable high-photon-number coherent-state superpositions; Phys. Rev. A **105** (2022) 033714/1-24

RMK22: N. Rana, M. S. Mrudul, D. Kartashov, M. Y. Ivanov, and G. Dixit; High-harmonic spectroscopy of coherent lattice dynamics in graphene; Phys. Rev. B **106** (2022) 064303/1-7

RPA22: M. Ruberti, S. Patchkovskii, and V. Averbukh; Quantum coherence in molecular photoionization; Phys. Chem. Chem. Phys. **24** (2022) 19673-19686

RSE22: H. Rottke, D. Schick, and S. Eisebitt; Vierwellenmischung im extremen UV; Physik in unserer Zeit **53** (2022) 216-217

SAH22: S. Staeck, A. Andrle, P. Hönicke, J. Baumann, D. Grötzsch, J. Weser, G. Goetzke, A. Jonas, Y. Kayser, F. Förste, I. Mantouvalou, J. Viefhaus, V. Soltwisch, H. Stiel, B. Beckhoff, and B. Kanngießer; Scan-free GEXRF in the soft x-ray range for the investigation of structured nanosamples; Nanomaterials **12** (2022) 3766/1-13

SHR22: R. Shayduk, J. Hallmann, A. Rodriguez-Fernandez, M. Scholz, W. Lu, U. Bösenberg, J. Möller, A. Zozulya, M. Jiang, U. Wegner, R.-C. Secareanu, G. Palmer, M. Emons, M. Lederer, S. Volkov, I. Lindfors-Vrejoiu, D. Schick, M. Herzog, M. Bargheer, and A. Madsen; Femtosecond x-ray diffraction study of multi-THz coherent phonons in $SrTiO_3$; Appl. Phys. Lett. **120** (2022) 202203/1-5

SES22: S. Sharma, P. Elliott, and S. Shallcross; Valley control by linearly polarized laser pulses: example of WSe_2; Optica **9** (2022) 947-952

SIJ22: R. E. F. Silva, M. Y. Ivanov, and Á. Jiménez-Galán; All-optical valley switch and clock of electronic dephasing; Opt. Express **30** (2022) 30347-30355

SJi22: R. E. F. Silva and Á. Jiménez-Galán; Reconstruction of attosecond beating by interference of two-photon interband transitions in solids; Phys. Rev. A **106** (2022) 053103/1-8

SKE22: S. Shallcross, C. von Korff Schmising, P. Elliott, S. Eisebitt, J. K. Dewhurst, and S. Sharma; Electronic origin of x-ray absorption peak shifts; Phys. Rev. B **106** (2022) L060302/1-6

SKZ22: L. Seiffert, S. Zherebtsov, M. F. Kling, and T. Fennel; Strong-field physics with nanospheres; Advanced in Physics: X **7** (2022) 2010595/1-60

SLD22: S. Shallcross, Q. Z. Li, J. K. Dewhurst, S. Sharma, and P. Elliott; Ultrafast optical control over spin and momentum in solids; Appl. Phys. Lett. **120** (2022) 032403/1-6

SNB22: G. Steinmeyer, T. Nagy, I. Babushkin, and C. Mei; Cage solitons; SPIE Proc. **11986** (2022) 1198602/1-6

SNC22: A. K. Schnack-Petersen, B. Nunes Cabral Tenório, S. Coriani, P. Decleva, J. Tross, K. Ramasesha, M. Coreno, R. Totan, and A. Röder; Core spectroscopy of oxazole; J. Chem. Phys. **157** (2022) 214305/1-14

SRL22: P. Stammer, J. Rivera-Dean, T. Lamprou, E. Pisanty, M. F. Ciappina, P. Tzallas, and M. Lewenstein; High photon number entangled states and coherent state superposition from the extreme ultraviolet to the far infrared; Phys. Rev. Lett. **128** (2022) 123603/1-7

SSE22a: F. Steinbach, N. Stetzuhn, D. Engel, U. Atxitia, C. v. K. Schmising, and S. Eisebitt; Accelerating double pulse all-optical write/erase cycles in metallic ferrimagnets; Appl. Phys. Lett. **120** (2022) 112406/1-7

SSE22b: S. Sharma, S. Shallcross, P. Elliott, S. Eisebitt, C. v. K. Schmising, and J. K. Dewhurst; Computational analysis of transient XMCD sum rules for laser pumped systems: When do they fail?; Appl. Phys. Lett. **120** (2022) 062409/1-8

SSE22c: S. Sharma, S. Shallcross, P. Elliott, and J. K. Dewhurst; Making a case for femto-phono-magnetism with FePt; Sci. Adv. **8** (2022) eabq2021/1-6

Ste22: G. Steinmeyer; Creating the perfect plasmonic wave; Light-Sci. Appl. **11** (2022) 229/1-2

SVN22: M. B. Soley, P. E. Videla, E. T. J. Nibbering, and V. S. Batista; Ultrafast charge relocation dynamics in enol−keto tautomerization monitored with a local soft-X-ray probe; J. Phys. Chem. Lett. **13** (2022) 8254-8263

SZG22a: P. Singh, J. Zhang, A. Ghalgaoui, K. Reimann, B. P. Fingerhut, M. Woerner, and T. Elsaesser; Coherent polaron dynamics of electrons solvated in polar liquids; PNAS Nexus **1** (2022) pgac078/1-8

SZG22b: P. Singh, J. Zhang, A. Ghalgaoui, K. Reimann, B. P. Fingerhut, M. Woerner, and T. Elsaesser; Coherent underdamped polarons in liquid alcohols; in *Ultrafast Phenomena 2022*, F. Légaré, T. Tahara, J. Biegert, T. Brixner, and N. Dudovich (eds.) (Optica Publishing Group, Montreal, Quebec, Canada, 2022) W4A.30/1-2

SZL22: S. Sun, H.-J. Zeng, Z.-L. Lin, W.-Z. Xue, G. Zhang, Z. Lin, V. Petrov, H. Lin, P. Loiko, X. Mateos, Y. Zhao, B. Teng, L. Wang, and W. Chen; SESAM mode-locked Yb:Sr3Y2(BO3)4 laser; Opt. Express **30** (2022) 11861-11871

TBC22: K. Tschernig, K. Busch, D. N. Christodoulides, and A. Perez-Leija; Branching high-order exceptional points in Non-Hermitian optical systems; Laser Photon. Rev. **16** (2022) 2100707/1-9

TKA22: J. Tarrant, M. Khokhlova, and V. Averbukh; Interferometry of quantum revivals; J. Chem. Phys. **157** (2022) 054304/1-8

TMB22: K. Tschernig, G. Martinez-Niconoff, K. Busch, M. A. Bandres, and A. Perez-Leija; Topological protection of partially coherent light; Photonics Res. **10** (2022) 1223-1231

TYW22: D. Turenne, A. Yaroslavtsev, X. Wang, V. Unikandanuni, I. Vaskivskyi, M. Schneider, E. Jal, R. Carley, G. Mercurio, R. Gort, N. Agarwal, B. V. Kuiken, L. Mercadier, J. Schlappa, L. L. Guyader, N. Gerasimova, M. Teichmann, D. Lomidze, A. Castoldi, D. Potorochin, D. Mukkattukavil, J. Brock, N. Z. Hagström, A. H. Reid, X. Shen, X. J. Wang, P. Maldonado, Y.Kvashnin, K. Carva, J. Wang, Y. K. Takahashi, E. E. Fullerton, S. Eisebitt, P. M. Oppeneer, S. Molodtsov, A. Scherz, S. Bonetti, E. Iacocca, and H. A. Dürr; Nonequilibrium sub–10 nm spin-wave soliton formation in FePt nanoparticle; Sci. Adv. **8** (2022) 0523/1-10

UJO22: A. J. Uzan-Narovlansky, Á. Jiménez-Galán, G. Orenstein, R. E. F. Silva, T. Arusi-Parpar, S. Shames, B. D. Bruner, B. Yan, O. Smirnova, M. Y. Ivanov, and N. Dudovich; Observation of light-driven band structure via multiband high-harmonic spectroscopy; Nat. Photonics **16** (2022) 428-432

Vra22: M. J. J. Vrakking; Ion-photoelectron entanglement in photoionization with chirped laser pulses; J. Phys. B **55** (2022) 134001/1-9

WFE22: M. Woerner, B. P. Fingerhut, and T. Elsaesser; Field-induced electron generation in water: solvation dynamics and many-body interactions; J. Phys. Chem. B **126** (2022) 2621-2634

WHZ22: M.-O. Winghart, P. Han, Z.-Y. Zhang, R. Mitzner, M. Fondell, E. Pines, M. Odelius, P. Wernet, and E. T. J. Nibbering; Ultrafast electronic structural dynamics of water-mediated photoacid-base proton transfer reactions; in *Ultrafast Phenomena 2022*, F. Légaré, T. Tahara, J. Biegert, T. Brixner, and N. Dudovich (eds.) (Optica Publishing Group, Montreal, Quebec, Canada, 2022) Th4A.6/1-2

WLZ22: Y. Wang, P. Loiko, Y. Zhao, Z. Pan, W. Chen, M. Mero, X. Xu, J. Xu, X. Mateos, A. Major, M. Guina, V. Petrov, and U. Griebner; Polarized spectroscopy and SESAM mode-locking of Tm,Ho:CALGO; Opt. Express **30** (2022) 7883-7893

WOS22: T. Witting, M. Osolodkov, F. Schell, F. Morales, S. Patchkovskii, P. Šušnjar, F. H. M. Cavalcante, C. S. Menoni, C. P. Schulz, F. J. Furch, and M. J. J. Vrakking; Generation and characterisation of isolated attosecond pulses at 100 kHz repetition rate; Optica **9** (2022) 145-151

WPG22: M. Woerner, S. Priyadarshi, I. González-Vallejo, C. Hauf, K. Reimann, and T. Elsaesser; Phonon-induced valence-charge relocation in cubic BN observed by ultrafast x-ray diffraction; in *Ultrafast Phenomena 2022*, F. Légaré, T. Tahara, J. Biegert, T. Brixner, and N. Dudovich (eds.) (Optica Publishing Group, Montreal, Quebec, Canada, 2022) Th2B.4/1-2

WSG22: C.-Y. Wang, S. Sharma, E. K. U. Gross, and J. K. Dewhurst; Dynamical Born effective charges; Phys. Rev. B **106** (2022) L180303/1-7

WSM22: C.-Y. Wang, S. Sharma, T. Müller, E. K. U. Gross, and J. K. Dewhurst; Coupled Bogoliubov equations for electrons and phonons; Phys. Rev. B **105** (2022) 174509/1-13

WVP22: L. Wang, S. R. Vangala, S. Popien, M. Beutler, V. L. Tassev, and V. Petrov; Second-harmonic generation in heteroepitaxially grown, orientation-patterned, ternary GaAsP periodic structures; Phys. Status Solidi-R **16** (2022) 2200198/1-9

XLQ22: S. P. Xu, M. Q. Liu, W. Quan, L. B. Zheng, Z. Q. Wang, M. Zhao, S. G. Yu, R. P. Sun, Y. L. Wang, L. Q. Hua, X. Y. Lai, W. Becker, J. Chen, and X. Liu; Wavelength scaling of strong-field Rydberg-state excitations: towards an effective S-matrix theory; Phys. Rev. A **106** (2022) 063106/1-7

XLZ22a: W.-Z. Xue, Z.-L. Lin, H.-J. Zeng, G. Zhang, P. Zhang, Z. Chen, Z. Li, V. Petrov, P. Loiko, X. Mateos, H. Lin, Y. Zhao, L. Wang, and W. Chen; Diode-pumped SESAM mode-locked Yb:(Y,Gd)AlO_3 laser; Opt. Express **30** (2022) 11825-11832

XLZ22b: W.-Z. Xue, Z.-L. Lin, H.-J. Zeng, G. Zhang, P. Loiko, L. Basyrova, A. Benayad, P. Camy, V. Petrov, X. Mateos, L. Wang, and W. Chen; Diode-pumped mode-locked Yb:BaF_2 laser; Opt. Express **30** (2022) 15807-15818

YSB22: K. Yao, F. Steinbach, M. Borchert, D. Schick, D. Engel, F. Bencivenga, R. Mincigrucci, L. Foglia, E. Pedersoli, D. D. Angelis, M. Pancaldi, B. Wehinger, F. Capotondi, C. Masciovecchio, S. Eisebitt, and C. v. K. Schmising; All-optical switching on the nanometer scale excited and probed with femtosecond extreme ultraviolet pulses; Nano Lett. **22** (2022) 4453-4458

ZBL22a: L. Zhang, R.-X. Bai, H. Lin, P. Loiko, X. Mateos, Z.-L. Lin, Z. Lin, G. Zhang, V. Petrov, L. Wang, and W. Chen; Disordered Yb:GdYCOB crystal: polarized spectroscopy, thermal lensing and diode-pumped lasers; SPIE Proc. **11980** (2022) 119800L/1-5

ZBL22b: L. Zhang, L. Basyrova, P. Loiko, P. Camy, Z. Lin, G. Zhang, S. Slimi, R. M. Solé, X. Mateos, M. Aguiló, F. Díaz, E. Dunina, A. Kornienko, U. Griebner, V. Petrov, L. Wang, and W. Chen; Growth, structure, and polarized spectroscopy of monoclinic Er^3+:$MgWO_4$ crystal; Opt. Mater. Express **12** (2022) 2028-2040

ZJS22: D. Zahn, F. Jakobs, H. Seiler, T. A. Butcher, D. Engel, J. Vorberger, U. Atxitia, Y. W. Windsor, and R. Ernstorfer; Intrinsic energy flow in laser-excited 3d ferromagnets; Phys. Rev. Research **4** (2022) 013104/1-13

ZKE22: J. Zhang, A. Kundu, T. Elsaesser, P. Macchi, M. Kalter, G. Eickerling, and W. Scherer; Ultrafast vibrational response of activated C-D bonds in a chloroform-platinum(II) complex; J. Phys. Chem. Lett. **13** (2022) 4447-4454

ZKH22: Z.-Y. Zhang, C. Kleine, P. Han, M.-O. Winghart, M. J. J. Vrakking, E. T. J. Nibbering, and A. Rouzée; Femtosecond soft X-ray absorption spectroscopy of photo-excited NO_2; in *Ultrafast Phenomena 2022*, F. Légaré, T. Tahara, J. Biegert, T. Brixner, and N. Dudovich (eds.) (Optica Publishing Group, Montreal, Quebec, Canada, 2022) Th4A:29/1-2

ZLP22: H.-J. Zeng, Z.-L. Lin, Z. Pan, P. Loiko, X. Mateos, H. Lin, W.-Z. Xue, G. Zhang, V. Petrov, L. Wang, and W. Chen; Continuous-wave and passively mode-locked operation of Yb:$Ca_3Gd_2(BO_3)_4$ laser; SPIE Proc. **11980** (2022) 119800M/1-5

ZLW22: N. Zhang, S. Liu, Z. Wang, J. Liu, X. Xu, J. Xu, J. Wang, P. Liu, J. Ma, D. Shen, D. Tang, H. Lin, J. Zhang, W. Chen, Y. Zhao, U. Griebner, and V. Petrov; SESAM mode-locked Tm:Y2O3 ceramic laser; Opt. Express **30** (2022) 29531-29538

ZLX22: H.-J. Zeng, Z.-L. Lin, W.-Z. Xue, G. Zhang, Y. Chen, Z. Pan, V. Petrov, P. Loiko, X. Mateos, Y. Zhao, H. Lin, L. Wang, and W. Chen; Soliton mode-locked Yb:$Ca_3Gd_2(BO_3)_4$ laser; Opt. Express **30** (2022) 11833-11839

ZWL22: N. Zhang, Z. Wang, S. Liu, W. Jing, H. Huang, Z. Huang, K. Tian, Z. Yang, Y. Zhao, U. Griebner, V. Petrov, and W. Chen; Watt-level femtosecond Tm-doped “mixed” sesquioxide ceramic laser in-band pumped by a Raman fiber laser at 1627 nm; Opt. Express **30** (2022) 23978/1-8

ZZF22: Q. Zhong, H. Zhao, L. Feng, K. Busch, Ş. K. Özdemir, and R. El-Ganainy; The missing link between standing- and traveling-wave resonators; Nanophotonics **11** (2022) 4427-4437

ZZH22: Y. Zhao, C. Zheng, Z. Huang, Q. Gao, J. Dong, K. Tian, Z. Yang, W. Chen, and V. Petrov; Twisted light in a single-crystal fiber: Toward undistorted femtosecond vortex amplification; Laser Photon. Rev. **online** (2022) 2200503/1-9

in press

BTM: A. Bercha, W. Trzeciakowski, G. Muziol, J. W. Tomm, and T. Suski; Evidence for “dark charge” from photoluminescence measurements in wide InGaN quantum wells; Opt. Express

BVR: F. Braußе, M. J. J. Vrakking, and A. Rouzée; Shape resonances in angle-resolved photoionization of aligned CF3I molecules; J. Phys. B: At. Mol. Opt. Phys.

CMB: J. Correa, M. Mehrjoo, R. Battistelli, F. Lehmkühler, A. Marras, C. B. Wunderer, T. Hirono, V. Felk, F. Krivan, S. Lange, I. Shevyakov, V. Vardanyan, M. Zimmer, M. Hoesch, K. Bagschik, N. Guerrini, B. Marsh, I. Sedgwick, G. Cautero, L. Stebel, D. Giuressi, R. H. Menk, A. Greer, T. Nicholls, W. Nichols, U. Pedersen, P. Shikhaliev, N. Tartoni, H. J. Hyun, S. H. Kim, S. Y. Park, K. S. Kim, F. Orsini, F. J. Iguaz, F. Büttner, B. Pfau, E. Plönjes, K. Kharitonov, M. Ruiz-Lopez, R. Pan, S. Gang, B. Keitel, and H. Graafsmaa; The PERCIVAL detector: first user experiments; J. Synchrotron Rad.

GEi: M. Genevriez and U. Eichmann; Isolated-core quadrupole excitation of highly excited autoionizing Rydberg states; Phys. Rev. A

GJLa: R. Grunwald, M. Jurke, M. Liebmann, and M. Bock; Orbital angular momentum encoded beam tracking and wavefront sensing; J. Lightwave Technol.

HWE: C. Hauf, M. Woerner, and T. Elsaesser; Femtosecond diffraction with laser-driven hard x-ray sources: Nuclear motions and transient charge densities; in *Structural Dynamics with X-ray and Electron Scattering*, K. Amini, A. Rouzée, and M. J. J. Vrakking (eds.) (RSC)

JPS: A. S. Johnson, D. Pérez-Salinas, K. M. Siddiqui, S. Kim, S. Choi, K. Volckaert, P. E. Majchrzak, S. Ulstrup, K. Hallman, R. F. Haglund, C. M. Günther, B. Pfau, S. Eisebitt, D. Backes, F. Maccherozzi, A. Fitzpatrick, S. Dhesi, P. Gargiani, M. Valvidares, N. Artrith, F. d. Groot, H. Choi, D. Jang, A. Katoch, S. Kwon, S. H. Park, H. Kim, and S. E. Wall; Ultrafast X-ray imaging of the light-induced phase transition in VO_2; Nat. Phys.

KBH: C. Klose, F. Büttner, W. Hu, C. Mazzoli, K. Litzius, R. Battitelli, I. Lemesh, J. M. Bartell, M. Huang, C. M. Günther, M. Schneider, A. Barbour, S. B. Wilkins, G. S. D. Beach, S. Eisebitt, and B. Pfau; Coherent correlation imaging: resolving fluctuating states of matter; Nature

KBU: K. Kato, V. V. Badikov, N. Umemura, K. Miyata, and V. Petrov; Phase-matching properties of $Ba_2Ga_8GeS_{16}$; J. Opt. Soc. Am. B

KHB: R. Kahvedzić, D. Habibović, W. Becker, S. Gräfe, and D. B. Milošević; Nondipole effects in atomic ionization induced by an intense counterrotating bicircular laser field; Ann. Phys.-Berlin

KUB: K. Kato, N. Umemura, V. V. Badikov, D. V. Badikov, T. Okamoto, K. Miyata, V. Petrov; Sellmeier and thermo-optic dispersion formulas for $BaGa_2GeS_{6,}$; SPIE Proc.

LKB: F. Loth, T. Kiel, K. Busch, and P. T. Kristensen; Surface roughness in finite-element meshes: application to plasmonic nanostructures; J. Opt. Soc. Am. B

MWC: R. T. Murray, L. Wang, W. Chen, R. A. Battle, A. Schirrmacher, E. Büttner, V. Petrov, Narrowband seeding of a PPLN nonresonant optical parametric oscillator; SPIE Proc.

PEi: B. Pfau and S. Eisebitt; X-ray resonant scattering and holography with application to magnetization dynamics; in *Structural Dynamics with X-ray and Electron Scattering*, A. Rouzée and M. J. J. Vrakking K. Amini (eds.)

PLS: Z. Pan, P. Loiko, J. M. Serres, H. Yuan, Y. Wang, L. Wang, Y. Zhao, R. M. Solé, M. Aguiló, F. Díaz, P. Camy, W. Chen, U. Griebner, V. Petrov, and X. Mateos; Tm,Ho:Ca(Gd,Lu)AlO_4 crystals: Polarized spectroscopy and laser operation; J. Lumin.

RCB: R. Rouzegar, A. L. Chekhov, Y. Behovits, B. R. Serrano, M. A. Syskaki, C. H. Lambert, D. Engel, U. Martens, M. Münzenberg, M. Wolf, G. Jakob, M. Kläui, T. S. Seifert, and T. Kampfrath; Broadband spintronic terahertz source with peak electric fields exceeding 1.5 MV/cm; Phys. Rev. Appl.

SÖB: L. Simonson, Ş. K. Özdemir, K. Busch, and R. El-Ganainy; Resolvent expansion for discrete non-Hermitian resonant systems [Invited]; Opt. Mater. Express

ZPJ: Z. Zang, S. Peng, W. Jin, Y. Zuo, G. Steinmeyer, Y. Dai, and D. Liu; In-situ measurement and compensation of complex spatio-temporal couplings in ultra-intense lasers; Opt. Las. Eng.

ZSZ: N. Zhang, Q. Song, J. Zhou, J. Liu, S. Liu, H. Zhang, X. Xu, Y. Xue, J. Xu, W. Chen, Y. Zhao, U. Griebner, and V. Petrov; 44-fs pulse generation at 2.05 µm from a SESAM mode-locked Tm:$GdScO_3$ laser; Opt. Lett.

Submitted

ARF: N. Acharyya, M. Richter, and B. P. Fingerhut; Coherent dynamics of the off-diagonal Spin-Boson model in the ultra-strong coupling regime; Phys. Rev. Research

BEK: M. Borchert, D. Engel, C. v. K. Schmising, B. Pfau, S. Eisebitt, and D. Schick; Picosecond x-ray magnetic circular dichroism spectroscopy at the Fe L-edges with a laser-driven plasma source; Optica

CKW: M.-A. Codescu, T. Kunze, M. Weiß, M. Brehm, O. Kornilov, D. Sebastiani, and E. T. J. Nibbering; Ultrafast proton transfer pathways mediated by amphoteric imidazole; J. Phys. Chem. Lett.

EAA: R. Y. Engel, O. Alexander, K. Atak, U. Bovensiepen, J. Buck, R. Carley, M. Cascella, V. Chardonnet, G. S. Chiuzbaian, C. David, F. Döring, A. Eschenlohr, N. Gerasimova, F. d. Groot, L. L. Guyader, O. S. Humphries, M. Izquierdo, E. Jal, A. Kubec, T. Laarmann, C.-H. Lambert, J. Lüning, J. P. Marangos, L. Mercadier, G. Mercurio, P. S. Miedema, K. Ollefs, B. Pfau, B. Rösner, K. Rossnagel, N. Rothenbach, A. Scherz, J. Schlappa, M. Scholz, J. O. Schunck, K. Setoodehnia, C. Stamm, S. Techert, S. M. Vinko, H. Wende, A. A. Yaroslavtsev, Z. Yin, and M. Beye; Electron dynamics at high-energy densities in Nickel from non-linear resonant X-ray absorption spectra; Phys. Rev. Lett.

FBM: B. Fetić, W. Becker, and D. B. Milošević; Can we measure the Wigner time delay in a photoionization experiment?; Phys. Rev. Lett.

FGS: M. Fleischmann, R. Gupta, S. Sharma, and S. Shallcross; Moiré quantum well states in tiny angle two dimensional semi-conductors; Phys. Rev. Lett.

GJL: R. Grunwald, M. Jurke, M. Liebmann, M. Bock, B. P. Bruno, H. Gowda, and U. Wallrabe; Structuring light by combining spatial modulation and fast angular shaping; SPIE Proc.

GLS: K. Gerlinger, R. Liefferink, M. Schneider, L.-M. Kern, C. Klose, D. Metternich, D. Engel, F. Capotondi, D. D. Angelis, M. Pancaldi, E. Pedersoli, F. Büttner, S. Eisebitt, J. H. Mentink, and B. Pfau; Robust scenario for the generation of non-equilibrium topological fluctuation states; Phys. Rev. Lett.

GPH: K. Gerlinger, B. Pfau, M. Hennecke, L.-M. Kern, I. Will, T. Noll, M. Weigand, J. Gräfe, N. Träger, M. Schneider, C. M. Günther, D. Engel, G. Schütz, and S. Eisebitt; Pump-probe x-ray microscopy of photo-induced magnetization dynamics at MHz repetition rates; Struct. Dyn.

HKY: M. Hennecke, C. von Korff Schmising, K. Yao, E. Jal, B. Vodungbo, V. Chardonnet, K. L. garé, F. Capotondi, D. Naumenko, E. Pedersoli, I. Lopez-Quintas, I. P. Nikolov, L. Raimondi, G. D. Ninno, L. Salemi, S. Ruta, R. Chantrell, T. Ostler, B. Pfau, D. Engel, P. M. Oppeneer, S. Eisebitt, and I. Radu; Ultrafast Opto-magnetic Effects in the Extreme Ultraviolet Spectral Range; Phys. Rev. Lett.

KGR: A. Koç, I. González-Vallejo, K. Reimann, L. Kremeyer, F. Thiemann, M. Horn von Hoegen, K. Sokolowski-Tinten, M. Woerner, and T. Elsaesser; Quantum pathways of carrier and coherent phonon excitation in bismuth; Phys. Rev. Lett.

KJY: C. von Korff Schmising, S. Jana, K. Yao, M. Hennecke, P. Scheid, S. Sharma, M. Viret, J.-Y. Chauleau, D. Schick, and S. Eisebitt; Ultrafast behavior of induced and intrinsic magnetic moments in CoFeB/Pt bilayers probed by element-specific spectroscopy in the extreme ultraviolet spectral range; Phys. Rev. Research

MKS: B. Major, K. Kovács, E. Svirplys, M. Anus, O. Ghafur, K. Varjú, M. J. J. Vrakking, V. Tosa, and B. Schütte; High-harmonic generation in a strongly overdriven regime; Phys. Rev. A

OSm: A. F. Ordonez and O. Smirnova; On the molecular information revealed by photoelectron angular distributions of isotropic samples; Phys. Rev. A

RRW: M. Runge, K. Reimann, M. Woerner, and T. Elsaesser; Nonlinear terahertz polarizability of electrons solvated in polar liquids; Phys. Rev. Lett.

RTG: J. Ruschel, J. W. Tomm, J. Glaab, T. Kolbe, A. Knauer, J. Rass, N. L. Ploch, T. Musengezi, and S. Einfeldt; Spatially resolved degradation effects in UVB LEDs stressed by constant current operation; Appl. Phys. Lett.

SBY: J. Schlipf, F. Berkmann, Y. Yamamoto, M. Reichenbach, M. Veleski, Y. Kawaguchi, F. Mörz, J. W. Tomm, D. Weißhaupt, and I. A. Fischer; Robust Si/Ge heterostructure metasurfaces as building blocks for wavelength-selective photodetectors; Appl. Phys. Lett.

Smi: O. Smirnova; Controlling, shaping and imaging quantum matter with intense light, in viewpoint on attosecond and FEL science; Nat. Rev. Phys.

STF: G. Steinmeyer, J. W. Tomm, P. Fuertjes, U. Griebner, S. S. Balabanov, and T. Elsaesser; Efficient electronic excitation transfer via phonon-assisted dipole-dipole coupling in Fe^{2+}:Cr^{2+}:ZnSe; Phys. Rev. Appl.

TSF: J. W. Tomm, G. Steinmeyer, P. Fuertjes, U. Griebner, and T. Elsaesser; Excitation transfer from Cr^{2+} to Fe^{2+} ions in co-doped ZnSe as a pumping scheme for infrared solid-state lasers; J. Electron. Mater.

WFG: D. Weckbecker, M. Fleischmann, R. Gupta, W. Landgraf, S. Leitherer, O. Pankratov, S. Sharma, V. Meded, and S. Shallcross; Moiré ordered current loops in the graphene twist bilayer; 2D Mat.

General Publications

EGS22: T. Elsaesser, M. Grötschel, M. Scheffler, J. H. Ullrich, and F. v. Blanckenburg; Open Research Data in Naturwissenschaften und Mathematik; in *Denkanstöße aus der Akademie* (Berlin-Brandenburgische Akademie der Wissenschaften, Berlin, 2022) Vol. 10, 1-10

Bachelor, Master and PhD Theses

Bachelor Theses

Lun22: L. Lunin; *Pulsgetriggerte Detektion resonanter magnetischer Kleinwinkelstreuung an einer Laser-getriebenen Röntgenquelle* (Supervisors: S. Eisebitt and B. Pfau), Technische Universität Berlin

OZü22: O. Zülich; *Direkte und indirekte Anregung ferromagnetisher Eisen-Nickel Legierungen untersucht durch elementspezifische EUV-Spektroskopie* (Supervisors: C. von Korff Schmising and S. Eisebitt), TU Berlin

Wei22: B. Weinmann; Magnetotransport Measurements of the Laser-Induced Nucleation of Skyrmions (Supervisors: S. Eisebitt and B. Pfau), Technische Universität Berlin

Master Theses

Dei22: V. Deinhart; *Ion-patterning of ferrimagnetic FeGd films* (Supervisors: S. Eisebitt and B. Pfau), Technische Universität Berlin

Sma22: P. Smaliukas; *Development of a front-end for an OPCPA system based on the Raman selffrequency shift* (Supervisor: G. Steinmeyer), Humboldt-Universität zu Berlin

PhD theses

Ben22: U. Bengs; *Driving strong-field processes with tailored laser pulses* (Supervisors: M. Y. Ivanov and N. Zhavaronkov), Humboldt-Universität zu Berlin

Cod22: M.-A. Codescu; *Photoinduced intermolecular proton transfer in solution monitored by femtosecond infrared spectroscopy* (Supervisor: T. Elsaesser), Humboldt-Universität zu Berlin

Li22: Q. Li; *Ultra long range effects in ultra fast spin dynamics* (Supervisors: P. Brouwer and S. Sharma), Freie Universität Berlin

Oso22: M. Osolodkov; *Attosecond XUV- IR pump- probe measurements of small molecules using 3D momentum spectroscopy* (Supervisors: M. J. J. Vrakking and T. Witting), Freie Universität Berlin

Sch22: J. Schauss; *The phosphate vibration as a sensor for ion-pair formation studied by nonlinear time-resolved vibrational spectroscopy* (Supervisor: T. Elsaesser), Humboldt-Universität zu Berlin

Sen22: B. Senfftleben; *Coherent diffractive imaging of electron dynamics in the attosecond domain* (Supervisors: S. Eisebitt and D. Rupp), Technische Universität Berlin

Tsc22: K. Tschernig; *Tailoring non-classical states of light for applications in quantum information processing* (Supervisors: K. Busch and A. Perez-Leija), Humboldt-Universität zu Berlin

Yao22: K. Yao; *Magnetization Dynamics: Ultrafast, Ultrasmall, Studied with Extreme Ultraviolet Radiation* (Supervisor: S. Eisebitt), Technische Universität Berlin

Appendix 2

External Talks, Teaching

Invited lectures at conferences

D. Ayuso and O. Smirnova; APS March Meeting 2022 (virtual, 2022-04): *Opportunities for imaging chiral nuclear dynamics on ultrafast timescales with synthetic chiral light*

K. Busch; NanoPhoton Conference 2022 (Rungstegaard, Denmark, 2022-06): *Time-domain simulations of nano-photonic systems: advances using the DGTD method*

K. Busch; MeepCon 2022 (Cambridge, MA, USA, 2022-07): *Advances in finite-element time-domain simulations*

K. Busch; DokDok 2022 (Arnstadt, Germany, 2022-08): *Multi-Photon dynamics in tight-binding lattices*

K. Busch; HIOS Symposium 2022 (Berlin, Germany, 2022-10): *Modelling Active Nano-Photonic Systems*

S. Carlström; ATTO-FEL 2022 (London, UK, 2022-06): *Spin-polarized photoelectrons in linearly polarized light*

W. Chen; CIOP 2022, 13th Int. Conference on Information Optics and Photonics (Xi'an, China, 2022-08): *Sub-40 fs Kerr-lens mode-locked Tm,Ho laser at ~2 µm*

W. Chen *together with* P. Loiko, X. Mateos, P. Camy, U. Griebner, and V. Petrov; Europhoton 2022 (Hanover, Germany, 2022-08): *Recent progress in laser crystals and ceramics for femtosecond mode-locked lasers at ~2 µm*

U. Eichmann; 14th Int. Conference on Synchrotron Radiation Instrumentation - SRI 2021 (virtual, 2022-03): *Photon-Recoil Imaging: expanding the view of nonlinear X-ray physics*

S. Eisebitt; Magnetofon, Joint Meeting of Working Groups 1 & 2 (Messina, Italy, 2022-03): *Watching magnetization evolve in space - what soft x-ray pulses can do for you*

S. Eisebitt; 762. WE-Heraeus-Seminar "Diffraction Limited Synchrotron Light Sources and Next Generation Free Electron Lasers" (Physikzentrum Bad Honnef, Germany, 2022-03): *Nano- to mesoscale magnetization dynamics: new insight enabled by coherent x-ray pulses*

S. Eisebitt; 12th Ultrafast Surface Dynamics Conference (USD12) (ICFO/Centro de Ciendias de Benasque Pedro Pascual, Spain, 2022-05): *Laser-driven nuleation of a topological phase & depth-profiling of magnetization dynamics*

S. Eisebitt; 5th Int. Conference on resonant elastic X-ray scattering (Paris, France, 2022-06): *REXS accessing magnetization dynamics: Following the birth of topological structures and some surprises when looking into the depth*

P. Elliott; Magnetofon, Joint Meeting of Working Groups 1 & 2 (Messina, Italy, 2022-03): *Ab-initio Simulation of Ultrafast Spin Dynamics and the Giant Optical Spin Hall Effect*

P. Elliott; 12th Ultrafast Surface Dynamics Conference (USD12) (ICFO/ Centro de Ciendias de Benasque Pedro Pascual, Spain, 2022-05): *Ab-initio simulation of ultrafast spin dynamics: Phonomagnetism and the giant optical spin hall effect*

P. Elliott; 5th Ultrafast Magnetism Conference (UMC 2022) (Nancy, France, 2022-09): *Ab-initio simulation of ultrafast spin dynamics: phonomagnetism and the giant optical spin hall effect*

T. Elsaesser; Spring Meeting of the American Society (San Diego, CA, USA, 2022-03): *Charge solvation in water: Ultrafast dynamics and electric interactions*

T. Elsaesser; Workshop 'Advances of Multidimensional Vibrational Spectroscopy in Water, Biology, and Materials Science' (Telluride, CO, USA, virtual, 2022-07): *Ultrafast solvation of electrons and ions in polar liquids*

T. Elsaesser; Nobel Symposium 173 'Exploring complex molecular and condensed phase processes and functions by multidimensional spectroscopy from THz to X-rays' (Baståd, Sweden, 2022-08): *Charge dynamics in water and hydrated biomolecules mapped by 2D infrared and terahertz spectroscopy*

T. Elsaesser; 2nd European Symposium on Ultrafast Laser-Driven Biophotonics (Jena, Germany, 2022-09): *Ultrafast vibrational probes of electric interactions in hydrated RNA*

B. P. Fingerhut; Undergraduate Research Conference on Molecular Sciences (URCUP) (Kloster Irsee, Germany, 2022-10): *Towards the numerically exact transfer dynamics in photoactive proteins*

U. Griebner *together with* L. von Grafenstein, M. Bock, T. Nagy, and T. Elsaesser; VII Ultrafast Dynamics and Metastability & Ultrafast Bandgap Photonics 2022 (Hersonissos, Crete, Greece, 2022-06): *2-µm chirped pulse amplifier system emitting >10 GW peak power at kHz repetition rate*

A. Husakou; Crete VII Ultrafast Dynamics Symposium (Crete, Greece, 2022-06): *Injection current and its role in harmonic generation in amorphous dielectrics*

M. Y. Ivanov; PQE'2022, The 51st Winter Colloquium on the Physics of Quantum Electronics (Snowbird, Utah, USA, 2022-01): *Toward Valleytronics at PHz Rates*

M. Y. Ivanov; Int. COST/ZCAM School on Computational methods for attosecond processes (Zaragoza, Spain, 2022-03): *Fundamentals of strong field dynamics*

M. Y. Ivanov; 4th Int. Workshop on Quantum and Topological Nanophotonics (Singapore, 2022-04): *Lightwave electronics in trivial and strongly correlated solids*

M. Y. Ivanov, Int. Workshop on Attosecond Science and Wolf prize award ceremony (Haifa and Jerusalem, Israel, 2022-06): *Towards Peta-Hertz light-wave electronics*

M. Y. Ivanov, ECAMP conference (Vilnius, Lithunia, 2022-06): Lightwave electronics in trivial, topological, and strongly correlated solids

M. Ivanov; ATTO VIII Conference (University of Central Florida, Orlando, FL, USA, 2022-07): Lightwave electronics in trivial and strongly correlated solids

M. Y. Ivanov; EPS Symposium on the Third Generation Metamaterials, METAMATERIALS 3.1 (Cetraro, Calabrien, Italy, 2022-08): Lightwave electronics in trivial and strongly correlated solids

P. Jürgens *together with* B. Liewehr, B. Kruse, C. Peltz, T. Witting, A. Husakou, A. Rouzée, M. Y. Ivanov, T. Fennel, M. J. J. Vrakking, and A. Mermillod-Blondin; CIOP 2022, The 13th Int. Conference on Information Optics and Photonics (Xi'an, China, 2022-08): *Reconstruction of strong-field-driven carrier generation dynamics from injection harmonics in solid dielectrics*

A. Koç together with C. Hauf, M. Woerner, L. von Grafenstein, D. Ueberschaer, U. Griebner, M. Bock, and T. Elsaesser; CLEO 2022 (San Jose, CA, USA, 2022-05): *High-flux table-top hard x-ray source driven by few-cycle 5 µm OPCPA at a 1 kHz repetition rate*

N. Mayer; DPG SAMOP, virtual (Erlangen, Germany 2022-03): *Synthetic chiral light for Control of achiral and chiral media*

A. Mermillod-Blondin; Photonics Days Berlin-Brandenburg (Optec Berlin-Brandenburg OpTecBB e.V., Berlin, 2022-10): *Rapid prototyping of photonic integrated circuits with ultrashort laser pulses*

J. Mikosch; 739. WE-Heraeus-Seminar/Molecular Physics and Physical Chemistry with Advanced Photon Sources (Bad Honnef, Germany, 2022-01): *Sensitivity of inner-shell photoelectron spectroscopy to non-Born-Oppenheimer and photodissociation dynamics in polyatomic molecules*

E. T. J. Nibbering; Ultrafast X-Ray Science@SXL (Stockholm, Sweden, 2022-06): *Ultrafast water-mediated proton transport dynamics between acids and bases*

Z. Pan *together with* Y. Wang, Y. Zhao, W. Chen, L. Wang, H. Yu, H. Zhang, H. Chu, D. Li, F. Rotermund, P. Loiko, J. M. Serres, X. Mateos, U. Griebner, and V. Petrov; LTO2022 The 17th National Conference on Laser Technology and Optoelectronics (Shanghai, China, 2022-08): *Development of disordered garnet laser crystals for the 2 µm band and ultrashort pulse laser research with them*

S. Patchkovskii, Int. COST/ZCAM School on Computational methods for attosecond processes, (Zaragoza, Spain, 2022-03): *Extreme/static ionization in atoms and molecules*

B. Pfau; 16th Meeting of GMM Working group "Materials for Nonvolatile Memories" (Technische Universität Dresden, virtual, 2022-03): *Magnetic skyrmions a candidate for data storage applications?*

B. Pfau; The world congress on optics and photonics ICO-25 and 16th Congress of the internatinal society on optics within life sciences (OWLS) (Technische Universität Dresden, Germany, 2022-09): *X-ray imaging and optical manipulation of chiral magnetic materials*

B. Pfau; XFEL School 2022 for condensed matter, physics in extreme conditions and dense plasmas (Aussois, France, 2022-10): *Ultrafast dynamics of magnetic skyrmions*

A. Rouzée; QUTIF Final Colloquium (Bad Honnef, Germany, 2022-08): *Strong laser-induced field-free alignment of molecules by tailored laser pulses*

B. Schütte *together with* M. Kretschmar, A. Hadjipittas, B. Major, J. Tümmler, I. Will, T. Nagy, M. Vrakking, and A. Emmanouilidou; ATTO FEL 2022 (London, UK, 2022-06): *Attosecond control of XUV mulit-photon ionization*

S. Sharma; Spin Phenomena Interdisciplinary Center, SPICE- Conferene Ultrafast Antiferromagnetic Writing (Ingelheim, Germany, 2022-05): *Ultrafast spin charge and nuclear dynamics*

S. Sharma; 50+2 years in science theory (Nijmegen, The Netherlands, 2022-05): *Ultrafast spin charge and nuclear dynamics*

S. Sharma; MORIS (Magnetics and Optics Research Int. Symposium) (Shimane, Japan, virtual, 2022-05): *Femto-Phono-Magnetism*

S. Sharma; Psi-k 2022 Conference (Lausanne, Switzerland, 2022-08): *Ultrafast spin charge and nuclear dynamics*

S. Sharma, Paris-Saclay Ultrafast X-ray Science School, Seminar "Femto-Phono-Magnetism" (Paris-Saclay University, France, 2022-10): *Transient x-ray spectroscopy for ultrafast magnetism: theoretical description*

S. Sharma; Theory meets XFELs (DESY, Hamburg, Germany, 2022-11): *Ultrafast spin charge and nuclear dynamics*

T. P. H. Sidiropoulos; 12th Ultrafast Surface Dynamics Conference (USD12) (ICFO/ Centro de Ciendias de Benasque Pedro Pascual, Spain, 2022-05): *Accessing the Real Time Flow of Energy Between Light, Carriers and Lattice in Solids with Attosecond Core-Level Spectroscopy*

O. Smirnova; PQE'2022, The 51st Winter Colloquium on the Physics of Quantum Electronics (Snowbird, Utah, USA, 2022-01): *Geometric Fields and New Enantio-Sensitive Observables in Photonionization of Chiral Molecules*

O. Smirnova; Int. COST/ZCAM School on New Computational Methods for Attosecond Processes (Zaragoza, Spain, 2022-03): *Fundamentals of high harmonic generation and high harmonic generation spectroscopy*

O. Smirnova; 4th Int. Workshop on Quantum and Topological Nanophotonics (QTN 2022) (Nanyang Technological University, Singapore, 2022-04): *Ultrafast chirality: twisting light to twist electrons*

O. Smirnova; Int. workshop on Attosecond Science and Wolf prize award ceremony (Haifa and Jerusalem, Israel, 2022-06): *Sub-cycle dynamics in strongly correlated systems*

O. Smirnova; Quantum Frontiers (Telluride, USA, 2022-06): *Ultrafast chirality: efficient dynamic approaches to chiral discrimination*

O. Smirnova; Adlershofer Forschungsforum (Berlin, Germany, 2022-06): *Ultrafast chirality: twisting light to twist electrons on ultrafast time scale*

O. Smirnova; ATTO VIII Conference (University of Central Florida, Orlando FL, USA, 2022-07): *Ultrafast Chirality: Twisting Light to Twist Electrons*

O. Smirnova; The 27th Int. Conference on Atomic Physics (Royal Conservatory of Music, Toronto, Canada, 2022-07): *Ultrafast chirality: twisting light to twist electrons*

O. Smirnova; ATTO FEL Conference (University College, London, UK, 2022-07): *Sub-cycle dynamics in strongly correlated systems*

O. Smirnova; Optica Incubator on On-Chip High-Field Nanophotonics, Workshop (Optica Global Headquarters, Washington DC, USA, 2022-07): *Synthetic chiral light & chiral topological light for efficient chiral light matter interaction*

O. Smirnova; EPS Symposium on the Third Generation Metamaterials, METAMATERIALS 3.1 (Cetraro, Calabrien, Italy, 2022-08): *Ultrafast molecular chirality: twisting light to twist electrons*

O. Smirnova; The 23rd European Conference on the Dynamics of Molecular Systems (MOLEC 2022) (Hamburg, Germany, 2022-08): *Ultrafast chirality: twisting light to twist electrons on ultrafast time scale, Keynote*

O. Smirnova; The 7th edition of the ELI Summer School (ELISS 2022) (Szeged, Hungary, 2022-08): *Synthetic chiral light for efficient chiral light matter interaction*

G. Steinmeyer; Workshop on Nonlinear Photonics and Applications (Helsinki, Finland, 2022-10): *Entropy loopholes in multimode fiber self-cleaning*

M. J. J. Vrakking; ATTO conference SOAL-2022 (Dongguan, China, 2022-01): *Control of ion-photoelectron entanglement in an attosecond experiment*

M. J. J. Vrakking; APS March Meeting 2022 (Chicago, USA, 2022-03): *Imaging "spooky action at a distance"*

M. J. J. Vrakking; ATTO-FEL 2022 (London, UK, 2022-06): *Control of attosecond entanglement and coherence*

M. J. J. Vrakking *together with* L.-M. Koll, L. Maikowski, L. Drescher, and T. Witting; Int. Workshop on Photoinization IWP & Resonant Inelastic X-ray Scattering (RIXS) (Zao-cho, Japan, 2022-11): *Control of attosecond entanglement and coherence*

Invited external talks at seminars and colloquia

K. Amini; Colloquium (Imperial College London, United Kingdom, 2022-11): *Ultrafast electron diffraction of structural dynamics below the space-charge limit*

K. Amini *together with* F. Rodriguez Diaz, T. Esnouf, M. J. J. Vrakking, C. Reiter, and M. Merö; Seminar (Oxford University, UK, 2022-11): *Ultrafast electron diffraction of structural dynamics below the space-charge limit*

K. Amini together with F. Rodriguez Diaz, M. J. J. Vrakking, and M. Meroe; Seminar (University of Oxford, UK, 2022-11): *A 100-kHz ultrafast electron diffraction set-up for 50-fs structural dynamics*

K. Amini together with F. Rodriguez Diaz, M. J. J. Vrakking, and M. Meroe; Colloquium (Imperial College London, UK, 2022-11): *A 100-kHz ultrafast electron diffraction set-up for 50-fs structural dynamics*

K. Amini *together with* F. Rodriguez Diaz, T. Esnouf, M. J. J. Vrakking, C. Reiter, and M. Merö; Colloquium (MPIK Heidelberg, Germany, 2022-11): *Ultrafast electron diffraction of structural dynamics below the space-charge limit*

W. Becker, Colloquium (Institute for Atomic and Molecular Physics, Jilin University, Changchun, China, 2022-07): *High-order harmonic generation in atoms and molecules in tailored fields*

U. Eichmann, (Université catholique de Louvain, Belgium, 2022-04): *Atomic strong-field excitation from low to high frequency fields*

T. Elsaesser, Colloquium Series (SLAC, Menlo Park, CA, USA, 2022-03): *Ultrafast electron dynamics in polar liquids and crystals*

B. P. Fingerhut, Physical and Theoretical Chemistry Seminar (Universität Regensburg, Germany, 2022-02): *From structure to function: Towards the numerically exact transfer dynamics in photoactive proteins*

B. P. Fingerhut, Theorieseminar (Heidelberg University, Germany, 2022-02): *From structure to function: Towards the numerically exact transfer dynamics in photoactive proteins*

B. P. Fingerhut, Physical and Theoretical Chemistry Seminar (Goethe-Universität Frankfurt, Germany, 2022-06): *From structure to function: Towards the numerically exact transfer dynamics in photoactive proteins*

B. P. Fingerhut, Dynamical Spectroscopies Group Seminar (Raitenhaslach, Germany, 2022-10): *Towards the numerically exact transfer dynamics in photoactive proteins*

F. J. Furch; Seminar (Lund University, Sweden, 2022-09): *Broadband OPCPAs in the NIR at high repetition rates*

M. Y. Ivanov, QUTIF meeting (Bad Honnef, Germany, 2022-08): All-optical Stückelberg spectroscopy of strongly driven Rydberg states

M. Y. Ivanov, Limati SFB Retreat Workshop (Gut Ulrihshusen, Germany, 2022-09): Fundamentals of strong field ionization

M. Y. Ivanov, Summer school on light-matter interaction at interfaces, (Rostock, Germany, 2022-09): Fundamentals of strong field ionization

M. Y. Ivanov, ICFO Colloquium (Barcelona, Spain, 2022-12): Attosecond control of electron dynamics in simple and strongly correlated materials

O. Kornilov; SFB-Seminar, Sonderforschungsbereich: SFB 1319 Extremes Licht für die Analyse und Kontrolle von molekularer Chiralität (ELCH) (Universität Kassel, Germany, 2022-12-22): *Ultrafast photoisomerization studied by time-resolved photoelectron spectroscopy*

A. Kundu, Seminar (Ashoka University, Chemistry department, Delhi, India, virtual, 2022-07): *Water dynamics in biological relevant systems & nonlinear ultrafast spectroscopy*

A. Kundu, Seminar (Laboratoire Interactions, Dynamique et Lasers (LIDYL), Université Paris-Saclay, CEA, CNRS, Paris, France, virtual, 2022-07): *2DIR spectroscopy reveals the unified picture of water hydrogen bonding dynamics in confined systems*

E. T. J. Nibbering, Department Seminar (Helmholtz-Zentrum Berlin, Germany, virtual, 2022-07): *Ultrafast water-mediated proton transport dynamics between acids and bases*

V. Petrov; Seminar (University of Central Florida, CREOL, Orlando, FL, USA 2022-10): *Spectral narrowing of non-resonant optical parametric oscillators*

B. Pfau, IKZ Kolloquium/Onlineseminar (Berlin, Germany, 2022-01): *X-raying magnetic skyrmions – Multidimensional imaging of quantum materials on the nanoscale*

D. Schick, FLASH FL24 Beamline Review Meeting (Hamburg, Germany, 2022-04): *Probing electron & hole colocalization*

S. Sharma, Colloquium, (Trinity College Dublin, Ireland, virtual, 2022-03): *Ultrafast spin charge and nuclear dynamics*

S. Sharma, joint Seminar/Colloquium, (TU Graz and KFU, Austria, virtual, 2022-05): *Ultrafast spin charge and nuclear dynamics*

S. Sharma, (TU Kaiserslautern, 2022-09): *Ultrafast spin charge and nuclear dynamics*

S. Sharma, Colloquium (Regensburg, Germany, 2022-11): *Ultrafast spin charge and nuclear dynamics*

O. Smirnova; Int. COS/ZCAM School on New Computational Methods for Attosecond Processes (Zaragoza, Spain, 2022-03): *Tutorial on strong-field physics 2*

O. Smirnova *together with* F. Morales, and S. Carlstrom; Int. COS/ZCAM School on New Computational Methods for Attosecond Processes (Zaragoza, Spain, 2022-03): *TDSE 1e simulation*

O. Smirnova, Seminar of Kassel University SFB on chirality (Bad Arolsen, Germany, 2022-10): Ultrafast chirality: twisting light to twist electrons on ultrafast time scale

O. Smirnova, Retreat Workshop of the Technical University (Gustrow, Germany, 2022-10): Ultrafast chirality: twisting light to twist electrons on ultrafast time scale

J. W. Tomm, Physikalisches Kolloquium (Institut für Physik, TU Chemnitz, Germany, virtual, 2022-01): *Spectroscopic studies of GaN-based devices*

M. J. J. Vrakking; HELIOS PIER Graduate week 2022 (Hamburg, Germany, 2022-02): *Hands-on work with inversion software*

M. J. J. Vrakking; HELIOS PIER Graduate week 2022 (Hamburg, Germany, 2022-02): *Velocity map imaging of atomic and molecular dynamics*

Z. Y. Zhang; SMART-X symposium, Optica student chapter (Politecnico di Milano, Milan, Italy, 2022-01): *From high-harmonic generation to table-top soft x-ray sources*

Z. Y. Zhang *together with* M.-O. Winghart, C. Kleine, P. Han, M. Segovia, A. Sen, D. Rana, A. Rouzée, and E. Nibbering; SMART-X 2nd symposium (Trieste, Italy, 2022-04): *Ultrafast photo-dissociation dynamics of NO2 by femtosecond time-resolved soft X-ray absorption spectroscopy at N K-edge*

Academic Teaching

K. Busch, *together with* O. Benson, A. Peters, A. Saenz, S. Ramelow, F. Intravaia, M. Krutzik, J. Volz, and P. Schneeweiß; Seminar, 2 SWS (Humboldt-Universität zu Berlin, WS 2021/2022): *Optik/Photonik: Projekt und Seminar*

K. Busch, *together with* F. Intravaia, and K. Höflich; Vorlesung und Übungen, 8 SWS (Humboldt-Universität zu Berlin, WS 2021/2022): *Fundamentals of optical sciences*

K. Busch, *together with* A. Perez-Leija, and K. Tschernig; Vorlesung und Übungen, 4 SWS (Humboldt-Universität zu Berlin, WS 2021/2022): *Diskrete Quantenoptik*

K. Busch, Vorlesung und Übung, 4 SWS (Humboldt-Universität zu Berlin SS 2022): *Computational Photonics*

K. Busch, *together with* A. Rauschenbeutel; Vorlesung, 4 SWS (Humbodt-Universität Berlin, WS 2022/2023): *Laserphysik*

K. Busch, *together with* O. Benson, A. Peters, A. Saenz, S. Ramelow, F. Intravaia, M. Krutzik, J. Volz, and P. Schneeweiß; Seminar, 2 SWS (Humboldt-Universität zu Berlin, WS 2022/2023): *Optik/Photonik: Projekt und Seminar*

K. Busch, *together with* A. Rauschenbeutel; Vorlesung, 6 SWS (Humboldt-Universität zu Berlin, WS 2022/2023): *Fundamentals in Optical Sciences*

U. Eichmann, Vorlesung, 2 SWS (Technische Universität Berlin, WS 2021/22): *Höhere Atomphysik*

S. Eisebitt, *together with* B. Kanngießer; Vorlesung und Übungen, 4 SWS (Technische Universität Berlin, Institut für Optik und Atomare Physik, SS 2022): *Röntgenphysik II*

S. Eisebitt, *together with* B. Kanngießer, B. Pfau, and C. von Korff Schmising; Vorlesung und Übungen, 4 SWS (Technische Universität Berlin, Institut für Optik und Atomare Physik, WS 2021/22): *Röntgenphysik I*

T. Elsaesser and K. Busch, Vorlesung, 4 SWS (Humboldt-Universität zu Berlin, WS 2021/22): *Laserphysik*

T. Elsaesser and G. Steinmeyer, Vorlesung, 4 SWS (Humboldt-Universität zu Berlin, SS 2022): *Physik ultraschneller Prozesse (Kurzzeitspektroskopie)*

F. Intravaia and M. Woerner, Übung, 4 SWS (Humboldt-Universität zu Berlin, WS 2021/22): *Laserphysik*

M. Y. Ivanov, *together with* T. Bredtmann; Vorlesung und Übungen, 4 SWS (Humboldt-Universität zu Berlin, WS 2021/2022): *Nichtlineare Optik*

M. Y. Ivanov, Vorlesung und Übungen, 4 SWS (Humboldt-Universität zu Berlin, WS 2022/2023): *Quantum dynamics in strong laser fields*

M. Y. Ivanov, Vorlesung und Übungen, 6 SWS (Humboldt-Universität zu Berlin, WS 2022/2023): *Nichtlineare Optik*

O. Smirnova, *together with* U. Woggon; Vorlesung und Übungen, 74,67 UE (Technische Universität Berlin, Institut für Optik und Atomare Physik, SS 2022): *Attosecond Physics*

G. Steinmeyer, Vorlesung, 4 SWS (Humboldt-Universität zu Berlin, WS 2022/23): *Physik III Optik*

G. Steinmeyer, Tutorial, 2 SWS (Humboldt-Universität zu Berlin, WS 2022/23): *Physik III Optik*

M. J. J. Vrakking, Vorlesungen und Übungen, 4 SWS (Freie Universität Berlin, WS 2021/2022): *Ultrafast Laserphysics*

M. J. J. Vrakking, Vorlesungen und Übungen, 4 SWS (Freie Universität Berlin, WS 2022/2023): *Ultrafast Laserphysics*

General talks (popular, science politics etc.)

T. Elsaesser: Vortrag: *Quantentechnologie - die physikalische Sicht*, Schiller-Gymnasium, Potsdam, 08.02.2022, Kurt-Tucholsky-Schule, Berlin, 09.12.2022

T. Elsaesser: Vortrag*: Licht und Materie - kann man Atome sichtbar machen?* Neues Gymnasium, Glienicke/Nordbahn, 10.01.2022, Johann-Wolfgang-von-Goethe Gymnasium, Pritzwalk, 26.01.2022, Städtisches Gymnasium Carl Friedrich Gauß, Frankfurt/Oder, 10.06.2022

T. Elsaesser: Vortrag: *Die Messung der Zeit - eine physikalische Herausforderung*, Leonardo da Vinci Campus, Nauen, 10.01.2022, Von Saldern Gymnasium/Europaschule, Brandenburg/Havel, 24.01.2022

Appendix 3

Ongoing Bachelor, Master, and PhD theses

Bachelor theses

D. Dahm; *Herstellung und Charakterisierung von Dünnschichtproben mittels Rotationsbeschichtung für zeitaufgelöste Röntgenabsorptionsspektroskopie* (Supervisors: B. Kanngießer and H. Stiel), Technische Universität Berlin

Master theses

M. Anus; *Optimization of XUV intensity using a novel compact HHG scheme* (Supervisors: C. Saraceno, and M. J. J. Vrakking), Ruhr Universität Bochum, Germany

L. Glöggler; *First pump-probe NEXAFS experiments using a laser-based plasma source* (Supervisors: B. Kanngießer and H. Stiel), Technische Universität Berlin

S. Dávila Lara; *Construction of a Velocity Map Imaging Spectrometer Beamline for Attosecond Pump Probe Experiments with a 100 kHz OPCPA Laser System* (Supervisors: T. Witting and R. Kienberger), TU München

X. Li; *Optical characterization of semiconductor saturable absorber mirrors* (Supervisor: G. Steinmeyer), Humboldt-Universität zu Berlin

A. Loehr; *Pulse compression by coherently rotating molecules* (Supervisors: M. Y. Ivanov and M. Khokhlova), Humboldt-Universität zu Berlin

Y. Ma; *Carrier-envelope phase stabilization of a Cr:ZnS laser oscillator* (Supervisor: G. Steinmeyer), Humboldt-Universität zu Berlin

A. Molodtsova; *Time- and angle-resolved scattering of magnetic nanostructures in the extreme ultraviolet spectral range* (Supervisor: S. Eisebitt), Technische Universität Berlin

S. Vengaladas; *Machine-learning optimized entanglement in photonic topological insulators* (Supervisors: K. Busch and K. Tschernig), Humboldt-Universität zu Berlin

PhD theses

N. Abdurakhimov; *Development and characterisation of an EUV/soft X-ray single-photon sensitive sCMOS Camera* (Supervisors: M. J. J. Vrakking and T. Kampfrath), Freie Universität Berlin and SMART-X network

V. Bender; *Modeling of non-linear and active material in interaction with plasmonic nanostructures* (Supervisor: K. Busch), Humboldt-Universität zu Berlin

M. Borchert; *Ultrafast magnetic spectroscopy in the extreme ultraviolet spectral range* (Supervisor: S. Eisebitt), Technische Universität Berlin

F. Branchi; *Ultrafast structural dynamics in molecules by time-resolved photoelectron holography* (Supervisors: J. Mikosch and M. J. J. Vrakking), Freie Universität Berlin

F. A. Rodriguez Diaz; *Development of a high-repetition rate, short pulse ultrafast electron diffraction set-up for time-resolved structural dynamics* (Supervisors: M. J. J. Vrakking and M. Weinelt), Freie Universität Berlin

P. Fuertjes; *Generation and application of ultrashort mid-infrared pulses* (Supervisor: T. Elsaesser), Humboldt-Universität zu Berlin

K. Gerlinger; *X-ray imaging of optically induced spin textures* (Supervisor: S. Eisebitt), Technische Universität Berlin

M. O. Segovia Guzman; *Ultrafast charge carrier dynamics in oxide semiconductors by time-resolved soft x-ray absorption spectroscopy* (Supervisors: M. J. J. Vrakking and M. Weinelt), Freie Universität Berlin

T. Kubail Kalousdian; *Strongfield dissociation of state-selected H_2^+ (v,J)* (Supervisors: M. J. J. Vrakking and H.-J. Freund), Freie Universität Berlin

L.-M. Kern; *Laser-driven magnetic switching at inhomogeneities and nanostructures* (Supervisor: S. Eisebitt), Technische Universität Berlin

C. Kleine; *Ultraschnelle Spektroskopie von Ladungstransferprozessen untersucht mit weichen Röntgenimpulsen* (Supervisor: T. Elsaesser), Humboldt-Universität zu Berlin

N. Klimkin; *Attosecond electron dynamics in light-driven solids* (Supervisor: M. Y. Ivanov), Humboldt-Universität zu Berlin

C. Klose; *Mesoscale Magnetization Dynamics* (Supervisor: S. Eisebitt), Technische Universität Berlin

L.-M. Koll; *2D XUV Spectroscopy* (Supervisors: M. J. J. Vrakking and G. Sansone), Freie Universität Berlin

N. Mayer; *Ultrafast spectroscopy and control of quantum dynamics in tailored multicolor laser fields* (Supervisor: M. Y. Ivanov), Humboldt-Universität zu Berlin

M. Osswald; *Theoretical description and simulation of non-linear spectroscopic signals of the light induced primary processes in (6-4) photolyase* (Supervisors: K. Busch and B. P. Fingerhut), Humboldt-Universität zu Berlin

L. Rammelt; *Direct laser writing of photonic chips for applicators in the classical and quantum regime* (Supervisors: M. J. J. Vrakking and T. Kampfrath), Freie Universität Berlin

J. Richter; *Exploring all optical magnetization switching-by ultrafast extreme ultraviolet spectroscopy* (Supervisor: S. Eisebitt), Technische Universität Berlin

M. Runge; *Nonlinear terahertz spectroscopy of biomolecules* (Supervisor: T. Elsaesser), Humboldt-Universität zu Berlin

P. Singh; *Ultrafast vibrational probes of electric fields in hydrated molecular systems* (Supervisors: J. Kneipp and T. Elsaesser), Humboldt-Universität zu Berlin

F. Steinbach; *All optical switching in complex magnetic structures* (Supervisor: S. Eisebitt), Technische Universität Berlin

N. Stetzuhn; *Ultrafast Magnetization Dynamics in van der Waals Ferromagnets* (Supervisors: K. Bolotin and S. Eisebitt), Freie Universität Berlin

E. Svirplys; *Entwicklung einer Attosekunden-Plasmalinse* (Supervisor: M. J. J. Vrakking), Freie Universität Berlin

Z. Zhang; *Soft X-ray spectroscopy of investigating charge transfer processes in push-pull chromophores* (Supervisor: M. J. J. Vrakking), Freie Universität Berlin

W. Zhao; *Free electron quantum optics* (Supervisor: K. Busch), Humboldt-Universität zu Berlin

Appendix 4

Guest Lectures at the MBI

M. Gühr, Potsdam University, Germany (virtual, 2022-01-12): *Time-resolved x-ray probing of the photorelaxation in thiouracil*

C. Tzschaschel, Harvard University, Cambridge, MA, USA (virtual, 2022-01-13): *Ultrafast optical manipulation and probing of antiferromagnetic states*

F. Légaré, Institut national de la recherche scientifique (IRNS), Québec, Canada (virtual, 2022-02-09): *Generation of few-cycle laser pulses and applications*

B. Winter, Fritz-Haber-Institut Berlin, Germany (virtual, 2022-03-02): *Advances in liquid-jet photoelectron spectroscopy*

R. Radloff, Technische Universität Berlin, Germany (Max-Born-Saal, 2022-03-04): *Spectroscopic properties of diamondoid radical cations: diamantane and 1-cyanoadamantane*

W. Bouckaert, École Polytechnique Fédérale de Lausanne, France & Carnegie Mellon University, EPFL, Pittsburgh, PA, USA (virtual, 2022-03-22): *Tunnel magnetoresistance detection of skyrmion*

J. Peschel, Lund University, Sweden (Max-Born-Saal, 2022-03-24): *Atomic and molecular dynamics probed by intense extreme ultraviolet attosecond pulses*

A. Khodko, Institute of Physics of NAS, Kyiv, Ukraine (Max-Born-Saal, 2022-04-01): *Optical characteristics and cyclization dynamics of photochromic diarylethene molecules*

X. Wang, SLAC National Accelerator Laboratory, Stanford, CA, USA (Max-Born-Saal, 2022-04-04): *Watch water molecules dancing with MeV electrons*

S. Cundiff, University of Michigan, MI, USA (virtual, 2022-04-06): *Tri-comb spectroscopy*

J. Lee, University of Seoul, South Korea (virtual, 2022-04-08): *Ultrafast fiber lasers in 1 μm-2 μm wavelength region*

S. A. Diaz, Universität Duisburg-Essen, Germany (virtual, 2022-04-11): *Correlated dynamics of driven magnetic skyrmions*

J. Richter, Freie Universität Berlin, Germany (Max-Born-Saal, 2022-04-29): *Dynamic photocurrent measurements and tunnelling spectroscopy of heterostructures including 2D magnets*

R. Riedel, Class 5 Photonics GmbH, Hamburg, Germany (Max-Born-Saal, 2022-05-20): *A review about Class 5 Photonics NIR-MIR optical-parametric chirped-pulse amplifiers*

M. Krikunova, ELI Beamlines – Int. Laser Research Centre, Czech Republic & TH Wildau, Germany (Max-Born-Saal, 2022-06-21): *A multipurpose end-station MAC for applications in AMO science and CDI at ELI Beamlines*

J. Carpenter, University of Queensland, Brisbane, Australia (Seminarraum A, 2022-06-28): *Arbitrary vector spatiotemporal beamshaping: Any amplitude, phase and polarisation at any delay*

U. Höfer, University of Marburg, Germany (Max-Born-Saal, 2022-07-06): *Lightwave ARPES – subcycle time-resolved photoemission of lightwave-driven processes*

M. Richardson, University of Central Florida, Orlando, FL, USA (Max-Born-Saal, 2022-07-06): *High power lasers in the outside!*

A. Johnson, The Institute of Photonic Sciences (ICFO), Barcelona, Spain (Max-Born-Saal, 2022-07-14): *Ultrafast and hyperspectral coherent X-ray imaging of the metal to insulator phase transition in VO2*

P. Kraus, Advanced Research Center for Nanolithography (ARCNL), Amsterdam, The Netherlands (Max-Born-Saal, 2022-07-28): *Coherent extreme-ultraviolet generation and manipulation from bulk and nanostructured solids*

C. Kufner, Center for Astrophysics, Harvard College Observatory, Cambridge, MA, USA (Max-Born-Saal, 2022-08-16): *UV-induced photochemistry in prebiotic lakes*

M. Volkov, University of Konstanz, Germany (Max-Born-Saal, 2022-08-18): *Towards petahertz electronics: exploring the dynamics of solids with pulsed electrons and light*

J. Rothhardt, Helmholtz Institute Jena, Germany (Max-Born-Saal, 2022-08-26): *Towards attosecond imaging at the nanoscale using extreme ultraviolet high harmonic sources*

R. Murray, Imperial Collgege, London, UK (Seminarraum A, 2022-09-06): *Fibre laser pumped nonlinear conversion sources from the visible to the mid-infrared: biomedical applications at Imperial College London*

E. Kachan, Hubert Curien Laboratory, University of Saint-Étienne, France (Seminarraum A, 2022-09-08): *Ab initio simulations of ultrafast laser excitation of solids*

D. Rolles, Kansas State University, Manhattan, KS, USA (Max-Born-Saal, 2022-09-14): *Gas-phase photochem-*

istry studies with free-electron lasers

A. Tsaturyan, University of Lyon, Université Jean Monnet Saint-Étienne, France (Seminarraum A, 2022-09-15): *First-principles calculations of fused silica electronic structure under strong laser-induced excitation*

A. Sanchez, The Institute of Photonic Sciences, Barcelona, Spain (Max-Born-Saal, 2022-09-21): *Laser-induced electron interferences from atoms and molecules*

D. Arena, University of South Florida, Tampa, FL, USA (Seminarraum C, 2022-09-23): *Spin dynamics in ferrimagnetic thin films: pump-probe studies using visible and extreme UV photons*

O. A. Naranjo-Montoya, University of Duisburg-Essen, Germany (Max-Born-Saal, 2022-10-10): *Towards a tabletop facility for ultrafast soft x-ray absorption spectroscopy*

J. Osterhoff, DESY Hamburg, Germany (Max-Born-Saal, 2022-10-12): *Plasma-based particle accelerators for scientific and societal applications driven by intense lasers and beams*

R. Forbes, SLAC National Accelerator Laboratory, CA, USA (Seminarraum A, 2022-10-24): *Multichannel excited state dynamics probed by structurally sensitive imaging and spectroscopic techniques*

C. R. Baiz, Department of Chemistry, University of Texas at Austin, TX, USA (Seminarraum C, 2022-10-25): *Improving signal-to-noise ratios in ultrafast spectroscopy: new 2D IR optical implementations and machine learning*

V. Unnikandanunni, Stockholm University, Sweden (Max-Born-Saal, 2022-11-28): *Ultrafast spin dynamics: The role of magneto-crystalline anisotropy*

V. Temnov, CNRS, Ecole Polytechnique, Palaiseau, France (Max-Born-Saal, 2022-11-30): *Ultrafast quantitative magneto-acoustics at the nano-scale*

P. Demekhin, Kassel University, Germany (Max-Born-Saal, 2022-12-07): *Molecular Frame Photoelectron Angular Distributions (MFPADs): A sensitive access to electronic structure and dynamics*

D. Afanasiev, Radboud University Nijmegen, The Netherlands (Max-Born-Saal, 2022-12-09): *Ultrafast control of spins using resonant light excitation*

P. Polynkin, University of Arizona, Tucson, AZ, USA (Seminarraum A, 2022-12-09): *Low-order harmonic generation and CEP effects in short- and mid-wave infrared laser filaments in gases*

Appendix 5

Grants and Contracts

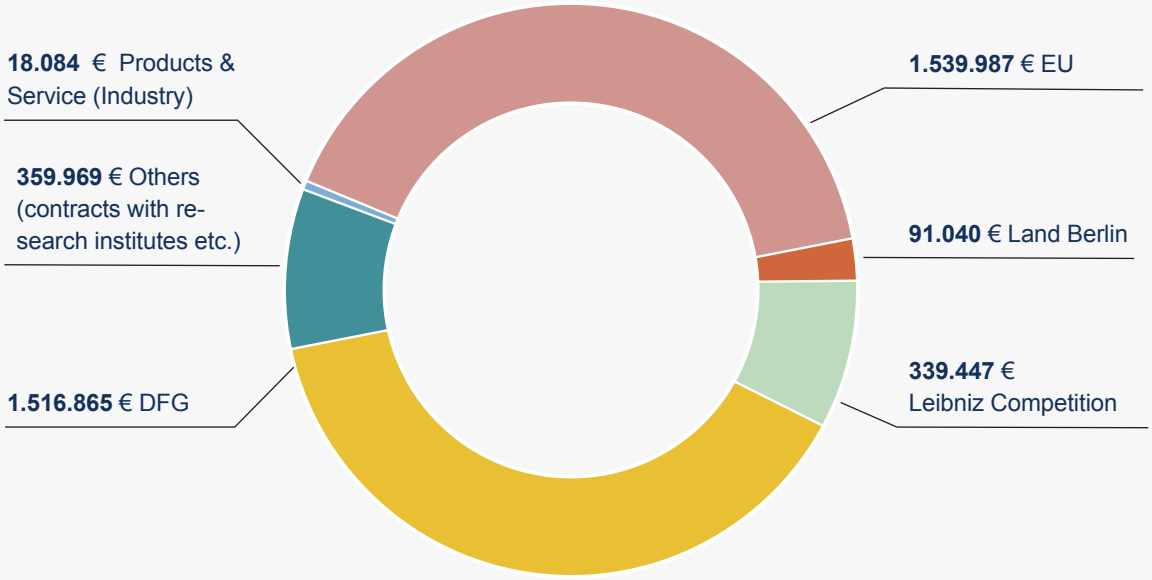

Total amount spent in 2022: 3.865.392 €

Appendix 6

Activities in Scientific Organizations

W. Becker

Member, Editorial Board, Applied Sciences,

Member, Editorial Board Science open,

Member, Editorial Board Laser Physics Letters,

Member of the Advisory and Program Committee and Co-Chair Seminar 2, 30th International Laser Physics Workshop - LPHYS'22, virtual format, Lyon, France

K. Busch

Editor-in-chief, Journal of the Optical Society of America B

S. Eisebitt

Vorsitzender Vorstand, PGzB (Physikalische Gesellschaft zu Berlin)

Member, FERMI Proposal Review Panel, Elettra Sincrotrone Trieste, Italy

Chair Scientific Advisory Council Elettra-Sincrotrone Trieste, Italy

Vice Chair, DESY Photon Science Comittee

Member, Scientific Advisory Committee (SAC) of the European XFEL

T. Elsaesser

Secretary of the Mathematics and Science Class, Berlin Brandenburg Academy of Sciences

Chair, TELOTA steering group, Berlin Brandenburg Academy of Sciences

Conference Chair, Program Committee, 15th Femtochemistry Conference (FEMTO 15)

Member, IRIS Adlershof, Humboldt-Universität zu Berlin (Berlin)

Member, Kuratorium of the Max Planck Institute for Quantum Optics, Garching, Germany

Member, Standing Committee for the Evaluation of International Max Planck Centers, Max Planck Society, Munich, Germany

Member, Editorial Board, Chem. Phys. Lett.

Member, Advisory Board, Conference Series on Time Resolved Vibrational Spectroscopy

Associate Editor, Struct. Dyn., AIP

Member, Science Policy Committee, SLAC, Menlo Park

Member, FXE Proposal, Review Panel, Schenefeld, European XFEL

Chair, Physics Group, Gesellschaft Deutscher Naturforscher und Ärzte (GdNÄ)

Member, Advisory Board, Int. Conference on Coherent Multidimensional Spectroscopy

B. P. Fingerhut

Member, Coblentz Award Committee of the Coblentz Society

U. Griebner

Member, Programm Committee, Ultrafast Optics 2023, Bariloche, Argentina

R. Grunwald

Member, SPIE Fellows Committee 2022

Member, Editorial Board, Applied Sciences (MDPI)

Associate Editor, Optics Express (Optica)

Member, Programm Committee Photonics West, OPTO, Complex light and optical forces XV

Member, International Committee of Optics (ICO), Dresden, Germany

E. T. J. Nibbering

Member, Advisory Board, Conference Series on Time Resolved Vibrational Spectroscopy

Member, Editorial Board, Journal of Photochemistry and Photobiology A

V. Petrov

Chair of programme committee, Photonics West 2022, Nonlinear freqency generation (San Francisco, USA)

A. Rouzée

Editor, Advances in Physics X

O. Smirnova

Member, Advisory Board of the Max Planck School of Photonics

Member, dynaMENT Mentoring for Women in Natural Sciences, University of Hamburg and DESY

Member, International Program Committee, International Conference on on Attosecond Science and Technology, ATTO

Member, General Committee, ICPEAC, International Conference on Photonic, Electronic and Atomic Collisions

G. Steinmeyer

Subcommittee Chair, Nonlinear Photonics 2022, Maastricht, Netherlands

Associate Editor, Optica

Member, Editorial Board, Phys. Lett. A

Member, Program Committee, Ultrafast Optics 2023, Bariloche, Argentina

H. Stiel

Member, Scientific Committee Int. Conference on X-ray Lasers, EMPA, Dübendorf, Switzerland

Member, Advisory board of Institute of Applied Photonics (IAP) eV, Berlin

J. W. Tomm

Permanent Member, Int. Steering Committee, Int. Conference on Defects - Recognition, Imaging and Physics of Semiconductors, DRIP (Yokohama, Japan)

Associate Editor, Journal of Electronic Materials (JEMS)

Member Editorial Board, Communications in Physics (CIP)

M. J. J. Vrakking

Editor-in-chief, Journal of Physics B

Chairman of the SAB, Institute of Physics, Universität Freiburg

Conference Chair, Program Committee, 15th Femtochemistry Conference (FEMTO 15)

Member of UED proposal review panel at LCLS, Stanford University

Chair of Session Molecular Physics 10: XUV-spectroscopy, DPG Spring Meeting, Erlangen, online

Honors and awards

P. Fuertjes: IPG Student Paper Award, IPG Photonics

T. Elsaesser: Ahmed Zewail Award, American Chemical Society

D. Schick: Junior Research Group in the Leibniz competition on the topic “Complex spin structures in time and space"

O. Smirnova: Senior-Award - Mildred Dresselhaus Gastprofessorinnenprogramm 2022 des Hamburg Centre for Ultrafast Imaging (CUI), Hamburg, Germany

O. Smirnova: ERC Advanced Grant on Ultrafast Molecular Chirality

Max-Born-Institut (MBI)
für Nichtlineare Optik und Kurzzeitspektroskopie
im Forschungsverbund Berlin e. V.

Mail Address: Max-Born-Institut
Max-Born-Straße 2 A
12489 Berlin
Germany

Phone: (++49 30) 6392 1505
Fax: (++49 30) 6392 1519
mbi@mbi-berlin.de
www.mbi-berlin.de

The Divisions of the Max-Born-Institut

Division A: Attosecond Physics
Prof. Dr. M. J. J. Vrakking

Division B: Transient Electronic Structure and Nanoscience
Prof. Dr. S. Eisebitt

Division C: Nonlinear Processes in Condensed Matter
Prof. Dr. T. Elsaesser

City district: Berlin Treptow-Koepenick
Subdistrict: Berlin-Adlershof

Site: Berlin-Adlershof
Street: Max-Born-Straße 2 A

S-Bahn: S45, S46, S85, S8, and S9
Station: Berlin-Adlershof
from there:
Bus 162, 164 to Magnusstraße
Tram: 61, 63 to Karl-Ziegler-Straße

Subway: U7
Station: Rudow
from there:
Bus 162 to Magnusstraße

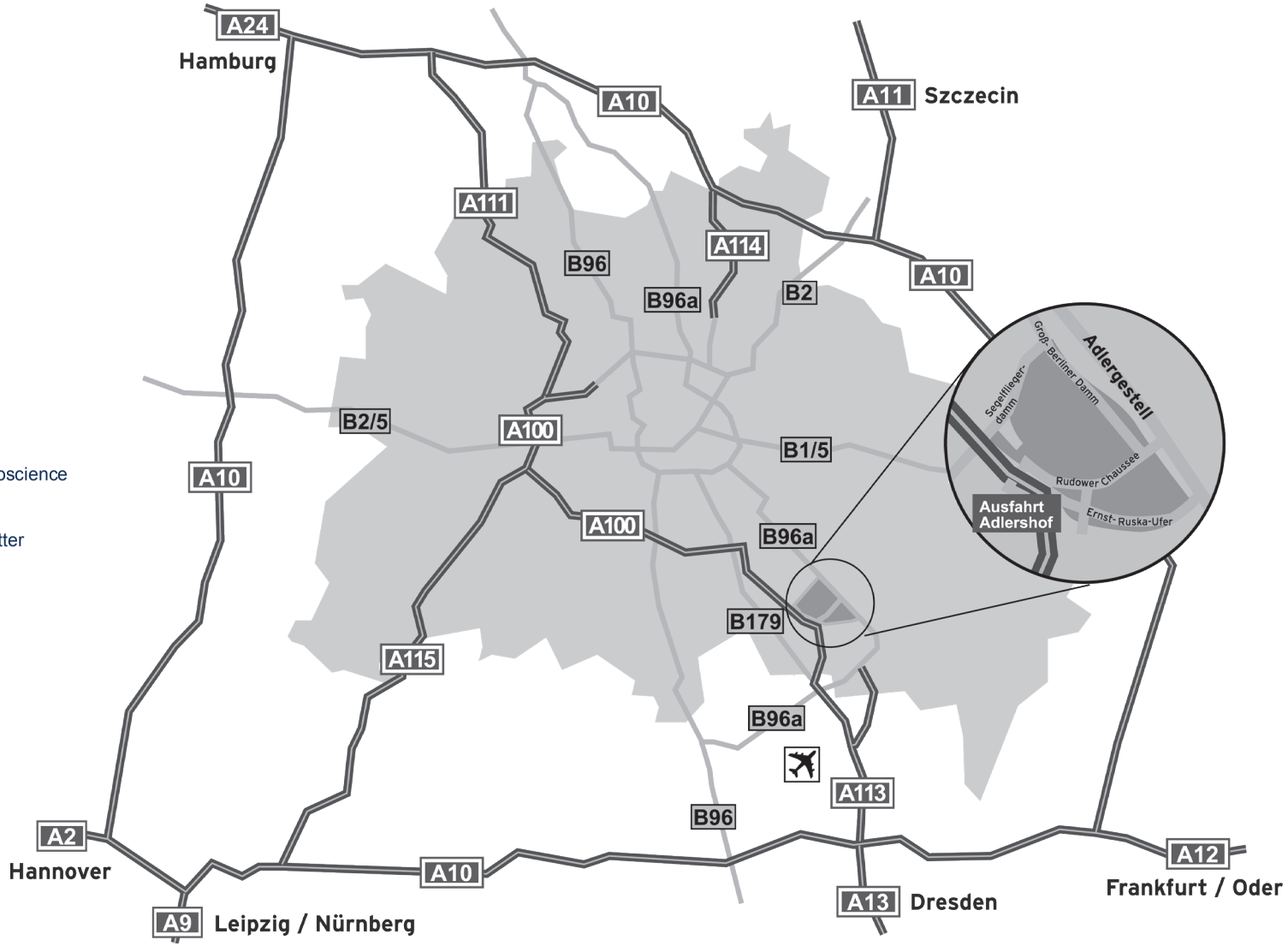

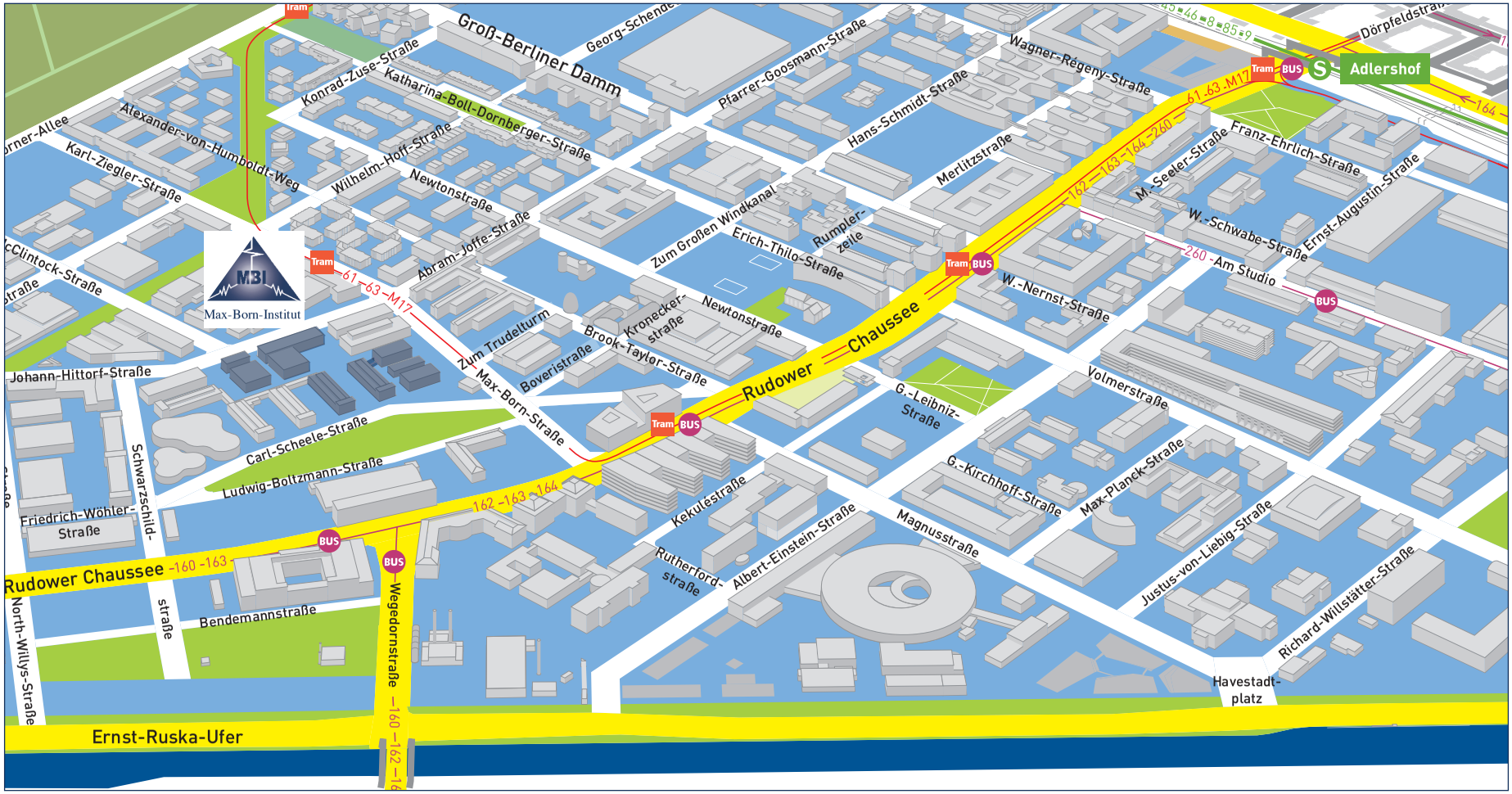
Groß-Berliner Damm
Georg-Schende
Konrad-Zuse-Straße
Katharina-Boll-Dornberger-Straße
Pfarrer-Goosmann-Straße
Wagner-Régeny-Straße
Dörpfeldstraße
Adlershof
Tram
BUS
S
-61 -63 -M17
-164
Alexander-von-Humboldt-Weg
Karl-Ziegler-Straße
Wilhelm-Hoff-Straße
Newtonstraße
Hans-Schmidt-Straße
Merlitzstraße
-162 -163 -164 -260
M. Seeler-Straße
Franz-Ehrlich-Straße
W.-Schwabe-Straße
Ernst-Augustin-Straße
Abram-Joffe-Straße
Zum Großen Windkanal
Erich-Thilo-Straße
Rumpler-zeile
-260 -Am Studio
W.-Nernst-Straße
Max-Born-Institut
MBI
Zum Trudelturm
Kronecker-straße
Newtonstraße
Boveristraße
Brook-Taylor-Straße
Rudower Chaussee
Johann-Hittorf-Straße
Max-Born-Straße
G.-Leibniz-Straße
Volmerstraße
Carl-Scheele-Straße
Ludwig-Boltzmann-Straße
Schwarzschild-
Friedrich-Wöhler-Straße
-162 -163 -164
Kekulestraße
G.-Kirchhoff-Straße
Max-Planck-Straße
Rudower Chaussee -160 -163
Albert-Einstein-Straße
Magnusstraße
Rutherford-straße
Justus-von-Liebig-Straße
Richard-Willstätter-Straße
North-Willys-Straße
straße
Bendemannstraße
Wegedornstraße -160 -162
Havestadt-platz
Ernst-Ruska-Ufer